Etude de nouveaux systèmes photoamorceurs pour la synthèse de polymères en impression 3D ou pour les composites

Fatima Hammoud

THÈSE

Présentée et soutenue le **30 Juin 2023** par :

Fatima HAMMOUD

Pour l'obtention du titre de Docteur en Chimie des Matériaux de
L'UNIVERSITÉ DE HAUTE ALSACE

Étude de nouveaux systèmes photo-amorceurs pour la synthèse des polymères pour l'impression 3D ou pour les composites.

Membres du Jury

Pr. Françoise Chuburu Université de Reims Champagne	Rapporteur
Pr. Laurent Rubatat Université de Pau et des Payes de l'Adour	Rapporteur
Pr. Jacques Lalevée Université de Haute Alsace	Directeur de thèse
Pr. Akram Hijazi Université Libanaise	Co-Directeur de thèse

« Cela parait toujours impossible, jusqu'à ce que ce soit fait », disait Nelson Mandela (1918-2013, Ancien président de l'Afrique du Sud).

« Tout commence par un rêve ! « La première étape est de croire que tu peux », disait même Will Smith. Et un jour tu pourras dire : ça n'a pas été facile, mais j'ai réussi ! »

« Seulement ceux qui prendront le risque d'aller trop loin découvriront jusqu'où on peut aller », murmurait Thomas Stearns Eliot (1888-1965, Poète).

« Dans la vie, tout est une affaire de risque. Ce que vous devez apprendre, c'est comment le gérer. Vous ne devez pas avoir peur d'échouer, vous devez avoir peur de ne pas essayer ! Pour ma part, je pense qu'on a le contrôle sur nos capacités et notre motivation. On n'est pas déterminé par le fait de gagner ou de perdre. On peut aller de l'avant avec ce qu'on a. »

Dédicace

***À ma très chère maman**,*

Quoi je fasse ou que je dise, je ne saurai point te remercier comme il se doit. Ton affection me couvre, ta bienveillance me guide et ta présence à mes côtés a toujours été ma source de force pour affronter les différents obstacles.

***À mon très cher papa**,*

Tu es toujours été à mes côtés pour me soutenir et m'encourager. Que ce travail traduit ma gratitude et mon affection.

À mon très cher frère Ali et mes belles sœurs Nejmeh, Walàa, Hanan et Hiba,

Vous avez partagé avec moi tous les moments difficiles lors de la réalisation de ce travail. Que Dieu me permette de vous rendre au moins une partie, aussi infime soit-elle, de tout ce que je vous dois.

À mes amours de nièces et neveux Lana, Monzer, Nohad, Hassan, et Ali,

Vous êtes les étoiles de mon ciel ! Écouter votre rire est le meilleur remède que je puisse prendre. Je veux que vous sachiez que vous occupez beaucoup de mon bonheur dans cette vie.

Rien n'aurait été possible sans vous !

Remerciements

Cette thèse m'a laissé un sentiment agréable et plaisant. Ce sentiment m'aide sans aucun doute à me sentir à l'aise pour accomplir la tâche qui m'a été confiée, et découle surtout de mon désir d'exprimer ma gratitude à ceux qui m'ont si chaleureusement soutenu tout au long de cette aventure.

Ce travail a été réalisé à l'Institut de Science des Matériaux de Mulhouse (IS2M) de l'Université de Haute Alsace (UHA) dans l'équipe de Chimie Radicalaire des Matériaux (CRM). Cette thèse est réalisée en codirection avec l'Université Libanaise (UL) – Liban.

Ma reconnaissance s'adresse à la France, qui m'a accueillie et m'a permis d'élargir et d'approfondir mes connaissances scientifiques dans le domaine de la recherche.

Ce travail n'aurait pu être mené à bien sans l'aide de la "Fondation Pierre et Jeanne Spiegel", qui a financé mes années de thèse. Un grand merci pour leur confiance et leur soutien.

Tout d'abord, je tiens à exprimer mes remerciements les plus sincères à mon directeur de thèse Pr. Jacques LALEVÉE, de m'avoir accueillie au sein de son équipe ainsi que pour sa confiance et soutien permanent. Un très grand Merci à lui pour ses encouragements, ses conseils et son intérêt porté à mon travail. J'ai beaucoup apprécié son enthousiasme et sa bonne humeur. Aucun mot ne peut exprimer mon extrême gratitude envers lui.

Je tiens aussi à remercier mon co-directeur de thèse Pr. Akram HIJAZI. Je lui exprime toute la gratitude, le respect et ma très vive reconnaissance pour son aide et sa confiance qui m'est très précieuse.

Un grand merci aux Dr. Michael SCHMITT et Dr. Fabrice MORLET-SAVARY pour leur aide indispensable, leurs conseils avisés et leur amicale disponibilité.

J'exprime encore mes remerciements au collaborateur Dr. Frédéric DUMUR qui a rythmé l'avancée de mes recherches en effectuant la synthèse de la majorité des produits sur lesquels porte mon travail de recherche.

Mes sincères remerciements sont adressés également aux membres du jury qui m'ont fait le grand honneur d'évaluer ces travaux de recherche.

Au Pr. Dominique BERLING, directeur de l'école doctorale, aux membres du laboratoire IS2M, spécialement Pr. Vincent ROUCOULES, directeur du laboratoire IS2M et à tous ceux que j'ai croisés lors des séminaires, des colloques et des conférences, je tiens à les remercier.

Je ne peux continuer ces remerciements sans évoquer mes collègues de l'équipe, passés et actuels : Noëlle, Tuba, Marie, Rania, Mariem, Romain, Rafael, Loïc, Estelle, Serife, Alexis, Loic, Elodie, Valentine, Aurore, Valentin, Yijun, Shaohui, Hong… Un merci tout particulier à Haifaa, Ahmad, Mahmoud, Mira et Adel pour leur soutient, les conseils et les discussions !
Au-delà de cette équipe dynamique, je tiens à remercier les autres personnes gravitant à l'IS2M, en particulier Stéphania, Marwan, Youssef, Carole et Rana pour leur bonne humeur et leur soutien.

Ces trois années n'auraient vraiment pas été les mêmes sans mes collègues de bureau ! Merci à Chaima, Asma et Hanine, pour tout le soutien psychologique, les discussions, merci de m'avoir encouragée et d'avoir créé un excellent environnement de travail. Merci notamment pour l'aide que vous m'avez apportée dans le domaine scientifique mais aussi en informatique et pour les formalités administratives. Merci d'avoir été là dans les bons comme les mauvais moments.

Je passe ensuite une dédicace spéciale à tous mes stagiaires que j'ai eu le plaisir d'encadrer durant ces quelques années, Aristea, Alex, Armelle et Burak. Je tiens à mentionner le plaisir que j'ai eu à travailler avec vous tous.

À ma collègue et chère amie, Mirna Zgheib, qui est restée à mes côtés tout au long de cette aventure du début à la fin. Merci beaucoup Mirna pour ta gentillesse, tes encouragements, ton empathie. Je suis heureuse d'avoir pu partager tous les détails de cette étape de ma vie avec toi. Je n'oublierai jamais nos moments de folie, de bonheurs, de tristesse, de stress… J'espère pourvoir commencer le prochain défi avec toi à mes côtés.

Enfin, aucun mot ne pourrait exprimer la gratitude et l'amour que je porte à mes parents. Ce travail est le fruit de leurs sacrifices, de leurs encouragements, de leur tendresse, de leur amour et de leur confiance indéfectible dans mes choix. Je ne pourrais vous remercierai jamais assez !

RÉSUMÉ/ABSTRACT

Résumé

Cette thèse vise principalement à étudier de nouveaux systèmes photo-amorceurs à haute performance qui sont capables de mener à bien à des processus efficaces sous des sources de lumière visible telles que les diodes électroluminescentes (LEDs) et de les utiliser pour des applications dans l'impression 3D ou dans la synthèse de composites. Les nouvelles molécules introduites sont le résultat de colloborations étroites et de plusieurs synthèses effectuées, majoritairement au sein de l'Institut de Chimie Radicalaire de Marseille mais certaines ont été préparées au Département d'Ingénierie Chimique et des Matériaux de l'Université Nationale des Sciences et Technologies de Kaohsiung (Taiwan)**. Dans une première partie**, l'état de l'art et la bibliographie seront présentés. **Dans une seconde partie**, des structures qui peuvent être considérées comme des photo-amorceurs (Type II) pour des systèmes multi-composants (deux ou trois composants) ont été testées sous LED@405 nm ; celles-ci ayant été choisies pour ce travail afin d'être compatible avec la plupart des imprimantes 3D qui fonctionnent en fait spécifiquement à cette longueur d'onde. La recherche a également porté sur des co-amorceurs ou des additifs de polymérisation en vue de les étudier comme des alternatives intéressantes aux amines toxiques et donc comme des candidats prometteurs pour le développement de systèmes sans amine. **Dans une troisième partie**, afin de réduire la complexité des systèmes et de résoudre les problèmes de solubilité, d'efficacité du transfert d'électrons et de viscosité des résines, on est passé, à des systèmes mono-composants, en introduisant la fonction oxime-ester dans la composition structurelle des molécules étudiées afin qu'elles puissent réagir comme des photoamorceurs Type I, sachant que les oxime-esters étaient connues depuis longtemps pour leur photoréactivité élevée dans le processus de photopolymérisation. Compte tenu du but principal de cette thèse, qui consiste à accéder à des applications dans la synthèse de composites en plus de l'impression 3D, les systèmes développés ont montré une bonne efficacité même pour des échantillons chargés. Pour finir, **dans une quatrième partie**, un projet a été réalisé dans le cadre d'une collaboration industrielle avec BASF à Ludwigshafen (Allemagne). Il s'est concentré sur la synthèse de composites (hautement chargés) à travers d'un processus de polymérisation frontale qui se déclenche habituellement à partir de la photopolymérisation en surface. Du fait de l'exothermicité de ce processus, un amorceur thermique peut se décomposer et poursuivre l'amorçage de la polymérisation en profondeur.

Abstract

This thesis mainly aims at studying new high performance photoinitiator systems that are able to carry out efficient processes under visible light sources such as light emitting diodes (LEDs) and to use them for applications in 3D printing or in the synthesis of composites. The new molecules introduced are the result of close colloborations and several syntheses performed, mostly at the Institute of Radical Chemistry of Marseille but some were prepared at the Department of Chemical and Materials Engineering of the National University of Science and Technology of Kaohsiung (Taiwan). **In a first part**, the state of the art and the bibliography will be presented. **In a second part**, structures that can be considered as photoinitiators (Type II) for multi-component systems (two or three components) have been tested under LED@405 nm; these having been chosen for this work in order to be compatible with most of the 3D printers that actually work specifically at this wavelength. The research also focused on co-initiators or polymerization additives in order to study them as interesting alternatives to toxic amines and thus as promising candidates for the development of amine-free systems. **In a third part**, in order to reduce the complexity of the systems and to solve the problems of solubility, electron transfer efficiency and viscosity of the resins, we moved to mono-component systems by introducing the oxime-ester function in the structural composition of the studied molecules so that they can react as Type I photoinitiators, knowing that the oxime-esters have been known for a long time for their high photoreactivity in the photopolymerization process. Considering the main goal of this thesis, which is to access applications in the synthesis of composites in addition to 3D printing, the developed systems showed a good efficiency even for loaded samples. Finally, **in a fourth part**, a project was carried out as part of an industrial collaboration with BASF in Ludwigshafen (Germany). It focused on the synthesis of (highly filled) composites through a frontal polymerization process which is usually initiated from the surface photopolymerization. Due to the exothermicity of this process, a thermal initiator can decompose and continue the polymerization in depth.

Introduction Générale, Structuration et Valorisation du Travail

TABLE DES MATIÈRES

Table des matières

INTRODUCTION GÉNÉRALE, STRUCTURATION ET VALORISATION DU TRAVAIL

I. Introduction Générale

1. Thème principal de la thèse

La recherche de nouveaux procédés de synthèse de polymères à faible coût, respectueux de l'environnement et économiques en énergie est plus importante que jamais dans divers domaines, tels que les transports, la santé, l'énergie, les nanotechnologies, etc.

Les polymères sont utilisés partout dans la vie quotidienne, notamment dans les cosmétiques, les revêtements, les aliments, les emballages, la dentisterie, l'électronique, les adhésifs, les peintures et l'optique. [1-5] Leur production devenant de plus en plus indispensable, et face aux nouvelles exigences, il est essentiel de trouver des procédés nouveaux, rapides, économiques et écologiques. [6-8]

L'activation thermique est depuis longtemps un sujet de recherche pour le déclenchement des réactions de polymérisation. Cette procédure est gourmande en énergie, nécessite l'utilisation de solvants et requiert souvent de longues périodes de réaction. [9-11] Il existe d'autres sources d'énergie qui peuvent amorcer une réaction, surtout les irradiations (lumière, micro-ondes, photons gamma…). Ces dernières années ont été marquées par le développement de sources lumineuses économiques, efficaces et à faible consommation grâce aux progrès techniques. [12-15] Les procédés de synthèse des polymères par voie photochimique connaissent actuellement un développement rapide.

Les réactions de polymérisation induites par la lumière ont connu un essor récent et sont utilisées dans de nombreuses applications industrielles, tels que le domaine du « radiation curing », l'imagerie laser, les revêtements, les encres et les peintures, (Schéma 1) ... [16-19]

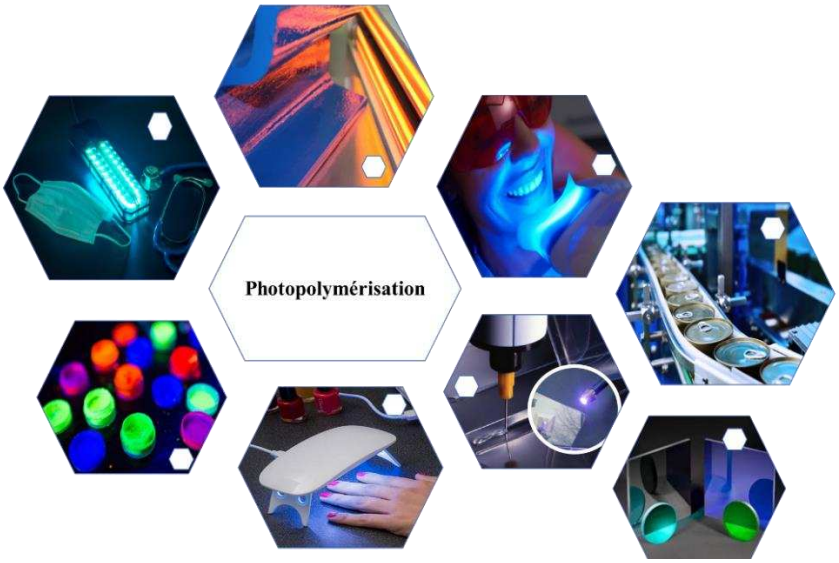

Schéma 1. Exemples de domaines d'application de la photopolymérisation.

À côté de ces utilisations, de nouvelles techniques basées sur la photopolymérisation ont été développées, en particulier l'impression 3D [20] et les différentes techniques regroupées sous ce terme générique (même si toutes ne sont pas basées sur la photopolymérisation). En termes de production de déchets, de complexité des articles et de coûts de fabrication, l'impression 3D, également connue sous le nom de fabrication additive, a véritablement révolutionné l'industrie de la fabrication et du prototypage. [21-23]

Ces temps derniers, les entreprises cherchent aussi à mettre sur le marché des composites présentant des caractéristiques mécaniques intéressantes, dont un poids réduit, une stabilité chimique et une résistance à la corrosion, et s'intéressent de plus en plus aux techniques de polymérisation induite par la lumière. [24-26] En raison de ces qualités, les composites sont le matériau dominant qui se développe dans plusieurs applications industrielles, tels que les secteurs de l'automobile, des articles de sport et de l'aérospatiale. [27-30]

L'idée de base de la photopolymérisation est qu'il suffit de quelques secondes d'exposition à la lumière pour transformer une substance liquide constituée de monomères ou oligomères (de petites molécules possédant une ou plusieurs fonctions réactives) en un matériau solide appelée polymère. [31]

Un ingrédient photosensible doit être présent dans la formulation pour qu'une réaction de photopolymérisation se produise (le photoamorceur ou système photoamorceur). Ce dernier, va produire des radicaux amorceurs lors d'une irradiation lumineuse, permettant l'amorçage de la polymérisation. [32-34]

INTRODUCTION GÉNÉRALE, STRUCTURATION ET VALORISATION DU TRAVAIL

Lorsque de nombreux composés sont combinés pour amorcer la réaction de photopolymérisation, on parle d'un "système photoamorceur" (PIS). Dans ce contexte, il y a un photoamorceur (PA) et un ou plusieurs coamorceurs (coA). Selon le type de polymérisation à mettre en œuvre, les espèces réactives créées par le rayonnement lumineux peuvent être de plusieurs natures, notamment des radicaux libres, des cations ou des anions. Un monomère approprié doit être utilisé en fonction de l'espèce générée, comme les monomères acryliques ou vinyliques pour les radicaux ou les époxydes pour les cations. [35-37]

De nombreuses études ont été réalisées sur les processus de polymérisation cationique et/ou radicalaire induits par la lumière. Ces procédés présentent un certain nombre d'avantages par rapport aux techniques de polymérisation thermique :

- Ces procédés nécessitent moins d'énergie que d'autres méthodes de synthèse de matériaux polymères. Comme les processus de photopolymérisation se déroulent à température ambiante tout en étant exposés à des sources lumineuses qui consomment beaucoup moins d'énergie que les équipements de chauffage traditionnels.
- En outre, le procédé de polymérisation photochimique est rapide. La production des espèces réactives et le processus d'amorçage de la polymérisation peuvent tous deux être réalisés en quelques secondes.
- Comme la formulation comprend très peu, voire pas du tout, de solvant, moins de composés organiques volatils (COV) sont libérés dans l'atmosphère. En outre, la réaction se produit à température ambiante, ce qui réduit encore les émissions de COV. En réalité, la procédure photochimique présente l'avantage d'être beaucoup plus respectueuse de l'environnement (classée comme technologie verte par la communauté européenne).
- Seules les parties exposées subissent une polymérisation, ce qui permet un contrôle spatial efficace du processus (par exemple, impression 3D, lithographie...).
- L'accès à des échantillons de polymères épais (jusqu'à quelques centimètres) est rendu possible par la possibilité de contrôler la longueur d'onde d'irradiation et/ou la concentration du photoamorceur. L'accès aux composites reste un grand challenge.
- Les polymères produits par voie photochimique présentent de bonnes caractéristiques physicochimiques, notamment une plus grande homogénéité, une bonne qualité de surface, une absence d'odeur et une bonne résistance chimique.

2. *Problématiques et challenges*

La synthèse des photopolymères au niveau industriel se fait par voie radicalaire ou ionique. La génération de radicaux et des ions se fait uniquement par l'absorption du système photoamorceur d'une énergie lumineuse appropriée. Cependant, la majorité des photoamorceurs commerciaux absorbent la lumière UV, ainsi les photopolymères synthétisés industriellement s'accompagnent d'une consommation d'énergie assez forte due à la forte intensité de la lumière UV. Ceci nécessite l'utilisation de dispositifs d'irradiation émettant des UV (lampes UV à vapeur de mercure) qui présentent plusieurs inconvénients : ils nécessitent un certain temps de chauffage, le rayonnement est nocif pour la santé humaine, le prix élevé, la faible durée de vie des ampoules, ainsi qu'une faible pénétration de la lumière en profondeur pour les échantillons épais (limite pour l'accès aux matériaux composites).

L'emploi d'une source de lumière plus douce, telle que la lumière visible, est très recherché en raison des limitations déjà mentionnées et afin de synthétiser des matériaux dans des conditions qui respectent les normes environnementales et préservent la sécurité humaine. Il s'agit d'un changement significatif dans la manière de traiter les problèmes liés à l'utilisation des sources de lumière UV. Cependant, les conditions d'irradiation douces impliquent des sources d'irradiation différentes.

Par rapport aux sources de lumière à diodes électroluminescentes (LED) modernes, les sources de lumière UV traditionnelles (telles que les lampes à mercure) présentent un certain nombre d'inconvénients, notamment une durée de vie limitée, des temps de fonctionnement lents, des périodes de chauffage parfois longues et une consommation d'énergie élevée. [38] En outre, la qualité de la surface des articles peut être affectée par la chaleur élevée générée par l'éclairage à large bande d'une lampe au mercure. De plus, l'ozone libéré pendant le fonctionnement est dangereux pour la santé. Bien que la polymérisation par UV soit déjà bien établie dans l'industrie, les inconvénients inhérents aux sources de lumière UV constituent un obstacle au développement plus large encore de la photopolymérisation. En raison de leur faible coût et de leur haut niveau de sécurité, les LEDs sont donc de plus en plus utilisées dans la photopolymérisation de nos jours (Schéma 2). [39]

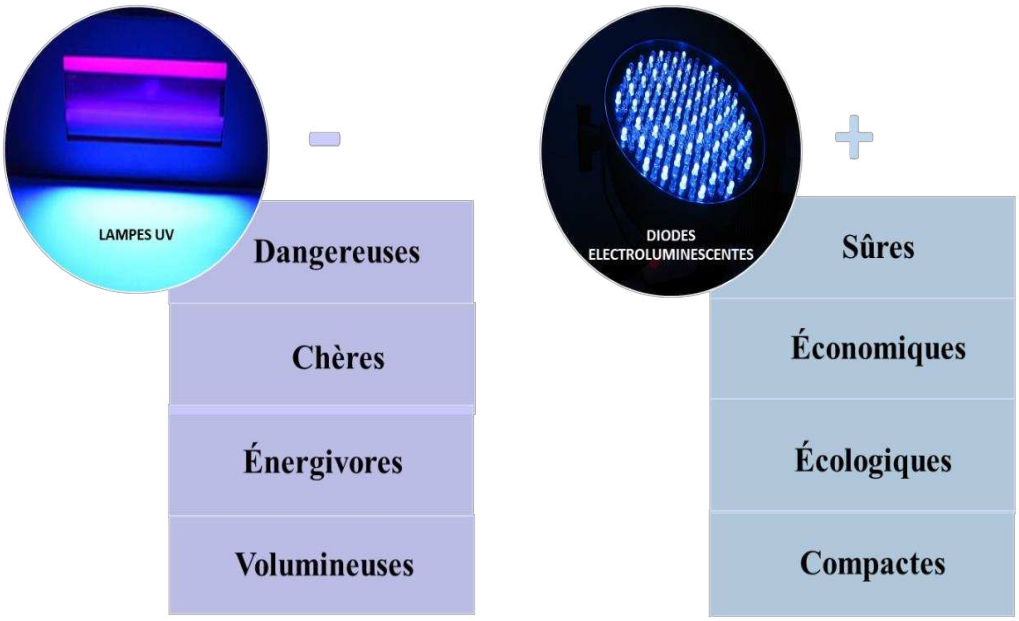

Schéma 2. Comparaison entre les Lampes UV à Vapeur de Mercure (Hg) et les Diodes Électroluminescentes (LEDs).

Les bandes d'émission des LEDs actuelles sont assez étroites (FWHM de l'ordre de 15 nm) et généralement situées à des longueurs d'onde de 365 nm, 395 nm, 405 nm et 455 nm. La plupart des PA commerciaux sont sensibles aux UV et absorbent peu la lumière dont la longueur d'onde est supérieure à 360 nm. Ainsi, la littérature citée pour plusieurs amorceurs commerciaux présente clairement l'impact des bandes d'émission étroites et du décalage des longueurs d'onde. Par conséquent, il est important de développer des PA qui peuvent être activés par la lumière des LED. Le développement de plusieurs PA pour travailler avec les LEDs s'est installé au cours des dix dernières années. Les exemples incluent les PA de Type I et de Type II, les PA à base de colorants, les PA à base de complexes métalliques, les PA à base de polyoxométalates et les PA à base de nanoparticules. Il s'agit de plusieurs efforts vraiment intéressants pour les PA à base de colorants et le remplacement des PA commerciaux de Type I et de Type II. La longueur d'onde d'absorption maximale (λ_{max}) et le coefficient d'absorption molaire (ε) sont d'autres caractéristiques de leurs qualités d'absorption de la lumière.

3. *Objectifs du travail*

Le but de mes recherches est de trouver des systèmes photo-amorceurs toujours plus performants. Pour cela, il est absolument nécessaire de développer de manière continue de nouvelles molécules qui puissent agir comme co-amorceurs (coA) ou photo-amorceurs (PA) dans ces processus de photopolymérisation. Le défi consiste à produire des espèces très réactives en consommant le moins d'énergie possible sous une irradiation modérée (LED, lumière halogène, etc.).

Les systèmes photosensibles développés devront répondre aux exigences suivantes afin de mener à bien ce travail :

- Pour produire des espèces réactives lorsqu'il est exposé à la lumière, le système de photoamorceur doit avoir de fortes capacités d'absorption. Il doit être spécifiquement modifié ou sélectionné pour la source de lumière choisie.
- Le système doit être bien soluble dans le monomère.
- Les sous-produits de la réaction ne doivent pas être toxiques ou le moins possible.
- Un état excité transitoire réactif pour la photodissociation de la molécule.
- Faible coût des réactifs et grande stabilité de stockage.

De plus, cette thèse répond à trois grands enjeux clairs du domaine :

i) La photopolymérisation dans une atmosphère aérée pour éviter les dispositifs d'inertage compliqués et coûteux.

ii) La photopolymérisation dans le domaine visible car la plupart des systèmes actuels fonctionnent dans le domaine UV.

iii) Les applications dans l'impression 3D et la synthèse de composites.

Ces trois enjeux seront abordés successivement dans les différentes parties de la thèse.

II. Structuration du Travail

Le manuscrit de cette thèse est structuré autour de quatre parties principales qui sont décrites brièvement ci-dessous et représentées dans le Schéma 3.

- Dans la **première partie**, un état de l'art est donné, il est divisé en trois chapitres traitant :
  - La Photopolymérisation Radicalaire (FRP).
  - L'impression 3D ou Fabrication additive.
  - Polymérisation Frontale pour l'accès aux composites.

- Dans la **deuxième partie**, deux chapitres seront traités :
  - **Chapitre I** : il est basé sur une large étude concernant les biscarbazoles en tant que photoamorceurs multicomposants et leurs applications dans l'impression 3D ainsi que la synthèse des composites.
  - **Chapitre II** : il traitera des nouveaux co-amorceurs ou additifs de polymérisation considérés comme des alternatives intéressantes aux amines aromatiques toxiques et donc des candidats prometteurs pour le développement de systèmes sans amine.

- Dans la **troisième partie**, des systèmes photoamorceurs (Type I) monocomposants seront présentés :
  - **Chapitre I** : il couvrira une famille de photoamorceurs à base d'oxime-esters. En effet, les oximes-esters ont attiré une grande attention comme photoamorceurs Type I efficaces. Plusieurs études ont été réalisées dans le but de modifier leurs structures chimiques en introduisant différents chromophores et/ou en faisant varier la substitution du groupe ester. Ce travail a contribué à établir une relation structure/réactivité/efficacité intéressante.

- **Chapitre II** : Des esters d'imidazolyl sont exposés dans ce chapitre. Ils sont inédits dans la littérature et peuvent être comparés aux oxime-esters développés précédemment. En effet, le but est de présenter cette nouvelle famille de PA et d'examiner la possibilité qu'ils se comportent comme des PA très efficaces par rapport aux oxime-esters.

➢ La **quatrième partie,** c'est un projet réalisé dans le cadre d'une collaboration industrielle avec BASF à Ludwigshafen (Allemagne). Il portait sur la synthèse de composites par un procédé de polymérisation frontale. Il combine les avantages de la photopolymérisation avec la robustesse de l'amorçage thermique.

L'idée de cette partie est de combiner un photoamorceur avec un amorceur thermique afin d'améliorer la polymérisation en profondeur dans les composites renforcés de fibres. En effet, les procédés de photopolymérisation ne sont pas encore suffisamment appliqués dans le domaine des composites car la pénétration de la lumière dans ces matériaux est très limitée. La stratégie de photopolymérisation frontale sera présentée comme une approche puissante pour la préparation de composites hautement chargés.

Les différentes parties seront présentées comme suit :

i) Chaque chapitre sera basé sur un article en anglais avec un résumé préalable en français.
ii) Les techniques expérimentales et leurs descriptions seront abordées directement dans les chapitres.

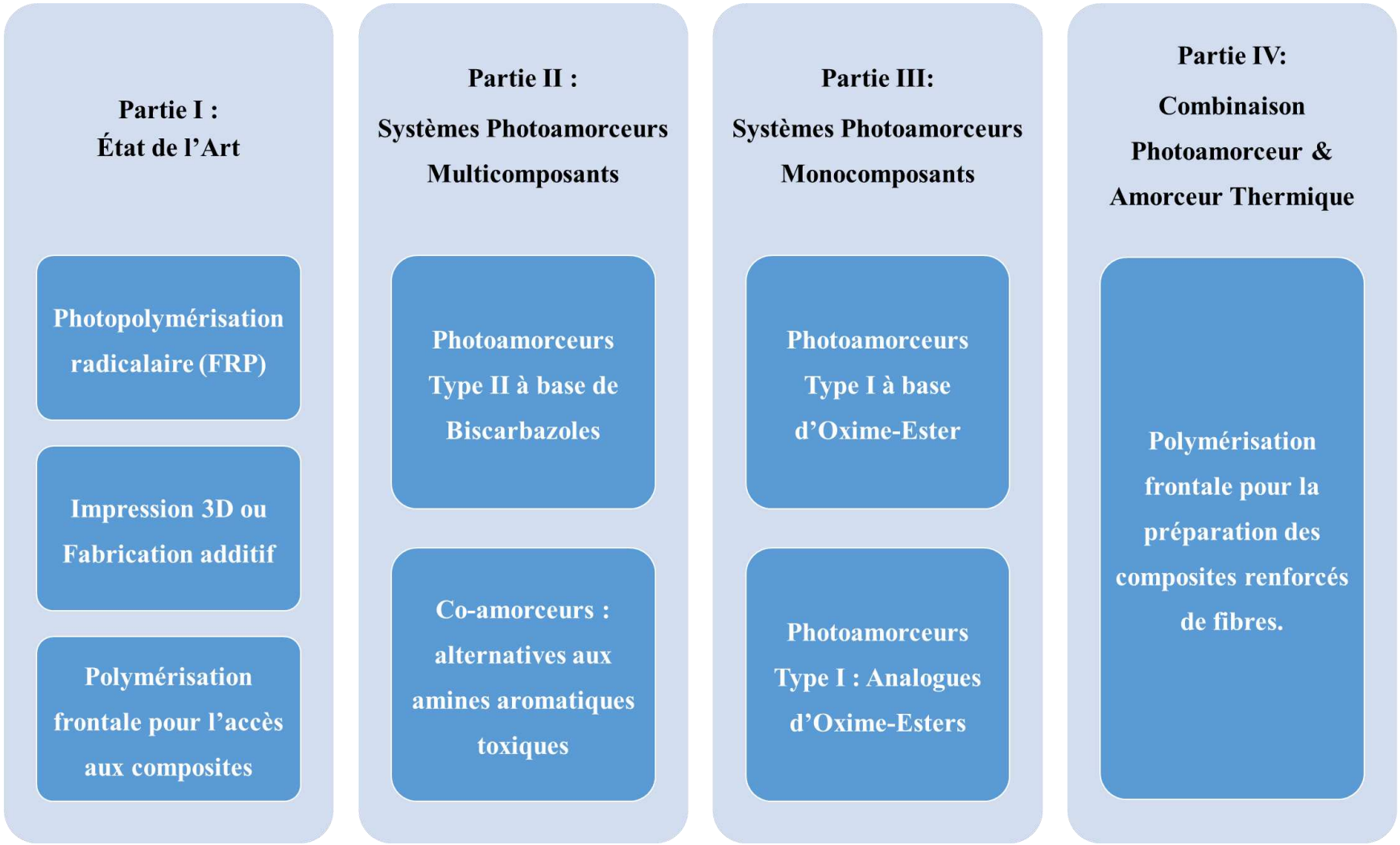

Schéma 3. Plan des quatre parties constituant ce travail de thèse.

III. Valorisation du Travail

Cette thèse a été valorisée par différentes publications dans des journaux internationaux. De plus, les résultats de cette thèse ont été présentés dans des conférences nationales et internationales.

Liste des publications :

11 publications (dont 8 comme premier auteur) dans des journaux internationaux à comité de lecture :

[1] Z. Lee, **F. Hammoud**, A. Hijazi, B. Graff, J. Lalevée, Y.C. Chen, Synthesis and free radical photopolymerization of triphenylamine-based oxime ester photoinitiators, Polymer Chemistry, 2021, 12, 1286-1297.

[2] **F. Hammoud**, M. Rahal, J. Egly, F. Morlet-Savary, A. Hijazi, S. Bellemin-Laponnaz, M. Mauro, J. Lalevée, Cubane Cu4I4(phosphine)4 complexes as new co-initiators for free radical photopolymerization: towards aromatic amine-free systems, Polymer Chemistry, 2021, 12, 2848–2859.

[3] **F. Hammoud**, Z.H. Lee, B. Graff, A. Hijazi, J. Lalevée, Y.C. Chen, Novel phenylamine-based oxime ester photoinitiators for LED-induced free radical, cationic, and hybrid polymerization, Journal of Polymer Science, 2021, 59, 1711–1723.

[4] **F. Hammoud**, N. Giacoletto, G. Noirbent, B. Graff, A. Hijazi, M. Nechab, D. Gigmes, F. Dumur, J. Lalevée, Substituent effects on the photoinitiation ability of coumarin-based oxime-ester photoinitiators for free radical photopolymerization, Materials Chemistry Frontier, 2021, 5, 8361–8370.

[5] **F. Hammoud**, A. Hijazi, S. Duval, J. Lalevée, F Dumur, 5,12-Dihydroindolo[3,2-a]carbazole: A promising scaffold for the design of visible light photoinitiators of polymerization, European Polymer Journal, 2022, 162, 110880.

[6] Z. H. Lee, T. L. Huang, **F. Hammoud**, C.C. Chen, A. Hijazi, B. Graff, J. Lalevée, Y. Chen, Effect of the Steric Hindrance and Branched Substituents on Visible Phenylamine Oxime Ester Photoinitiators: Photopolymerization Kinetics Investigation through Photo-DSC Experiments. Photochemistry and Photobiology, 2021.

[7] **F. Hammoud**, N. Giacoletto, M. Nechab, B. Graff, A. Hijazi, F. Dumur and J. Lalevée, 5,12-Dialkyl-5,12-dihydroindolo[3,2-a]carbazole-based oxime-esters for LED photoinitiating systems and application on 3D printing, Macromolecular Materials and Engineering, 2022.

[8] **F. Hammoud**, A. Hijazi, M. Ibrahim-Ouali, J. Lalevée and F. Dumur, Chemical engineering around the 5,12-dihydroindolo[3,2-a]carbazole scaffold: Fine tuning of the optical properties of visible light photoinitiators of polymerization, European Polymer Journal, 2022.

[9] **F. Hammoud**, A. Pavlou, A. Petropoulos, B. Graff, M.G. Siskos, A. Hijazi, F. Morlet-Savary, F. Dumur, J. Lalevée, Naphthoquinone-based imidazolyl esters as blue-light-sensitive Type I photoinitiators, Polymer Chemistry, 2022, 13, 4817-4831.

[10] Z.H. Lee, S.C. Yen, **F. Hammoud**, A. Hijazi, B. Graff, J. Lalevée, YC Chen, Naphthalene-Based Oxime Esters as Type I Photoinitiators for Free Radical Photopolymerization, Polymers, 2022, 14, 5261.

[11] **F. Hammoud**, A. Hijazi, M. Schmitt, F. Dumur, J. Lalevée, A Review on Recently Proposed Oxime Ester Photoinitiators, European Polymer Journal, 2023, 111901, 0014-3057.

Participation aux conférences :

Congrès nationaux

[1] **F. Hammoud**, M. Rahal, J. Egly, F. Morlet-Savary, A. Hijazi, S. Bellemin-Laponnaz, M. Mauro, J. Lalevée, Les Cubanes comme Nouveaux Co-amorceurs pour la Photopolymérisation Radicalaire : Vers des Systèmes sans Amine Toxiques, 17ème Journée Scientifique - GFP section Grand-Est.

[2] **F. Hammoud**, N. Giacoletto, M. Nechab, B. Graff, A. Hijazi, F. Dumur and J. Lalevée, 5,12-Dialkyl-5,12-dihydroindolo[3,2-a]carbazole-based oxime-esters for LED photoinitiating systems and application on 3D printing, 1ères Journées Scientifiques SCF-GFP Grand-Est, Besançon 05-07 Juillet 2022.

Congrès internationaux

[1] **F. Hammoud**, A. Hijazi, M. Schmitt, F. Dumur, J. Lalevée, Recently Proposed Oxime-Ester as Blue- Light-Sensitive Type I Photoinitiators, APME2023, April 2023.

Références

[1] J. P. Fouassier, Photoinitiation, Photopolymerization, and Photocuring: Fundamentals and Applications, Hanser Publishers, New York, 1995.

[2] P. Garra, C. Dietlin, F. Morlet-Savary, F. Dumur, D. Gigmes, J.P. Fouassier, J. Lalevée, Photopolymerization processes of thick films and in shadow areas: a review for the access to composites, Polymer Chemistry, 2017, 8.46, 7088-7101.

[3] J. P. Fouassier, J. Lalevée, Photoinitiators: Structures, Reactivity and Applications in Polymerization, Wiley, Weinhein, 2021.

[4] Y. Yagci, S. Jockusch, N. J. Turro, Photoinitiated polymerization: advances, challenges, and opportunities, Macromolecules, 2010, 43, 6245-6260.

[5] F. Karasu, C. Croutxé-Barghon, X. Allonas, D. V. Van, G. J. Leendert, Free radical photopolymerization initiated by UV and LED: Towards UV stabilized, tack free coating, Journal of Polymer Science Part A: Polymer Chemistry, 2015, 52.24, 3597-607.

[6] Y. Yagci, S. Jockusch, N. J. Turro, Photoinitiated polymerization: advances, challenges, and opportunities, Macromolecules, 2010, 43, 6245-6260.

[7] K. Dietliker, T. Jung, J. Benkhoff, H. Kura, A. Matsumoto, H. Oka, D. Hristova, G. Gescheidt, G. Rist, New developments in photoinitiators, Macromolecular Symposia. Weinheim : WILEY-VCH Verlag, 2004, 217.1, 77-98.

[8] J. Lalevée, J. P. Fouassier, Dye Photosensitized Polymerization Reactions: Novel Perspectives, RSC Photochemistry Reports, Ed. A. Albini, E. Fasani, Photochemistry, London, UK, 2015, 42, 215–232.

[9] A. Kowalska, J. Sokolowski, K. Bociong, The photoinitiators used in resin based dental composite—a review and future perspectives, Polymers, 2021, 13.3, 470.

[10] J. Shao, Y. Huang, Q. Fan, Visible light initiating systems for photopolymerization: status, development and challenges, Polymer Chemistry, 2014, 5.14, 4195-4210.

[11] K. Sun, P. Xiao, F. Dumur, J. Lalevée, Organic dye-based photoinitiating systems for visible-light-induced photopolymerization, Journal of Polymer Science, 2021, 59.13, 1338-1389.

[12] N. Corrigan, J. Yeow, P. Judzewitsch, J. Xu, C. Boyer, Seeing the light: advancing materials chemistry through photopolymerization, Angewandte Chemie International Edition, 2019, 58.16, 5170-5189.

[13] J. W. Stansbury, Curing dental resins and composites by photopolymerization, Journal of esthetic and restorative dentistry, 2000, 12.6, 300-308.

[14] K. D. Jandt, R. W. Mills, A brief history of LED photopolymerization, Dental Materials, 2013, 29.6, 605-617.

[15] M. A. Tehfe, F. Louradour, J. Lalevée, J. P. Fouassier, Photopolymerization reactions: On the way to a green and sustainable chemistry, Applied Sciences, 2013, 3.2, 490-514.

[16] M. Kaur, A. K. Srivastava, Photopolymerization: A review, Journal of Macromolecular Science, Part C: Polymer Reviews, 2002, 42.4, 481-512.

[17] D. Zhou, Y. Ito, Visible light-curable polymers for biomedical applications, Science China Chemistry, 2014, 57, 510-521.

[18] F. Dumur, Recent advances on visible light Thiophene-based photoinitiators of polymerization, European Polymer Journal, 2022, 111120.

[19] S. Zakeri, M. Vippola, E. Levänen, A comprehensive review of the photopolymerization of ceramic resins used in stereolithography, Additive Manufacturing, 2020, 35, 101177.

[20] A. Bagheri, J. Jin, Photopolymerization in 3D Printing, ACS Applied Polymer Materials, 2019, 1, 593–611.

[21] M. Layani, X. Wang, S. Magdassi, Novel materials for 3D printing by photopolymerization, Advanced Materials, 2018, 30.41, 1706344.

[22] P. Fiedor, M. Pilch, P. Szymaszek, A. Chachaj-Brekiesz, M. Galek, J. Ortyl, Photochemical study of a new bimolecular photoinitiating system for vat photopolymerization 3D printing techniques under visible light, Catalysts, 2020, 10.3, 284.

[23] Y. Bao, Recent Trends in Advanced Photoinitiators for Vat Photopolymerization 3D Printing, Macromolecular Rapid Communications, 2022, 43.14, 2200202.

[24] V. Narayanan, A. B. Scranton, Photopolymerization of composites, Trends in polymer science, 1997, 12.5, 415-419.

[25] A. Al Rashid, W. Ahmed, M. Y. Khalid, M. Koc, Vat photopolymerization of polymers and polymer composites: Processes and applications, Additive Manufacturing, 2021, 47, 102279.

[26] A. Knezevic, M. Ristic, N. Demoli, Z. Tarle, S. Music, V. N. Mandic, Composite photopolymerization with diode laser, Operative dentistry, 2007, 32.3, 279-284.

[27] T. Dikova, J. Maximov, V. Todorov, G. Georgiev, V. Panov, Optimization of photopolymerization process of dental composites, Processes, 2021, 9.5, 779.

[28] M. Atai, D. C. Watts, A new kinetic model for the photopolymerization shrinkage-strain of dental composites and resin-monomers, Dental Materials, 2006, 22.8, 785-791.

[29] Y. Zhang, L. Josien, J. P. Salomon, A. Simon-Masseron, J. Lalevée, Photopolymerization of zeolite/polymer-based composites: toward 3D and 4D printing applications, ACS Applied Polymer Materials, 2020, 3.1, 400-409.

[30] K. Ikemura, T. Endo, A review of the development of radical photopolymerization initiators used for designing light-curing dental adhesives and resin composites, Dental Materials Journal, 2010, 29.5, 481-501.

[31] I. Gibson, D. W. Rosen, B. Stucker, Photopolymerization processes, Additive Manufacturing Technologies: Rapid Prototyping to Direct Digital Manufacturing, 2010, 78-119.

[32] I. Chiulan, E. B. Heggset, S. I. Voicu, G. Chinga-Carrasco, Photopolymerization of bio-based polymers in a biomedical engineering perspective, Biomacromolecules, 2021, 22.5, 1795-181.

[33] E. I. Paruli, O. Soppera, K. Haupt, C. Gonzato, Photopolymerization and photostructuring of molecularly imprinted polymers, ACS Applied Polymer Materials, 2021, 3.10, 4769-4790.

[34] E. Andrzejewska, Free radical photopolymerization of multifunctional monomers. In Three-Dimensional Microfabrication Using Two-Photon Polymerization, 2016, William Andrew Publishing, 62-81.

[35] C. Dietlin, S. Schweizer, P. Xiao, J. Zhang, F. Morlet-Savary, B. Graff, J. P Fouassier, J. Lalevée, Photopolymerization upon LEDs: new photoinitiating systems and strategies, Polymer Chemistry, 2015, 6.21, 3895-3912.

[36] F. Karasu, C. Croutxé-Barghorn, X. Allonas, L. G. Van Der Ven, Free radical photopolymerization initiated by UV and LED: towards UV stabilized, tack free coatings, Journal of Polymer Science Part A: Polymer Chemistry, 2014, 52.24, 3597-3607.

[37] E. Hola, P. Fiedor, A. Dzienia, J. Ortyl, Visible-light amine thioxanthone derivatives as photoredox catalysts for photopolymerization processes, ACS Applied Polymer Materials, 2021, 3.11, 5547-5558.

[38] M. Lecompere, X. Allonas, D. Marechal, A. Criqui, Dual-cure Photo-thermal Initiating System for Cationic Polymerization of Epoxy under LED Visible Light, Journal of Photopolymer Science and Technology, 2017, 30.4, 399-404.

Cette Thèse est composée de Quatre Parties Principales :

Partie I : État de l'Art

Partie II : Systèmes Photoamorceurs Multicomposants

Partie III : Systèmes Photoamorceurs Monocomposants

Partie IV : Combinaison : Photoamorceur & Amorceur Thermique

Partie I : État de l'Art

TABLE DES MATIÈRES

Table des matières

TABLE DES MATIÈRES

Chapitre I : Photopolymérisation Radicalaire (FRP)

Le procédé de photopolymérisation radicalaire (FRP) reste le plus polyvalent parmi les types courants de photopolymérisation. Il offre le plus grand choix de monomères et un grand nombre de systèmes de photoamorceurs éventuels. [1-2] En outre, la photopolymérisation radicalaire offre plusieurs avantages par rapport aux autres méthodes de synthèse, tels que : la rapidité du processus, l'insensibilité à l'humidité, les propriétés intéressantes du polymère final et bien d'autres caractéristiques. En raison de ces avantages, de nombreux secteurs industriels modernes sont intéressés par l'utilisation de ce procédé : dentisterie, revêtements, encres, peintures, adhésifs, holographie, impression 3D, et bien d'autres domaines. [3-5]

1. Mécanismes réactionnels

Le principe de photopolymérisation radicalaire est la transformation d'une résine liquide en un polymère solide lorsqu'elle est exposée à la lumière. De manière générale, ces procédés sont applicables aux monomères contenant des insaturations, comme les acrylates, les méthacrylates ou les polyesters insaturés. Un photoamorceur, ou un système de photoamorceur, qui est un système chimique capable de créer des radicaux libres sous l'influence de la lumière, est dissout dans un monomère dans une photopolymérisation radicalaire. [6-8] Dans ces conditions, le procédé de photopolymérisation radicalaire se déroule de la même manière qu'une polymérisation radicalaire thermique classique, à l'exception de la première étape, qui est différente [8] (Schéma 1).

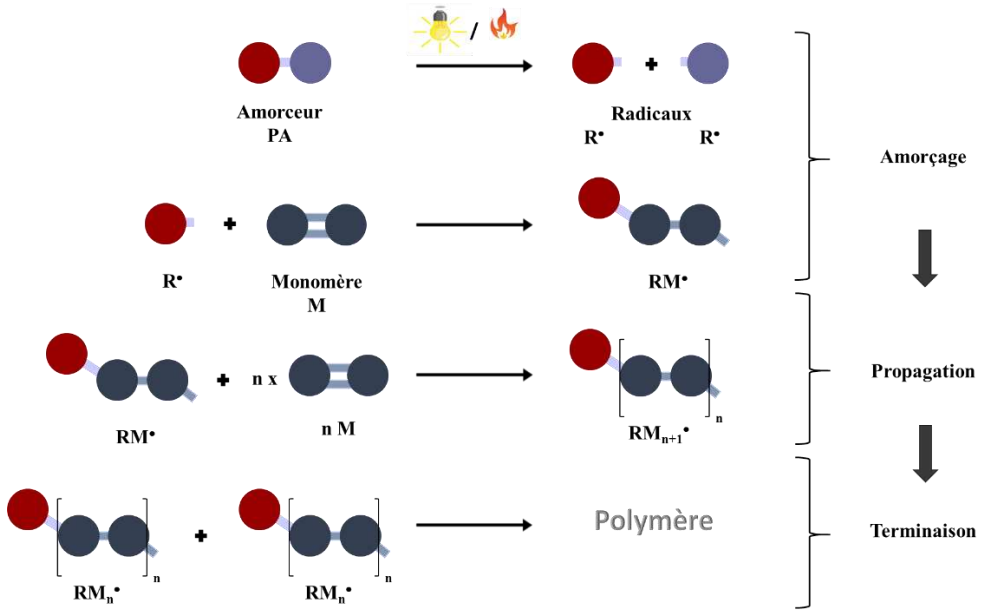

Schéma 1. Étapes de la polymérisation radicalaire.

La présence d'oxygène (O_2) dans l'atmosphère est le principal obstacle à cette forme de polymérisation. La désactivation des états excités du photoamorceur et des radicaux amorceurs ou propageants est, en effet, provoquée par l'oxygène. En fait, la présence d'O_2 ralentit ou, dans certaines situations, arrête même la réaction de polymérisation. L'inhibition par l'oxygène est le terme qui désigne ce phénomène. Il constitue un obstacle important à la photopolymérisation. [9]

L'amorçage, la propagation et la terminaison sont les trois étapes essentielles du processus de création d'un polymère par voie photochimique et ceci en présence d'un photoamorceur (Schéma 1).

1.1. Photoamorçage

Un processus de photoamorçage doit passer par deux étapes afin d'amorcer une réaction de polymérisation :

a) Production des radicaux primaires :

Le photoamorceur absorbe l'énergie lumineuse lors de son exposition aux rayons UV ou visibles, passant ensuite à un état électronique excité (singulet ou triplet). Les radicaux libres (primaires) $R^{\bullet}$ peuvent être produits lorsqu'une liaison chimique dans une molécule excitée est coupée de manière homolytique (photoamorceur de Type I), ou lorsqu'un électron ou un proton est transféré (photoamorceur de Type II). L'étude de ces deux types de photoamorceurs sera détaillée par la suite. [10-12]

$PA \rightarrow PA^{*} \rightarrow R^{\bullet}$ (Type I)

$PA \rightarrow PA^{*}$ + coamorceur $\rightarrow R^{\bullet}$ (Type II)

b) L'amorçage :

Les radicaux primaires formés réagissent ensuite de manière efficace avec le monomère (M) pour former un radical alkyle ($RM^{\bullet}$) qui peut ensuite propager la réaction de polymérisation en chaîne. [10-12]

1.2. Propagation

C'est l'étape principale de la polymérisation radicalaire. Le radical RM• produit lors de l'étape d'amorçage attaque la double liaison d'un autre monomère pour créer un macroradical. Ainsi, un très grand nombre de molécules de monomères sont successivement ajoutées.

Ce phénomène entraîne une réaction en chaîne. Le démarrage de cette réaction est rapide mais se ralentit lorsque la proportion de monomères diminue et que la viscosité du milieu augmente. [10-12]

1.3. Terminaison

La dernière étape consiste à une étape de terminaison. Les macroradicaux crées réagissent ensemble et mettent fin à la croissance des chaînes de polymère. Cette réaction se fait essentiellement par voie bimoléculaire (recombinaison ou dismutation).

a) Recombinaison :

Cette réaction se distingue par la formation d'une liaison covalente par la recombinaison de deux macroradicaux, qui donne lieu à une chaîne plus longue.

$RM_m^{\bullet} + RM_n^{\bullet} \rightarrow RM_{(n+m)}$

b) Dismutation :

Au cours de cette terminaison, un atome d'hydrogène est transféré d'une macromolécule à une autre, ce qui entraîne la formation de deux chaînes polymères, dont l'une a une extrémité saturée et l'autre une extrémité insaturée.

$RM_m^{\bullet} + RM_n^{\bullet} \rightarrow RM_{n(-H)} + RM_{m(+H)}$

Un autre mode de terminaison peut également conduire à la disparition du centre actif : la terminaison monomoléculaire. Ce mode aura lieu lorsque le milieu réactionnel devient très visqueux, la diffusion du monomère vers les radicaux actifs ne sera plus possible. Ainsi, les chaînes polymères en croissance sont piégées dans la matrice polymère. [10-12]

2. Aspect cinétique

La cinétique d'une réaction de polymérisation est décrite simplement par les étapes d'amorçage, de propagation et de terminaison (ces étapes ont déjà été décrites en détail dans la partie précédente) (Tableau 1).

Tableau 1. Cinétique de la réaction de polymérisation radicalaire. [13]

Étape	Réaction	Vitesse associée
Amorçage	$A \rightarrow 2R^{\bullet}$	$v_d = 2.\ k_d.\ [A]$
	$R^{\bullet} + M \rightarrow RM^{\bullet}$	$v_a = k_a\ [R^{\bullet}][M]$
	$(v_a)_{globale} = f\ v_d = 2.\ f.\ k_d\ [A]$ où f est l'efficacité de l'amorceur	
Propagation	$RM_n^{\bullet} + M \rightarrow RM^{\bullet}_{n+1}$	$v_p = -\ d[M]/dt = k_p\ [RM^{\bullet}][M]$
	Temps de demi réaction de polymérisation : $t_{1/2} = \ln(2)/k_p[RM^{\bullet}_n]$	
Terminaison	Recombinaison : $RM_m^{\bullet} + RM_n^{\bullet} \rightarrow RM_{(n+m)}$	$v_t = k_t\ [RM^{\bullet}_n]^2$
	Dismutation : $RM_m^{\bullet} + RM_n^{\bullet} \rightarrow RM_{n(-H)} + RM_{m(+H)}$	

A est l'amorceur qui se décompose en un composé **R** ; **M** est le monomère.

$\mathbf{k_d}$ est la constante de dissociation de [A].

$\mathbf{k_a}$ est la constante d'amorçage.

$\mathbf{v_d}$ est la vitesse de dissociation.

$\mathbf{k_p}$ est la constante de propagation.

$\mathbf{k_t}$ est la constante de terminaison.

3. Systèmes photoamorceurs

En exposant la formulation à un rayonnement lumineux, une molécule excitée créera des espèces actives qui amorceront le processus de polymérisation. Il est donc nécessaire d'utiliser des matériaux photosensibles capables d'absorber la lumière et de former des espèces réactives (radicaux, cations et anions), qui déclencheront ensuite la réaction de polymérisation. En effet, la majorité des monomères sont incapables d'absorber les radiations lumineuses émises par les sources UV conventionnelles (300-400 nm). [15-18]

L'efficacité de ces substances, appelées photoamorceurs (PA), dépend de trois facteurs :
1) la quantité de lumière qui est absorbée par le système photosensible ;
2) la quantité d'espèces excitées qui produisent des espèces actives (radicaux, cations, etc.) ;
3) la quantité d'espèces actives qui réussissent à former de nouvelles chaînes polymères. [17]

La réaction en chaîne, une fois lancée, peut se poursuivre comme une polymérisation classique (Schéma 2). Le photoamorceur est ajouté à une résine polymérisable avant l'exposition à la lumière. Généralement, un oligomère multifonctionnel utilisé pour créer cette résine est réticulé pour former un réseau polymère 3D. De plus, une variété d'additifs peut être appliquée au matériau pour améliorer ses qualités finales. [19-20]

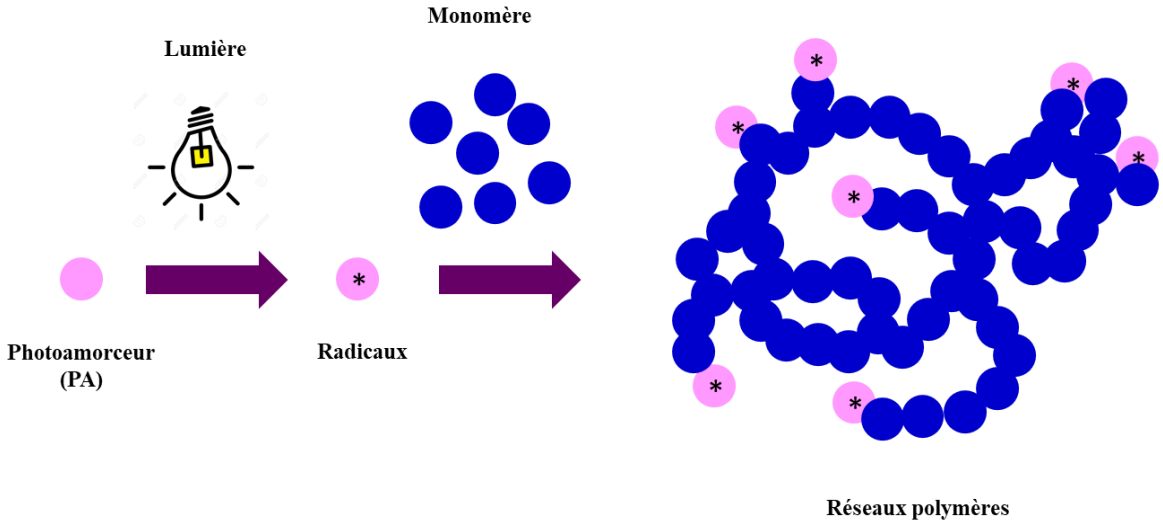

Schéma 2. Représentation schématique du processus de photopolymérisation.

Le choix du photoamorceur est crucial dans le processus de polymérisation induite par la lumière puisque la vitesse de la réaction est directement contrôlée par le photoamorceur, qui est souvent le composant clé de la réaction de polymérisation.

Pour être efficace, un photoamorceur approprié doit répondre à un certain nombre de critères. Il doit présenter les propriétés suivantes : une forte absorption dans le domaine d'émission de la source lumineuse, une courte durée de vie de l'état excité réactif pour éviter les réactions secondaires avec d'autres molécules, un rendement quantique élevé pour la formation de radicaux, et une réactivité élevée des radicaux formés par rapport au monomère (amorçage). Selon la façon dont il répond à ces différentes exigences, un changement de photoamorceur peut aboutir à des résultats plus ou moins intéressants. [21-23]

Une fois excité, le photoamorceur passe à un niveau d'énergie supérieur, dans lequel il pourra agir comme catalyseur de différentes réactions photochimiques et moléculaires (état excité singulet ou triplet : S_1 ou T_1). Généralement, un diagramme de Perrin-Jablonski (Schéma 3), propre à chaque molécule, est utilisé pour expliquer ces processus. [24]

Tout d'abord, le schéma 3 montre les transitions entre les niveaux électroniques qui correspondent à une molécule spécifique. Il existe en fait deux catégories de transitions :

1) les transitions radiatives, dans lesquelles des photons sont émis spontanément d'un niveau d'énergie électronique à un autre qui est plus bas en énergie.

2) les transitions non radiatives, qui ont lieu entre des états d'énergie électroniques, soit entre des états vibrationnels, mais qui ne génèrent pas de photons.

En fait, deux modes de désactivation concurrents sont à l'origine des changements radiatifs :

i) cette phase de désactivation fait passer de S_1 à S_0 par émission (Fluorescence)
ii) le passage de S_1 à T_1 puis le retour à S_0 (Phosphorescence).

La durée de l'émission après excitation, qui est de l'ordre de la nanoseconde pour la fluorescence et de la microseconde pour la phosphorescence, distingue ces deux types de luminescence. [25]

Les relaxations non radiatives peuvent se produire soit par une conversion interne, qui entraîne une transition de l'état S_1 à l'état S_0 sans émission de photons, soit par un croisement intersystème, qui se produit après la transition d'un état S_1 à T_1, suivi d'une transition électronique de l'état T_1 à l'état S_0 sans émission de lumière. Ces processus de relaxation non radiatifs entraînent une relaxation thermique. [26-27]

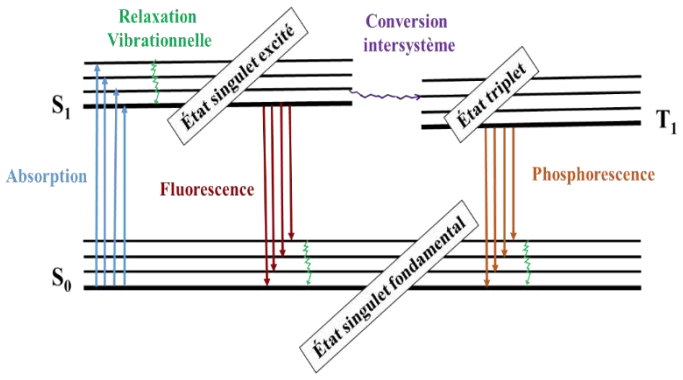

Schéma 3. Diagramme de Perrin-Jablonski.

Outre les processus photophysiques susmentionnés, qui n'entraînent aucune modification chimique de la molécule concernée, des processus photochimiques peuvent également se produire à partir des états excités S_1 ou T_1. A noter que ces processus sont à l'origine de la production d'espèces réactives (radicaux ou ions) capables d'amorcer les processus de photopolymérisation. [27]

En effet, selon le mécanisme de photogénération des radicaux libres primaires, les photoamorceurs sont principalement classés en deux grandes catégories : les photoamorceurs de Type I ou de Type II. Il s'agit d'un photoamorceur de Type I lorsque le PA peut générer des radicaux par lui-même, et d'un PA de Type II lorsqu'un co-amorceur (donneur d'hydrogène) est inclus. Il existe donc deux approches pour obtenir les radicaux :

a) Par clivage homolytique pour le Type I. Ce mode permet la formation directe de deux radicaux.

$$PA \rightarrow {}^1PA \text{ et/ou } {}^1PA \rightarrow {}^3PA \ (h\nu)$$

$$^3PA \rightarrow R_1^{\bullet} + R_2^{\bullet}$$

Des conditions préalables à un clivage homolytique doivent être respectées :

- La molécule doit comporter une liaison à faible énergie de dissociation (Bond Dissociation Energy : BDE). Mais cette liaison ne doit pas avoir une énergie de dissociation trop faible, au risque de provoquer une décomposition thermique de la molécule et de la rendre instable.
- L'énergie de la liaison engagée dans le processus de dissociation doit être inférieure ou égale à l'énergie de l'état excité de la molécule.
- L'énergie d'activation la plus faible possible E_a ($J.mol^{-1}$) est requise pour la coupure.

b) Type II : par le transfert d'hydrogène. Il existe deux façons de réaliser ce mode :

- Soit en arrachant l'hydrogène sur un donneur (D-H) vers le photoamorceur (PA) :

$$^3PA \rightarrow DH \rightarrow PA\text{-}H^{\bullet} + D^{\bullet}$$

- Soit par un transfert d'électron suivi d'un proton du donneur (D-H) vers le PA :

$$^3PA + De\text{-}H \rightarrow [PA^{\bullet -} \ldots De\text{-}H^{\bullet +}] \rightarrow PA\text{-}H^{\bullet} + De^{\bullet}$$

Bien que les mécanismes réactionnels soient différents, ces deux réactions produisent le même résultat. Les éthers aliphatiques (hydrogène en alpha de l'oxygène), les amines aliphatiques tertiaires (hydrogène en alpha de l'azote), les thiols et les silanes dont l'hydrogène est directement lié au silicium ou au soufre, respectivement, sont souvent les donneurs d'hydrogène les plus réactifs. [28-30]

3.1.Photoamorceurs de Type I

Les photoamorceurs de Type I sont souvent constitués d'un groupement benzoyle. Ce chromophore peut subir un clivage homolytique à partir de l'état excité après absorption de la lumière (souvent l'état triplet). Ce clivage peut se produire :

- en position α par rapport au groupe carbonyle : appelé aussi clivage de type Norrish I, il aboutit à la production de deux radicaux libres (Schéma 4). Un radical benzoyle est l'un des deux radicaux produits par ce clivage. En utilisant des monomères acryliques comme point de départ, celui-ci présente une excellente réactivité en polymérisation radicalaire. Des radicaux supplémentaires créés lors de la coupure du PA peuvent aussi potentiellement démarrer le processus de polymérisation. [30]

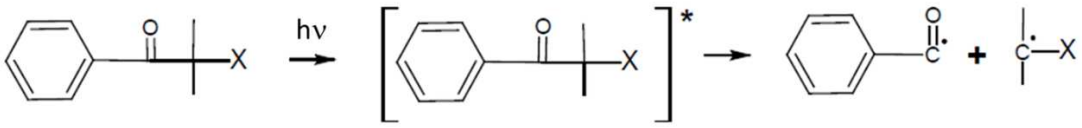

Schéma 4. Coupure en α d'un photoamorceur de Type I.

- en position β par rapport au groupe carbonyle (Schéma 5), principalement pour les liaisons C-X où X=halogène.

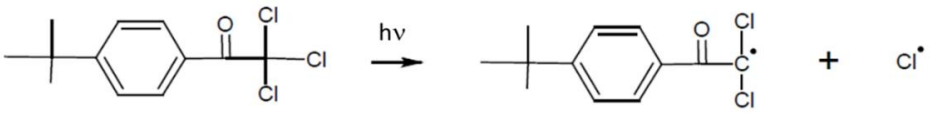

Schéma 5. Coupure en β de la 2,2,2 trichloro tert-butylacétophénone (TAP).

Les PA de Type I existent en plusieurs variétés, dont certains exemples sont illustrés dans la Figure 1.

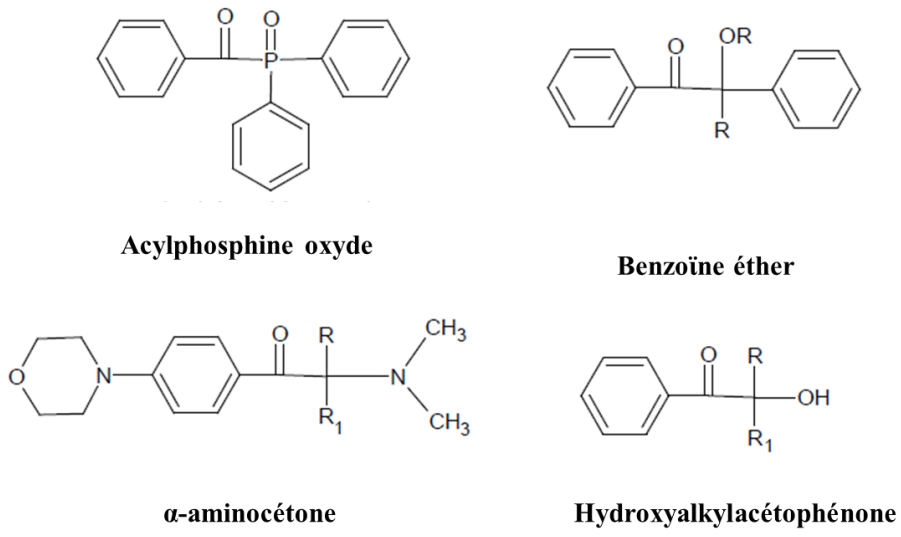

Figure 1. Exemples de photoamorceurs de Type I.

3.2. Photoamorceurs de Type II

Un photoamorceur de Type II est une molécule qui nécessite l'ajout d'un coamorceur afin de générer des radicaux libres après avoir été exposé à la lumière (Schéma 6). Ce dernier sera constitué de :

- Un donneur d'électrons qui, après un transfert de proton (De-H), produit deux radicaux ; ces donneurs peuvent être des amines, des thiols ou des silanes (Figure 2).
- Un donneur d'hydrogène pur (DH), comme les alcools ou les éthers.

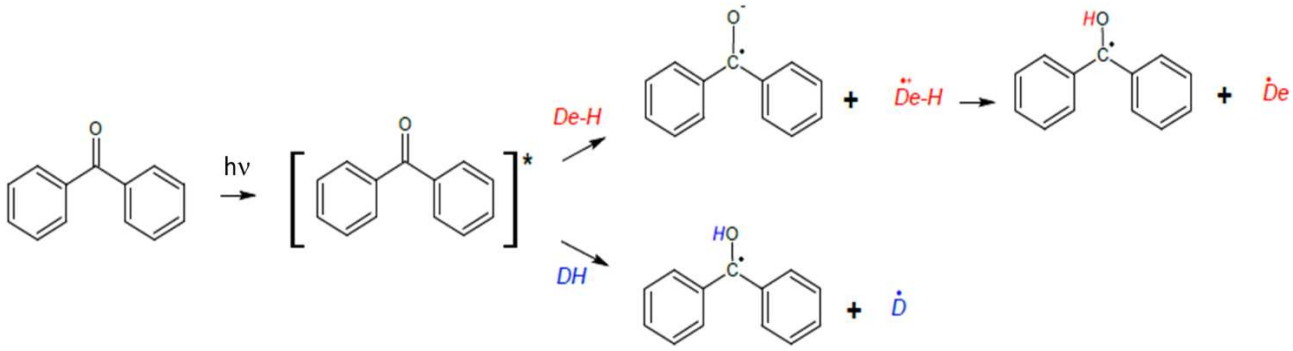

Schéma 6. Formation de radicaux à partir d'un photoamorceur de Type II : cas de la benzophénone.

Ainsi, dans le Schéma 6, De• ou D•, le radical provenant de la source d'hydrogène est celui qui amorce la polymérisation. Le radical cétyle stable (BPH•) participe à la réaction de terminaison en réagissant avec les macroradicaux en croissance. Certains PA de Type II, comme l'isopropylthioxanthone (ITX) ou la camphorquinone (CQ), sont fréquemment utilisés dans les formulations de revêtements photoréticulables pour les surfaces protectrices (Figure 2). Comme co-initiateur, une amine aromatique comme l'éthyldiméthylaminobenzoate (EDB) est généralement utilisée avec ces photoinitiateurs (Figure 3). Les amines présentent cependant un certain nombre d'inconvénients, comme le fait qu'elles provoquent fréquemment une dégradation du substrat et sont mutagènes. La Figure 2 présente quelques exemples de formations de PA de Type II. [29-30]

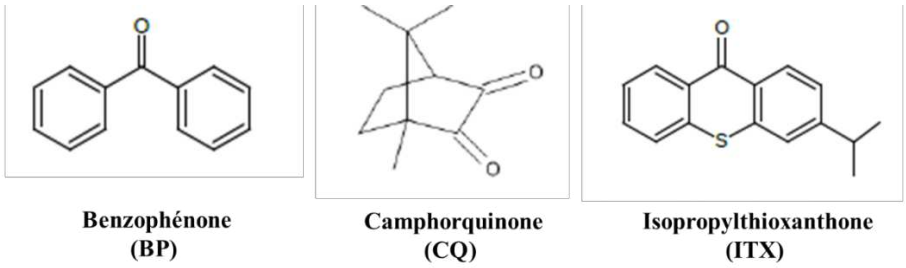

Benzophénone (BP) | **Camphorquinone (CQ)** | **Isopropylthioxanthone (ITX)**

Figure 2. Exemples de photoamorceurs de Type II.

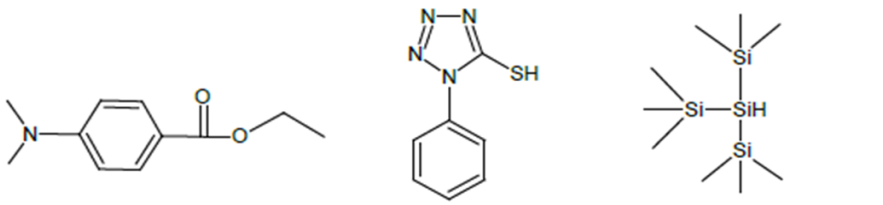

Éthyldiméthylaminobenzoate (EDB) | **Phényltétrazole thiol** | **Tris(triméthylsilyl)silane (TTMSS)**

Figure 3. Structures de co-amorceurs.

Du fait de la rareté des photoamorceurs sensibles à la lumière visible, l'objectif principal de cette thèse est basé sur la nécessité de développer de nouveaux photoamorceurs avec d'excellentes propriétés d'absorption dans la région visible, afin d'amorcer les processus de polymérisation radicalaire induits par des dispositifs d'irradiation douce dans le visible. De nombreux exemples de colorants ont été synthétisés et développés dans notre laboratoire ; ils seront étudiés en détail dans la suite de ce manuscrit.

4. Limitations de la Photopolymérisation Radicalaire (FRP)

Le procédé de photopolymérisation radicalaire présente un certain nombre de désavantages qui affectent les caractéristiques finales des matériaux produits.

4.1. Inhibition par l'oxygène

La molécule de dioxygène, en tant que biradical, possède deux électrons célibataires situés dans des orbitales moléculaires dégénérées. Le dioxygène peut contenir des spins parallèles ou antiparallèles dans ces orbitales moléculaires, tout comme les autres biradicaux. La Figure 4 montre les diagrammes d'orbitales moléculaires de l'oxygène dans son état fondamental (triplet) et dans son premier état excité (singulet). [31-33]

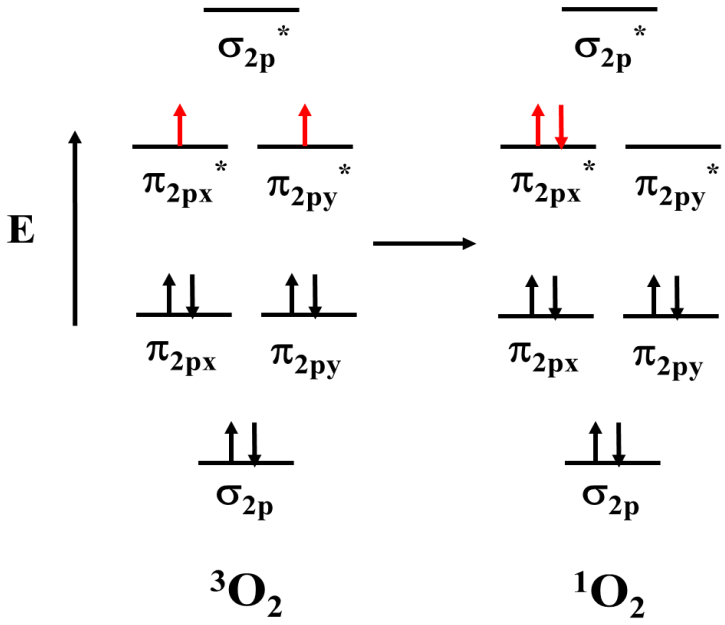

Figure 4. Diagrammes des orbitales moléculaires de l'oxygène dans son état fondamental ($^3O_2$) et dans son premier état excité ($^1O_2$). [34]

Le dioxygène triplet est un inhibiteur puissant de la polymérisation. En effet, il se combine facilement avec les radicaux produits lors de la polymérisation pour créer des radicaux peroxyles ROO• stables. Ce phénomène arrête la propagation de la réaction.

La délocalisation de l'électron non apparié autour de la liaison O-O est à l'origine de la stabilité de ces radicaux peroxyles. [32] De plus, l'oxygène (O_2) désactive les états excités.

Cette inhibition a des effets négatifs sur la polymérisation. En fait, la présence de radicaux peroxyles ralentit à la fois le rythme de la polymérisation et la conversion finale, la polymérisation ne commençant que lorsque la plus grande partie de l'oxygène dissous a été consommée. L'inhibition entraîne une mauvaise réticulation à la surface du polymère qui devient collant. Ceci a une influence négative significative sur les caractéristiques mécaniques finales. En raison de la faible épaisseur des échantillons et de la prédominance fréquente de la surface du polymère, cette faible réticulation est particulièrement défavorable dans le cas de la photopolymérisation.

De nombreuses stratégies peuvent être utilisées pour surmonter cet obstacle. Tout d'abord, le dioxygène présent peut être éliminé en effectuant la polymérisation dans un environnement inerte tel que le diazote. Il est toutefois difficile d'utiliser cette méthode dans le cadre d'une photopolymérisation industrielle. Une autre méthode pour empêcher le dioxygène de pénétrer dans le milieu réactionnel consiste à utiliser une barrière physique. En outre, la polymérisation en laminé est une méthode plus pratique que l'inertage. Pour produire plus de radicaux et accélérer la polymérisation, la longueur d'onde, l'intensité de la source lumineuse et la concentration du photoamorceur peuvent être ajustées. En fait, comme le dioxygène dans le milieu environnant a moins de temps pour diffuser dans le milieu lorsque la polymérisation est achevée rapidement, le dioxygène est moins susceptible de réagir avec les radicaux. La viscosité ne doit pas être négligée en tant qu'élément permettant d'éviter que le processus de polymérisation ne soit entravé par le dioxygène. En fait, la réoxygénation se produit beaucoup plus rapidement dans les échantillons à faible viscosité que dans les échantillons épais. L'utilisation de monomères à haute fonctionnalité est une autre stratégie potentielle pour surmonter cette restriction. En dernier lieu, des molécules peuvent être utilisées pour capturer le dioxygène dissous ou pour convertir le dioxygène triplet en dioxygène singulet.

4.2. Difficulté de pénétration de la lumière

Comme déjà évoqué, pour créer des radicaux et amorcer la photopolymérisation, un amorceur doit être excité par une source lumineuse. Cependant, la lumière a souvent du mal à pénétrer profondément dans le milieu réactionnel. Ce problème peut être expliqué par deux facteurs.

L'effet de filtre interne est la première explication de la difficulté de pénétration de la lumière. Comme ce dernier, les molécules situées dans les couches inférieures du milieu reçoivent en fait une intensité lumineuse plus faible que celles situées dans les couches supérieures de par l'absorption du PA en surface. De plus, la présence de particules insolubles comme des charges ou des pigments, qui diffusent la lumière dans le milieu et diminuent donc sa pénétration, est le deuxième facteur contribuant à la difficulté de la lumière à traverser le milieu. [35]

Pour pallier ce problème, plusieurs stratégies peuvent être appliquées. Dans un premier cas, l'effet de filtre interne peut être limité en diminuant la quantité de PA absorbant la lumière émise par la source lumineuse et en réduisant la profondeur du milieu. Une source de lumière visible ou proche de l'infrarouge peut aussi être utilisée pour compenser l'existence de particules insolubles. En fait, comme le montre la Figure 5, la lumière produite par des sources lumineuses de grande longueur d'onde est moins dispersée dans le milieu, ce qui améliore sa pénétration.

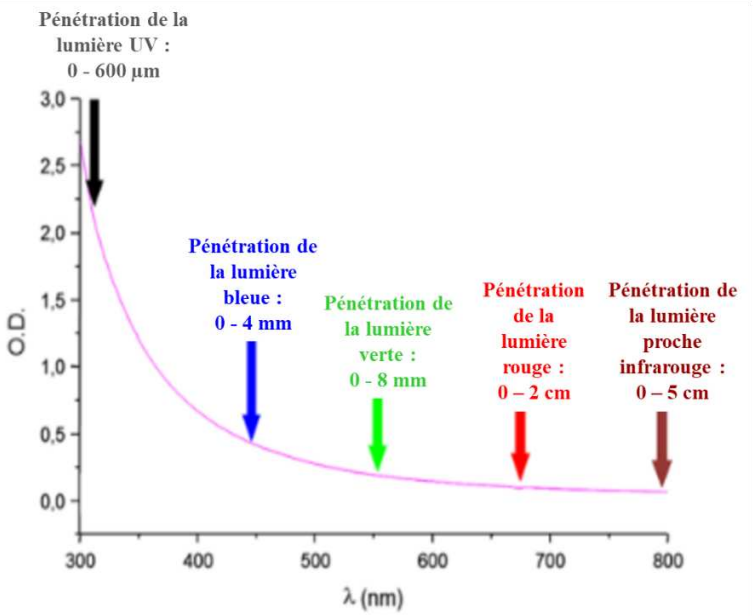

Figure 5. Pénétration de la lumière en fonction de la longueur d'onde pour un latex de polystyrène. [35]

Références

[1] J. P. Fouassier, Photoinitiation, photopolymerization, and photocuring: fundamentals and applications, Hanser, 1995.

[2] P. Suppan, Chemistry and light, Royal Society of Chemistry, 1994.

[3] M. Sangermano, M. Tonin, Y. Yagci, Degradable Epoxy Coatings by Photoinitiated Cationic Copolymerization of Bisepoxide with ε-Caprolactone, European Polymer journal, 2010, 46, 254-259.

[4] J. V. Crivello, M. Sangermano, Visible and long-wavelength photoinitiated cationic polymerization, Journal of Polymer Science Part A: Polymer Chemistry, 2001, 39, 343-356.

[5] Y. Yagci, W. Schnabel, New aspects on the photoinitiated free radical promoted cationic Polymerization, Macromolecular Symposia, 1992, 60, 133-143.

[6] R. Bensasson, A. Bernas, Polymérisation radiochimique de l'acrylonitrile quelques observations sur le post effet, Journal of Polymer Science 1958, 30.121, 163-173.

[7] T. Wang, L. J. Ma, P. Y. Wan, J. P. Liu, F. Wang, A study of the photoactivities and thermomechanical properties of epoxy resins using novel [cyclopentadien-Fe-arene]+PF6−photoinitiators, Journal of Photochemistry and Photobiology A: Chemistry, 2004, 163, 77-86.

[8] M. A. Tehfe, J. Lalevée, F. Morlet-Savary, B. Graff, J. P. Fouassier, A Breakthrough toward Long Wavelength Cationic Photopolymerization: Initiating Systems Based on Violanthrone Derivatives and Silyl Radicals, Macromolecules, 2011, 44, 8374-8379.

[9] C. Decker, Real-time monitoring of polymerization quantum yields, Macromolecules, 1990, 23, 5217-5220.

[10] H. Gu, W. Zhang, K. Feng, D. C. Neckers, Photolysis of ((3-(Trimethylsilyl)propoxy)phenyl)phenyliodonium Salts in the Presence of 1-Naphthol and 1-Methoxynaphthalene, Journal of Organic Chemistry, 2000, 65, 3484-3488.

[11] G. Hizal, Y. Yagci, W. Schnabel, Charge-transfer complexes of pyridinium ions and methyland methoxy-substituted benzenes as photoinitiators for the cationic polymerization of cyclohexene oxide and related compounds, Polymer. 1994, 35, 2428-2431.

[12] J. Lalevée, N. Blanchard, M. El-Roz, B. Graff, X. Allonas, J. P. Fouassier, New Photoinitiators Based on the Silyl Radical Chemistry: Polymerization Ability, ESR Spin Trapping, and Laser Flash Photolysis Investigation, Macromolecules, 2008, 41, 4180-4186.

[13] E. Andrzejewska, Photopolymerization kinetics of multifunctional monomers, Progress in polymer science, 2001, 26.4, 605-665.

[14] G. Hizal, S. E. Emiroglu, Y. Yagci, Photoinitiated radical polymerization using charge transfer complex of N-ethoxy-p-cyanopyridinium salt and 1,2,4-trimethoxybenzene, Polymer International, 1998, 47, 391-392.

[15] M. El-Roz, J. Lalevée, F. Morlet-Savary, X. Allonas, J. P. Fouassier, Radical and cationic photopolymerization: New pyrylium and thiopyrylium salt-based photoinitiating systems, Journal of Polymer Science Part A: Polymer Chemistry, 2008, 46, 7369-7375.

[16] J. P. Fouassier, F. Morlet-Savary, J. Lalevée, X. Allonas, C. Ley, Dyes as photoinitiators or photosensitizers of polymerization reactions, Materials, 2010, 3.12, 5130-5142.

[17] Z. Gomurashvili, J. V. Crivello, Phenothiazine photosensitizers for onium salt photoinitiated cationic polymerization, Journal of Polymer Science Part A: Polymer Chemistry, 2001, 39.8, 1187-1197.

[18] J. Lalevee, M. A. Tehfe, F. Dumur, D. Gigmes, B. Graff, F. Morlet Savary, J. P. Fouassier, Light harvesting organic photoinitiators of polymerization, Macromolecular Rapid Communication, 2013, 34, 239 245.

[19] M. V. Encinas, E. A. Lissi, C. Majmud, J. J. Cosa, Photopolymerization in aqueous solutions initiated by the interaction of excited pyrene derivatives with aliphatic amines, Macromolecules, 1993, 26.23, 6284-6288.

[20] S. Telitel, F. Dumur, T. Faury, B. Graff, M. A. Tehfe, D. Gigmes, J.P. Fouassier, J. Lalevée, New core-pyrene π structure organophotocatalysts usable as highly efficient photoinitiators, Beilstein journal of organic chemistry, 2013, 9.1, 877-890.

[21] J. Barth, M. Buback, P. Hesse, T. Sergeeva, Termination and Transfer Kinetics of Butyl Acrylate Radical Polymerization Studied via SP-PLP-EPR, Macromolecules, 2010, 43.9, 4023-4031.

[22] H. Arikawa, H. Takahashi, T. Kanie, S. Ban, Effect of various visible light photoinitiators on the polymerization and color of light-activated resins, Dental Materials Journal, 2009, 28, 454–460.

[23] K. Dietliker, T. Jung, J. Benkhoff, H. Kura, A. Matsumoto, H. Oka, D. Hristova, G. Gescheidt, G. Rist, New developments in photoinitiators, Macromolecular Symposia. Weinheim : WILEY-VCH Verlag, 2004, 217.1, 77-98.

[24] Y. Yagci, S. Jockusch, N. J. Turro, Photoinitiated polymerization: advances, challenges, and opportunities, Macromolecules, 2010, 43, 6245-6260.

[25] J. V. Crivello, J. H. W. Lam, Diaryliodonium Salts. A New Class of Photoinitiators for Cationic Polymerization, Macromolecules, 1977, 10, 1307-1315.

[26] J. Lalevée, F. Dumur, C. R. Mayer, D. Gigmes, G. Nasr, M. A. Tehfe, S. Telitel, F. Morlet Savary, B. Graff, J. P. Fouassier, Photopolymerization of N-Vinylcarbazole Using Visible-Light Harvesting Iridium Complexes as Photoinitiators, Macromolecules, 2012, 45, 4134-4141.

[27] S. S. Liow, V. T. Lipik, L. K. Widjaja, M. J. M. Abadie, Synthesis, Characterization and Photopolymerization of Vinyl Ether and Acrylate Functionalized Hybrid Oligo-Caprolactone, Journal of Polymer Research, 2011, 19, 9748.

[28] C. Jing, G. Ding, X. Qin, G. Peng, H. Huang, J. Wang, S. Zhang, H. Li, Z. Luo, F. Gao, New near UV photoinitiators containing benzophenone part for photoinitiating polymerization of methyl methacrylate, Progress in Organic Coatings, 2017, 110, 150 161.

[29] M. Popal, J. Volk, G. Leyhausen, W. Geurtsen, Cytotoxic and genotoxic potential of the type I photoinitiators BAPO and TPO on human oral keratinocytes and V79 fibroblasts, Dental Materials 2018, 34.12, 1783 1796.

[30] M. D. Purbrick, In: Photoinitiation, Photopolymerization and Photocuring, Hanser Publishers, Munich, GER 1995.

[31] A. Chapiro, Radiation induced polymerization, Radiation Physics and Chemistry, (1977) 1979, 14.12, 101-116.

[32] C. Decker, A novel method for consuming oxygen instantaneously in photopolymerizable films, Die Makromolekulare Chemie, 1979, 180.8, 2027-2030.

[33] T. Scherzer, H. Langguth, Temperature Dependence of the Oxygen Solubility in Acrylates and Its Effect on the Induction Period in UV Photopolymerization, Macromolecular Chemistry and Physics, 2005, 206.2, 240-245.

[34] F. Arndt, A. Kalischek, Beiträge zur Konstitution der sogenannten γ Pyridone, Berichte Der Deutschen Chemischen Gesellschaft, 1930, 63.3, 587-596.

[35] A. H. Bonardi, F. Dumur, T. M. Grant, G. Noirbent, D. Gigmes, B. H. Lessard, J. P. Fouassier, J. Lalevée, High Performance Near Infrared (NIR) Photoinitiating Systems Operating under Low Light Intensity and in the Presence of Oxygen, Macromolecules, 2018, 51.4, 1314-1324.

Chapitre II : L'impression 3D ou fabrication additive

La fabrication additive (additif manufacturing : AM) (également connue sous le nom d'impression 3D) a permis la fabrication personnalisée d'objets ayant des géométries et des fonctions complexes en termes de propriétés mécaniques et électriques. Les technologies de fabrication additive utilisent généralement des polymères et des composites et ont progressé dans une variété d'applications industrielles émergentes. [1-3] Malgré les progrès récents de l'impression 3D de composites polymères, de nombreux défis, tels que la qualité sous-optimale des produits fabriqués et le nombre limité de matériaux disponibles pour l'impression 3D, doivent être relevés pour que les matériaux fabriqués de manière additive soient plus largement adoptés. Ce chapitre présente d'abord un bref historique des technologies de fabrication additive et de l'impression 3D de polymères. Par la suite, l'état de l'art en matière de conception des polymères et matériaux et les principes des processus d'AM sont abordés.

1. *Évolution de l'impression 3D polymère*

1.1. *Impression 3D à partir de polymère : histoire*

La chronologie de l'impression 3D, ainsi que le développement des matériaux polymères, sont résumés dans la Figure 1. Le développement des matériaux de base, en particulier des polymères, est indispensable à l'invention de l'impression 3D. La plupart des polymères, notamment les polyamides, l'acide polylactique (PLA) et l'époxy, ont été synthétisés et développés dans les années 1920 et 1940. Les concepts fondamentaux de l'AM ont été étudiés il y a plus de 50 ans. Les années 1980 et 1990 ont été les décennies de la naissance et de la croissance de l'impression 3D. La première méthode d'impression 3D, la stéréolithographie, a été commercialisée en 1987. D'autres techniques d'impression 3D, telles que la fabrication par filament fondu (FFF) et le frittage sélectif par laser (SLS), ont également été inventées au cours de cette période. À la fin des années 1990, la plupart des premières versions des techniques d'impression 3D sont apparues et ont évolué rapidement, grâce aux progrès des technologies informatiques. Au début des années 2000, les techniques d'impression 3D ont commencé à être largement explorées dans des secteurs tels que le prototypage, la médecine et l'aérospatiale. [4-6]

Dans le même temps, de nombreux brevets relatifs aux versions antérieures des techniques d'impression 3D ont expiré et de nombreuses entreprises ont commencé à fabriquer leurs propres marques d'imprimantes 3D, les rendant ainsi accessibles au grand public. Après 2010, l'accès généralisé aux techniques d'impression 3D a conduit à des techniques d'impression avancées avec une précision, une exactitude et une vitesse accrues. [8] Au début, les techniques d'AM ont principalement adopté des matériaux polymères existants et les ont adaptés à l'AM. Aujourd'hui, une attention croissante est accordée au développement de polymères spécifiques pour l'impression 3D. Avec le développement rapide de matériaux d'impression 3D à haute performance (par exemple, les polymères intelligents), l'AM est devenu un processus fondamental et a conduit à une nouvelle révolution industrielle dans divers domaines. [9-11] Par exemple, des polymères nouvellement conçus, tels que les polymères à mémoire de forme (SMP), les hydrogels intelligents, les polymères à cristaux liquides (LCP) et les élastomères à cristaux liquides (LCE), ont conduit à un nouveau paradigme de fabrication, notamment l'impression 4D, et donnent aux industries une chance de produire de nouveaux dispositifs intelligents, des robots et des produits biomédicaux. [12-15] Actuellement, l'impression 3D est en train de passer du prototypage aux produits d'utilisation finale, ce qui aura un impact sociétal plus large. D'autre part, il existe un mouvement parmi les fabricants qui rend la technologie de l'impression 3D bon marché et facile à utiliser. L'impression d'un objet nécessite un logiciel de conception assistée par ordinateur (CAO) (dont le prix peut atteindre 50 000 dollars) ; toutefois, il existe des logiciels de CAO libres. En outre, les fabricants d'imprimantes 3D permettent aux utilisateurs de télécharger des conceptions 3D dans le nuage, ce qui favorisera encore la prolifération de l'impression. [14]

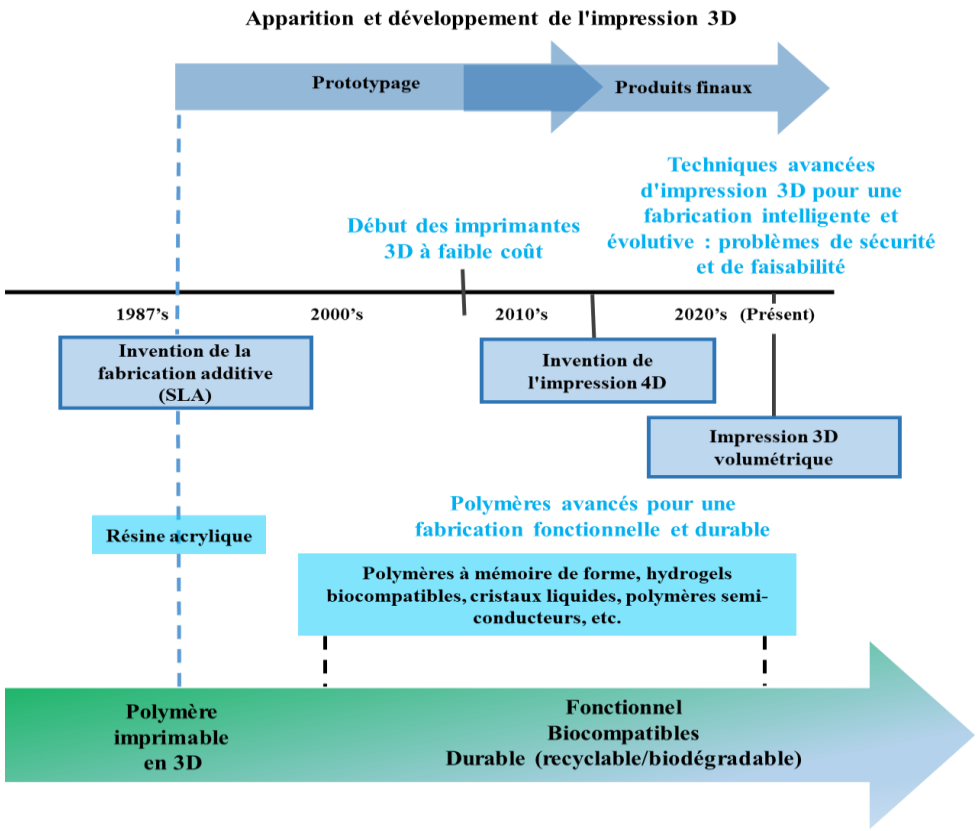

Figure 1. Histoire de l'impression 3D et développement de polymères pour l'impression 3D : transition du prototypage rapide vers une production évolutive et personnalisable.

1.2. *De la conception aux objets 3D*

L'impression 3D commence par un modèle 3D réalisé à l'aide d'un logiciel de CAO et convertit le modèle en un fichier STL (langage de tessellation de surface). Le fichier STL sera découpé en couches 2D pour planifier le chemin d'impression des objets 3D. Cependant, il ne convient que pour un seul type de matériau. Un autre format de fichier, tel que les fichiers OBJ, peut stocker des informations sur la couleur, le matériau et la texture, et les fichiers PLY peuvent contenir des objets scannés en 3D. De nouveaux formats de fichiers ont également été développés, notamment le format de fabrication 3D (3MF) et le format de fabrication additive (AMF). Ces deux formats décrivent les informations internes des modèles 3D, notamment la couleur, les matériaux et la texture. Contrairement au STL, l'AMF stocke des données géométriques codées en tessellation triangulaire qui peut se courber, ce qui permet d'obtenir une géométrie précise. Le 3MF, une version avancée de l'AMF, possède toutes les propriétés techniques de l'AMF et les données sont enregistrées dans un format XML lisible par l'homme pour faciliter le contrôle. [16-18]

En ce qui concerne les matériaux, les polymères sont populaires dans l'impression 3D en raison de leur souplesse de conception, de leur facilité d'utilisation et de leur rentabilité. En général, les propriétés physiques, mécaniques et chimiques des polymères dépendent de la composition chimique, de la structure des polymères et du degré de polymérisation. Au stade de la conception et de la synthèse des matériaux, on a la capacité de concevoir les propriétés inhérentes des matériaux au niveau moléculaire, puis de les transformer en formes, tailles et rhéologies adaptées aux processus d'impression 3D. Pendant l'impression, différents paramètres de fabrication (par exemple, la température et le taux de chauffage/refroidissement) peuvent influencer les microstructures du matériau, telles que la taille et le degré de cristallinité, et finalement déterminer les propriétés mécaniques et autres des objets imprimés. Il est donc essentiel de comprendre les relations processus/structure/propriété dans l'impression 3D. [19]

Dans la VAT photopolymérisation (VP), l'impression 3D est généralement réalisée par le biais du processus de polymérisation UV, qui est un processus photochimique dans lequel la lumière UV est utilisée pour amorcer la polymérisation (ou le réseau de réticulation) des résines (généralement des monomères et des oligomères) avec l'aide de photoamorceurs. [20] Les polymères photosensibles (c'est-à-dire le photopolymère) doivent être conçus pour avoir une viscosité appropriée de moins de 5 Pa·s pour une bonne fluidité et un coefficient d'absorption relativement élevé, selon le type de photoamorceurs, pour une haute résolution d'impression. La viscosité de ces photopolymères peut être ajustée à une valeur inférieure en ajoutant un diluant réactif ou en chauffant la résine au cours du processus d'impression. Bien que le diluant réactif permette de contrôler la viscosité, le module de flexibilité et de compression et la contrainte à la rupture diminuent progressivement avec l'augmentation de la fraction pondérale du diluant. La profondeur de pénétration de la lumière UV peut être contrôlée par l'ajout d'un photo-absorbant qui augmente l'absorption de la lumière. L'absorption plus élevée de la lumière entraîne une production plus importante de radicaux libres en tant qu'amorceurs, ce qui provoque une réticulation élevée de la chaîne polymère et un degré de durcissement plus élevé.

Pour avoir une impression 3D efficace, il faut d'abord avoir une bonne connaissance des matériaux et choisir le bon procédé, puis optimiser le processus de fabrication et enfin examiner la qualité des impressions. Le post-traitement, tel que le nettoyage, la finition de surface, le durcissement et la peinture, est nécessaire dans la plupart des processus d'impression. Le nettoyage consiste à couper le matériau de support. Après le nettoyage des parties inutiles, une finition de surface peut être nécessaire pour rendre le produit plus beau grâce à des traitements

mécaniques (par exemple, le sablage et le microbillage) et chimiques (par exemple, la réaction à la vapeur). Dans le cas de la technique VP, un processus de durcissement supplémentaire utilisant la lumière UV peut être nécessaire pour améliorer les propriétés mécaniques du produit imprimé. Dans certains cas, l'objet imprimé est peint à l'aide d'un pinceau ou d'un spray pour la visualisation. [20-22]

2. *Procédé d'impression 3D pour les polymères et les composites*

Les processus d'impression 3D sont bien établis pour produire des objets 3D composés de polymères et de composites. Certaines techniques d'impression 3D sont bien développées, telles que l'extrusion de matériaux (ME), la VP (ou stéréolithographie [SLA]), le jet de matériau (MJ), le jet de liant (BJ), et le PBF, mais beaucoup d'autres sont encore en cours de développement. Chaque procédé d'impression 3D présente ses propres avantages et défis dans la fabrication de polymères/composites et requiert des conditions spécifiques pour le polymère, telles que la forme, l'état (solide ou liquide) et les propriétés physiques (viscosité et température de fusion). Par conséquent, lors du choix des techniques d'impression 3D, l'utilisateur doit tenir compte des matériaux, du coût et des exigences de l'application (y compris la résolution, la complexité de la géométrie et les propriétés mécaniques). [23-25] Ci-dessous, se trouve un aperçu de chaque mécanisme d'impression 3D. Six méthodes d'impression 3D courantes sont illustrées dans la Figure 2, avec les composants clés étiquetés. Leurs caractéristiques (principe d'impression, polymères typiques et état des polymères, avantages et inconvénients) sont résumées dans le Tableau 1.

2.1. *Extrusion de matériaux (ME)*

La ME distribue sélectivement un matériau à travers une buse et dépose le matériau couche par couche pour construire un objet en 3D. Le processus d'impression de la ME diffère selon le type de matériau (liquide ou solide). Dans la ME, le procédé FFF, également connu sous le nom de marque déposée "fused deposition molding" (FDM), est le plus couramment utilisé en raison de sa simplicité d'installation. Le procédé FFF est une forme d'impression 3D dans laquelle le filament solide est fondu à l'état semi-liquide à l'extrémité chaude, extrudé à travers la buse et déposé couche par couche sur la plateforme ou sur les couches imprimées précédemment. [26] Les matériaux thermoplastiques, tels que les l'acrylonitrile butadiène styrène (ABS), le PLA et le nylon, sont utilisés comme matières premières en raison de leur faible température de fusion et de leur viscosité appropriée lorsqu'ils sont fondus.

Si des filaments composites sont utilisés comme matières premières en ajoutant aux polymères des renforts ou des charges actives, tels que des nanomatériaux de carbone, des métaux, des biomatériaux et des céramiques, la FFF peut produire des produits fonctionnels, tels que des appareils électroniques, des dispositifs de stockage d'énergie et des os artificiels. Il est également possible d'utiliser des matériaux multiples (matière première principale et matière première sacrificielle) pour fabriquer des structures complexes. Les matériaux sacrificiels sont utilisés comme structures de soutien, qui peuvent être complètement enlevées et laisser une bonne finition de surface. Les matières premières sacrificielles sont généralement constituées de matériaux dissolubles dans un produit chimique ou dans l'eau, tels que l'alcool polyvinylique (PVA) et l'Hydrofill. [26-28]

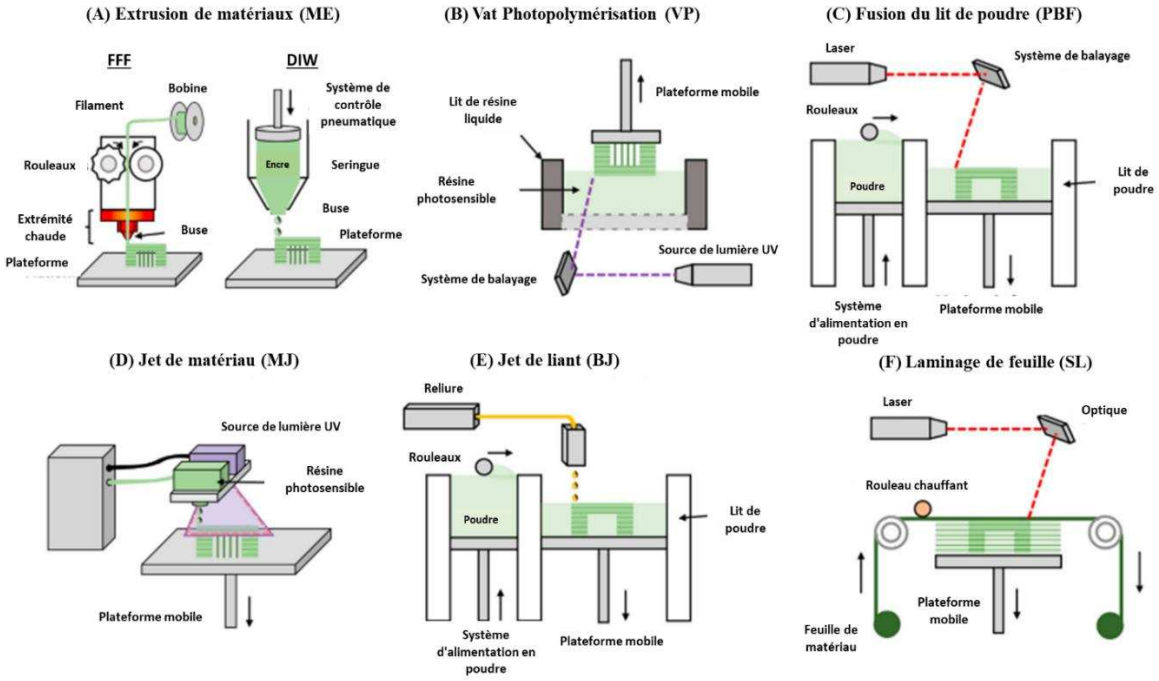

Figure 2. Représentation schématique des techniques d'impression 3D ; (A) Dans l'extrusion de matériaux (ME), la fabrication par fusion de filaments (FFF) est une méthode d'impression 3D dans laquelle le filament solide est fondu, extrudé à travers la buse et déposé couche par couche. L'écriture directe à l'encre (DIW) utilise une encre viscoélastique et l'encre est extrudée à travers une petite buse avec un débit contrôlé. (B) La photopolymérisation en cuve (VP) utilise la lumière UV pour polymériser la résine photopolymère dans le bain liquide en formant des réseaux réticulés. (C) La fusion sur lit de poudre (PBF) utilise l'énergie thermique pour faire fondre un matériau en poudre et imprimer un objet en 3D. (D) La projection de matériaux (MJ) imprime des produits 3D en déposant de manière sélective des gouttelettes de matériaux de construction. (E) Le jet de liant (BJ) dépose un liant liquide sur des matériaux en poudre, qui sont les principaux composants des objets finaux. (F) Le laminage de feuilles (SL) utilise de fines feuilles de matériau et les assemble couche par couche pour fabriquer un objet en 3D.

Autre type de ME, l'écriture directe à l'encre (DIW) est un processus de dépôt d'encre dans lequel l'encre viscoélastique est extrudée à travers une petite buse à des débits contrôlés et déposée couche par couche pour créer des structures en 3D. En raison de sa résolution relativement élevée (jusqu'à 200 µm) et de sa capacité à imprimer des structures périodiques en 3D à l'échelle méso et microscopique, le DIW est activement utilisé pour des applications fonctionnelles, telles que les dispositifs microfluidiques et les capteurs. De plus, elle bénéficie d'une flexibilité matérielle grâce à l'ajout de diverses charges dans l'encre imprimable. Pour les matières premières, il existe des liquides polymères, des hydrogels et des suspensions colloïdales. L'écriture directe à l'aide de gels colloïdaux est aussi utilisée. Le point essentiel à prendre en compte est la rhéologie du matériau : l'encre doit s'amincir sous certaines contraintes de cisaillement et présenter des propriétés mécaniques relativement bonnes pour les caractéristiques autoportantes après la dispersion. Dans la plupart des cas, les encres comprennent un mélange de matériaux en poudre dans des polymères liquides, et elles sont systématiquement ajustées pour atteindre une limite d'élasticité suffisante et un comportement d'amincissement par cisaillement par le démoussage et le refroidissement ou le chauffage. [28-30]

2.2. *VP ou SLA*

La VP, également appelé SLA, utilise des photopolymères (résine à base d'époxy ou d'acrylique) solidifiés par la lumière UV. Les principales configurations de machines sont la VP descendante et la VP ascendante. Dans la technique VP descendante, la lumière UV se déplace dans la trajectoire souhaitée au-dessus de la cuve et solidifie le photopolymère dans le bain liquide situé sur le dessus en formant des réseaux réticulés. Une fois qu'une couche est imprimée, la plateforme s'éloigne de la zone de réaction d'une épaisseur de couche donnée pour permettre à la résine fraîche, non polymérisée, de réapprovisionner la zone. L'imprimante imprime ensuite la couche suivante et répète les processus jusqu'à ce que l'objet soit complet. La technique VP ascendante nécessite moins de résine pour remplir le bain et permet de produire des volumes plus importants que la technique VP descendante. Les imprimantes VP ascendantes placent la source lumineuse sous le bain de résine et la plate-forme mobile est construite à l'envers. Le bain de résine a un fond transparent qui laisse passer la lumière du laser mais empêche la pièce durcie d'y adhérer. Après l'impression d'une couche, la pièce durcie s'éloigne de la zone de réaction du bain au fur et à mesure que la plate-forme se déplace vers le haut. [31] En outre, si le mécanisme d'excitation de la polymérisation est modifié (de l'absorption

monophotonique à l'absorption multiphotonique), la VP peut fabriquer des objets en 3D avec une résolution élevée dans la région submicronique. Contrairement à la VP traditionnelle, où la polymérisation se produit sur la surface irradiée par le laser, la polymérisation à deux photons (TPP) ne polymérise que dans un point étroitement focalisé (généralement à l'intérieur du photopolymère). Dans la TPP, le processus photochimique est induit par un faisceau laser pulsé, et une molécule photosensible absorbe deux photons simultanément pour activer la polymérisation. [31-33]

Les photopolymères se composent généralement de monomères/oligomères et de photoamorceurs, mais pour un processus de photoamorçage adéquat et des produits de haute qualité, des diluants et des agents de transfert de chaîne peuvent être ajoutés. Les agents de dilution contrôlent la viscosité de la résine pour un bon mouillage et une bonne imprégnation, et les agents de transfert de chaîne modifient le réseau de réticulation pendant l'impression. Pour un bon processus de polymérisation, plusieurs facteurs de réaction de polymérisation, notamment l'intensité du laser, la viscosité et le comportement de mouillage de la résine, doivent être bien contrôlés. Comme la cuve limite la présence de plusieurs photopolymères à l'état non mélangé, il est difficile d'imprimer des matériaux multiples avec cette technologie, à moins d'utiliser plusieurs réservoirs pour différents photopolymères ou de les intégrer à un système microfluidique pour échanger activement différents photopolymères. [32]

2.3. *La fusion sur lit de poudre (PBF)*

La technologie PBF est l'une des technologies les plus polyvalentes, qui est déjà très répandue dans la production de masse. Elle utilise des poudres et imprime des formes en 3D en injectant sélectivement de l'énergie thermique, par exemple des lasers. Le laser passe sur la surface des poudres, les frittant de manière sélective et fusionnant les poudres pour former la forme souhaitée pour chaque couche 2D. Pendant l'impression, la température du lit de poudre est légèrement inférieure à la température de fusion afin de minimiser la chaleur nécessaire pour faire fondre la poudre, mais supérieure à la température de cristallisation afin de retarder la cristallisation. Après l'impression d'une couche, un rouleau apporte des poudres supplémentaires depuis la plate-forme d'approvisionnement, recouvre la couche imprimée, puis répète les opérations. Bien qu'en théorie n'importe quelle poudre de polymère thermoplastique puisse être utilisée comme matière première, les poudres de polyamide et de polycaprolactone (PCL) sont les principaux matériaux utilisés dans la pratique, car elles présentent une large

fenêtre de frittage et un comportement de consolidation. [33] En PBF, les principaux paramètres d'impression sont la granulométrie de la poudre, la puissance du laser, l'épaisseur de la couche et la vitesse de balayage. Ces paramètres doivent être pris en compte pour une étape de recouvrement de la poudre appropriée, une mobilité adéquate de la poudre fondue, une faible porosité et une grande précision géométrique, respectivement. [31-32]

2.4. *Procédés basés sur le jet (MJ et BJ)*

Dans les processus basés sur le jet de matière, MJ et BJ sont des techniques typiques d'impression 3D. La MJ a été introduite pour produire un prototype visuel en couleur dans les années 1990. La MJ fabrique des produits 3D en déposant de manière sélective des gouttelettes de matériaux de construction. C'est l'une des technologies d'impression les plus précises (jusqu'à 16 µm) et elle peut imprimer des produits multi-matériaux en utilisant plusieurs buses. Les résines à l'état liquide (généralement des photopolymères) sont déposées aux endroits souhaités et durcies par la lumière UV située à proximité de la tête d'impression. Une fois que chaque couche est terminée, la plate-forme de construction descend ou la tête d'impression remonte, et le processus se répète jusqu'à ce que la pièce entière soit imprimée. Comme pour les autres méthodes d'impression 3D, il est courant de procéder à un post-traitement, tel que l'enlèvement du support, la finition de la surface et la teinture. [25]

En MJ, la rhéologie (viscosité et amincissement par cisaillement) de la résine liquide est le principal paramètre. Le polymère doit avoir un comportement d'amincissement par cisaillement pour se fluidifier et s'écouler à travers la petite buse, puis retrouver rapidement son module après la sortie de la buse afin de maintenir la structure imprimée. En outre, le polymère liquide doit avoir une viscosité appropriée pour tomber à la demande. C'est pourquoi les photopolymères sont préchauffés à une température comprise entre 30 et 60 °C. La viscosité limitée entre 20 et 40 centipoises est le point le plus problématique pour la formation de gouttelettes, ce qui rend difficile la conception de matériaux imprimables. En outre, d'autres facteurs, notamment la densité du liquide et la tension superficielle, doivent être ajustés avec précision pour convertir avec succès un matériau d'impression d'un liquide continu en petites gouttelettes. Les propriétés mécaniques des objets imprimés ne conviennent pas aux prototypes structurels en raison de la fragilité attribuée à la formation de réseaux de polymères à forte densité de réticulation, mais elles peuvent être améliorées par l'ajout de nanocharges (silice et argile) dans l'encre. Toutefois, ces nanocharges sont discontinues et l'amélioration des propriétés mécaniques n'est pas suffisante pour des applications structurelles. [34-37]

Le procédé BJ dépose un liant liquide sur un lit de poudre, qui deviendra le principal composant des objets finaux. Les étapes d'impression sont pratiquement les mêmes que celles du procédé PBF, à l'exception du processus de durcissement, car la soudure par solvant ou la réaction chimique se produit entre la poudre et le liant sans traitement thermique. Ce processus non thermique élargit la gamme des matériaux par rapport à la PBF : les produits finaux peuvent être fabriqués à partir de nombreux matériaux différents à condition qu'ils soient fournis sous forme de poudre, et le liant peut varier en fonction de la poudre utilisée. Comme la PBF, elle est efficace pour la production de masse et permet la production de produits à haute résolution (~235 µm), mais les produits finaux présentent de nombreux pores à l'intérieur de la structure après l'élimination du liant, ce qui nécessite un post-traitement supplémentaire pour remplir des matériaux à l'intérieur des structures poreuses afin d'en améliorer les propriétés mécaniques. En général, une ligne est installée pour injecter des matériaux dans les pores à l'intérieur des produits pendant le traitement au four. En outre, la surface du produit est rugueuse et nécessite un post-traitement pour la lisser. Dans le procédé BJ, la granulométrie de la poudre, la viscosité du liant, la vitesse d'impression et le mouillage de la poudre avec le liant liquide doivent être contrôlés pour obtenir des produits de haute qualité. [35-37]

2.5. *Laminage de feuille (SL)*

Le laminage de feuilles est l'une des méthodes typiques de la fabrication additive et peut également être utilisé pour la fabrication assistée par ordinateur de composites polymères en collant des feuilles de matériaux pour former une pièce en trois dimensions. Les composites polymères peuvent être imprimés par la technologie de fabrication d'objets laminés, qui utilise des feuilles minces de matériau et de l'adhésif au lieu du soudage. Dans ce processus d'impression, la chaleur et la pression sont utilisées conjointement pour faire fondre et coller les feuilles ensemble. La manipulation des matériaux est aisée en SL, ce qui permet une production rapide. Cependant, la résolution (normalement de 50 à 1 000 µm dans la direction z) est limitée en raison de l'épaisseur fixe de la feuille, et les propriétés mécaniques sont déterminées par la force de l'adhésif. En outre, il peut être nécessaire de procéder à un post-traitement pour polir la surface et à un traitement thermique pour améliorer l'adhérence entre les couches. [31] L'une des entreprises les plus performantes, Impossible Objects, a réussi à imprimer des objets en 3D en SL à l'aide de matériaux composites (par exemple, des feuilles de fibre de carbone et de fibre de verre).

Tableau 1. Les caractéristiques des technologies d'impression 3D pour les polymères et les composites.

	Principe d'impression	Polymère/composite état	Matériaux polymères typiques	Avantages	Désavantages
ME (FFF/DIW)	Extrusion	Filament solide	Les thermoplastiques, tels que l'ABS, PLA, et le nylon	Simple, peu coûteux (300 dollars pour un usage domestique et jusqu'à 2 000 à 8 000 dollars pour un usage professionnel) et rapide (de 50 à 150 mm/h jusqu'à 500 mm/h)	Bouchage de la buse et mauvaise qualité
	Extrusion sous pression	Polymère liquide	Polymère liquide, hydrogel et suspension colloïdale	Flexibilité des matériaux et haute résolution (jusqu'à 200 µm)	Faible débit
VP	Polymérisation induite par les UV	Photopolymère liquide	Résine photosensible (résine à base d'époxy ou d'acrylate)	Haute résolution (6-140 µm)	Faible débit (14 mm/h : ProJet 1200) et un coût élevé (à partir d'environ 3 000 et jusqu'à 10 000 $ pour l'impression de grands volumes)
PBF	Frittage induit par la chaleur	Poudre solide	Le polyamide, polystyrène et PCL poudre	Bonne pour la production de masse et la conception flexibilité	Coût élevé (à partir d'environ 100 000 $), surface rugueuse et génération de cavités
MJ	Goutte-à-la-demande jet de matière avec solidification UV	Photopolymère liquide	Résine photosensible	Haute résolution (jusqu'à 16 µm), capacités multimatériaux et propriétés homogènes	Coût élevé (100 à 250 000 $: CONNEX3 OBJET350) et ne convient pas aux applications structurelles
BJ	Goutte à goutte sur demande jet de liant	Polymère liquide	Agents d'adhérence + poudre à base d'acrylate (métal et sable)	Flexibilité des matériaux et de la conception et aptitude à la production de masse	Surface rugueuse et la formation de cavités ; retrait
SL	Adhésif couche par couche	Feuille de polymère	Agents de liaison + composites polymères	Facilité de manutention et rapidité (45 in^3/h : CBAM)	Finition variée, résolution limitée des pièces (50 à 1 000 mm) et propriétés mécaniques limitées

Ce processus SL applique de l'adhésif sur les feuilles, dépose de la poudre de polymère sur chaque feuille, puis colle les feuilles. L'objet imprimé est chauffé dans un four pour faire fondre le polymère et compressé pour consolider la pièce. L'excédent de matériau est ensuite éliminé par un procédé mécanique ou chimique. L'imprimante peut construire une structure d'un volume maximal de 12 x 12 x 4 pouces à grande vitesse (45 in^3/h : CBAM). [34]

3. *Conception et sélection des polymères pour l'AM de polymères*

Les technologies AM ont des exigences spécifiques en matière de propriétés des matériaux, telles que le point de fusion et les propriétés rhéologiques. Les polymères thermodurcissables et les composites sont essentiels pour les structures légères et économes en énergie dans les secteurs de l'aérospatiale, de l'automobile et de l'énergie. Cependant, la fabrication de thermodurcissables à hautes performances, à l'exception des résines photosensibles, nécessite des températures élevées (environ 180°C) pour durcir les monomères pendant plusieurs heures. Il est donc difficile d'utiliser ces thermodurcissables comme matières premières pour l'impression 3D. En concevant le polymère, en particulier la cinétique de polymérisation, une polymérisation rapide à la température ambiante est devenue possible, ce qui a permis d'élargir le choix des matériaux pour l'impression 3D. Il est donc essentiel de concevoir et de sélectionner des polymères pour l'AM sur la base d'une compréhension fondamentale des caractéristiques des polymères. [35-37]

Les deux polymères largement utilisés pour l'impression 3D sont les thermoplastiques et les photopolymères, qui polymérisent sous l'effet des UV. Une autre classe spéciale de polymères sont les hydrogels, qui possèdent un réseau de chaînes polymères hydrophiles. Ces trois types de polymères sont populaires dans l'impression 3D, et leur structure moléculaire, leurs propriétés physiques critiques, leurs sous-catégories (telles que les polymères représentatifs) et les méthodes d'impression courantes sont présentées dans la Figure 3.

3.1. *Polymères thermoplastiques*

Les polymères thermoplastiques sont des polymères couramment utilisés qui se ramollissent lorsqu'ils sont chauffés, ce qui permet de les façonner, et qui se solidifient à nouveau lorsqu'ils refroidissent. Les polymères thermoplastiques peuvent être divisés en plastiques amorphes ou semi-cristallins sur la base de leur structure moléculaire illustrée à la Figure 3A. Les thermoplastiques amorphes ont une structure moléculaire ordonnée de manière aléatoire et n'ont pas de point de fusion précis, ce qui les rend faciles à thermoformer.

En revanche, les thermoplastiques semi-cristallins ont une structure moléculaire ordonnée et un point de fusion élevé. Après l'absorption d'une certaine quantité de chaleur, ils passent brusquement de l'état solide à l'état liquide. Les polymères semi-cristallins ont de bonnes propriétés mécaniques en raison de leurs fortes forces intermoléculaires. Tous les polymères thermoplastiques ont une capacité de traitement réversible, ce qui les rend adaptés à l'impression 3D par extrusion, telle que la FFF. Sous l'effet de la chaleur externe d'une imprimante 3D, les particules de polymères solides (ou filaments) sont fondues en brisant les chaînes de polymères. À ce stade, les chaînes de polymères peuvent se déplacer librement et, après l'impression, le polymère fondu est solidifié dans l'arrangement souhaité. [38-40]

3.2. *Les thermodurcissables*

Les polymères thermodurcissables sont irréversiblement durcis par la polymérisation d'un prépolymère liquide visqueux ou d'une résine. Plutôt que de croître dans une seule direction, les sites de réaction actifs à l'intérieur de la chaîne polymère réagissent avec leurs chaînes adjacentes pour former un réseau polymère étroitement connecté. Plus la densité de réticulation des thermodurcissables est élevée, plus la résistance mécanique et la dureté sont importantes et plus la résistance à la dégradation par la chaleur et aux attaques chimiques sont élevées. Ces polymères peuvent être durcis par la chaleur ou un rayonnement approprié et être favorisés par une pression élevée et l'ajout de catalyseurs. La Figure 3B montre la structure moléculaire connectée des thermodurcissables et décrit les différents composants en fonction des méthodes de durcissement. Dans le cas des polymères thermodurcissables, la réaction de durcissement devient active à mesure que la température augmente, mais la réaction devient lente lorsque le système atteint la transition vitreuse et se poursuit jusqu'au durcissement complet de la résine. En revanche, les photopolymères sont amorcés par un rayonnement UV, qui est plus énergique que le visible. La lumière UV déclenche la rupture d'une liaison covalente ou ionique des photoamorceurs et génère des radicaux libres actifs ou des groupes cationiques/anioniques actifs pour la polymérisation rapide des monomères dans les résines photopolymères. Une fois amorcée, la réaction en chaîne se développe comme dans une polymérisation thermique conventionnelle, à l'exception de la phase d'amorçage, dans laquelle la vitesse d'amorçage peut être augmentée par une irradiation élevée. Parmi les différents photopolymères, les polymères à base d'acrylate, y compris les polyesters acryliques, les silicones acryliques et les uréthanes acryliques, ont été activement utilisés parce que la vitesse de polymérisation est très rapide. [38-39]

Les résines photopolymères (à base d'époxy ou d'acrylate) sont principalement utilisées dans l'impression 3D à base de VP et de gouttelettes (comme l'impression à jet d'encre). Elles polymérisent généralement sous une lumière UV d'une longueur d'onde comprise entre 355 et 405 nm. Dans cette approche, une faible viscosité ou une bonne fluidité du photopolymère est nécessaire. Les photopolymères à faible viscosité sont composés de monomères et d'oligomères de faible poids moléculaire. Ces photopolymères sont faciles à polymériser avec un degré de réticulation élevé, ce qui donne des structures dures et cassantes. Si la résine est composée d'éléments de poids moléculaire élevé, la viscosité sera élevée. Pour faire face à cette viscosité élevée, des diluants réactifs sont ajoutés à la résine, mais ils peuvent s'intégrer à la structure finale des polymères et potentiellement détériorer les performances des impressions. Idéalement, le développement d'une résine photopolymère devrait répondre à deux critères : faible viscosité et haute performance. [35]

3.3. *Les hydrogels*

Les hydrogels sont des matériaux intéressants pour l'impression 3D car ils sont l'un des matériaux d'encre les plus faisables pour l'impression 3D basée sur l'extrusion. L'hydrogel est un réseau polymère hydrophile réticulé en 3D (illustré à la Figure 3C) et peut être classé, selon les méthodes de préparation, en homopolymère, copolymère et réseau semi-interpénétré (semi-IPN). Les homopolymères sont composés d'un seul type de monomères, tels que le poly(méthacrylate d'hydroxyéthyle) (PHEMA) et le polyéthylène glycol (PEG). Les copolymères contiennent deux types de monomères : par exemple, PEGMA et carboxyméthylcellulose. Les semi-IPN, par exemple le copolymère acrylamide/acide acrylique, se forment lorsqu'un polymère linéaire pénètre dans un autre réseau réticulé sans qu'il y ait de liaison chimique entre eux. Des solvants typiques, tels que l'eau, l'éthanol, les mélanges eau-éthanol et l'alcool benzylique, sont utilisés pour la polymérisation en solution. [37-39]

Grâce à leur élasticité et à leur souplesse, les hydrogels occupent une place de choix dans les domaines de la bioingénierie, des appareils intelligents et de l'agriculture. L'impression 3D est activement adoptée pour créer des échafaudages poreux 3D à petite échelle, tels que des os artificiels, mais il peut être difficile de fabriquer des produits complexes et de grande taille en raison de la faible stabilité structurelle et de la grande capacité de gonflement.

Pour être imprimés en 3D avec succès, les hydrogels doivent avoir des propriétés rhéologiques appropriées (viscosité et amincissement par cisaillement) pour l'impression et une forte intégrité mécanique pour maintenir la structure pendant et après l'impression. La viscosité de l'hydrogel dépend de la concentration en monomères et de la longueur de chaîne macromoléculaire (Figure 3C). La concentration plus élevée en monomères et la longueur de chaîne plus importante des macromolécules augmentent le contact entre elles et renforcent les attractions intermoléculaires, ce qui se traduit par une viscosité plus élevée. [39]

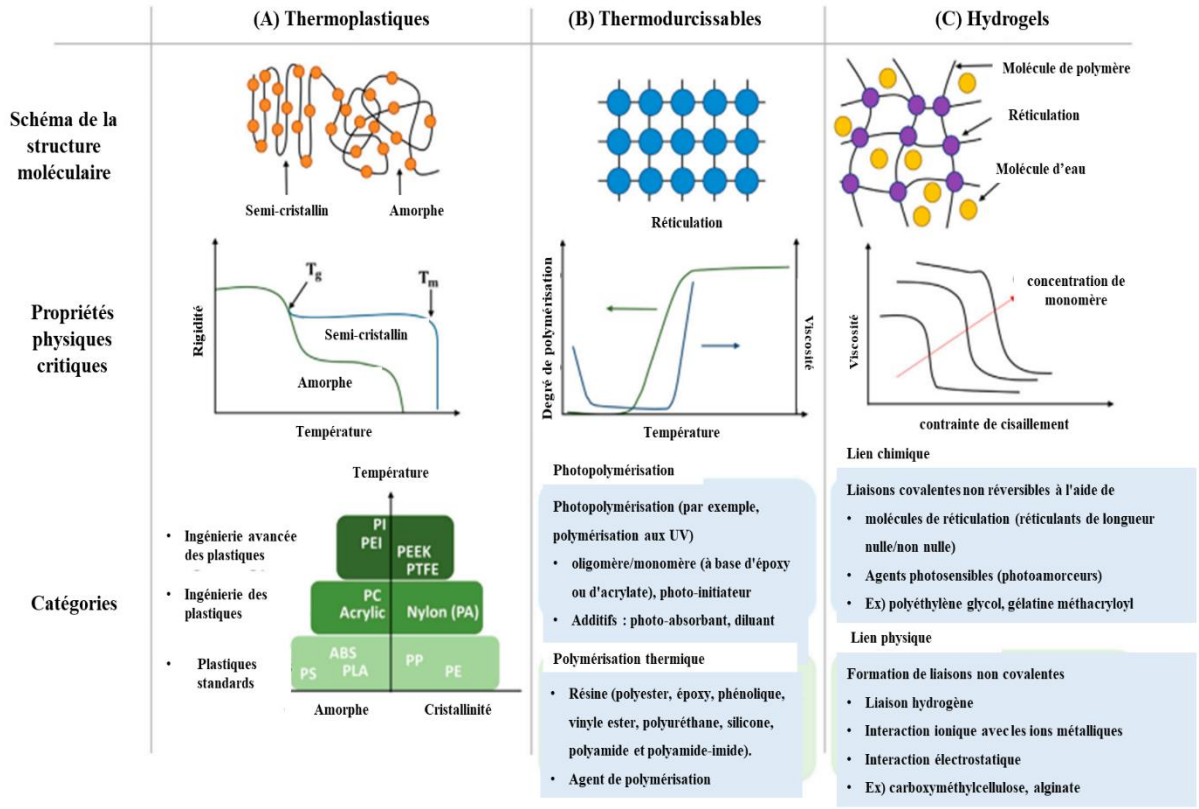

Figure 3. Polymères les plus utilisés dans l'impression 3D et leurs propriétés (A) Thermoplastiques, (B) thermodurcissables et (C) hydrogels.

Références

[1] C. M. Spadaccini, Additive manufacturing and processing of architected materials, MRS Bulletin, 2019, 44.10, 782-788.

[2] T. Van Manen, S. Janbaz, A. A. Zadpoor, Programming 2D/3D shape-shifting with hobbyist 3D printers. Materials horizons, 2017, 4.6, 1064-1069.

[3] A. Kotikian, R. L. Truby, J. W. Boley, T. J. White, J. A. Lewis, 3D printing of liquid crystal elastomeric actuators with spatially programed nematic order, Advanced materials, 2018, 30.10, 1706164.

[4] D. Drummer, M. Medina-Hernández, M. Drexler, K. Wudy, Polymer powder production for laser melting through immiscible blends, Procedia engineering, 2015, 102, 1918-1925.

[5] J. R. Greer, V. S. Deshpande, Three-dimensional architected materials and structures: Design, fabrication, and mechanical behavior, MRS Bulletin, 2019, 44.10, 750-757.

[6] D. Raviv, W. Zhao, C. McKnelly, A. Papadopoulou, A. Kadambi, B. Shi, S. Hirsch, D. Dikovsky, M. Zyracki, C. Olguin, R. Raskar, S. Tibbits, Active printed materials for complex self-evolving deformations, Scientific reports, 2014, 4.1, 1-8.

[7] C. Yuan, D. J. Roach, C. K. Dunn, Q. Mu, X. Kuang, C. M. Yakacki, T. J. Wang, K. Yu and H. J. Qi, 3D printed reversible shape changing soft actuators assisted by liquid crystal elastomers, Soft Matter, 2017, 13.33, 5558-5568.

[8] T. Ching, Y. Li, R. Karyappa, A. Ohno, Y. C. Toh, M. Hashimoto, Fabrication of integrated microfluidic devices by direct ink writing (DIW) 3D printing, Sensors and Actuators B: Chemical, 2019, 297, 126609.

[9] S. Z. Guo, K. Qiu, F. Meng, S. H. Park, M. C. McAlpine, 3D printed stretchable tactile sensors, Advanced Materials, 2017, 29.27, 1701218.

[10] Y. Yang, L. Li, Total volatile organic compound emission evaluation and control for stereolithography additive manufacturing process, Journal of Cleaner Production, 2018, 170, 1268-1278.

[11] W. Xiong, Y. Liu, L. J. Jiang, Y. S. Zhou, D. W. Li, L. Jiang, J. F. Silvain, Y. F. Lu, Laser-directed assembly of aligned carbon nanotubes in three dimensions for multifunctional device fabrication, Advanced Materials, 2016, 28.10, 2002-2009.

[12] J. T. Muth, D. M. Vogt, R. L. Truby, Y. Mengüç, D. B. Kolesky, R. J. Wood, J. A. Lewis, Embedded 3D printing of strain sensors within highly stretchable elastomers. Advanced materials, 2014, 26.36, 6307-6312.

[13] J. Z. Manapat, Q. Chen, P. Ye, R. C. Advincula, 3D printing of polymer nanocomposites via stereolithography, Macromolecular Materials and Engineering, 2017, 302.9, 1600553.

[14] V. Kishore, C. Ajinjeru, A. Nycz, B. Post, J. Lindahl, V. Kunc, C. Duty, Infrared preheating to improve interlayer strength of big area additive manufacturing (BAAM) components, Additive Manufacturing, 2017, 14, 7-12.

[15] Y. S. Rim, S. H. Bae, H. Chen, N. De Marco, Y. Yang, Recent progress in materials and devices toward printable and flexible sensors, Advanced Materials, 2016, 28.22, 4415-4440.

[16] R. D. Goodridge, M. L. Shofner, R. J. Hague, M. McClelland, M. R. Schlea, R. B. Johnson, C. J. Tuck, Processing of a Polyamide-12/carbon nanofibre composite by laser sintering, Polymer Testing, 2011, 30.1, 94-100.

[17] H. Gu, F. AlFayez, T. Ahmed, Z. Bashir, Poly (ethylene terephthalate) powder—a versatile material for additive manufacturing, Polymers, 2019, 11.12, 2041.

[18] F. Guo, S. Aryana, Y. Han, Y. Jiao, A review of the synthesis and applications of polymer–nanoclay composites, Applied Sciences, 2018, 8.9, 1696.

[19] J. R. Tumbleston, D. Shirvanyants, N. Ermoshkin, R. Janusziewicz, A. R. Johnson, D. Kelly, K. Chen, R. Pinschmidt, J. P. Rolland, A. Ermoshkin, E. T. Samulski, and J. M. DeSimone, Continuous liquid interface production of 3D objects, Science, 2015, 347.6228, 1349-1352.

[20] J. T. Muth, D. M. Vogt, R. L. Truby, Y. Mengüç, D. B. Kolesky, R. J. Wood, J. A. Lewis, Embedded 3D printing of strain sensors within highly stretchable elastomers. Advanced materials, 2014, 26.36, 6307-6312.

[21] M. Singh, H. M. Haverinen, P. Dhagat, G. E. Jabbour, Inkjet printing—process and its applications, Advanced materials, 2010, 22.6, 673-685.

[22] C. B. Sweeney, B. A. Lackey, M. J. Pospisil, T. C. Achee, V. K. Hicks, A. G. Moran, B. R. Teipel, M. A. Saed, M. J. Green, Welding of 3D-printed carbon nanotube–polymer composites by locally induced microwave heating, Science advances, 2017, 3.6, e1700262.

[23] K. N. Long, T. F. Scott, H. J. Qi, C. N. Bowman, M. L. Dunn, Photomechanics of light-activated polymers, Journal of the Mechanics and Physics of Solids, 2009, 57.7, 1103-1121.

[24] R. L. Truby, J. A. Lewis, Printing soft matter in three dimensions, Nature, 2016, 540.7633, 371-378.

[25] A. Mokrane, M. H. Boutaous, S. Xin, Process of selective laser sintering of polymer powders: Modeling, simulation, and validation, Comptes Rendus Mécanique, 2018, 346.11, 1087-1103.

[26] H. B. Muralidhara, S. Banerjee, Eds., 3D Printing Technology and Its Diverse Applications, CRC Press, 2021.

[27] M. He, Y. Zhao, B. Wang, Q. Xi, J. Zhou, Z. Liang, 3D printing fabrication of amorphous thermoelectric materials with ultralow thermal conductivity, Small, 2015, 11.44, 5889-5894.

[28] R. Ni, B. Qian, C. Liu, X. Liu, J. Qiu, A cross-linking strategy with moderated pre-polymerization of resin for stereolithography, RSC advances, 2018, 8.52, 29583-29588.

[29] C. A. Chatham, T. E. Long, C. B. Williams, A review of the process physics and material screening methods for polymer powder bed fusion additive manufacturing, Progress in Polymer Science, 2019, 93, 68-95.

[30] Y. H. Cho, I. H. Lee, D. W. Cho, Laser scanning path generation considering photopolymer solidification in micro-stereolithography, Microsystem technologies, 2005, 11.2-3, 158-167.

[31] A. Haleem, M. Javaid, R. Vaishya, 3D printing applications for the treatment of cancer. Clinical Epidemiology and Global Health, 2020, 8.4, 1072-1076.

[32] M. R. Cutkosky, S. Kim, Design and fabrication of multi-material structures for bioinspired robots, Philosophical Transactions of the Royal Society A: Mathematical, Physical and Engineering Sciences, 2009, 367.1894, 1799-1813.

[33] L. R. Meza, A. J. Zelhofer, N. Clarke, A. J. Mateos, D. M. Kochmann, J. R. Greer, Resilient 3D hierarchical architected metamaterials, Proceedings of the National Academy of Sciences, 2015, 112.37, 11502-11507.

[34] S. Park, W. Shou, L. Makatura, W. Matusik, K. K. Fu, 3D printing of polymer composites: Materials, processes, and applications. Matter, 2022, 5.1, 43-76.

[35] D. Kazmer, Three-dimensional printing of plastics, In Applied plastics engineering handbook, 2017, William Andrew Publishing, 617-634.

[36] A. Vashist, A. Vashist, Y. K. Gupta, S. Ahmad, Recent advances in hydrogel based drug delivery systems for the human body, Journal of Materials Chemistry B, 2014, 2.2, 147-166.

[37] H. Yang, W. R. Leow, T. Wang, J. Wang, J. Yu, K. He, D. Qi, C.Wan, X. Chen, 3D printed photoresponsive devices based on shape memory composites, Advanced Materials, 2017, 29.33, 1701627.

[38] S. Y. Wu, C. Yang, W. Hsu, L. Lin, 3D-printed microelectronics for integrated circuitry and passive wireless sensors, Microsystems & Nanoengineering, 2015, 1.1, 1-9.

[39] W. Wu, D. Qi, H. Liao, G. Qian, L. Geng, Y. Niu, J. Liang, Deformation mechanism of innovative 3D chiral metamaterials, Scientific reports, 2018, 8.1, 12575.

[40] V. K. Balla, K. H. Kate, J. Satyavolu, P. Singh, J. G. D. Tadimeti, Additive manufacturing of natural fiber reinforced polymer composites: Processing and prospects, Composites Part B: Engineering, 2019, 174, 106956.

Chapitre III : Polymérisation frontale pour l'accès aux composites

Dans un monde où la réduction des coûts est un objectif constant, les matériaux composites, qui allient légèreté et résistance mécanique élevée, constituent une alternative viable aux matériaux traditionnels tels que les métaux ou les plastiques. Bien que leur champ d'application s'étende de l'aérospatiale aux équipements sportifs haut de gamme, leurs coûts de production élevés semblent être le principal obstacle à un passage universel de l'acier aux matériaux composites. [1-3] Ces dernières années, la plupart des travaux ont été réalisés pour augmenter leur niveau de compétitivité, mais il reste encore beaucoup de progrès à faire pour résoudre ce problème persistant. Aujourd'hui, la polymérisation thermique est la principale méthode de production des matériaux composites. Cela signifie que les réactions ont lieu soit à des températures élevées, nécessitant beaucoup d'énergie, soit à des températures ambiantes, nécessitant peu de contrôle et étant lentes. [4] Les inconvénients techniques de la polymérisation thermique peuvent être surmontés par une évolution vers une procédure entièrement contrôlée par les UV. Il s'agit d'une technologie fiable qui fonctionne à température ambiante et dont les temps de réaction sont de l'ordre de quelques minutes plutôt que de quelques heures. Malgré tous ses avantages, la lumière n'est encore que récemment et très rarement utilisée dans la production de matériaux composites.

1. Les matériaux composites : généralités

Un matériau composite est un matériau hétérogène constitué d'au moins deux composants distincts et non miscibles : une matrice homogène qui assure la cohésion du matériau et un renfort qui lui offre une résistance aux différentes pressions extérieures. Il est ainsi possible d'améliorer les qualités du matériau final, telles que la densité, la résistance à l'abrasion, la conductivité électrique et thermique, la résistance chimique, la rigidité, la résistance mécanique et la résistance à la fatigue. En outre, des additifs peuvent être ajoutés pour modifier les caractéristiques et faciliter la mise en œuvre. [5-6]

Les matériaux composites peuvent être divisés en deux catégories en fonction de la matrice (céramique, métallique ou organique) ou du type de renfort utilisé (fibres, particules, composants structurels), [6] comme le montre la figure ci-dessous.

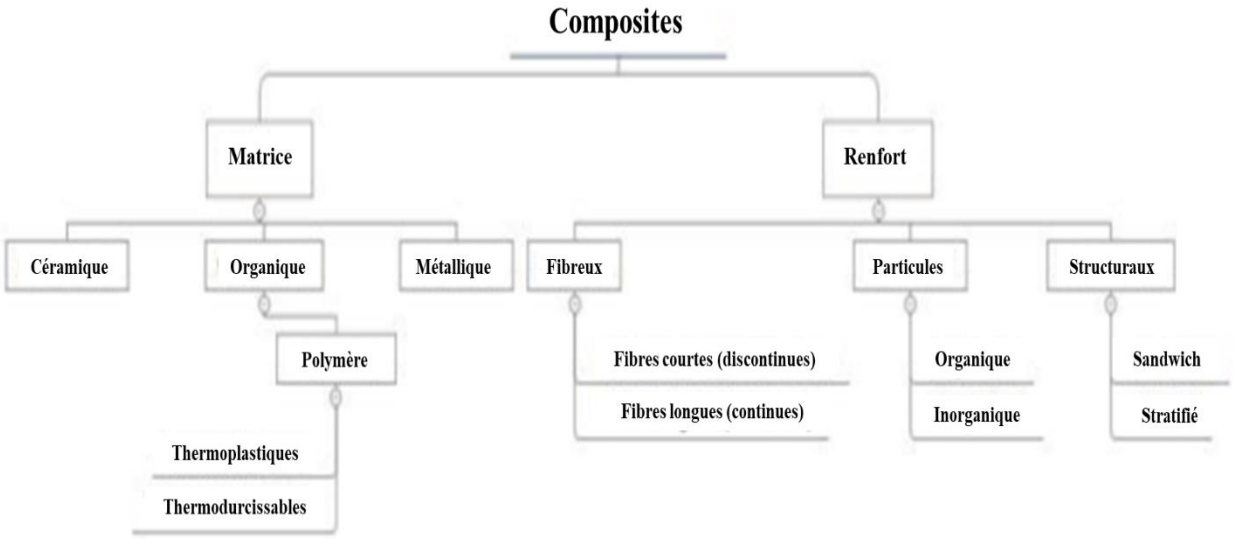

Figure 1. Classification des composites. [6]

2. Classification selon le renfort

2.1. Les composites fibreux

Le matériau industriel le plus utilisé sur le marché, en particulier les polymères renforcés de fibres (FRP fiber reinforced polymers), est employé dans de nombreuses applications, notamment dans l'aérospatiale, l'aviation et l'automobile. Le diamètre et la section (cylindrique ou rectangulaire), l'orientation (unidirectionnelle, bidirectionnelle, multidirectionnelle, aléatoire) et le type de fibre ont tous un impact sur l'efficacité du renforcement par fibres (synthétiques ou naturelles, continues ou discontinues). Le choix se fait en fonction des exigences à satisfaire. La résistance à la traction des fibres est généralement plus connue que leur résistance à la compression. [7-9]

La fibre synthétique la plus utilisée dans les matériaux composites est le verre, reconnu pour sa résistance exceptionnelle, sa flexibilité, sa souplesse et sa résistance chimique. En tant que renfort pour les matériaux utilisés dans la grande distribution, leur faible coût encourage leur utilisation en grand nombre dans la matrice. En raison de leur résistance mécanique extrêmement élevée, de leur module de traction élevé et de leur excellente résistance à l'usure, les fibres de carbone sont également fréquemment employées dans les composites, et elles sont principalement utilisées dans la formulation de matériaux à haute performance. [8-9] Les fibres aramides de type Kevlar constituent une autre option. Comparées à d'autres types de fibres

synthétiques, elles présentent une résistance à la traction et un module élevés, mais un faible allongement à la rupture. [7-10]

Les études sur les fibres naturelles dans les matériaux composites se sont récemment développées en raison des préoccupations environnementales. Malheureusement, les propriétés techniques et mécaniques de ces matériaux (Tableau 1) ne sont pas comparables à celles des matériaux fabriqués à partir de fibres synthétiques. [11]

Tableau 1. Propriétés mécaniques des fibres utilisées dans les matériaux composites. [11]

Fibre	Type	Densité (10^3 kg/m^3)	Élongation (%)	Ténacité (MPa)	Module d'Young (GPa)
Aramide	Synthétique organique	1,4	3,3 - 3,7	3000 - 3450	63 - 67
Kevlar 49	Synthétique organique	1,45	2	2800	124
SiC	Synthétique organique	3,08	0,8	3440	400
Verre E	Synthétique inorganique	2,5	2,5	2000 - 3500	70
Verre S	Synthétique inorganique	2,5	2,8	4570	86
Alumine	Synthétique inorganique	3,95	0,4	1900	379
Carbone	Synthétique inorganique	1,4	1,4 – 1,8	4000	230 - 240
Coton	Naturel	1,5	7,0 - 8,0	287 -597	5,5 – 12,6
Jute	Naturel	1,3	1,5 – 1,8	393 -773	26,5
Lin	Naturel	1,5	2,7 – 3,5	345 -1035	27,6
Chanvre	Naturel	-	1,5	690	-
Ramie	Naturel	-	3,6 – 3,8	400 - 938	61,1 - 128
Sisal	Naturel	1,5	4 -6	511 - 635	9,4 - 22
Coco	Naturel	1,2	30	175	4,0 – 6,0
Bananier	Naturel	1,3	2 - 4	750	29 - 32
Ananas	Naturel	1,56	-	172	62
Huile de palme	Naturel	1,55	-	100 - 400	26,5
Bois	Naturel	1,5	-	1000	40

2.2. Les composites à particules

Dans ce cas, les particules ou les charges ajoutées à la matrice du composite sont destinées à la renforcer, principalement en réduisant la ductilité du matériau et en augmentant son module d'Young. Contrairement aux fibres, les particules confèrent au matériau une résistance et une rigidité dans deux directions en raison de leur géométrie qui est principalement bidimensionnelle (renforcement unidirectionnel). Enfin, les qualités barrière des composites sont améliorées par l'inclusion de particules. [12-14]

Par rapport aux composites à base de fibres, les composites à base de particules offrent un avantage significatif. Des matériaux plus denses peuvent être créés en introduisant des particules en plus grande quantité et en les dispersant plus facilement et plus uniformément. Cela simplifie le recouvrement des particules et nécessite moins de matrice. Les composites renforcés par des particules de verre en sont un exemple. [12] Ils sont plus résistants et plus rigides que le GRFP (glass fiber reinforced polymer), voire plus performants. Contrairement au GRFP, dont les fibres ont une surface assez uniforme, les caractéristiques mécaniques du matériau final peuvent être affectées si la qualité de la surface des particules est médiocre ou présente des défauts. [15]

L'industrie du bâtiment, par exemple, utilise des composites contenant des particules inorganiques. Le béton est un composite composé d'une matrice de ciment et de particules de sable et de gravier pour le renforcement. Pour améliorer la conductivité électrique et thermique, réduire les phénomènes de dilatation thermique et renforcer la résistance à l'usure des composites, des particules métalliques peuvent également être ajoutées à une matrice plastique. [12-13]

Dans les matériaux composites, les particules organiques sont également utilisées comme renfort. La matrice peut être renforcée par l'ajout de microsphères de polymères, telles que des particules sphériques d'époxy ou de phénol. Les matériaux les plus populaires dans cette catégorie sont les particules de carbone et de graphène. [15-16]

2.3. Les composites structuraux

Les composites structuraux stratifiés sont constitués d'au moins deux couches de divers matériaux qui sont collées ensemble et empilées l'une sur l'autre. Les fibres de chaque couche sont alignées de manière unidirectionnelle ou bidirectionnelle avec une orientation variable (0°, 45°, 90°), comme illustré à la Figure 2. Chaque couche est constituée de fibres imprégnées de résine. Une fois de plus, l'objectif est de mélanger les qualités des différents composants pour créer un matériau plus performant. Dans les domaines du sport de haut niveau, de l'automobile, de l'aérospatiale et de l'aviation, ces matériaux de haute performance sont particulièrement appréciés. [15-17]

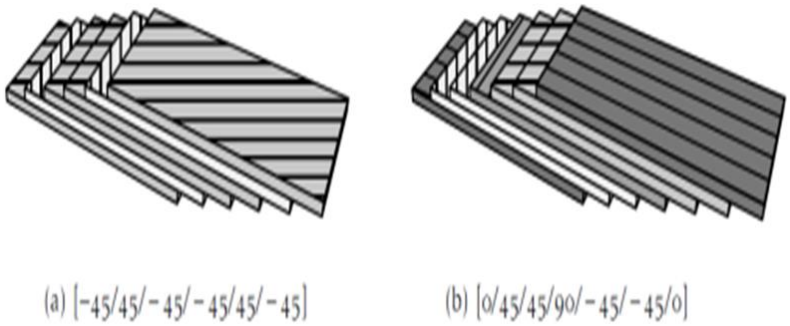

Figure 2. Représentation de différentes structures composites stratifiées. [15]

Les composites structuraux peuvent être organisés en sandwich, en fonction des exigences ou des limites de l'application. Ils se composent alors d'un centre et de deux peaux assemblées par une résine appropriée au système choisi. Les composants utilisés peuvent être en mousse, ondulés ou en nid d'abeille. Grâce à son mode de construction, ce composant du composite est extrêmement résistant aux forces de compression et de cisaillement hors plan. Les peaux garantissent la résistance aux contraintes dans le plan et sont généralement des stratifiés de différents types. Ces matériaux sont également largement utilisés dans les secteurs de l'automobile, de l'aviation et de l'aérospatiale, où ils sont soumis à d'importantes contraintes de flexion et/ou de torsion. [16-18]

3. *Classification selon le renfort*

Le composant du composite qui donne à la substance sa cohésion et sa forme est appelé la matrice. En général, ses propriétés sont médiocres par rapport à celles du renfort. Toutefois, un renfort et une matrice combinés intelligemment peuvent donner des matériaux présentant des caractéristiques mécaniques, thermiques et autres supérieures. Selon le type de matrice, il existe trois grandes familles de composites, comme le montre le système de classification des matériaux composites (Figure 1) :

- les composites à matrice organique ou polymère (CMO / CMP)
- les composites à matrice métallique (MMC)
- Les composites à matrice céramique (CMC)

Les CMO sont constitués d'un renfort et d'une matrice polymère. Il existe deux groupes principaux de polymères : les thermodurcissables (TD) et les thermoplastiques (TP) (Figure 3). Chaque catégorie possède des caractéristiques uniques qui permettent de produire des matériaux utilisés dans diverses applications industrielles. [18-20]

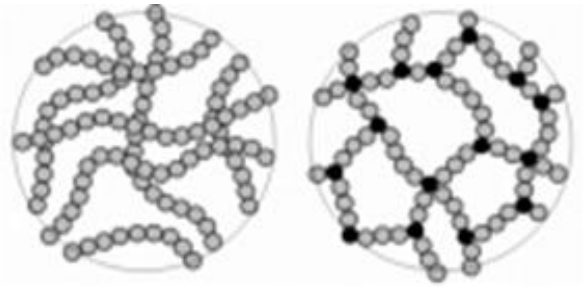

Figure 3. Représentation schématique de l'organisation des chaînes de polymères dans un réseau thermoplastique (à gauche) et un réseau thermodurcissable (à droite). [17]

4. Photopolymérisation des composites : limites et difficultés

Le passage à un processus entièrement contrôlé par la lumière pourrait constituer une alternative viable au polymérisation thermique et permettre de résoudre bon nombre des problèmes énergétiques et écologiques. Il s'agit en effet d'une technologie fiable qui fonctionne à température ambiante et dont les temps de réaction durent quelques minutes plutôt que quelques heures. [4] Malgré tous les avantages qu'elle présente, l'utilisation de la lumière pour fabriquer des pièces en matériaux composites est récente et encore très limitée.

En présence de charge, l'intensité lumineuse traversant la résine composite est réduite. Par conséquent, l'intensité de la lumière est atténuée et l'efficacité de la polymérisation correspondante est réduite à mesure que la profondeur augmente. En général, de nombreux facteurs affectent le processus de photopolymérisation, notamment la diffusion de la lumière, l'absorption de la lumière, la distribution des charges, la forme et la taille des charges, etc. Par conséquent, pour obtenir un matériau composite présentant de bonnes propriétés mécaniques et de bonnes fonctionnalités, ces enjeux doivent être étudiés et résolus.

4.1. Absorption de la lumière

L'amorçage de la photopolymérisation est basée sur l'absorption de photons par les amorceurs pour générer des espèces réactives. Cependant, les photoamorceurs utilisés sont normalement colorés et doivent avoir une bonne capacité d'absorption de la lumière. Ainsi, la présence de pigments et la génération d'espèces réactives font que la lumière peut être principalement absorbée à la surface supérieure, ce qui signifie que plus la capacité d'absorption est élevée, plus la pénétration de la lumière dans la formulation photosensible est faible, en particulier en profondeur. Par conséquent, lorsqu'un photoamorceur est utilisé, il convient de maintenir un équilibre entre la teneur correspondante et la performance d'absorption de la lumière dans la formulation photosensible. [21-22]

Les charges absorbent ou diffusent également la lumière pendant la photopolymérisation. Avec l'ajout de charges dans la résine, une compétition a lieu en termes d'absorption ou diffusion de la lumière entre le photoamorceur et les charges. En général, cette compétition conduit à un processus de photopolymérisation moins efficace. Normalement, les charges blanches absorbent peu ou pas du tout la lumière, mais lorsque la couleur de la charge est foncée voire noire, l'absorption de la lumière est très évidente. Par exemple, en tant que matériau de recherche très populaire, le graphène a une très bonne capacité d'absorption de la lumière. Lorsque le graphène est ajouté à la formulation, la pénétration de la lumière peut être facilement bloquée et lorsque la teneur en graphène dépasse une certaine quantité, elle interfère avec le durcissement de la résine. [22-25]

4.2. Diffusion de la lumière et indice de réfraction

La photopolymérisation est un processus dynamique, ce qui signifie que l'état de la résine photosensible passe de la phase liquide à la phase solide avec le temps sous l'effet de l'irradiation lumineuse. Au cours de ce processus, la réticulation ou la gélification et la vitrification du composite peuvent normalement avoir des effets négatifs sur l'indice de réfraction de la résine photosensible et la modification de la diffusion de la lumière, ce qui entraîne une détérioration des propriétés optiques de la matrice de résine. Simultanément, la nature exothermique de la réaction de photopolymérisation provoque un changement transitoire de l'indice de réfraction de la résine en raison d'un changement de densité. [23-25]

La capacité des matériaux à diffuser la lumière est liée à la différence d'indice de réfraction entre le polymère et la charge. Au cours du processus de photopolymérisation, l'indice de réfraction du polymère augmente en raison de l'augmentation de la densité et de la réduction de la polarisabilité, tandis que l'indice de réfraction des charges reste constant. Par conséquent, leur inadéquation augmente ou diminue, en fonction de leurs valeurs initiales. Lorsque l'indice de réfraction initial du monomère est inférieur à celui de la charge, le décalage de l'indice de réfraction diminue au cours du processus de photopolymérisation, ce qui entraîne une augmentation progressive de la transmission de la lumière. De même, si l'indice de réfraction initial du monomère est plus élevé que celui de la charge, la photopolymérisation ultérieure augmente le décalage de l'indice de réfraction, ce qui diminue progressivement la transmission. [24]

En outre, il est également possible que l'indice de réfraction initial du monomère soit égal à celui de la charge et qu'il continue à augmenter par la suite. [24]

4.3. Influence de la charge sur la transmission de la lumière

Comme indiqué ci-dessus, la réduction de la transmission de la lumière peut être liée à l'absorption de la lumière par le photoamorceur et la charge, ainsi qu'à la diffusion de la lumière et la différence d'indices de réfraction entre le monomère et la charge. En outre, la forme géométrique, la taille et le contenu des charges ont également un effet considérable sur la transmission ou la pénétration de la lumière au cours du processus de photopolymérisation. [26-27]

En général, la présence de charges, a un effet négatif sur la transmission de la lumière ; plus il y a de charges, plus la transmission de la lumière est faible. Cela s'explique par le fait qu'une grande quantité de charges peut bloquer le chemin de la lumière et entraîner par conséquent une plus faible pénétration de la lumière. Simultanément, lorsque de nombreuses charges sont ajoutées à la résine, la transparence de la formulation est également réduite de manière significative. [25-27]

Normalement, la taille des charges peut avoir une influence sur la quantité de lumière qui passe à travers le composite à base de résine pendant la période d'irradiation. Les charges de plus grandes tailles créent une zone d'ombre plus importante ce qui peut entraîner une faible transmission de la lumière. [27]

4.4. Autres problèmes

En plus des difficultés principalement décrites ci-dessus, de nombreuses autres peuvent être observées, telles que la présentation de l'interface ou de la zone d'interphase (espace ou formation de bulles) entre la charge et la matrice polymère, la mauvaise distribution de la nanocharge dans la formulation (dépôt facile de la charge, agglomérat de la charge), et une viscosité élevée, etc. Normalement, ces problèmes sont dus à l'inadéquation entre la charge et le polymère et aux propriétés physiques de la charge. Normalement, les nanotubes de carbone (NTC) ont une échelle nanométrique avec une grande surface, en raison des rapports d'aspect supérieurs à 1000. [28-30]

Pour les microparticules, une distribution homogène peut être facilement obtenue dans la matrice. Toutefois, lorsque les NTC sont placés dans le même volume de matrice, il est difficile de disperser les particules individuelles de manière égale en raison de leur échelle nanométrique. En outre, compte tenu de la mauvaise répartition dans la matrice, la grande surface des NTC entraîne également la présence d'une grande interface ou d'une zone d'interphase entre la charge et la matrice polymère. [29-30]

5. *Polymérisation frontale : pour un accès efficace aux composites*

La polymérisation frontale (FP), étudiée depuis plusieurs années, est une solution efficace face aux obstacles rencontrés lors d'un processus de photopolymérisation classique. C'est une réaction auto-entretenue, dans laquelle un stimulus initial (par exemple, la lumière) induit une zone de réaction localisée, appelée "front de polymérisation". La chaleur dégagée par la polymérisation exothermique dans cette zone fournit une augmentation de température suffisante pour amorcer une polymérisation supplémentaire à la limite entre le polymère et les phases de monomères non réagies, ce qui entraîne souvent une propagation de la réaction. Cet aspect frontal du processus de polymérisation est particulièrement important dans la photopolymérisation (et la réticulation) de matériaux épais (millimètre-centimètre). [31-34]

La FP a trouvé un intérêt croissant dans de nombreuses applications. Ainsi, sa capacité à polymériser des échantillons épais avec différentes charges jusqu'à 50 % en poids par l'application locale d'une portion raisonnable d'énergie rend cette approche de polymérisation très prometteuse. Elle est utilisée en lithographie, en prototypage rapide, dans les revêtements et dans bien d'autres domaines. [31-33]

Le principe de fonctionnement de la polymérisation frontale photo-induite (FPP) est assez différent de la polymérisation frontale thermique traditionnelle (TPF). Dans l'approche classique, le système chauffé subit une polymérisation auto-catalytique qui est la somme des effets thermiques du système. En revanche, la FPP n'est pas entièrement auto-catalytique. Le front solide est créé après photopolymérisation, et il est déplacé par une exposition continue aux rayons UV. En raison de ces propriétés, la FPP est aujourd'hui une méthode intéressante dans le processus de fabrication. [35-38]

Il est important que le processus de propagation soit lui-même exothermique, de sorte que des effets thermiques peuvent également se produire dans le FPP. Il a été rapporté que plus le processus d'amorçage et de polymérisation est rapide, plus l'augmentation de la température pendant la FPP est importante. Cela se traduit par une accélération encore plus grande du front qui s'enfonce dans la formulation. Cet effet est très actif au cours des premières étapes du processus et disparaît lorsque le front franchit un certain point critique auquel le rayonnement UV parvient, ce qui ralentit l'ensemble du processus. Toutefois, il convient de rappeler que si cet effet peut être bénéfique, dans une FPP contrôlée, il peut conduire à une situation dans laquelle, après l'arrêt de la source de rayonnement, le processus de polymérisation lui-même se poursuit pendant un certain temps, ce qui est appelé "heat rush" (ruée vers la chaleur). [37-39]

Il existe également une approche qui combine les techniques de polymérisation frontale thermique et photochimique. Dans la polymérisation thermique frontale (TFP), après le démarrage du système, il n'y a pratiquement aucune possibilité de contrôler le processus. En outre, la température du front de propagation thermique peut atteindre plus de 200 °C, ce qui entraîne la création de bulles ou même une dégradation de la matrice organique. Les bulles apparaissant dans le mélange réactionnel peuvent entraîner une rupture du front de propagation en raison d'une conversion très faible du monomère. Ces inconvénients peuvent être surmontés grâce aux systèmes de polymérisation thermique frontale photo-induite. Deux types d'amorceurs sont introduits dans le système : le photoamorceur et l'amorceur thermique. [37-38]

Lors de l'exposition de l'échantillon à la lumière, le photoamorceur se clive et démarre le processus de polymérisation. La chaleur créée pendant la polymérisation photo-induite entraîne le clivage de l'amorceur thermique, des radicaux sont créés et le processus s'accélère (Figure 4). La vitesse de polymérisation peut également être contrôlée par des changements d'intensité lumineuse. [37-38]

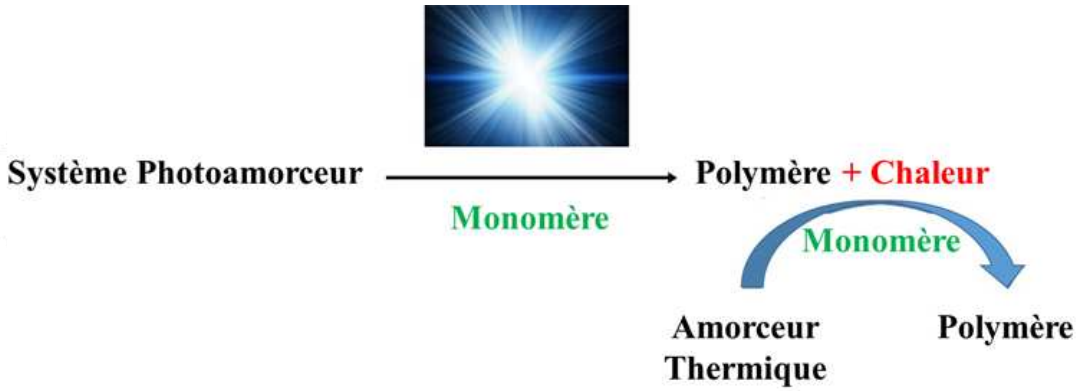

Figure 4. Représentation de l'approche adoptée combinant un système photoamorceur et un amorceur thermique.

Lors du choix d'un amorceur pour le FPP, il est nécessaire de prêter attention à plusieurs aspects importants. Tout d'abord, il convient de choisir le type d'amorceur approprié pour le système d'amorçage. L'amorceur doit absorber la lumière émise par la source tout en présentant une capacité de photoblanchiment afin de ne pas couvrir les rayons lumineux en profondeur pour que le front solide puisse se propager davantage. La sélection de la concentration du photoamorceur joue également un rôle clé. La concentration choisie doit permettre une pénétration profonde du rayonnement lumineux ; simultanément, elle doit fonctionner efficacement, en créant un nombre suffisant de radicaux. [35-37]

Références

[1] R. M. Jones, Mechanics of composite materials, CRC press, 2018.

[2] T. P. Sathishkumar, S. Satheeshkumar, J. Naveen, Glass fiber-reinforced polymer composites - A review, Journal of Reinforced Plastics and Composites, 2014, 33, 1258–1275.

[3] S. S. Yao, F. L. Jin, K. Y. Rhee, D. Hui, S. J. Park, Recent advances in carbon-fiber-reinforced thermoplastic composites: A review, Composites Part B: Engineering, 2018, 142, 241-250.

[4] M. R. Sanjay, G. R. Arpitha, L. L. Naik, K. Gopalakrishna, B. J. N. R. Yogesha, Applications of natural fibers and its composites: An overview, Natural Resources, 2016, 7.3, 108-114.

[5] S. Ahmed, F. R. Jones, A review of particulate reinforcement theories for polymer composites, Journal of materials science, 1990, 25, 4933-4942.

[6] S. Ray, A. J. Easteal, Advances in polymer-filler composites: Macro to nano, Materials and manufacturing processes, 2007, 22.6, 741-749.

[7] L. Gornet, Généralités sur les matériaux composites, 2008.

[8] J. P. Jose, K. Joseph, Advances in polymer composites: macro-and microcomposites–state of the art, new challenges, and opportunities, Polymer composites, 2012, 1-16.

[9] K. Van de Velde, P. Kiekens, Thermoplastic polymers: overview of several properties and their consequences in flax fibre reinforced composites, Polymer testing, 2001, 20.8, 885-893.

[10] A. Vitale, M. Sangermano, R. Bongiovanni, P. Burtscher, N. Moszner, Visible light curable restorative composites for dental applications based on epoxy monomer, Materials, 2014, 7.1, 554-562.

[11] D. Işın, N. Kayaman-Apohan, A. Güngör, Preparation and characterization of UV-curable epoxy/silica nanocomposite coatings, Progress in Organic Coatings, 2009, 65.4, 477-483.

[12] M. Atif, R. Bongiovanni, J. Yang, Cationically UV-cured epoxy composites, Polymer Reviews, 2015, 55.1, 90-106.

[13] A. Ashori, Wood–plastic composites as promising green-composites for automotive industries!, Bioresource technology, 2008, 99.11, 4661-4667.

[14] R. Karnani, M. Krishnan, R. Narayan, Biofiber-reinforced polypropylene composites, Polymer Engineering & Science, 1997, 37.2, 476-483.

[15] V. K. Lindroos, M. J. Talvitie, Recent advances in metal matrix composites, Journal of Materials Processing Technology, 1995, 53.1-2, 273-284.

[16] S. Prashanth, K. M. Subbaya, K. Nithin, S. Sachhidananda, Fiber reinforced composites-a review, Journal of Material Sciences and Engineering, 2017, 6.03, 2-6.

[17] S. M. Rangappa, S. Siengchin, H. N. Dhakal, Green-composites: Ecofriendly and sustainability, Applied Science and Engineering Progress, 2020, 13.3, 183-184.

[18] S. V. Joshi, L. T. Drzal, A. K. Mohanty, S. Arora, Are natural fiber composites environmentally superior to glass fiber reinforced composites?, Composites Part A: Applied science and manufacturing, 2004, 35.3, 371-376.

[19] Q. T. Shubhra, A. M. Alam, M. A. Quaiyyum, Mechanical properties of polypropylene composites: A review. Journal of thermoplastic composite materials, 2013, 26.3, 362-391.

[20] B. D. Agarwal, L. J. Broutman, Analysis and performance of fiber composites Second edition, John Wiley & Sons, 1990.

[21] L. Musanje, B. W. Darvell, Curing-light attenuation in filled-resin restorative materials, Dental Materials, 2006, 22.9, 804-817.

[22] H. Arikawa, T. Kanie, K. Fujii, H. Takahashi, S. Ban, Effect of filler properties in composite resins on light transmittance characteristics and color, Dental materials journal, 2007, 26.1, 38-44.

[23] A. Ogunyinka, W. M. Palin, A. C. Shortall, P. M. Marquis, Photoinitiation chemistry affects light transmission and degree of conversion of curing experimental dental resin composites, Dental Materials, 2007, 23.7, 807-13.

[24] S. M. Lim, B. S. Shin, K. Kim, Characterization of products using additive manufacturing with graphene/photopolymerresin nano-fluid, Journal of Nanoscience and Nanotechnology, 2017, 17.8, 5492-5495.

[25] S. L. d. A. Hernández, S. Fernández-Villamarín, Y. Ballesteros, J. C. D. Real, N. J. Dunne, E. Paz, 3D Printing of a Graphene-Modified Photopolymer Using Stereolithography for Biomedical Applications: A Study of the Polymerization Reaction, International Journal of Bioprinting, 2022, 8.1.

[26] L. Breuer, M. Raue, M. Kirschbaum, T. Mang, M. J. Schöning, R. Thoelen, T. Wagner, Light-controllable polymeric material based on temperature-sensitive hydrogels with incorporated graphene oxide, physica status solidi (a), 2015, 212.6, 1368-1374.

[27] M. Shibayama, S. Ozeki, T. Norisuye, Real-time dynamic light scattering on gelation and vitrification, Polymer, 2005, 46 .7, 2381-2388.

[28] B. Howard, N. D. Wilson, S. M. Newman, C. S. Pfeifer, J. W. Stansbury, Relationships between conversion, temperature and optical properties during composite photopolymerization, Acta Biomaterialia, 2010, 6.6, 2053-2059.

[29] M. Par, D. Marovic, H. Skenderovic, O. Gamulin, E. Klaric, Z. Tarle, Light transmittance and polymerization kinetics of amorphous calcium phosphate composites, Clinical Oral Investigations, 2017, 21.4, 1173-1182.

[30] M. Taira, M. Okazaki, J. Takajashi, Studies on optical properties of two commercial visible-light-cured composite resins by diffuse reflectance measurements, Journal of Oral Rehabilitation, 1999, 26, 329–337.

[31] F. Petko, A. Świeży, J. Ortyl, Photoinitiating systems and kinetics of frontal photopolymerization processes–the prospects for efficient preparation of composites and thick 3D structures, Polymer Chemistry, 2021, 12.32, 4593-4612.

[32] Q. Li, H. X. Shen, C. Liu, C. F. Wang, L. Zhu, S. Chen, Advances in frontal polymerization strategy: from fundamentals to applications, Progress in Polymer Science, 2022, 101514.

[33] J. A. Pojman, V. M. Ilyashenko, A. M. Khan, Free-radical frontal polymerization: Self-propagating thermal reaction waves, Journal of the Chemical Society, Faraday Transactions, 1996, 92.16, 2825-2837.

[34] J. T. Cabral, S. D. Hudson, C. Harrison, J.F. Douglas, Frontal photopolymerization for microfluidic applications, Langmuir, 2004, 20.23, 10020-10029.

[35] A. Vitale, M. G. Hennessy, O. K. Matar, J. T. Cabral, Interfacial profile and propagation of frontal photopolymerization waves, Macromolecules, 2015, 48.1, 198-205.

[37] M. Retailleau, A. Ibrahim, X. Allonas, Dual-cure photochemical/thermal polymerization of acrylates: a photoassisted process at low light intensity, Polymer Chemistry, 2014, 5.22, 6503-6509.

[38] D. P. Gary, S. Bynum, B. D. Thompson, B. R. Groce, A. Sagona, I. M. Hoffman, C. Morejon-Garcia, C. Weber, J. A. Pojman, Thermal transport and chemical effects of fillers on free-radical frontal polymerization, Journal of Polymer Science, 2020, 58.16, 2267-2277.

[39] M. Belk, K. G. Kostarev, V. Volpert, T. M. Yudina, Frontal photopolymerization with convection, The Journal of Physical Chemistry B, 2003, 107.37, 10292-10298.

Partie II : Systèmes Photoamorceurs Multicomposants

Table des matières

TABLE DES MATIÈRES

PARTIE II : SYSTÈMES PHOTOAMORCEURS MULTICOMPOSANTS

Introduction

La photopolymérisation peut être utilisée dans une variété de domaines allant des industries traditionnelles (par exemple, les revêtements, les encres et les adhésifs) aux industries de haute précision (par exemple, la biomédecine et la microélectronique). La formulation photosensible contient un oligomère, un diluant, un système photoamorceur et d'autres additifs fonctionnels. [1-3] Les systèmes photoamorceurs comprennent généralement un photoamorceur et un coamorceur, qui requièrent des qualités désirables telles qu'une absorption élevée dans la région spectrale des émissions de la lampe et une photoréactivité élevée. [2-3] Il est important de comprendre la relation entre amorceur et coamorceur, car toute connaissance peut clairement guider la recherche de nouveaux systèmes photoamorceurs efficaces dans les matériaux photopolymérisables.

Un grand nombre de systèmes photoamorceurs à deux composants ont été développés parce que les colorants et les additifs appropriés sont facilement disponibles en ce qui concerne le transfert d'électrons, le transfert d'électron/proton ou le transfert direct d'hydrogène. Cependant, le transfert d'électron en retour et la recombinaison des radicaux diminuent la concentration potentielle des centres actifs (radicaux libres) dans les systèmes photoamorceurs à deux composants, ce qui entraîne de nombreuses limitations cinétiques. [4-6]

La capacité de photoamorçage des systèmes photoamorceurs à deux composants est remarquablement améliorée par l'ajout d'un troisième additif pour pallier le manque de photoréactivité des systèmes photoamorceurs traditionnels, Le système photoamorceur à trois composants comprend trois ingrédients : un composé absorbant la lumière, un accepteur d'électron et un donneur d'électrons. Les mécanismes des systèmes photoamorceurs à trois composants, tels que colorant/amine/sel de d'iodonium (Iod), colorant/composé bromo/Iod, colorant/amine/maléimide et colorant/sel de borate/dérivé de triazine, peuvent être résumés en deux catégories. La première est le mécanisme en série parallèle, dans lequel le co-amorceur réagit indépendamment avec le colorant excité, et le nombre de radicaux libres formés dépend de la réactivité de chaque co-amorceur à l'état excité. Deuxièmement, deux des trois composants réagissent d'abord ensemble, et le troisième composant réagit avec l'un des photoproduits. Les radicaux libres sont formés par la conversion des co-amorceurs et des colorants dans leur forme réduite ou oxydée. Le colorant à l'état fondamental est alors récupéré et peut participer à d'autres photoréactions, et une véritable réaction cyclique à la lumière se produit avant que les réactifs ne soient complètement consommés. [6-8]

Références

[1] J. P. Fouassier, J. Lalevée, Photoinitiators: Structures, Reactivity and Applications in Polymerization, Wiley, Weinhein, 2021.

[2] Y. Yagci, S. Jockusch, N. J. Turro, Photoinitiated polymerization: advances, challenges, and opportunities, Macromolecules, 2010, 43, 6245-6260.

[3] K. Dietliker, T. Jung, J. Benkhoff, H. Kura, A. Matsumoto, H. Oka, D. Hristova, G. Gescheidt, G. Rist, New developments in photoinitiators, Macromolecular Symposia. Weinheim : WILEY-VCH Verlag, 2004, 217.1, 77-98.

[4] J. Kabatc, J. Pączkowski, One Photon− Two Free Radical Photoinitiating Systems. Novel Approach to the Preparation of Dissociative, Multicomponent, Electron-Transfer Photoinitiators for Free Radical Polymerization, Macromolecules, 2005, 38.24, 9985-9992.

[5] J. Zhang, M. Frigoli, F. Dumur, P. Xiao, L. Ronchi, B. Graff, F. Morlet-Savary, J. P. Fouassier, D. Gigmes, J. Lalevée, Design of Novel Photoinitiators for Radical and Cationic Photopolymerizations under Near UV and Visible LEDs (385, 395, and 405 nm), Macromolecules, 2014, 47.9, 2811-2819.

[6] X. Allonas, J. P. Fouassier, H. Obeid, M. Kaji, Y. Ichihashi, New Multi-Component Photoinitiating Systems based on Bisimidazole Derivative, Proceedings of RadTech Asia, 2005.

[7] J. Kabatc, K. Jurek, Free radical formation in three-component photoinitiating systems, Polymer, 2012, 53.10, 1973-1980.

[8] J. P. Fouassier, F. Morlet-Savary, J. Lalevée, X. Allonas, C. Ley, Dyes as photoinitiators or photosensitizers of polymerization reactions, Materials, 2010, 3.12, 5130-5142.

Chapitre I : Photoamorceurs Type II à base de biscarbazoles

L'étude des dérivés de carbazole en tant que photoamorceurs (PA) de haute performance pour l'amorçage des processus de polymérisation radicalaire (FRP) et cationique (CP) dans des conditions d'irradiation à la lumière visible est le sujet principal de ce chapitre. L'un des principaux objectifs de cette étude est d'introduire les diodes électroluminescentes (LEDs) en tant que sources d'irradiation sûres et accessibles. Cet objectif sera fortement soutenu tout au long du travail de cette thèse. Dans un premier temps, un aperçu général sur les carbazoles sera donné, puis le contenu de ce chapitre sera présenté de manière plus approfondie.

Depuis plusieurs années, et compte tenu du fait que les familles classiques de photoamorceurs UV ne sont pas adaptées à la conception de photoamorceurs pour la lumière visible, même après des travaux étendus en ingénierie chimique, de nouvelles familles de composés, et en particulier de colorants, qui n'ont jamais été explorées dans le contexte de la photopolymérisation, sont désormais testées de manière classique par les polymeristes. Si l'on considère que les photoamorceurs de lumière visible doivent absorber fortement dans le domaine visible, être chimiquement stables et que ces composés doivent également être capables d'être réduits ou oxydés dans une gamme électrochimique acceptable, tous les colorants organiques examinés dans l'électronique organique (cellules solaires organiques, diodes électroluminescentes organiques, transistors à effet de champ organiques) sont des candidats potentiels pour la photoamorçage. [1-5]

Dans ce domaine, le carbazole est un exemple représentatif. Cette structure symétrique extrêmement bon marché a été largement étudiée en électronique organique en raison de sa remarquable capacité à donner des électrons, de son faible potentiel d'oxydation et de sa facilité de modification chimique, de sorte qu'une large gamme de matériaux de transport de trous, de verres moléculaires ou de matériaux émettant de la lumière a été conçue avec le carbazole. Étant donné que les colorants push-pull peuvent être facilement synthétisés avec ce donneur d'électrons, le carbazole était également un excellent candidat pour la conception de matériaux de collecte de la lumière pour les cellules solaires, et de nombreux colorants présentant des coefficients d'extinction molaire élevés et des spectres d'absorption larges ont été obtenus avec ce donneur d'électrons planaire. [6-10]

PARTIE II : SYSTÈMES PHOTOAMORCEURS MULTICOMPOSANTS

Le carbazole est une structure polyaromatique comprenant deux cycles de benzène fusionnés de part et d'autre d'un cycle à cinq chaînons contenant de l'azote. La position centrale de l'atome d'azote permet de produire des formes de résonance avec une délocalisation électronique s'étendant sur les deux cycles aromatiques. Grâce à la présence de l'amine, l'atome d'azote peut être fonctionnalisé avec des chaînes d'alkyle pour améliorer la solubilité des photoamorceurs. La préparation de sels de carbazolium est également possible par quaternisation de l'amine. Les positions 3- et 6- du carbazole peuvent également être facilement fonctionnalisées avec divers groupes tels que l'aldéhyde, les halogènes et les groupes nitro, de sorte qu'une extension de la conjugaison ou l'introduction de divers groupes peut être effectuée. Parallèlement à la modification du noyau carbazole, le carbazole est également un groupe polyaromatique riche en électrons qui peut être utilisé pour la conception de sels de ferrocénium, ces complexes de fer étant préparés par échange de ligands sur le ferrocène. [11-15]

Une étude approfondie sur plusieurs séries de dérivés de carbazole a été accomplie tout en se focalisant sur leur capacité à amorcer les processus de polymérisation, leur aptitude à réagir en tant que catalyseurs photoredox, et éventuellement leur application dans la génération des motifs en 3D avec une épaisseur allant jusqu'à 2.2 mm dans un temps d'irradiation très court (< 1 min) et avec une très haute résolution spatiale, ainsi que dans la synthèse des composites ayant une excellente profondeur de durcissement. Ce chapitre sera divisé en deux sections présentées sous forme d'articles après de brèves introductions de chacun d'eux.

Références

[1] C. Dietlin, S. Schweizer, P. Xiao, J. Zhang, F. Morlet-Savary, B. Graff, J. P. Fouassier, J. Lalevée, Photopolymerization upon LEDs: New photoinitiating systems and strategies, Polymer Chemistry, 2015, 6.21, 3895-3912.

[2] P. Xiao, J. Zhang, F. Dumur, M. A. Tehfe, F. Morlet-Savary, B. Graff, D. Gigmes, J. Lalevée, Visible light sensitive photoinitiating systems: Recent progress in cationic and radical photopolymerization reactions under soft conditions, Progress in Polymer Science, 2015, 41, 32-66.

[3] N. Corrigan, J. Yeow, P. Judzewitsch, J. Xu, C. Boyer, Seeing the Light: Advancing Materials Chemistry through Photopolymerization, Angewandte Chemie International Edition, 2019, 58, 5170–5189.

[4] J. P. Fouassier, J. Lalevée, Photoinitiators: Structures, Reactivity and Applications in Polymerization, Wiley, Weinhein, 2021.

[5] Y. Yagci, S. Jockusch, N. J. Turro, Photoinitiated polymerization: advances, challenges, and opportunities, Macromolecules, 2010, 43, 6245-6260.

[6] J. Lalevée, J. P. Fouassier, Dye Photosensitized Polymerization Reactions: Novel Perspectives, RSC Photochemistry Reports, Ed. A. Albini, E. Fasani, Photochemistry, London, UK, 2015, 215–232.

[7] F. Dumur, Recent advances on carbazole-based photoinitiators of polymerization, European Polymer Journal, 2020, 125, 109503.

[8] M. Sangermano, G. Malucelli, A. Priola, S. Lengvinaite, J. Simokaitiene, J. V. Grazulevicius, Carbazole derivatives as photosensitizers in cationic photopolymerization of clear and pigmented coatings, European polymer journal, 2005, 41.3, 475-480.

[9] W. Liao, Q. Liao, Y. Xiong, Z. Li, H. Tang, Design, synthesis and properties of carbazole-indenedione based photobleachable photoinitiators for photopolymerization. Journal of Photochemistry and Photobiology A: Chemistry, 2023, 435, 114297.

[10] F. Dumur, L. Beouch, S. Peralta, G. Wantz, F. Goubard, D. Gigmes, Solution-processed blue phosphorescent OLEDs with carbazole-based polymeric host materials, Organic Electronics, 2015, 25, 21–30.

[11] G. Sathiyan, E.K.T. Sivakumar, R. Ganesamoorthy, R. Thangamuthu, P. Sakthivel, Review of carbazole based conjugated molecules for highly efficient organic solar cell application, Tetrahedron Letters, 2016, 57, 243–252.

[12] W. J. Kuo, G. H. Hsiue, R. J. Jeng, All Organic NLO Sol-Gel Material Containing a One-Dimensional Carbazole Chromophore, Macromolecular Chemistry and Physics, 2001, 202, 1782–1790.

[13] A. Al Mousawi, F. Dumur, P. Garra, J. Toufaily, T. Hamieh, B. Graff, D. Gigmes, J.P. Fouassier, J. Lalevée, Carbazole Scaffold Based Photoinitiator/Photoredox Catalysts: Toward New High Performance Photoinitiating Systems and Application in LED Projector 3D Printing Resins, Macromolecules, 2017, 50, 2747–2758.

[14] K. Kawamura, Y. Aotani, H. Tomioka, Photoinduced intramolecular electron transfer between carbazole and bis (trichloromethyl)-s-triazine generating radicals, The Journal of Physical Chemistry B, 2003, 107.19, 4579-4586.

[15] C. Xu, S. Gong, X. Wu, Y. Wu, Q. Liao, Y. Xiong, Z. Li, H. Tang, High-efficient carbazole-based photo-bleachable dyes as free radical initiators for visible light polymerization, Dyes and Pigments, 2022, 198, 110039.

PARTIE II : SYSTÈMES PHOTOAMORCEURS MULTICOMPOSANTS

Section 1 : 5,12-Dihydroindolo[3,2-a] carbazole : un chromophore prometteur pour le développement de photoamorceurs de polymérisation à la lumière visible

Le but de cette section est orienté vers le développement d'un couple de dérivés de carbazole, qui se caractérisent par des coefficients d'extinction molaire élevés dans le visible, en tant que photoamorceurs (PAs) à caractère polyvalent pour l'amorçage des réactions de polymérisation (radicalaire-FRP et cationique-CP) photoinduites par des dispositifs d'irradiation visible douce sûrs et économiques (diode électroluminescente (LED) à 405 nm), en présence de sel d'iodonium).

L'utilisation de ces dérivés en tant que catalyseurs photoredox (PCs) dans les procédés de photopolymérisation a été soulignée pour la première fois. De même, de très faibles concentrations en photoamorceur sont suffisantes pour amorcer efficacement le processus de polymérisation, assurant par conséquent une moindre toxicité dans la formulation. Notons que 0.2% de carbazoles proposés est une quantité assez suffisante en présence de 1% du sel d'iodonium pour amorcer efficacement la polymérisation d'une résine acrylique ou époxy. D'excellents résultats ont été obtenus en présence des différents systèmes testés à base de carbazoles du fait que ces dérivés combinent des potentiels d'oxydation appropriés à l'état excité, des variations d'énergie libre très favorables (ΔG_{et}) et une bonne absorbance sous la LED à 405 nm. Une image complète des mécanismes photochimiques impliqués est fournie. Et éventuellement, la production des polymères en 3D sous une diode laser à 405 nm a été également accomplies en présence de ces carbazoles. La synthèse de ce couple de carbazoles a été faite par nos collaborateurs de l'Université de Aix-Marseille (Dr. Frédéric Dumur). Ce travail a été publié dans "European polymer journal" sous la citation suivante : Hammoud F. et al. "5, 12-Dihydroindolo [3, 2-a] carbazole: A promising scaffold for the design of visible light photoinitiators of polymerization." European Polymer Journal 162 (2022): 110880, et est présenté à cette suite.

European Polymer Journal 162 (2022) 110880

Contents lists available at ScienceDirect

European Polymer Journal

journal homepage: www.elsevier.com/locate/europolj

5,12-Dihydroindolo[3,2-a]carbazole: A promising scaffold for the design of visible light photoinitiators of polymerization

Fatima Hammoud [a,b,c], Akram Hijazi [c], Sylvain Duval [d], Jacques Lalevée [a,b,*], Frédéric Dumur [e,*]

[a] Université de Haute-Alsace, CNRS, IS2M UMR 7361, F-68100 Mulhouse, France
[b] Université de Strasbourg, France
[c] EDST, Université Libanaise, Campus Hariri, Hadath, Beyrouth, Liban
[d] Université de Lille, CNRS, Centrale Lille, ENSCL, Univ. Artois, UMR 8181 - UCCS - Unité de Catalyse et Chimie du Solide, F-59000 Lille, France
[e] Aix Marseille Univ, CNRS, ICR UMR7273, F-13397 Marseille France

ARTICLE INFO

Keywords:
Carbazole
Photopolymerization
Dyes
Asymmetric substitution

ABSTRACT

5,12-Dihydroindolo[3,2-*a*]carbazole is a polycyclic structure combining in its scaffold two carbazole moieties sharing a fused aromatic ring. Since the pioneering works reported in 2019 on this structure concerning the substitution of the two carbazoles by similar functional groups, no recent investigation has been devoted to asymmetrize the substitution of the two carbazoles. In this work, a series of 13 compounds based on the 5,12-dihydroindolo[3,2-*a*]carbazole scaffold is presented. By carefully controlling the reaction conditions, functional groups such as a formyl, a nitro or an acetyl group could be selectively introduced on one of the two carbazoles. By combining X-ray diffraction and 2D NMR experiments, the higher reactivity of one of the two carbazoles could be clearly evidenced, enabling to generate asymmetrically substituted structures. Thanks to this unprecedented approach on the 5,12-dihydroindolo[3,2-*a*]carbazole scaffold, the absorption of the resulting dyes could be shifted towards the visible range whereas the parent structure (5,12-dihexyl-6,7-diphenyl-5,12-dihydroindolo [3,2-*a*]carbazole) exhibits a strongly UV-centered absorption. In light of their visible light absorption properties, several dyes have been examined as photoinitiators of polymerization activable at 405 nm and under low light intensity in two-component photoinitiating systems for the free radical polymerization of acrylates or the cationic polymerization of epoxides. Chemical mechanisms supporting the different polymerization processes have been fully elucidated by combining several techniques including cyclic voltammetry, UV–visible absorption and photoluminescence spectroscopy as well as photolysis experiments.

1. Introduction

During the last decades, carbazole which is a tricyclic aromatic heterocyclic compound comprising two aromatic rings fused on either side of a five-membered ring bearing a nitrogen as a ring hetero atom has been the focus of intense research efforts.[1] Interest for carbazole is notably supported by the different applications in which this poly-aromatic structure is involved including Organic Electronics (Organic Light-Emitting Diodes (OLEDs),[2–7] Organic Photovoltaics (OPVs), [8–10] Organic Field Effect Transistors (OFETs)),[11–13] Non Linear Optics[14–17] to compounds exhibiting biological activities (antimicrobial, antiepileptic, anti-inflammatory, antihistaminic, antidiarrheal, antitumor, analgesic and neuroprotective properties),[18] solid state emitters for two-photon imaging[19] and photoinitiators of polymerization.[20] From a photophysical viewpoint, carbazole is characterized by a wide bandgap[21] and a high triplet energy level [22,23] which has been advantageously used for the design of hosts materials for triplet emitters for OLEDs, enabling to prevent back energy transfer from the triplet emitters to the host.[24] Carbazole is also extensively used for the design of polymeric hosts for OLEDs and, in this field, the most representative polymer is undoubtedly poly(*N*-vinyl-carbazole) (PVK)[25] which exhibits a good film-forming ability, a high morphological stability and a high thermal decomposition temperature. [26] When used as photoinitiators of polymerization, carbazole was notably used as an electron donor for the design of push–pull dyes, [27–32] as a π-conjugated spacer to connect pyrenes or triphenylamines [33], enabling to generate polyaromatic structures of extended π-conjugation,[31] but also as a basis for the design of helicenes[34] or

* Corresponding authors at: Université de Haute-Alsace, CNRS, IS2M UMR 7361, F-68100 Mulhouse, France (J. Lalevée).
E-mail addresses: Jacques.lalevee@uha.fr (J. Lalevée), frederic.dumur@univ-amu.fr (F. Dumur).

https://doi.org/10.1016/j.eurpolymj.2021.110880
Received 4 October 2021; Received in revised form 30 October 2021; Accepted 13 November 2021
Available online 17 November 2021

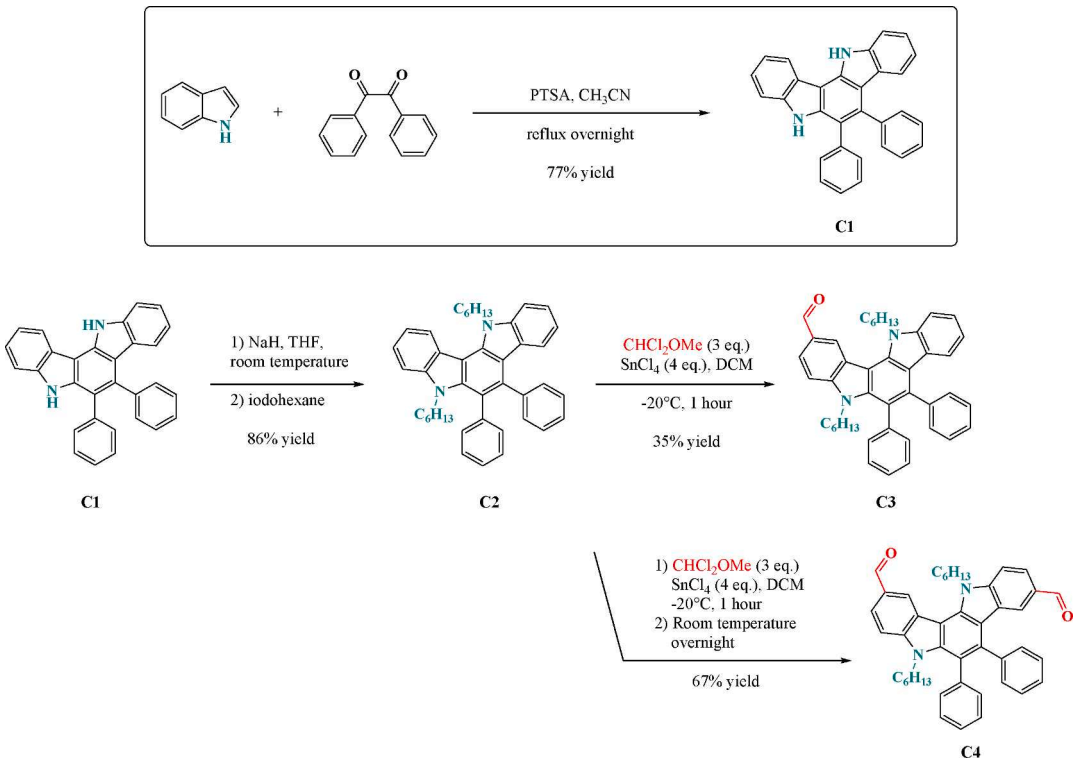

Scheme 1. Synthetic route to **C1-C4**.

benzophenone derivatives.[35] Beyond the absorption property which is one of the key parameter governing the polymerization efficiency, migratability of photoinitiators within the polymer is another major issue that can adversely affect the potential use of polymers, especially for applications such as food packaging[36–38] or different biological applications[39]. In fact, photopolymerization constitutes an efficient and environmentally friendly approach to prepare polymers for food packaging. However, photoinitiators are often small molecules that can migrate in the foodstuff, even if not necessarily harmful. This migration is undesirable and the subject of various legislative requirements. To address these issues, the development of macrophotoinitiators constitutes an efficient strategy. Indeed, the bigger the photoinitiator is, the more difficult the migration of photoinitiators within the polymer network is. In order to meet these requirements, oligomeric photoinitiators have notably been proposed.[40,41] Another efficient strategy consists in introducing crosslinkable functional groups onto photoinitiators.

However, if this strategy is appealing to reduce the migratability of small molecules, it also requires the photoinitiators to be chemically modified, what can constitute a challenge for certain photoinitiators. [42–48] When the synthesis of macrophotoinitiators is privileged as the option, in order to maximize the photoinitiating ability of macrophotoinitiators while minimizing the non-photoinitiating portion of the molecules, the combination of well-known photoinitiators within a unique molecule constitutes an efficient strategy. In this field, a relevant example has been proposed with truxene, which has notably been substituted with acridine-1,8-diones,[49] DMPA (2,2′-dimethoxy-2-phenyl acetophenone)[50] or pyrene.[51] By electronic coupling of the molecular orbitals of the truxene central core with that of the peripheral groups, a major enhancement of the molar extinction coefficients could be obtained, enabling to reduce the photoinitiator content. With aim at developing macromolecular photoinitiators based on carbazole, 5,12-dihydroindolo[3,2-a]carbazole which comprises two carbazole units sharing a fused aromatic ring is a perfect candidate. This structure, reported for the first time in 2019,[52] has notably been studied for its regioselective *bis*(acetylation) and *bis*(formylation) at the C2,9-positions. To date, no asymmetrically substituted derivatives of this structure (5,12-dihydroindolo[3,2-a]carbazole) have been reported yet. It has to be noticed that asymmetrically substituted carbazoles have already been reported in the literature as visible light photoinitiators of polymerization, but not on *bis*-carbazole structures. Thus, push–pull dyes based on carbazole have been reported as soon as 2013. [53] Final monomer conversions of 55% and 45% could respectively be obtained during the cationic polymerization of (3,4-epoxycyclohexane)methyl 3,4-epoxycyclohexylcarboxylate (EPOX) and the free radical polymerization of trimethylolpropane triacrylate (TMPTA) upon irradiation at 473 nm of photocurable resins comprising three-component carbazole/NVK/Ph_2I^+ photoinitiating systems (where NVK and Ph_2I^+ stand for *N*-vinylcarbazole and diphenyliodonium hexafluorophosphate).[54] While using indane-1,3-dione-based push–pull dyes, a TMPTA conversion of 58% could be obtained using three-component carbazole/NVK/Ph_2I^+ photoinitiating systems upon irradiation at 457 nm. Nitration of carbazole constitutes an efficient strategy to red-shift the absorption spectra of carbazole and this strategy was notably reported with a series of four dyes in 2017.[32] Interestingly, the four carbazole derivatives could be used photoredox catalysts and comparison of the photoinitiating abilities of the four dyes with that of *bis*(2,4,6-trimethylbenzoyl)phenylphosphine oxide (BAPO) revealed the four dyes to outperform BAPO at 405 nm. Thus, by using two-component carbazole/(*t*-Bu)Ph_2I^+ photoinitiating systems (where (*t*-Bu)Ph_2I^+ stands for *bis*-(4-*tert*-butylphenyl)iodonium hexafluorophosphate), final monomer conversions ranging between 50 and 76% could be obtained during the cationic polymerization of EPOX, contrarily to 15% for BAPO/iodonium in the same irradiation conditions. Asymmetrically substituted carbazoles of extended aromaticities were also examined in 2017 as photoinitiators activable at 405 nm for the cationic polymerization of EPOX [29]. In this series, an EPOX conversion of 57% could be obtained with a naphthalene-based dye while using two-component carbazole/(*t*-Bu)Ph_2I^+ photoinitiating systems. As interesting feature, colourless coatings could be obtained with this series of dyes, the carbazole derivatives being designed with weak electron-acceptors enabling to get high molar extinction coefficients at 405 nm while maintaining a low absorption

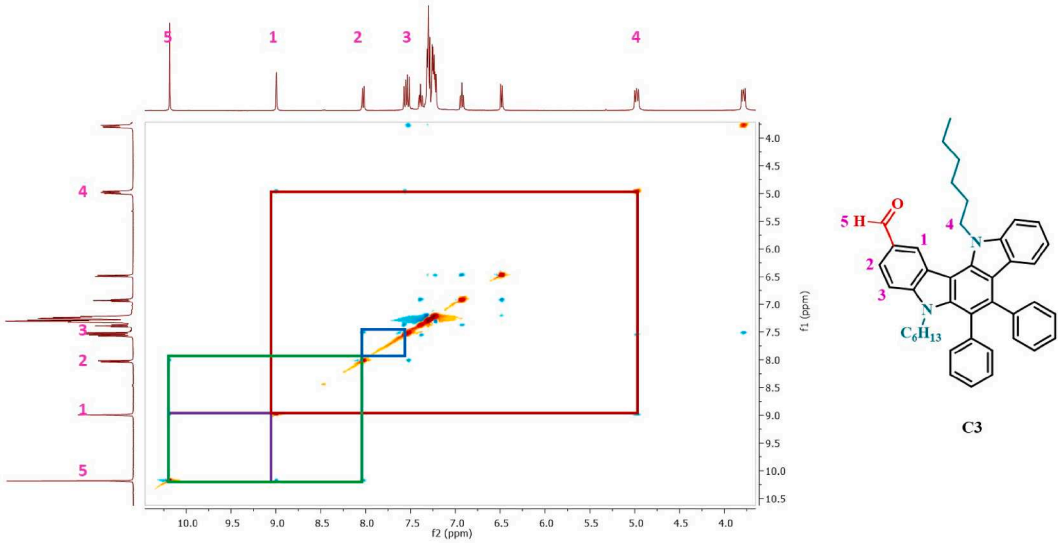

Fig. 1. NOESY spectrum of **C3** recorded in $CDCl_3$ as the deuterated solvent.

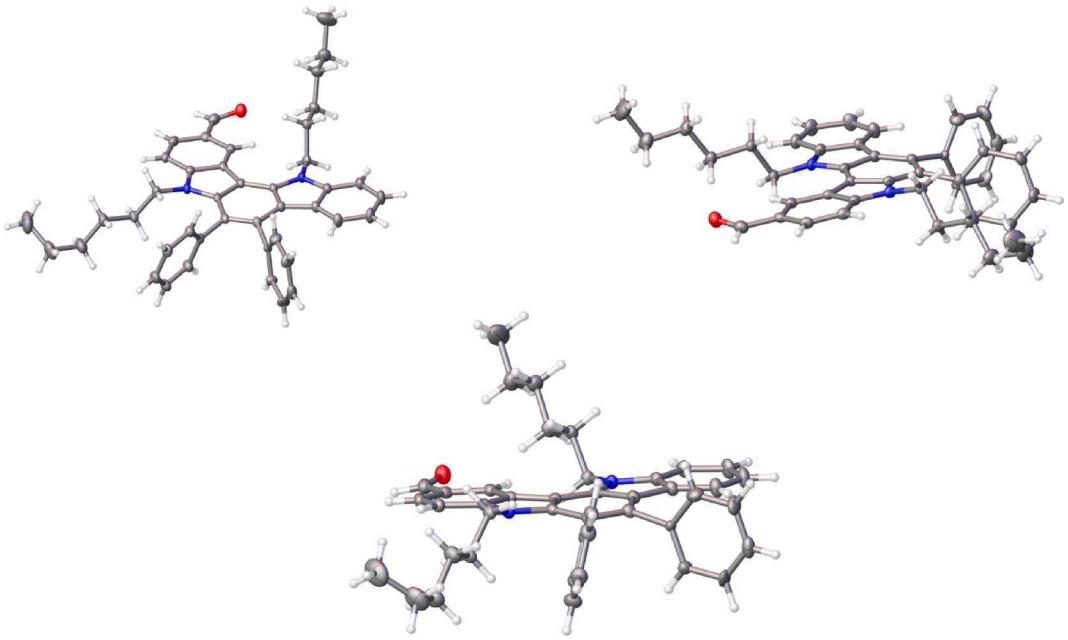

Fig. 2. Crystal structure of **C3**.

beyond 420 nm. Similar performances were obtained for dyes based on 1,4-dimethyl-9*H*-carbazole.[30] In this case, best performances were obtained for a formyl-substituted carbazole and an EPOX conversion of 48% using two-component carbazole/(*t*-Bu)Ph_2I^+ photoinitiating systems at 405 nm. Once again, the formyl-substituted carbazole could outperform BAPO as iodonium sensitizer (15% conversion at 405 nm). While substituting carbazole with a BODIPY, polymerization reactions could be initiated with near-infrared lights, demonstrating the versatility of the carbazole scaffold for designing photoinitiating activable between 400 and 1100 nm.[55] In this work, a series of 5,12-dihydroindolo[3,2-*a*]carbazole derivatives asymmetrically substituted with different functional groups such as formyl, acetyl or nitro groups have been designed and synthesized. The different syntheses revealed the functionalization of the C2-position to be easier than the C9-position. By mean of this asymmetric substitution, dyes absorbing beyond 400 nm could be obtained. To evidence the interest of these new structures, photopolymerization experiments have been carried out upon irradiation at 405 nm.

2. Experimental part

2.1. Synthesis of the different dyes

For this study, 5,12-dihexyl-6,7-diphenyl-5,12-dihydroindolo[3,2-*a*] carbazole **C2** was selected as the parent structure. Notably, hexyl chains were selected to provide a sufficient solubility to this polyaromatic structure. It can be synthesized in one step, by alkylation of 6,7-diphenyl-5,12-dihydroindolo[3,2-a]carbazole **C1** that was prepared in one step by an acid-catalyzed cycloaddition of two equivalents of indole with benzil, according to a procedure previously reported in the literature (See Scheme 1).[56] Interestingly, formylation of **C2** by mean of the Rieche method[57,58] that consists in treating **C2** with 1,1-dichloromethyl methyl ether in the presence of tin tetrachloride ($SnCl_4$) only furnished after one hour of reaction at −20 °C 5,12-dihexyl-6,7-

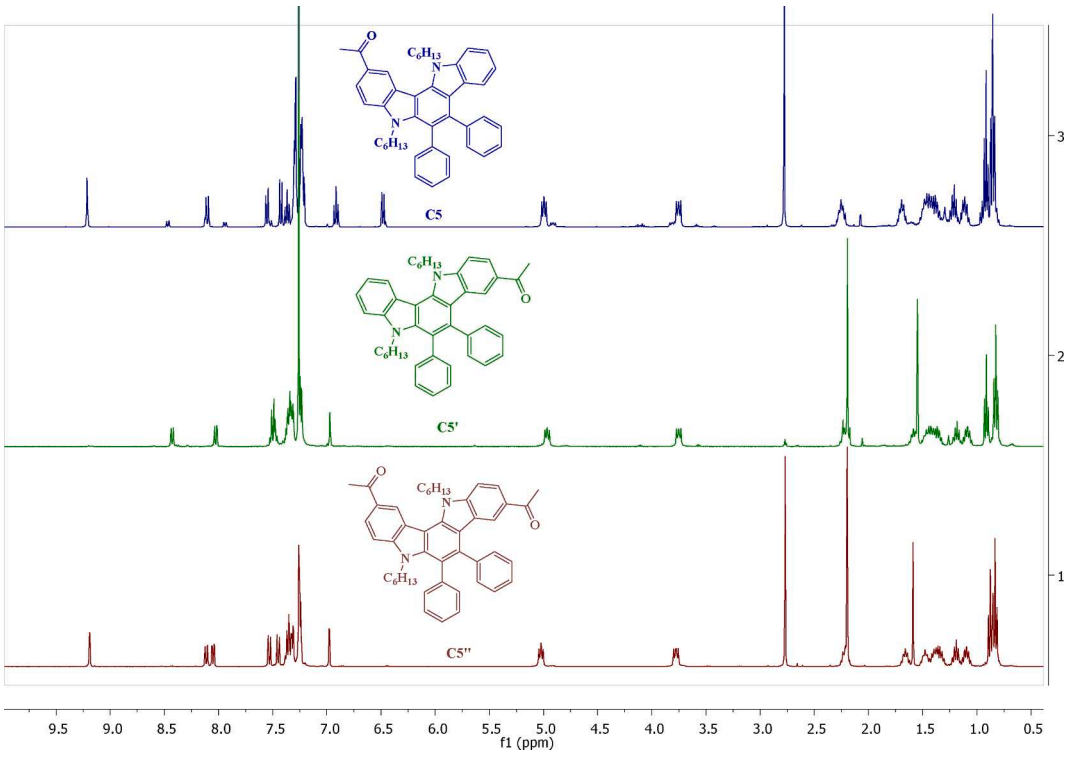

Fig. 3. ^{1}H NMR spectra of **C5**, **C5′** and **C5″** recorded in chloroform.

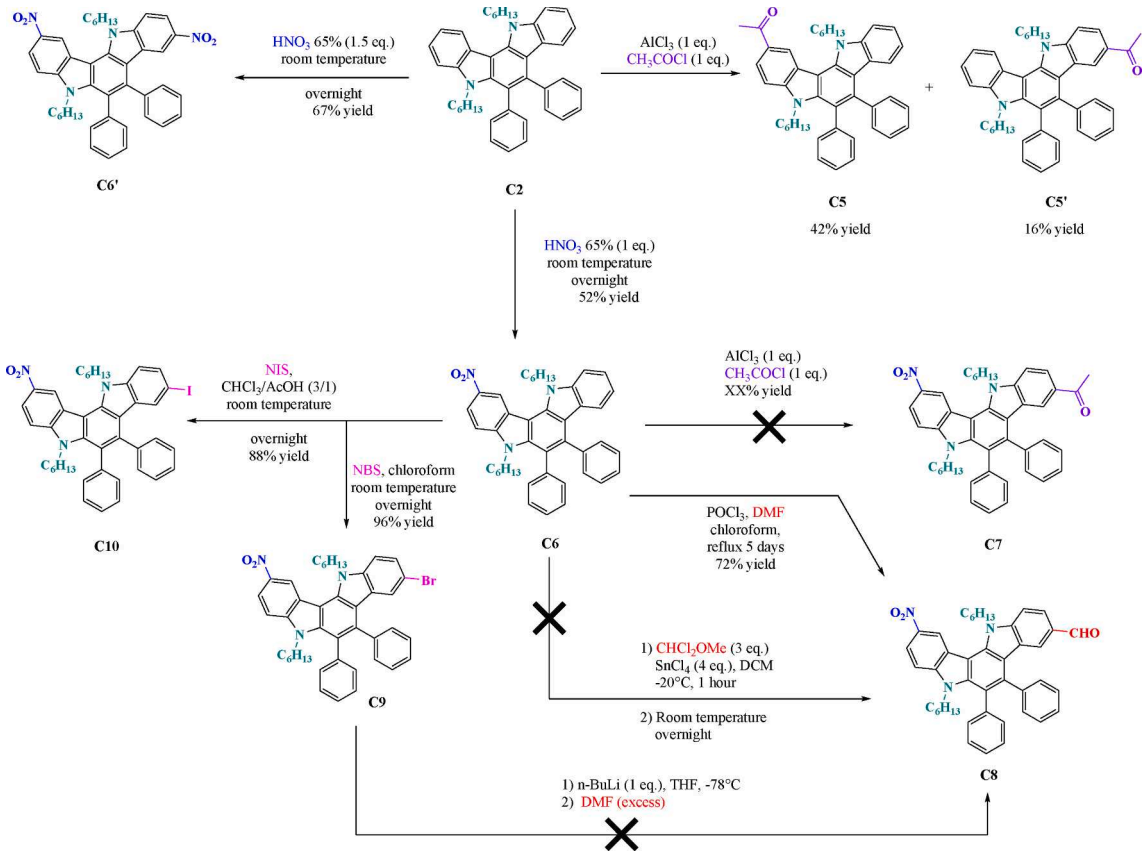

Scheme 2. Synthetic routes to **C5-C10**.

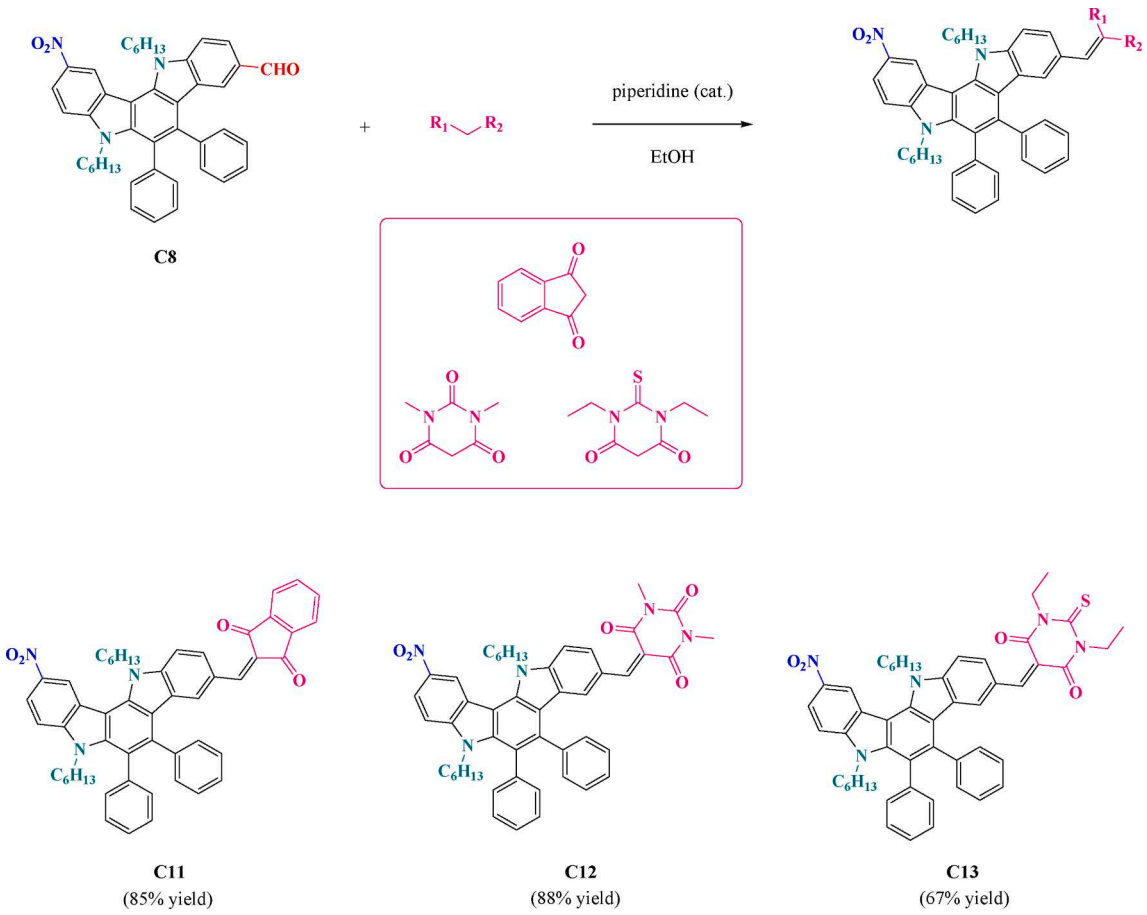

Scheme 3. Chemical structures of push–pull dyes **C11-C13** prepared with **C8** as the electron donor.

diphenyl-5,12-dihydroindolo[3,2-*a*]carbazole-2-carbaldehyde **C3** in moderate yield (35%), the rest corresponding to the unreacted starting compound **C2**. Conversely, by performing the reaction in the same conditions, but by stirring the solution at room temperature overnight, 5,12-dihexyl-6,7-diphenyl-5,12-dihydroindolo[3,2-*a*]carbazole-2,9-dicarbaldehyde **C4** could be selectively prepared in 67% yield.

In order to determine on which position (C2 or C9-positions) the formyl group was introduced on **C3**, 2D NMR experiments were carried out. As shown on the NOESY spectrum presented in the Fig. 1, a NOESY peak could be clearly identified between the aromatic proton (proton 1) at 9.00 ppm adjacent to the formyl peak (10.19 ppm, proton 5) and the CH_2 group at 4.98 ppm (proton 4). It could thus be concluded that the formyl group was introduced at the C2-position. Indeed, if introduced at the C9 position, no through space interaction could occur with any of the CH_2 groups of the alkyl chains. By slow evaporation of chloroform, crystals of **C3** could be obtained, confirming the previous assignment done by NMR spectroscopy (See Fig. 2).

Following these initial attempts, the possibility to selectively introduce other groups than a formyl group was examined. Notably, an acetyl group could be selectively introduced on **C5** in 42% yield while realizing a Friedel-Craft reaction with one equivalent of acetyl chloride at room temperature overnight. However, formation of the second regioisomer **C5′** could also be evidenced. This isomer could only be obtained in 16% yield. As shown in the Fig. 3, clear difference could be seen on their ^{1}H NMR spectra. Thus, if the acetyl group for the regioisomer at the C2-position could be detected at 2.78 ppm, conversely, a shift as high as 2.5 ppm could be demonstrated for the regioisomer at the C9-position, the acetyl group being detected at 2.19 ppm. Interestingly, comparison with the ^{1}H NMR spectrum of 1,1′-(5,12-dihexyl-6,7-diphenyl-5,12-dihydroindolo[3,2-*a*]carbazole-2,9-diyl)*bis*(ethan-1-one) **C5″** revealed the positions of the acetyl groups to be at similar positions to that of the *bis*-substituted compound **C5″**. Thus, acetyl groups are respectively detected at 2.77 and 2.20 ppm.

Similarly, by use of one equivalent of HNO_3 65% and by stirring the solution at room temperature overnight, **C6** could be obtained in 52% yield. Interestingly, the nitro-derivative could be easily separated from **C2** by precipitation in diethyl ether, providing **C6** as an orange powder. All attempts to improve the reaction by elongating the reaction time or by slightly increasing the number of equivalents of HNO_3 65% only produced *the* bis-functionalized compound **C6‘**. Considering that **C6** could be obtained in reasonable yield and that its colour was indicative of a strong absorption in the visible range, the introduction of functional groups that could be later used for generating push–pull dyes or Suzuki cross-coupling reaction was examined. Thus, attempt to perform a Friedel-Craft reaction with acetyl chloride did not provide the targeted product **C7** and only a mixture of compounds that could not be separated was obtained. Similarly, the Rieche method ($SnCl_4$, 1,1-dichloromethyl methyl ether) applied on **C6** only furnished after treatment the initial product **C6**. Conversely, the Vilsmeier-Haack reaction applied to **C6** could provide **C8** in 72% yield after five days of reflux in chloroform (See Scheme 2). Halogenation of **C6** was also examined. Thus, bromination of **C6** with one equivalent of *N*-bromosuccinimide furnished **C9** in 96% yield respectively. Similarly, by using *N*-iodosuccinimide, **C10** could be obtained in 88% yield. Interestingly, all attempts to convert **C9** as **C8** using the standard procedure *n*-BuLi/DMF failed.

With aim at developing dyes strongly absorbing in the visible range with **C8**, push–pull dyes which consist in connecting a strong electron donor to an electron acceptor by mean of a π-conjugated spacer was examined. Especially, these dyes exhibit an intense absorption band corresponding to the intramolecular charge transfer band so that these

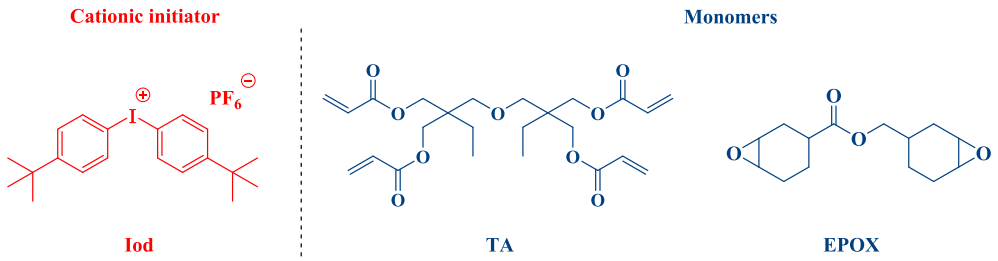

Scheme 4. Chemical structures of monomers and additives used in this study.

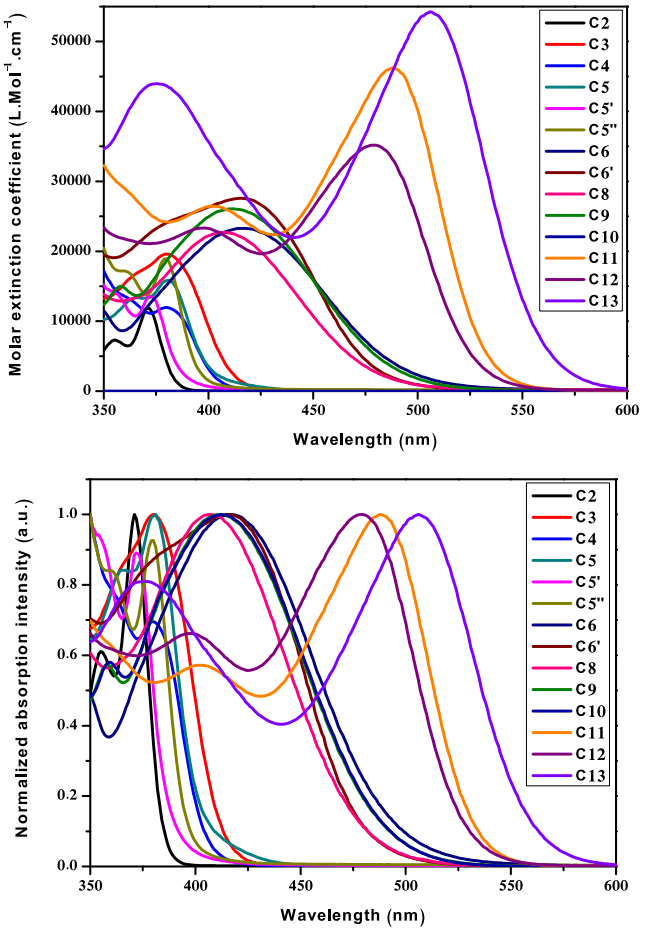

Fig. 4. UV visible absorption spectra of different dyes in chloroform. top: molar extinction coefficient. bottom: normalized absorption.

dyes can be advantageously used as visible light photoinitiators of polymerization. Even if numerous electron acceptors exist, only benchmark acceptors were examined in this study, namely, indane-1,3-dione, 1,3-dimethylbarbituric acid and 1,3-diethylthiobarbituric acid. The different Knoevenagel reactions could be carried out using ethanol as the solvent and piperidine as the catalyst. However, it has to be noticed that contrarily to the classical conditions of Knoevenagel reactions consisting in introducing both the aldehyde and the electron accepting group in stoichiometric conditions, three equivalents of electron accepting group had to be used in order to improve the reaction yield. Similar, a large excess of base had to be used and the reaction had to be maintained at reflux overnight. Using this procedure, all dyes **C11-C13** could be prepared with reaction yields ranging from 67% for **C13** to 88% for **C12** respectively (See Scheme 3).

2.2. Other chemicals compounds

Bis-(4-*tert*-butylphenyl)iodonium hexafluorophosphate (Iod; Speed-Cure 938) was obtained from Lambson Ltd (UK). The monomers ((3,4-epoxycyclohexane)methyl 3,4-epoxycyclohexylcarboxylate (EPOX) and di(trimethylolpropane)tetraacrylate (TA)) were obtained from Allnex. Chemical structures of monomers and additives are shown in the Scheme 4.

2.3. Irradiation source

The following light-emitting diode (LED) was used as the irradiation source: LED@405 nm with an incident light intensity at the sample surface: $I_0 = 110$ mW.cm^{-2}.

2.4. UV–visible absorption and photolysis experiments

The UV–visible absorption properties of the different compounds as well as the steady state photolysis experiments were studied using a JASCO V730 UV–visible spectrometer.

2.5. Photopolymerization kinetics (RT-FTIR)

The experimental conditions for each photosensitive formulation are indicated in the caption of the figures. All the polymerizations were performed at room temperature and the irradiation was started at t = 10 s. The weight content of the photoinitiating system is calculated from the monomer content. The photoinitiator concentrations in each photosensitive formulation have been chosen to ensure good light absorption at 405 nm. The conversion of the acrylate functions of TA and the epoxide functions of EPOX were continuously followed by real time FTIR spectroscopy (JASCO FTIR 4100). For the thin samples (~25 μm of thickness), the photosensitive formulations were deposited on polypropylene films under air for the cationic polymerizations of EPOX while the free radical polymerizations of TA were performed in laminate (the

Table 1
Optical characteristics of different dyes in chloroform as the solvent.

Compounds	C2	C3	C4	C5	C5′	C5″	C6
λ (nm)	370	380	379	380	372	380	417
ε ($M^{-1}.cm^{-1}$)	12,000	19,500	11,800	15,900	13,500	18,800	23,500
Compounds	**C6′**	**C8**	**C9**	**C10**	**C11**	**C12**	**C13**
λ (nm)	417	408	412	412	489	479	505
ε ($M^{-1}.cm^{-1}$)	27,500	22,700	25,900	17,400	42,600	34,900	54,100

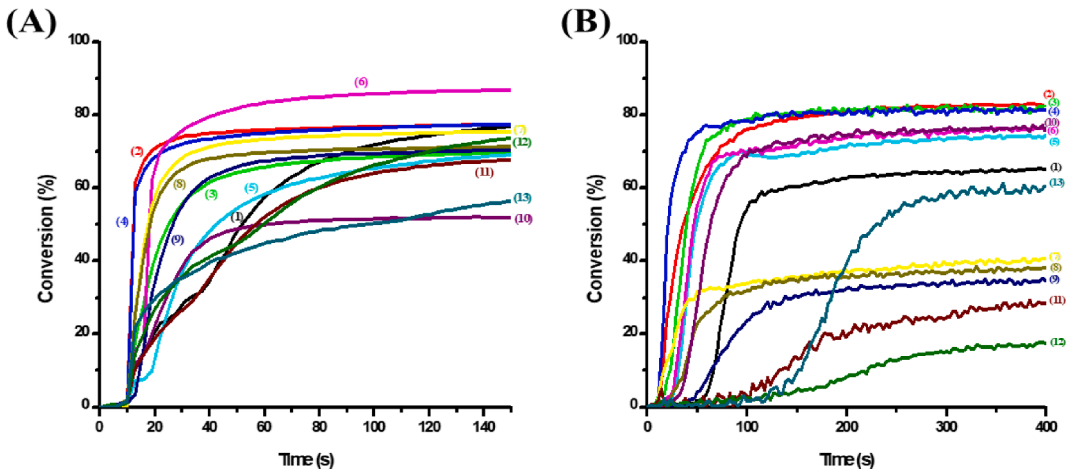

Fig. 5. (A) Polymerization profiles of TA (acrylate function conversion vs. irradiation time) in laminate (thickness = 25 μm) upon exposure to LED light λ = 405 nm in the presence of two-component photoinitiating systems: (1) **C2**/Iod (0.2%/1% w/w); (2) **C3**/Iod (0.2%/1% w/w); (3) **C4**/Iod (0.2%/1% w/w); (4) **C5**/Iod (0.2%/1% w/w); (5) **C5′**/Iod (0.2%/1% w/w); (6) **C5″**/Iod (0.2%/1% w/w); (7) **C6**/Iod (0.2%/1% w/w); (8) **C6′**/Iod (0.2%/1% w/w); (9) **C8**/Iod (0.2%/1% w/w); (10) **C9**/Iod (0.2%/1% w/w); (11) **C11**/Iod (0.2%/1% w/w); (12) **C12**/Iod (0.2%/1% w/w); and (13) **C13**/Iod (0.2%/1% w/w); respectively. The irradiation starts at t = 10 s. (B) Polymerization profiles of TA (acrylate function conversion vs. irradiation time) under air (thickness = 1.4 mm) upon exposure to LED light λ = 405 nm in the presence of two-component photoinitiating systems: (1) **C2**/Iod (0.2%/1% w/w); (2) **C3**/Iod (0.2%/1% w/w); (3) **C4**/Iod (0.2%/1% w/w); (4) **C5**/Iod (0.2%/1% w/w); (5) **C5′**/Iod (0.2%/1% w/w); (6) **C5″**/Iod (0.2%/1% w/w); (7) **C6**/Iod (0.2%/1% w/w); (8) **C6′**/Iod (0.2%/1% w/w); (9) **C8**/Iod (0.2%/1% w/w); (10) **C9**/Iod (0.2%/1% w/w); (11) **C11**/Iod (0.2%/1% w/w); (12) **C12**/Iod (0.2%/1% w/w); and (13) **C13**/Iod (0.2%/1% w/w); respectively. The irradiation starts at t = 10 s.

Table 2
Final acrylate function conversion (FCs) for TA using Dyes/Iod (0.2%/1% w/w) as photoinitiating systems, after 100 s of irradiation with the LED emitting at 405 nm.

	Thin sample (25 μm) in laminate PI/Iod (0.2%/1% w/w)	Thick sample (1.4 mm) under air PI/Iod (0.2%/1% w/w)
C2	77%	66%
C3	77%	83%
C4	70%	82%
C5	77%	81%
C5′	69%	75%
C5″	87%	76%
C6	75%	40%
C6′	71%	38%
C8	70%	34%
C9	52%	77%
C11	68%	28%
C12	74%	17%
C13	56%	61%

formulation is sandwiched between two polypropylene films to reduce the O_2 inhibition). The decrease of C═C double bond band or the epoxide group was continuously monitored from 1581 to 1662 cm^{-1} or from 768 to 825 cm^{-1} respectively. For the thicker samples (~1.4 mm of thickness), the formulations were deposited on a polypropylene film inside a 1.4 mm mold under air. The evolution of the C═C band and the epoxide group band were continuously followed from 6117 to 6221 cm^{-1} and from 3710 to 3799 cm^{-1} respectively.

2.6. Steady state fluorescence

Fluorescence spectra were acquired in a quartz cell at room temperature using a JASCO FP-750 spectrofluorometer.

2.7. Redox potentials

The oxidation potentials (E_{ox}) were measured in acetonitrile by cyclic voltammetry using tetrabutylammonium hexafluorophosphate (0.1 M) as the supporting electrolyte (potential vs. Saturated Calomel

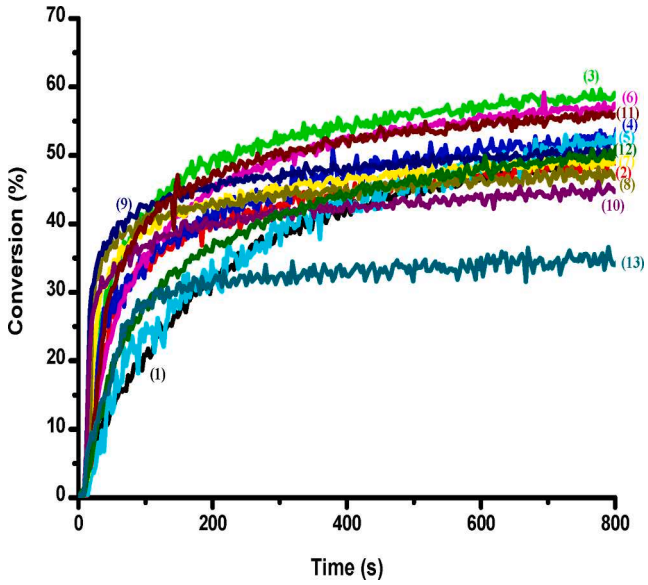

Fig. 6. Photopolymerization profiles of EPOX (epoxy function conversion vs. irradiation time) under air (thickness = 25 μm) upon exposure to LED light λ = 405 nm in the presence of different two component photoinitiating systems: PI/Iod (0.2%/1% w/w): (1) **C2**/Iod; (2) **C3**/Iod; (3) **C4**/Iod; (4) **C5**/Iod; (5) **C5′**/Iod; (6) **C5″**/Iod; (7) **C6**/Iod; (8) **C6′**/Iod; (9) **C8**/Iod; (10) **C9**/Iod; (11) **C11**/Iod; (12) **C12**/Iod; and (13) **C13**/Iod; respectively. The irradiation starts after t = 10 s.

Electrode – SCE). The free energy change ΔG_{et} for an electron transfer reaction was calculated from Eq. (1), [29] where E_{ox}, E_{red}, E*, and C are the oxidation potential of the electron donor (the carbazole derivatives), the reduction potential of the electron acceptor (the iodonium salt), the excited state energy and the coulombic term for the initially formed ion pair, respectively. Here, C is neglected for polar solvents.

$$\Delta G_{et} = E_{ox} - E_{red} - E^* + C \quad (1)$$

Table 3
Final epoxy function conversions (FCs) for EPOX using different two-component dyes/Iod (0.2%/1% w/w) photoinitiating systems after 800 s of irradiation with LED light (λ = 405 nm).

Thin sample (25 μm) in laminate												
C2	C3	C4	C5	C5′	C5″	C6	C6′	C8	C9	C11	C12	C13
50%	49%	59%	54%	53%	57%	49%	47%	51%	45%	56%	51%	34%

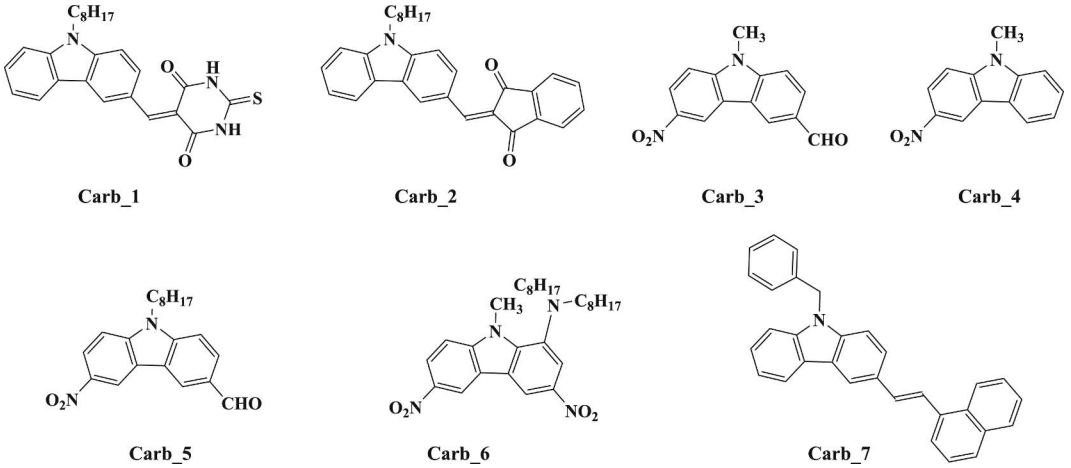

Fig. 7. Chemical structures of carbazole derivatives previously used as visible photoinitiators of polymerization for the cationic polymerization of EPOX.

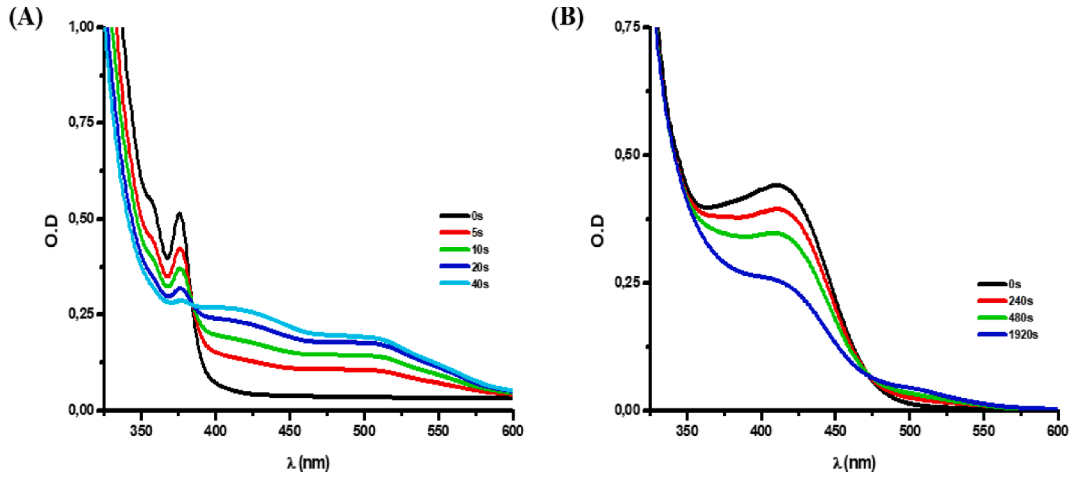

Fig. 8. (A) Photolysis of **C5″** with Iod (10^{-2} M) in acetonitrile; (B) Photolysis of **C6′** with Iod (10^{-2} M) in acetonitrile.

2.8. Direct laser write

For direct laser write experiments, a laser diode emitting at 405 nm (spot size around 50 μm) was used for the spatially controlled irradiation. The photosensitive resin was polymerized under air and the generated 3D patterns were analyzed using a numerical optical microscope (DSX-HRSU from Olympus Corporation).

3. Results and discussion

3.1. UV–visible absorption properties of the different dyes

Among all compounds reported in this work, except **C2** which exhibits a UV-centred absorption (λ_{max} = 370 nm), all dyes showed absorption spectra extending until the visible range, making these dyes suitable candidates for photopolymerization experiments done under visible light. As shown in the Fig. 4, three groups of dyes could be identified. First, dyes such as **C2, C3, C4, C5, C5′** and **C5″** proved to exhibit a strongly UV centred absorption so that only an onset could be detected in the visible range. As specificity, these dyes are substituted with weak electron accepting groups such as aldehyde and acetyl groups.

Conversely, for all dyes substituted with a nitro group i.e. **C6, C6′, C8** and **C8**, absorption maxima ranging from 408 nm for **C8** to 417 nm for **C6** and **C6′** could be determined. Interestingly, contrarily to **C6** and **C6′** that are only substituted with one or two nitro groups, introduction of additional groups such as a bromine on **C9**, an iodine on **C10** or an aldehyde on **C8** slightly blue-shifted their absorption maxima compared to the parent structure **C6**. Finally, by converting **C8** as an electron donating group for push–pull dyes, a major redshift of the absorption maxima could be determined. Thus, the absorption maxima of **C11-C13** could be determined respectively at 488, 479 and 505 nm. Interestingly, even if a stronger electron-withdrawing group was used in **C12** compared to **C11**, a hypsochromic shift of the absorption maxima of ca.

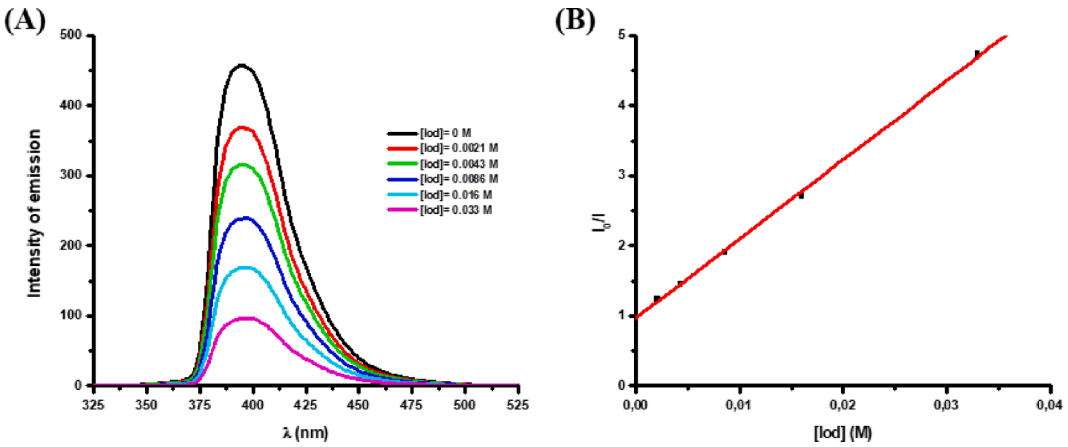

Fig. 9. (A) Quenching of ^{1}**C2** by Iod in acetonitrile. (B) Determination of the Stern-Volmer coefficient.

Table 4
Parameters characterizing the chemical mechanisms associated with ^{1}dyes/Iod interaction in acetonitrile: oxidation potentials (E_{ox}), singlet state energy levels (E_{S1}), free energy changes for the electron transfer reaction (ΔG_{S1}), Stern-Volmer quenching coefficients (K_{SV}) and electron transfer quantum yields (ϕ_{et}).

PI	E_{ox} (eV)	E_{s1} (eV)	$\Delta G_{s1\ (Iod)}$ (eV)[a]	K_{sv} (M^{-1})[b]	$\Phi_{et\ (Dye/Iod)}$
C2	0.88	3.28	−1.7	113	0.79
C3	1.04	3.04	−1.3	99	0.61
C4	1.17	3.11	−1.24	82	0.55
C5	1.01	3.10	−1.39	245	0.78
C5′	0.95	3.23	−1.58	18	0.21
C5″	1.12	3.19	−1.37	76	0.68
C6	1.11	–	–	–	–
C6′	1.15	–	–	–	–
C8	1.24	–	–	–	–
C9	1.19	–	–	–	–
C11	1.22	–	–	–	–
C12	1.21	–	–	–	–
C13	1.21	–	–	–	–

a: evaluated from $\Delta G_{S1} = E_{ox} - E_{red}(Iod) - E_{S1}$; $E_{red}(Iod) = -0.7$ V.
b: Stern-Volmer coefficient (K_{sv}); slope of the quenching curve: $I/I_0=(1 + ksv\ [Iod])$.

10 nm could be determined. This unexpected result can be assigned to the steric hindrance existing between the phenyl groups of the electron donor with the 6-membered ring of the electron acceptor in **C12**, enforcing the π-conjugated system to twist. Conversely, a more planar structure can be obtained in **C11**, due to the presence of an electron accepting group bearing a five-membered ring (see Table 1).

3.2. Photopolymerization abilities of the different dyes

3.2.1. Free radical polymerization (FRP) of acrylates

For the polymerization of the acrylate monomer TA, the photoinitiation abilities of the different dyes in the presence of an iodonium salt as the additive were investigated using real-time Fourier transform infrared spectroscopy (RT-FTIR) upon irradiation with LED@405 nm at room temperature. Typical acrylate function conversions vs. irradiation time profiles are given in Fig. 5 and the associated final acrylate function conversions (FCs) are summarized in Table 2.

Upon exposure to LED irradiation at 405 nm, the experimental results showed that almost all dyes, when combined with an iodonium salt, can effectively initiate free radical polymerizations (e.g. FC = 87% with 0.2% **C5′′** (w/w) and FC = 77% with 0.2% **C2**, or **C3** or **C5** (w/w) for thin sample (25 μm, in laminate); Fig. 5 (A), Table 2). For dyes alone, no polymerization is observed showing the interest of the two-component systems. The efficiency trend for dyes/Iod couples for the FRP in thin samples (25 μm, in laminate) respects the following order: **C5″ > C2 ~ C3 ~ C5 > C6 > C12 > C6′ > C4 ~ C8 > C5′ > C11 > C13 > C9** which is not directly related to the absorption properties of the different dyes, but also to the photochemical reactivity with the iodonium salt and also probably by the different reactivity of the generated radicals to initiate the free radical polymerization. For thick samples (1.4 mm, under air), the dye/Iod systems also showed high final acrylic conversions, but for some dyes (e.g., **C12** and **C13**) the polymerization was low compared to the results obtained in thin samples. This behaviour can be attributed to an internal filter effect (See Fig. 5 (B), Table 2).

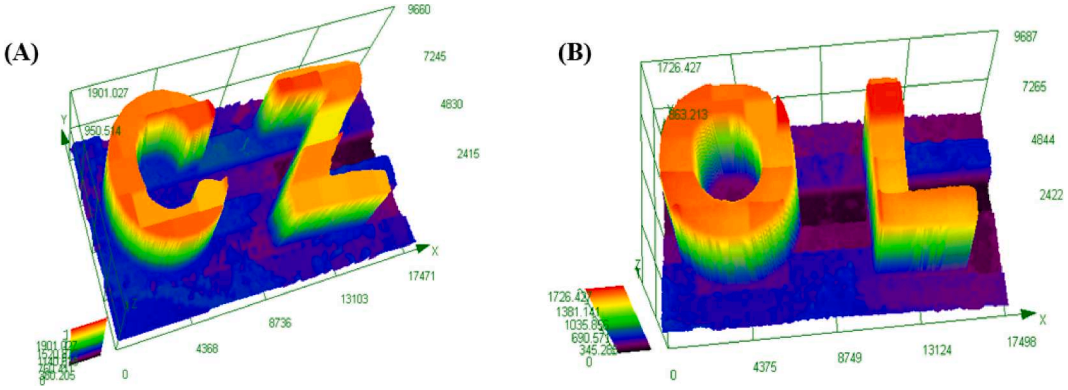

Fig. 10. 3D patterns obtained upon exposure to a laser diode @405 nm: characterization by numerical microscopy; (A): **C4**/Iod (0.2%/1% w/w) in TA (thickness = 1900 μm); (B): **C5**/Iod (0.2%/1% w/w/) in TA (thickness = 1700 μm).

3.2.2. Cationic polymerization (CP) of epoxides

The investigated dyes were also tested as photosensitizers for the iodonium salt (Iod) in the cationic polymerization (CP) of EPOX upon irradiation with a LED@405 nm. Epoxy function conversion versus irradiation time profiles are shown in Fig. 6 and the associated final epoxy function conversions (FC's) are gathered in Table 3. For Iod alone in EPOX, no polymerization occurs in agreement with the lack of absorption of the iodonium salt at 405 nm.

Actually, the different dyes can efficiently absorb the light at 405 nm, and then the corresponding generated excited states are expected to interact with the iodonium salt as a photoinitiator in order to generate reactive species ($Dye^{\bullet+}$; see reactions r(1) and r(2) below), which are able to initiate the cationic polymerization of thin (25 μm) epoxy films as shown in the Fig. 6. The two-component dyes/Iod (0.2%/1% w/w) photoinitiating systems are very efficient to initiate the CP under air where very high final functional conversions (FCs) and also high rates of polymerization (Rp) were achieved i.e., FC = 57% for **C5″**/Iod (0.2%/1% w/w) (curve 6 in Fig. 6; see also in Table 3 for the other dyes). The efficiency trend for dyes/Iod couples for the CP respects the following order: **C4** > **C5″** > **C11** > **C5** > C5′ > C8 ~ **C12** > **C2** > **C3** ~ **C6** > **C6′** > **C9** > **C13** which also is not directly linked to the absorption properties of the investigated dyes. Therefore, the photochemical reactivity with the iodonium salt is probably affected by the dye structure and also probably different reactivity of the generated radical cations ($Dye^{\bullet+}$) to initiate the CP. Interestingly, comparisons of the EPOX conversions obtained in this work for **C5″** and **C11** with results previously reported in the literature for carbazole-based structures revealed **C5″** and **C11** to furnish similar conversions at 405 nm to that obtained with the three-component carbazole/NVK/Ph_2I^+ (0.3%/3%/2% w/w) photoinitiating systems comprising **Carb_1** (55%) [53] or **Carb_2** (58%).[54] If **C5″** and **C11** can compete the two-component carbazole/(*t*-Bu)Ph_2I^+ (0.2%/2% w/w) photoinitiating systems based on **Carb_4** (50%) and **Carb_5** (58%), the EPOX conversions were lower than that obtained with other nitrated carbazoles such as **Carb_3** (76%) and **Carb_6** (70%).[32] However, EPOX conversions obtained with **C5″** and **C11** remain comparable to that of **Carb_7** (57 % yield) [29] (See Fig. 7).

3.3. Chemical mechanisms

3.3.1. Steady state photolysis

Steady-state photolysis of the dyes/Iod (10^{-2} M) systems is performed in acetonitrile under light irradiation, using an LED@375 nm. It is remarkable that, for example for **C5′'** (Fig. 8 (A)), there is an efficient photolysis with the rapid formation of photoproducts after 40 s, and for **C6′** after 1920s (Fig. 8 (B)), which may suggest a photochemical reaction between the studied dyes and the iodonium salt, in agreement with the results observed in the photopolymerization experiments. Isobestic points were observed suggesting photochemical processes without side-reactions.

3.3.2. Fluorescence quenching

In order to better understand the interaction between the studied dyes and the iodonium salt (Iod), fluorescence quenching experiments were carried out. For example, as Fig. 4 shows, a strong fluorescence quenching process of **C2** by Iod was detected (see Fig. 9 and Table 4); this clearly shows a very strong interaction of **C2** (and even the other dyes) with the iodonium salt ((r1) and (r2)). The oxidation potentials (E_{ox}) for the different carbazole derivatives determined by cyclic voltammetry (Table 4) allow the evaluation of the free energy change (ΔG) for this electron transfer reaction (Table 4); highly favorable ΔG are found in agreement with the strong ^{1}**C2**/Iod interaction observed above in fluorescence quenching. The associated electron transfer quantum yields (Φ_{et}) were determined according to the following equation: $\Phi_{et} = ksv[Iod]/(1 + ksv[Iod])$ and high Φ_{et} are found (e.g., $\Phi_{et} = 0.79$ for **C2**, Table 4).

$$Dye\ (h\nu) \rightarrow {}^{*}Dye \quad \text{(r1)}$$

$$^{*}Dye\ + Ar_2I^+ \rightarrow Dye^{\bullet+} + Ar_2I^{\bullet} \rightarrow Dye^{\bullet+} + Ar^{\bullet} + ArI \quad \text{(r2)}$$

3.4. 3D printing experiment

Some 3D printing experiments upon laser diode irradiation at 405 nm were successfully performed under air using **C4**/Iod and **C5**/Iod systems in TA (See Fig. 10). Indeed, the high photosensibility of these systems allows an efficient polymerization in the irradiated area. 3D patterns elaborated with high resolution and very short writing time (~2 min), were characterized by numerical optical microscopy.

4. Conclusion

In the present paper, a series of 5,12-dihydroindolo[3,2-*a*]carbazole derivatives characterized by strong visible light absorptions in the visible range are proposed for the development of new high performance photoinitiators for both the free radical polymerization of acrylates and the cationic polymerization of epoxides upon blue LED irradiation. Both high final conversions and polymerization rates are achieved. The high performance of these proposed dyes in initiating systems is also shown for new photosensitive 3D printing resins upon exposure to a laser diode. The challenge remains, therefore, to develop new photoinitiating systems absorbing at longer wavelengths for example in the near-infrared range for a better penetration of light into thick samples.

CRediT authorship contribution statement

Fatima Hammoud: Data curation, Formal analysis, Investigation, Validation, Writing – original draft, Writing – review & editing. **Akram Hijazi:** Data curation, Formal analysis, Investigation, Validation, Writing – original draft, Writing – review & editing. **Sylvain Duval:** Data curation, Formal analysis, Investigation, Validation, Writing – original draft, Writing – review & editing. **Jacques Lalevée:** Conceptualization, Data curation, Formal analysis, Funding acquisition, Investigation, Methodology, Project administration, Resources, Supervision, Validation, Writing – original draft, Writing – review & editing. **Frédéric Dumur:** Conceptualization, Data curation, Formal analysis, Funding acquisition, Investigation, Methodology, Project administration, Resources, Supervision, Validation, Writing – original draft, Writing – review & editing.

Declaration of Competing Interest

The authors declare that they have no known competing financial interests or personal relationships that could have appeared to influence the work reported in this paper.

Acknowledgments

Aix Marseille University and the Centre National de la Recherche Scientifique (CNRS) are acknowledged for financial supports.

Appendix A. Supplementary material

Supplementary data to this article can be found online at https://doi.org/10.1016/j.eurpolymj.2021.110880.

References

[1] K.L. Woon, A. Ariffin, K.W. Ho, S.-A. Chen, Effect of conjugation and aromaticity of 3,6 di-substituted carbazoles on triplet energy and the implication of triplet energy in multiple-cyclic aromatic compounds, RSC Adv. 8 (18) (2018) 9850–9857, https://doi.org/10.1039/C8RA00674A.

[2] A. Arai, H. Sasabe, K. Nakao, Y. Masuda, J. Kido, Kido, π-Extended Carbazole Derivatives as Host Materials for Highly Efficient and Long-Life Green Phosphorescent Organic Light-Emitting Diodes, Chem. Eur. J. 27 (15) (2021) 4971–4976, https://doi.org/10.1002/chem.v27.1510.1002/chem.202005144.

[3] Y. Nagai, H. Sasabe, S. Ohisa, J. Kido, Effect of substituents in a series of carbazole-based host-materials toward high-efficiency carbene-based blue OLEDs, J. Mater. Chem. C. 4 (40) (2016) 9476–9481, https://doi.org/10.1039/C6TC03067J.

[4] Z.-J. Gao, T.-H. Yeh, J.-J. Xu, C.-C. Lee, A. Chowdhury, B.-C. Wang, S.-W. Liu, C.-H. Chen, Carbazole/Benzimidazole-Based Bipolar Molecules as the Hosts for Phosphorescent and Thermally Activated Delayed Fluorescence Emitters for Efficient OLEDs, ACS Omega 5 (18) (2020) 10553–10561, https://doi.org/10.1021/acsomega.0c0096710.1021/acsomega.0c00967.s001.

[5] G. Li, J. Zheng, K. Klimes, Z.-Q. Zhu, J. Wu, H. Zhu, J. Li, Novel Carbazole/Fluorene-Based Host Material for Stable and Efficient Phosphorescent OLEDs, ACS Appl. Mater. Interfaces. 11 (43) (2019) 40320–40331, https://doi.org/10.1021/acsami.9b1324510.1021/acsami.9b13245.s00110.1021/acsami.9b13245.s00210.1021/acsami.9b13245.s003.

[6] F. Dumur, Carbazole-based polymers as hosts for solution-processed organic light-emitting diodes: Simplicity, efficacy, Org. Electron. 25 (2015) 345–361, https://doi.org/10.1016/j.orgel.2015.07.007.

[7] F. Dumur, L. Beouch, S. Peralta, G. Wantz, F. Goubard, D. Gigmes, Solution-processed blue phosphorescent OLEDs with carbazole-based polymeric host materials, Org. Electron. 25 (2015) 21–30, https://doi.org/10.1016/j.orgel.2015.06.013.

[8] G. Sathiyan, E.K.T. Sivakumar, R. Ganesamoorthy, R. Thangamuthu, P. Sakthivel, Review of carbazole based conjugated molecules for highly efficient organic solar cell application, Tetrahedr. Lett. 57 (3) (2016) 243–252, https://doi.org/10.1016/j.tetlet.2015.12.057.

[9] I.V. Martynov, A.V. Akkuratov, S.Y. Luchkin, S.A. Tsarev, S.D. Babenko, V. G. Petrov, K.J. Stevenson, P.A. Troshin, Impressive Radiation Stability of Organic Solar Cells Based on Fullerene Derivatives and Carbazole-Containing Conjugated Polymers, ACS Appl. Mater. Interfaces. 11 (24) (2019) 21741–21748, https://doi.org/10.1021/acsami.9b0172910.1021/acsami.9b01729.s001.

[10] J. Ouyang, G. Zeng, Y. Xin, X. Zhao, X. Yang, A Novel Carbazole-Based Nonfullerene Acceptor for High-Efficiency Polymer Solar Cells, Solar RRL. 4 (3) (2020) 1900417, https://doi.org/10.1002/solr.v4.310.1002/solr.201900417.

[11] B. Souharce, C.J. Kudla, M. Forster, J. Steiger, R. Anselmann, H. Thiem, U. Scherf, Amorphous Carbazole-based (Co)polymers for OFET Application, Macromol. Rapid Commun. 30 (2009) 1258–1262, https://doi.org/10.1002/marc.200900214.

[12] P. Jha, S.P. Koiry, V. Saxena, P. Veerender, A. Gusain, A.K. Chauhan, A.K. Debnath, D.K. Aswal, S.K. Gupta, Air-stability and bending properties of flexible organic field-effect transistors based on poly[N-9′-heptadecanyl-2,7-carbazole-alt-5,5-(4′,7′-di-2-thienyl-2′,1′,3′-benzothiadiazole)], Org. Electron. 14 (10) (2013) 2635–2644, https://doi.org/10.1016/j.orgel.2013.06.031.

[13] C.-H. Chen, Y. Wang, T. Michinobu, S.-W. Chang, Y.-C. Chiu, C.-Y. Ke, G.-S. Liou, Donor-Acceptor Effect of Carbazole-Based Conjugated Polymer Electrets on Photoresponsive Flash Organic Field-Effect Transistor Memories, ACS Appl. Mater. Interfaces. 12 (5) (2020) 6144–6150, https://doi.org/10.1021/acsami.9b2096010.1021/acsami.9b20960.s001.

[14] M. Khalid, A. Ali, R. Jawaria, M.A. Asghar, S. Asim, M.U. Khan, R. Hussain, M. Fayyaz ur Rehman, C.J. Ennis, M.S. Akram, First principles study of electronic and nonlinear optical properties of A-D–π–A and D–A–D–π–A configured compounds containing novel quinoline–carbazole derivatives, RSC Adv. 10 (37) (2020) 22273–22283, https://doi.org/10.1039/D0RA02857F.

[15] L. MayuriM, D. Kadam, N.S. Patil, Fluorescent carbazole based pyridone dyes – Synthesis, solvatochromism, linear and nonlinear optical properties, Opt. Mater. 85 (2018) 308–318, https://doi.org/10.1016/j.optmat.2018.08.072.

[16] W.-J. Kuo, G.-H. Hsiue, R.-J. Jeng, All Organic NLO Sol-Gel Material Containing a One-Dimensional Carbazole Chromophore, Macromol. Chem. Phys. 202 (2001) 1782–1790, https://doi.org/10.1002/1521-3935(20010601)202:9<1782::AID-MACP1782>3.0.CO;2-O.

[17] M. Rajeshirke, M.C. Sreenath, S. Chitrambalam, I.H. Joe, N. Sekar, Enhancement of NLO Properties in OBO Fluorophores Derived from Carbazole-Coumarin Chalcones Containing Carboxylic Acid at the N-Alykl Terminal End, J. Phys. Chem. C. 122 (26) (2018) 14313–14325, https://doi.org/10.1021/acs.jpcc.8b0293710.1021/acs.jpcc.8b02937.s001.

[18] M. Bashir, A. Bano, A.S. Ijaz, B.A. Chaudhary, Recent Developments and Biological Activities of N-Substituted Carbazole Derivatives: A Review, Molecules 20 (2015) 13496–13517, https://doi.org/10.3390/molecules200813496.

[19] M. Lepeltier, F. Appaix, Y.Y. Liao, F. Dumur, J. Marrot, T. Le Bahers, C. Andraud, C. Monnereau, Carbazole-Substituted Iridium Complex as a Solid State Emitter for Two-Photon Intravital Imaging, Inorg. Chem. 55 (19) (2016) 9586–9595, https://doi.org/10.1021/acs.inorgchem.6b0125310.1021/acs.inorgchem.6b01253.s00110.1021/acs.inorgchem.6b01253.s002.

[20] F. Dumur, Recent advances on carbazole-based photoinitiators of polymerization, Eur. Polym. J. 125 (2020) 109503, https://doi.org/10.1016/j.eurpolymj.2020.109503.

[21] N. Blouin, A. Michaud, D. Gendron, S. Wakim, E. Blair, R. Neagu-Plesu, M. Belletête, G. Durocher, Y.e. Tao, M. Leclerc, Toward a Rational Design of Poly (2,7-Carbazole) Derivatives for Solar Cells, J. Am. Chem. Soc. 130 (2) (2008) 732–742, https://doi.org/10.1021/ja077198910.1021/ja0771989.s00410.1021/ja0771989.s00510.1021/ja0771989.s006.

[22] K.H. Choi, J.M. Kim, W.J. Chung, J.Y. Lee, Effects of Substitution Position of Carbazole-Dibenzofuran Based High Triplet Energy Hosts to Device Stability of Blue Phosphorescent Organic Light-Emitting Diodes, Molecules 26 (2021) 2804, https://doi.org/10.3390/molecules26092804.

[23] A. van Dijken, J.J.A.M. Bastiaansen, N.M.M. Kiggen, B.M.W. Langeveld, C. Rothe, A. Monkman, I. Bach, P. Stössel, K. Brunner, Carbazole Compounds as Host Materials for Triplet Emitters in Organic Light-Emitting Diodes: Polymer Hosts for High-Efficiency Light-Emitting Diodes, J. Am. Chem. Soc. 126 (2004) 7718–7727, https://doi.org/10.1021/ja049771j.

[24] S.O. Jung, Y.-H. Kim, S.-K. Kwon, H.-Y. Oh, J.-H. Yang, New hole blocking material for green-emitting phosphorescent organic electroluminescent devices, Org. Electron. 8 (4) (2007) 349–356, https://doi.org/10.1016/j.orgel.2006.12.005.

[25] F. Dumur, D. Bertin, C.R. Mayer, A. Guerlin, G. Wantz, G. Nasr, E. Dumas, F. Miomandre, G. Clavier, D. Gigmes, Design of blue or yellow emitting devices controlled by the deposition process of a cationic iridium (III) complex, Synth. Met. 161 (17-18) (2011) 1934–1939, https://doi.org/10.1016/j.synthmet.2011.06.038.

[26] D. Sun, Q. Fu, Z. Ren, W. Li, H. Li, D. Ma, S. Yan, Carbazole-based polysiloxane hosts for highly efficient solution-processed blue electrophosphorescent devices, J. Mater. Chem. C. 1 (2013) 5344–5350, https://doi.org/10.1039/C3TC31108B.

[27] J. Zhang, D. Campolo, F. Dumur, P.u. Xiao, D. Gigmes, J.P. Fouassier, J. Lalevée, The carbazole-bound ferrocenium salt as a specific cationic photoinitiator upon near-UV and visible LEDs (365–405 nm), Polym. Bull. 73 (2) (2016) 493–507, https://doi.org/10.1007/s00289-015-1506-1.

[28] A. Al Mousawi, D.M. Lara, G. Noirbent, F. Dumur, J. Toufaily, T. Hamieh, T.-T. Bui, F. Goubard, B. Graff, D. Gigmes, J.P. Fouassier, J. Lalevée, Carbazole Derivatives with Thermally Activated Delayed Fluorescence Property as Photoinitiators/Photoredox Catalysts for LED 3D Printing Technology, Macromolecules 50 (13) (2017) 4913–4926, https://doi.org/10.1021/acs.macromol.7b0111410.1021/acs.macromol.7b01114.s001.

[29] A. Al Mousawi, P. Garra, F. Dumur, T.-T. Bui, F. Goubard, J. Toufaily, T. Hamieh, B. Graff, D. Gigmes, J.P. Fouassier, J. Lalevée, Novel Carbazole Skeleton-Based Photoinitiators for LED Polymerization and LED Projector 3D Printing, Molecules 22 (2017) 2143, https://doi.org/10.3390/molecules22122143.

[30] A. Al Mousawi, A. Arar, M. Ibrahim-Ouali, S. Duval, F. Dumur, P. Garra, J. Toufaily, T. Hamieh, B. Graff, D. Gigmes, J.-P. Fouassier, J. Lalevée, Carbazole-based compounds as photoinitiators for free radical and cationic polymerization upon near visible light illumination, Photochem. Photobiol. Sci. 17 (5) (2018) 578–585, https://doi.org/10.1039/C7PP00400A.

[31] M. Abdallah, D. Magaldi, A. Hijazi, B. Graff, F. Dumur, J.-P. Fouassier, T.-T. Bui, F. Goubard, J. Lalevée, Development of new high-performance visible light photoinitiators based on carbazole scaffold and their applications in 3d printing and photocomposite synthesis, J. Polym. Sci., Part A: Polym. Chem. 57 (20) (2019) 2081–2092, https://doi.org/10.1002/pola.v57.2010.1002/pola.29471.

[32] A. Al Mousawi, F. Dumur, P. Garra, J. Toufaily, T. Hamieh, B. Graff, D. Gigmes, J. P. Fouassier, J. Lalevée, Carbazole Scaffold Based Photoinitiator/Photoredox Catalysts: Toward New High Performance Photoinitiating Systems and Application in LED Projector 3D Printing Resins, Macromolecules 50 (7) (2017) 2747–2758, https://doi.org/10.1021/acs.macromol.7b0021010.1021/acs.macromol.7b00210.s001.

[33] S. Telitel, F. Dumur, T. Faury, B. Graff, M.-A. Tehfe, D. Gigmes, J.-P. Fouassier, J. Lalevée, New core-pyrene π structure organophotocatalysts usable as highly efficient photoinitiators, Beilstein J. Org. Chem. 9 (2013) 877–890, https://doi.org/10.3762/bjoc.9.101.

[34] A. Al Mousawi, F. Dumur, P. Garra, J. Toufaily, T. Hamieh, F. Goubard, T.-T. Bui, B. Graff, D. Gigmes, J. Pierre Fouassier, J. Lalevée, Azahelicenes as visible light photoinitiators for cationic and radical polymerization: Preparation of photoluminescent polymers and use in high performance LED projector 3D printing resins, J. Polym. Sci., Part A: Polym. Chem. 55 (7) (2017) 1189–1199, https://doi.org/10.1002/pola.v55.710.1002/pola.28476.

[35] S. Liu, D. Brunel, K.e. Sun, Y. Xu, F. Morlet-Savary, B. Graff, P.u. Xiao, F. Dumur, J. Lalevée, A monocomponent bifunctional benzophenone–carbazole type II photoinitiator for LED photoinitiating systems, Polym. Chem. 11 (21) (2020) 3551–3556, https://doi.org/10.1039/D0PY00644K.

[36] C.Y. Barlow, D.C. Morgan, Polymer film packaging for food: An environmental assessment, Resour. Conserv. Recycl. 78 (2013) 74–80, https://doi.org/10.1016/j.resconrec.2013.07.003.

[37] J.L. Aparicio, M. Elizalde, Migration of Photoinitiators in Food Packaging: A Review, Packaging Technology and Science. 28 (3) (2015) 181–203, https://doi.org/10.1002/pts.v28.310.1002/pts.2099.

[38] M.A. Lago, A.-R.-B. de Quirós, R. Sendón, J. Bustos, M.T. Nieto, P. Paseiro, Photoinitiators: a food safety review, Food Additives & Contaminants: Part A. 32 (2015) 779–798, https://doi.org/10.1080/19440049.2015.1014866.

[39] A.K. Nguyen, R.J. Narayan, Two-photon polymerization for biological applications, Mater. Today 20 (6) (2017) 314–322, https://doi.org/10.1016/j.mattod.2017.06.004.

[40] G. Ye, H. Zhou, J. Yang, Z. Zeng, Y. Chen, Synthesis and characterization of oligomers containing the α-aminoalkylphenone chromophore as oligomeric photoinitiator, J. Appl. Polym. Sci. 99 (6) (2006) 3417–3424, https://doi.org/10.1002/(ISSN)1097-462810.1002/app.v99:610.1002/app.22956.

[41] E. Ay, Z. Raad, O. Dautel, F. Dumur, G. Wantz, D. Gigmes, J.-P. Fouassier, J. Lalevée, Oligomeric Photocatalysts in Photoredox Catalysis: Toward High Performance and Low Migration Polymerization Photoinitiating Systems, Macromolecules 49 (6) (2016) 2124–2134, https://doi.org/10.1021/acs.macromol.5b0276010.1021/acs.macromol.5b02760.s001.

[42] P. Xiao, F. Dumur, M. Frigoli, M.-A. Tehfe, B. Graff, J.P. Fouassier, D. Gigmes, J. Lalevée, Naphthalimide based methacrylated photoinitiators in radical and cationic photopolymerization under visible light, Polym. Chem. 4 (2013) 5440–5448, https://doi.org/10.1039/C3PY00766A.

[43] J. Yang, W. Liao, Y. Xiong, Q. Wu, X. Wang, Z. Li, H. Tang, Naphthalimide dyes: Polymerizable one-component visible light initiators, Dyes Pigm. 148 (2018) 16–24, https://doi.org/10.1016/j.dyepig.2017.08.053.
[44] J. Yang, C. Xu, Y. Xiong, X. Wang, Y. Xie, Z. Li, H. Tang, A Green and Highly Efficient Naphthalimide Visible Photoinitiator with an Ability Initiating Free Radical Polymerization under Air, Macromol. Chem. Phys. 219 (24) (2018) 1800256, https://doi.org/10.1002/macp.201800256.
[45] J. Yang, W. Liao, Y. Xiong, X. Wang, Z. Li, H. Tang, A multifunctionalized macromolecular silicone-naphthalimide visible photoinitiator for free radical polymerization, Prog. Org. Coat. 115 (2018) 151–158, https://doi.org/10.1016/j.porgcoat.2017.11.010.
[46] H. Chen, G. Noirbent, K.e. Sun, D. Brunel, D. Gigmes, F. Morlet-Savary, Y. Zhang, S. Liu, P.u. Xiao, F. Dumur, J. Lalevée, Photoinitiators derived from natural product scaffolds: monochalcones in three-component photoinitiating systems and their applications in 3D printing, Polym. Chem. 11 (28) (2020) 4647–4659, https://doi.org/10.1039/D0PY00568A.
[47] H. Chen, G. Noirbent, Y. Zhang, K.e. Sun, S. Liu, D. Brunel, D. Gigmes, B. Graff, F. Morlet-Savary, P.u. Xiao, F. Dumur, J. Lalevée, Photopolymerization and 3D/4D applications using newly developed dyes: Search around the natural chalcone scaffold in photoinitiating systems, Dyes Pigm. 188 (2021) 109213, https://doi.org/10.1016/j.dyepig.2021.109213.
[48] H. Chen, G. Noirbent, Y. Zhang, D. Brunel, D. Gigmes, F. Morlet-Savary, B. Graff, P. u. Xiao, F. Dumur, J. Lalevée, Novel D–π-A and A–π-D–π-A three-component photoinitiating systems based on carbazole/triphenylamino based chalcones and application in 3D and 4D printing, Polym. Chem. 11 (40) (2020) 6512–6528, https://doi.org/10.1039/D0PY01197E.
[49] M.-A. Tehfe, F. Dumur, E. Contal, B. Graff, D. Gigmes, J.-P. Fouassier, J. Lalevée, Novel Highly Efficient Organophotocatalysts: Truxene–Acridine-1,8-diones as Photoinitiators of Polymerization, Macromol. Chem. Phys. 214 (19) (2013) 2189–2201, https://doi.org/10.1002/macp.201300362.
[50] M.-A. Tehfe, F. Dumur, B. Graff, J.-L. Clément, D. Gigmes, F. Morlet-Savary, J.-P. Fouassier, J. Lalevée, New Cleavable Photoinitiator Architecture with Huge Molar Extinction Coefficients for Polymerization in the 340–450 nm Range, Macromolecules 46 (3) (2013) 736–746, https://doi.org/10.1021/ma3024359.
[51] M.-A. Tehfe, J. Lalevée, S. Telitel, E. Contal, F. Dumur, D. Gigmes, D. Bertin, M. Nechab, B. Graff, F. Morlet-Savary, J.-P. Fouassier, Polyaromatic Structures as Organo-Photoinitiator Catalysts for Efficient Visible Light Induced Dual Radical/Cationic Photopolymerization and Interpenetrated Polymer Networks Synthesis, Macromolecules 45 (11) (2012) 4454–4460, https://doi.org/10.1021/ma300760c.
[52] N.A. Kazin, N.S. Demina, R.A. Irgashev, E.F. Zhilina, G.L. Rusinov, Modifications of 5,12-dihydroindolo[3,2-a]carbazole scaffold via its regioselective C2,9-formylation and C2,9-acetylation, Tetrahedron 75 (33) (2019) 4686–4696, https://doi.org/10.1016/j.tet.2019.07.015.
[53] M.-A. Tehfe, F. Dumur, B. Graff, F. Morlet-Savary, D. Gigmes, J.-P. Fouassier, J. Lalevée, Push–pull (thio)barbituric acid derivatives in dye photosensitized radical and cationic polymerization reactions under 457/473 nm laser beams or blue LEDs, Polym. Chem. 4 (2013) 3866–3875, https://doi.org/10.1039/C3PY00372H.
[54] P.u. Xiao, F. Dumur, B. Graff, F. Morlet-Savary, L. Vidal, D. Gigmes, J.P. Fouassier, J. Lalevée, Structural Effects in the Indanedione Skeleton for the Design of Low Intensity 300–500 nm Light Sensitive Initiators, Macromolecules 47 (1) (2014) 26–34, https://doi.org/10.1021/ma402149g.
[55] A. Bonardi, F. Bonardi, G. Noirbent, F. Dumur, C. Dietlin, D. Gigmes, J.-P. Fouassier, J. Lalevée, Different NIR dye scaffolds for polymerization reactions under NIR light, Polym. Chem. 10 (47) (2019) 6505–6514, https://doi.org/10.1039/C9PY01447K.
[56] V. Nair, V. Nandialath, K.G. Abhilash, E. Suresh, An efficient synthesis of indolo[3,2-a]carbazoles via the novel acid catalyzed reaction of indoles and diaryl-1,2-diones, Org. Biomol. Chem. 6 (2008) 1738–1742, https://doi.org/10.1039/B803009J.
[57] A. Rieche, H. Gross, E. Höft, I.V. Über α-Halogenäther, Synthesen aromatischer Aldehyde mit Dichlormethyl-alkyläthern, Ber. 93 (1) (1960) 88–94, https://doi.org/10.1002/(ISSN)1099-068210.1002/cber.v93:110.1002/cber.19600930115.
[58] I. Ramos-Tomillero, M. Paradís-Bas, I. De Pinho Ribeiro, J.M. Moreira, E. Bofill, F. A. Nicolás, Formylation of Electron-Rich Aromatic Rings Mediated by Dichloromethyl Methyl Ether and TiCl4: Scope and Limitations, Molecules 20 (2015) 5409–5422, https://doi.org/10.3390/molecules20045409.

Section 2 : Ingénierie chimique autour de la structure du 5,12-dihydroindolo[3,2-a]carbazole : optimisation des propriétés optiques des photoamorceurs de polymérisation à la lumière visible

Le 5,12-dihydroindolo[3,2-a]carbazole est un chromophore prometteur pour la conception de photoamorceurs de polymérisation à la lumière visible en raison de la présence de deux groupements carbazole qui peuvent être fonctionnalisés différemment. Notamment, le décalage vers le rouge des spectres d'absorption peut être facilement obtenu par nitration de l'un des deux carbazoles, le second groupe carbazole pouvant être fonctionnalisé avec différents substituants.

Dans cette section, une série de 36 composés jamais rapportés dans la littérature et différant par la substitution ont été synthétisés par nos collaborateurs de l'Université de Aix-Marseille, et développés dans cette thèse en tant que photoamorceurs à hautes performances sous lumière visible (diode électroluminescente (LED) à 405 nm). Notre recherche s'est d'abord concentrée sur la capacité de ces divers dérivés à photo-amorcer les monomères acryliques et époxys pour les processus de photopolymérisation radicalaire (FRP) et cationique (CP), respectivement. Cette étude photochimique a été menée de manière innovante en utilisant des procédures de photo-oxydation ou de photo-réduction. Par conséquent, ces structures ont plusieurs fonctions. Elles peuvent donc fonctionner comme photoamorceurs de Type II en présence de donneurs d'hydrogène (tels que les amines), mais elles peuvent également agir comme photosensibilisateurs ou photoamorceurs (PSs/PAs) lorsqu'elles sont combinées avec des sels d'iodonium pour amorcer une polymérisation radicalaire ou cationique. Ces composés ont produit d'excellentes capacités de photoamorçage ainsi que des conversions finales extrêmement élevées en fonctions réactives. Les nouveaux dérivés ont également permis de produire des photopolymères tack-free (sec à toucher). Plusieurs techniques ont été employées pour examiner les différentes caractéristiques photophysiques, photochimiques et électrochimiques de ces nouveaux photoamorceurs, afin de mieux comprendre leurs mécanismes réactionnels. La photoréactivité remarquable de ces composés a également été démontrée lors de tests d'impression 3D et de la synthèse de composites. Ce travail a été publié dans "European Polymer journal" sous la citation suivante : Hammoud F. et al. "Chemical engineering around the 5, 12-dihydroindolo [3, 2-a] carbazole scaffold: Fine tuning of the optical properties of visible light photoinitiators of polymerization." European Polymer Journal 172 (2022) : 111218, et est donné ci-dessous.

European Polymer Journal 172 (2022) 111218

Contents lists available at ScienceDirect

European Polymer Journal

journal homepage: www.elsevier.com/locate/europolj

Chemical engineering around the 5,12-dihydroindolo[3,2-*a*]carbazole scaffold: Fine tuning of the optical properties of visible light photoinitiators of polymerization

Fatima Hammoud [a,b,c], Akram Hijazi [c], Malika Ibrahim-Ouali [d], Jacques Lalevée [a,b,*], Frédéric Dumur [e,*]

[a] Université de Haute-Alsace, CNRS, IS2M UMR 7361, F-68100 Mulhouse, France
[b] Université de Strasbourg, France
[c] EDST, Université Libanaise, Campus Hariri, Hadath, Beyrouth, Lebanon
[d] Aix Marseille Univ, CNRS, Centrale Marseille, iSm2, F-13397 Marseille, France
[e] Aix Marseille Univ, CNRS, ICR UMR 7273, F-13397 Marseille, France

ARTICLE INFO

Keywords:
Carbazole
Photopolymerization
Dyes
Asymmetric substitution

ABSTRACT

5,12-Dihydroindolo[3,2-*a*]carbazole is a promising scaffold for the design of visible light photoinitiators of polymerization due to the simultaneous presence of two carbazole moieties that can be differently functionalized. Notably, redshift of the absorption spectra can be facilely obtained by nitration of one of the two carbazoles, the second carbazole group being functionalized with various groups. Dinitration of 5,12-dihydroindolo[3,2-*a*]carbazole is another efficient approach for designing dyes with strong absorptions extending over the visible range. In this work, a series of 36 compounds never reported in the literature and differing by the substitution pattern have been designed and synthesized. Notably, the possibility to design push–pull dyes by Knoevenagel and Claisen Schmidt reactions, to introduce electroactive groups such as thiophene by Suzuki cross-coupling reactions or to design water soluble chromophore has been explored. To evidence the interest of these structures, photopolymerization experiments have been carried out at 405 nm and the polymerization of acrylates has been examined in thick and thin films. To support the polymerization efficiency, mechanisms involved in the free radical polymerization of acrylates have been established by the combination of various techniques including UV–visible absorption and fluorescence spectroscopy, cyclic voltammetry and photolysis experiments.

1. Introduction

In recent years, visible light photopolymerization has been the focus of intense research efforts due to the wide range of applications in which this polymerization technique is involved [1–6]. Among the most popular applications, 3D printing, dentistry or microelectronics have boosted the development of new photoinitiators [7–16]. With aim at designing visible light photoinitiators, two competitive approaches can be developed [17]. The first one is based on the chemical modification of historical UV photoinitiators aiming at red-shifting their absorptions towards the visible range [18–20]. However, considering that these chromophores were UV-centered, shift of their absorptions towards the visible range can only be obtained at the cost of difficult syntheses and most of the dyes only absorb not far from the near-UV/visible range [21–29]. Face to these considerations, a second approach consists in developing new molecules totally disconnected from these historical structures [30–48]. Considering that visible light photoinitiators of polymerization should exhibit a strong absorption over the visible range, long-living excited state lifetimes but also appropriate electrochemical properties in order to efficiently interact with the different additives introduced into the photocurable resins, structures commonly used in Organic Electronics are candidates of choice for photoinitiation [49]. In this field, carbazole is a popular structure in Organic Electronics and interest for this structure is supported by the easiness of chemical modification, its good photochemical and thermal stability, good electron-donating ability, high triplet energy level [50,51] and wide bandgap [52]. Thus, carbazole can be used for the design of small-molecules and polymeric hosts for triplet emitters in Organic Light

* Corresponding authors at: Université de Haute-Alsace, CNRS, IS2M UMR 7361, F-68100 Mulhouse, France (J. Lalevée).
E-mail addresses: Jacques.lalevee@uha.fr (J. Lalevée), frederic.dumur@univ-amu.fr (F. Dumur).

https://doi.org/10.1016/j.eurpolymj.2022.111218
Received 19 March 2022; Received in revised form 13 April 2022; Accepted 19 April 2022
Available online 23 April 2022

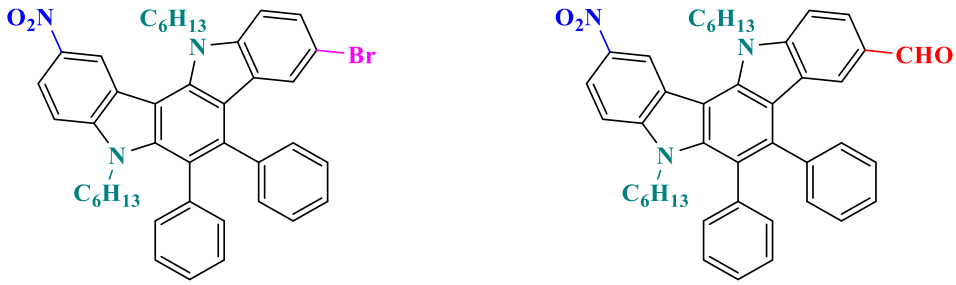

Scheme 1. Chemical structures of **Carb_1** and **Carb_2** used for the design of various dyes.

Emitting Diodes [51,53–56], molecular glasses for organic and hybrid solar cells [57–60], solid-state emitters for two-photon imaging [61], chromophores for Non-Linear optical applications [62–65], semiconductors for Organic Field Effect Transistors (OFETs)) [66–68], Aside from Organic Electronics, carbazole can also be used for the design of compounds exhibiting biological activities (antihistaminic, antitumor, antiepileptic, anti-inflammatory, antimicrobial, antidiarrheal, analgesic and neuroprotective properties) [69]. Carbazole has also been extensively used in photopolymerization [70], acting as an electron donor in push–pull dyes [71–76], a conjugated spacer for triphenylamine and pyrene-based structures [75,77], as an elemental building block for the design of polycyclic structures such as helicenes [78], or as chromophore for Type I photoinitiators [79].

In 2019, an interesting structure combining within a unique molecule two carbazole moieties has been proposed, namely 5,12-dihydroindolo[3,2-*a*]carbazole [80]. In this pioneering work, the symmetrical and regioselective *bis*(acetylation) and *bis*(formylation) at the C2,9-positions of the 5,12-dihydroindolo[3,2-*a*]carbazole core has been examined. However, absorptions of the resulting dyes were strongly UV-centered. Only in 2022, first attempts to asymmetrize the substitution of this structure have been reported [81]. Notably, the possibility to selectively nitrate one of the two carbazoles enabled first to redshift the absorption of the resulting dyes towards the visible range and second to introduce various groups onto the second carbazole such as formyl, acetyl, halogens that can advantageously be used for further chemical transformations. Asymmetrization of the substitution pattern is notably based on the difference of reactivity between the C2 and C9-positions, the C2-position being more reactive than the C9-position. Capitalizing on these preliminary results, a series of 30 dyes **Carb_1-Carb_36** based on the 5,12-dihydroindolo[3,2-*a*]carbazole scaffold have been designed and synthesized. Notably, innovative structures based on Suzuki cross-coupling reactions, Claisen-Schmidt and Knoevenagel reactions have been proposed. In fact, only **Carb_1** and **Carb_2** have been published in our previous work [81]. For all the other dyes i.e. **Carb_3-Carb_36**, none of these structures i.e. 33 compounds have previously been reported in the literature. To evidence the interest of these structures, the different dyes were used as Type II photoinitiators of polymerization upon photoactivation at 405 nm with a LED. The free radical polymerization of acrylates has been examined. Chemical mechanisms have been fully detailed by combining UV–visible absorption and

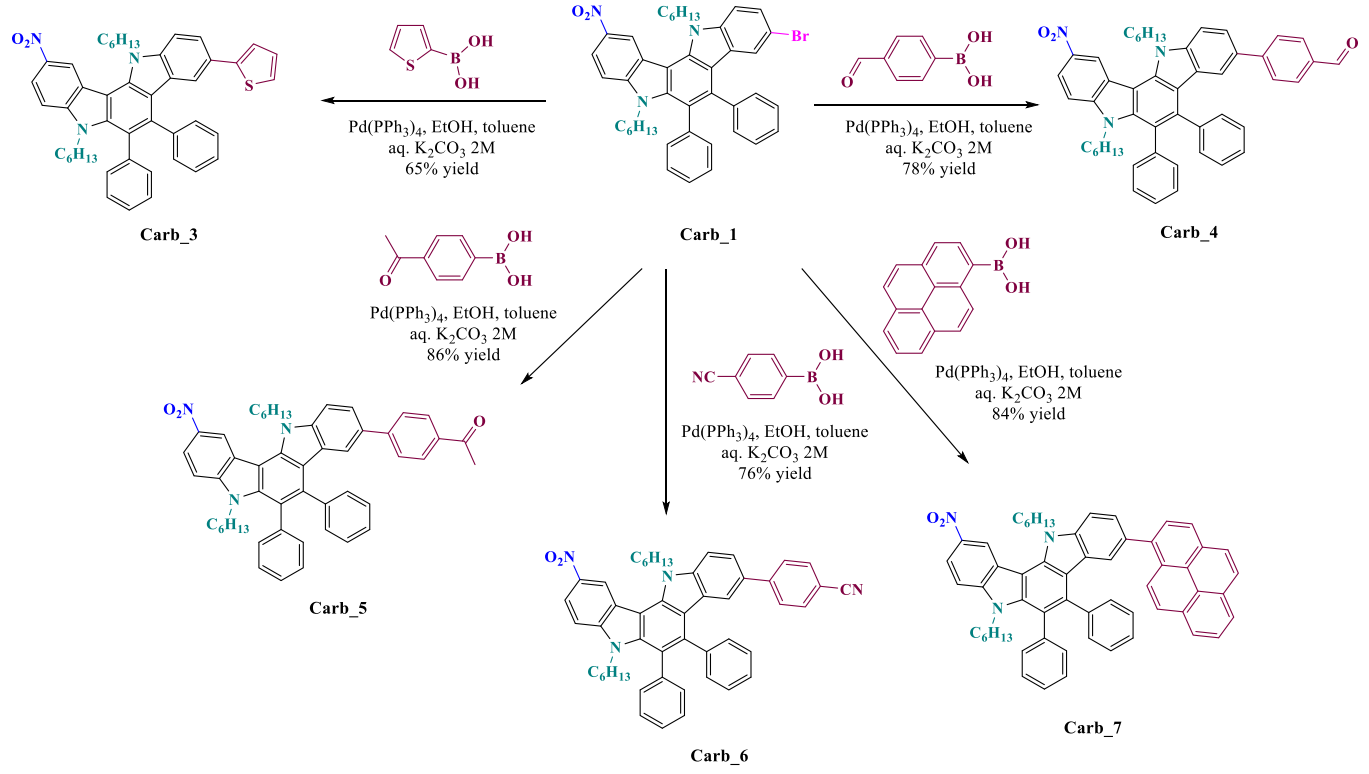

Scheme 2. Synthetic route to **Carb_3-Carb_7**.

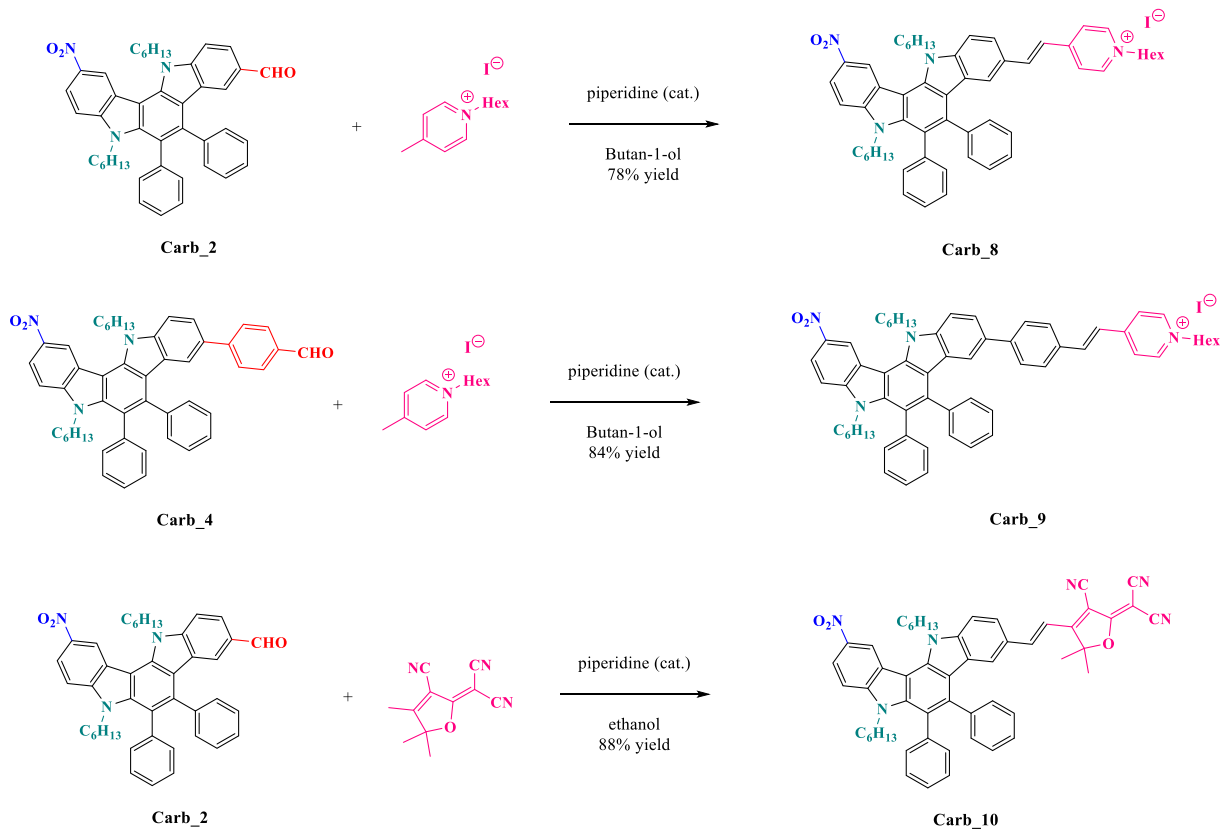

Scheme 3. Synthesis of **Carb_8** and **Carb_10** by Claisen-Schmidt condensation.

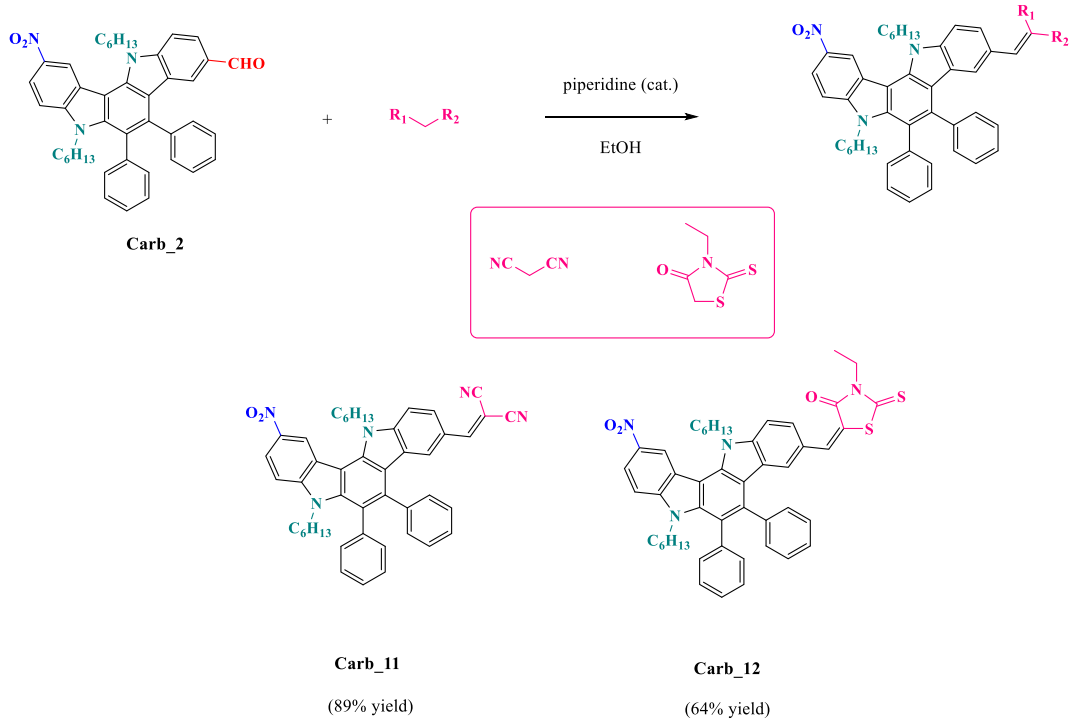

Scheme 4. Synthetic routes to **Carb_11-Carb-12**.

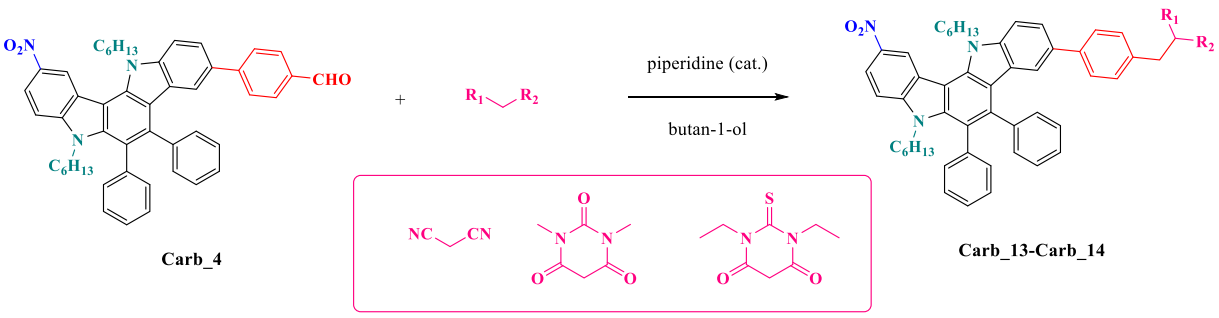

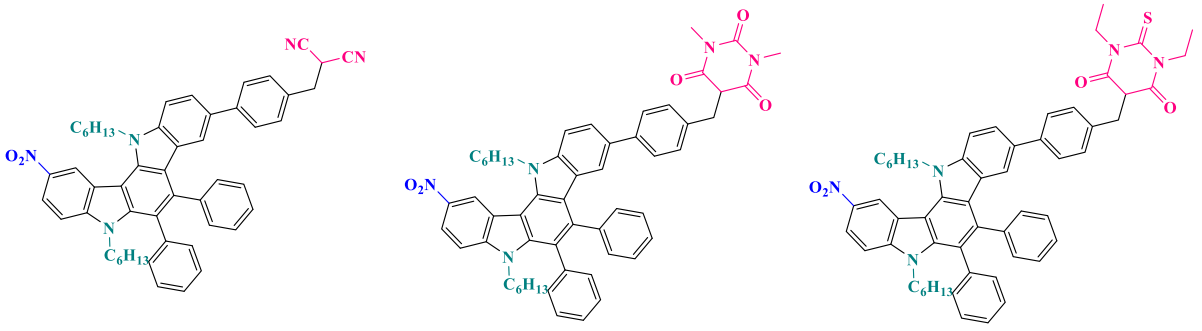

Carb_13 (55% yield)

Carb_14 (67% yield)

Carb_15 (61% yield)

Scheme 5. Synthetic routes to **Carb_13-Carb_15**.

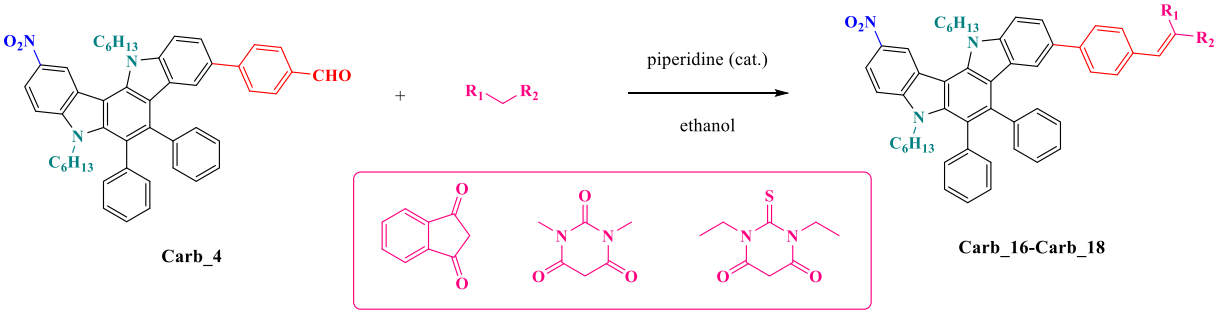

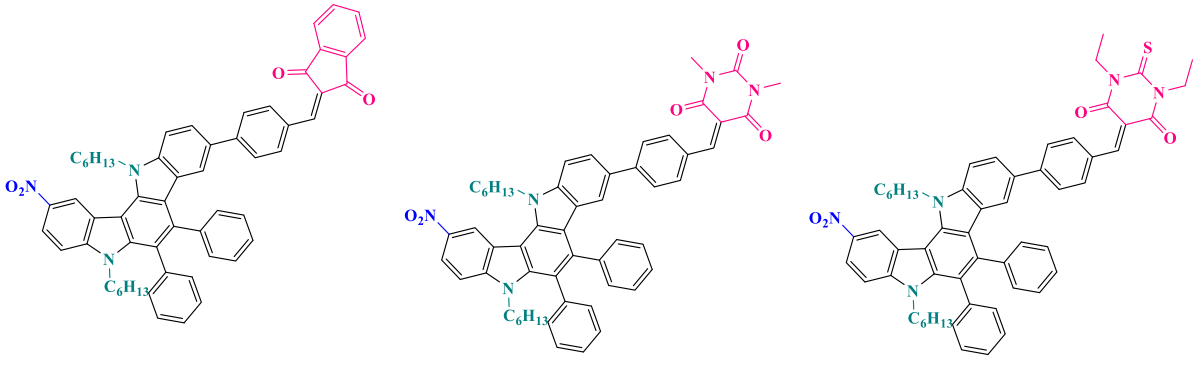

Carb_16 (78% yield)

Carb_17 (81% yield)

Carb_18 (86% yield)

Scheme 6. Synthetic routes to **Carb_16-Carb_18**.

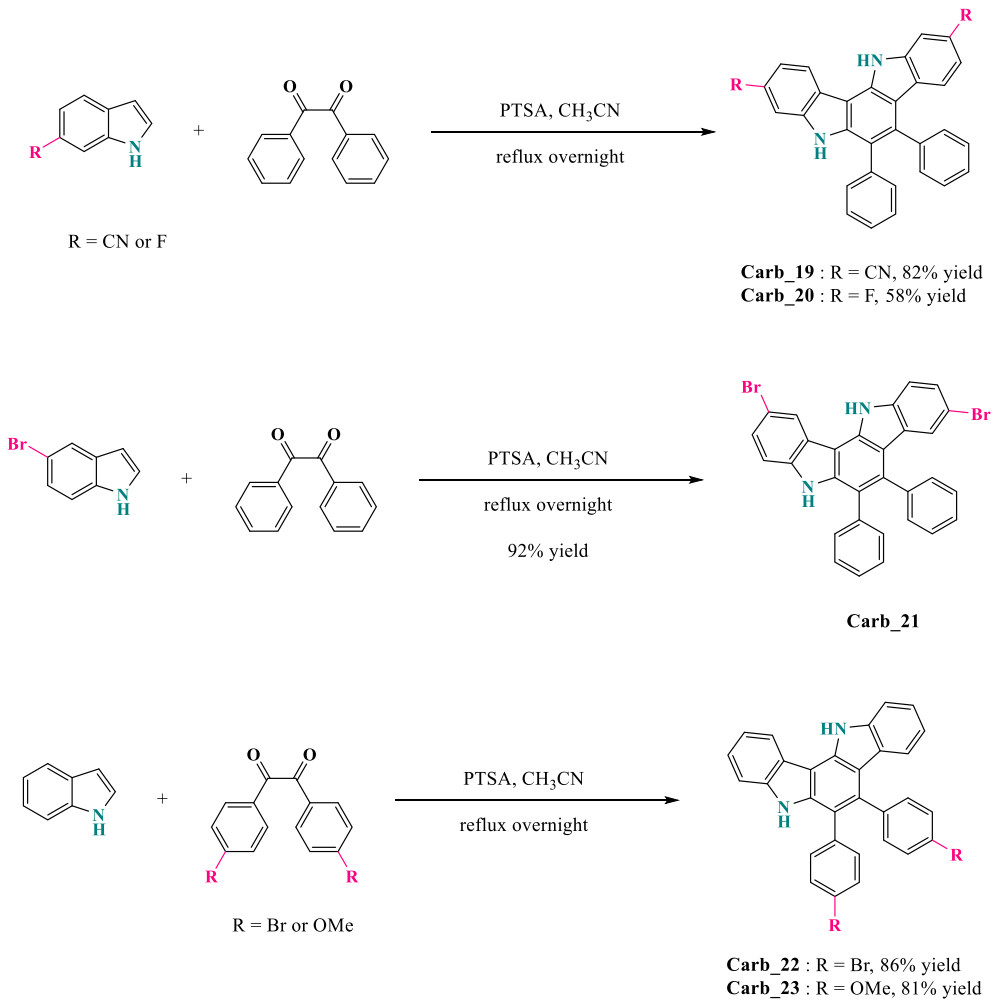

Scheme 7. Synthetic routes to **Carb_19-Carb_23**.

fluorescence spectroscopy, photolysis experiments and cyclic voltammetry.

2. Synthesis of the different dyes

2.1. Synthesis of Carb_1-Carb_7 by Suzuki cross-coupling reactions

In this work, two structures, namely 9-bromo-5,12-dihexyl-2-nitro-6,7-diphenyl-5,12-dihydroindolo[3,2-*a*]carbazole **Carb_1** and 5,12-dihexyl-2-nitro-6,7-diphenyl-5,12-dihydroindolo[3,2-*a*]carbazole-9-carbaldehyde **Carb_2** previously reported in the literature [81] have been used as reagents for the design of new structures (See Scheme 1).

Due to the presence of bromine onto **Carb_1**, Suzuki cross-coupling reactions could be carried out and **Carb_3-Carb_7** could be obtained with reaction yields ranging from 65 to 86% yields. Notably, electron-donating groups such as thiophene or pyrene, but also electron-withdrawing groups such as 4-formylphenyl, 4-acetylphenyl and 4-cyanophenyl substituents could be introduced as peripheral groups (See Scheme 2).

2.2. Synthesis of push–pull dyes by Claisen-Schmidt and Knoevenagel reactions

By connecting an electron donor to an electron acceptor by mean of a π-conjugated spacer, the resulting molecules that are named push–pull dyes are characterized an intense and broad absorption band extending over the visible range, namely, the intramolecular charge transfer band [82]. In the context of visible light photopolymerization which requires dyes to absorb in the visible range, Claisen-Schmidt and Knoevenagel reactions are reactions of choice for the design of push–pull dyes [42,83–87]. Additionally, these reactions can be carried out in green conditions, an alcohol being used as the solvent and a few drops of amine are sufficient to catalyze the two reactions. To end, push–pull dyes can be easily recovered in pure form by precipitation in alcohols, facilitating the purification process.

Thus, two dyes **Carb_8** and **Carb_9** were respectively prepared starting from **Carb_2** and **Carb_4** in 78 and 84% yields by a Claisen-Schmidt condensation of methyl picolinium iodide in butanol in the presence of a catalytic amount of piperidine (See Scheme 3). Noticeably, the same reactions carried out in ethanol did not furnish **Carb_8** and **Carb_9** under reflux, even if ethanol is commonly used as a solvent for Claisen Schmidt condensation. Conversely, while using 2-(3-cyano-4,5,5-trimethylfuran-2(5*H*)-ylidene)malononitrile (TCF) as the electron acceptor, **Carb_10** could be prepared from **Carb_2** in ethanol, still using piperidine as the base and the dye could be isolated in pure form by precipitation in 88% yield.

Carb_2 and **Carb_4** were also used as aldehydes for the design of push–pull dyes by Knoevenagel reactions. Thus, **Carb_11-Carb_12** could be obtained with reactions yields ranging from 64% for **Carb_13** to 89% for **Carb_11** in ethanol as the solvent (See Scheme 4).

While performing the Knoevenagel reaction in butan-1-ol with **Carb_4** as the aldehyde, an unexpected reaction occurred, furnishing **Carb_13-Carb_15** as the unique reaction products. The unexpected reduction reaction detected in butan-1-ol for **Carb_13-Carb_15** was

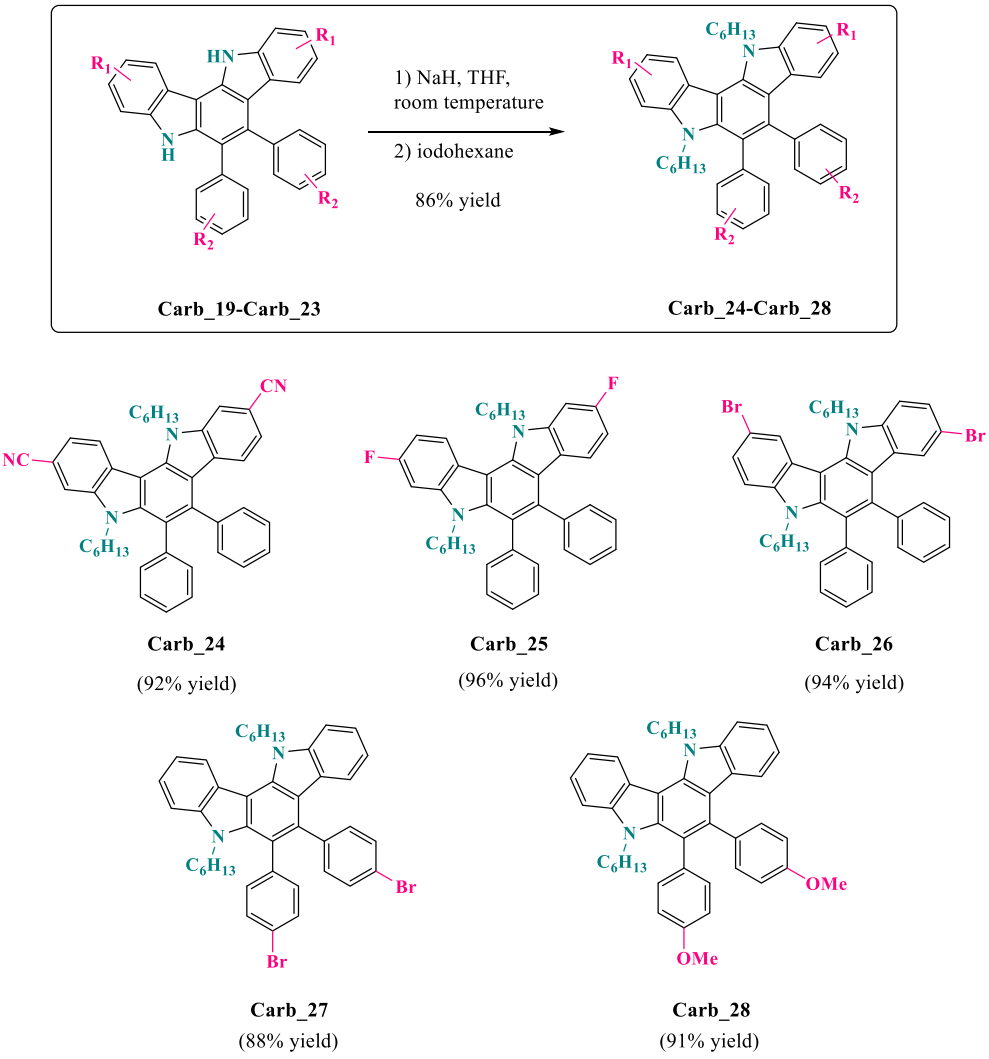

Scheme 8. Synthetic routes to **Carb_24-Carb_28**.

assigned to the contamination of **Carb_4** by traces of Pd(0) (Pd(0) is a side product of the Suzuki cross-coupling reaction), favouring the hydrogenation reaction subsequent to the Knoevenagel reaction [88]. Indeed, avoidance of trace catalysts residues is a major issue of organocatalyzed reactions [89–95]. The different dyes could be obtained with reaction yields ranging from 55% for **Carb_13** to 67% for **Carb_14** (See Scheme 5). Noticeably, all attempts to condense **Carb_4** to indane-1,3-dione failed, the unique reaction product being the dimerization product of indane-1,3-dione, namely bindone [66,67].

By performing the Knoevenagel reaction in ethanol exhibiting a lower boiling point, the targeted dyes **Carb_16-Carb_18** could be obtained with reaction yields ranging from 78 to 86% yields (See Scheme 6). Surprisingly, using ethanol as the solvent, no condensation reaction of **Carb_4** was detected with malononitrile. Conversely, due to its lower boiling point, condensation of indane-1,3-dione with **Carb_4** could be obtained, providing **Carb_16** in 78% yield. Overall, it can be concluded that the undesired hydrogenation reaction observed during the synthesis of **Carb_13-Carb_15** results from the higher boiling point of butan-1-ol compared to ethanol used for **Carb_16-Carb_18**, around 40 °C, favouring the hydrogenation reaction when butan-1-ol is used as the solvent.

2.3. Syntheses of new 5,12-dihydroindolo[3,2-a]carbazole derivatives

5,12-Dihydroindolo[3,2-*a*]carbazole is typically obtained by cycloaddition of two equivalents of indole with one equivalent of diphenylethanedione (benzil) in the presence of a catalytic amount of *para*-toluenesulfonic acid or RuO_2 nanoparticles (PTSA) [96–99]. In this context, substituted indoles and benzils were examined as potential reagents for the design of unreported 5,12-dihydroindolo[3,2-*a*]carbazole derivatives. Notably, **Carb_19-Carb_23** could be obtained with reaction yields ranging from 58% for **Carb_20** to 92% for **Carb_21** (See Scheme 7). To improve the solubility of **Carb_19-Carb_23**, the different dyes were alkylated with iodohexane using sodium hydride as the base. All dyes **Carb_25-Carb_28** could be obtained in high yields (See Scheme 8). Due to the presence of two bromine atoms on **Carb_26**, this compound was thus used for Suzuki cross-coupling reactions with 2-thienylboronic acid and 2-pyrenylboronic acid so that **Carb_29** and **Carb_30** could be obtained in 79 and 84% yields. Nitration of **Carb_27** and **Carb_28** was also examined and by controlling the number of equivalents of HNO_3 65%, mono or *bis*-nitrated compounds **Carb_31-Carb_34** could be obtained in moderate yields. Notably, lower reaction yields were obtained during *bis*-nitration due to the formation of numerous side-products (See Scheme 9). Finally, considering that the heavy atom effect is important in photochemistry, **Carb_31** and **Carb_33** were brominated with NBS, providing **Carb_35** and **Carb_36** in almost quantitative yields.

2.4. Other chemicals compounds

Bis-(4-*tert*-butylphenyl)iodonium hexafluorophosphate (Iod; Speed-Cure 938) was obtained from Lambson Ltd (UK). Ethyl 4-

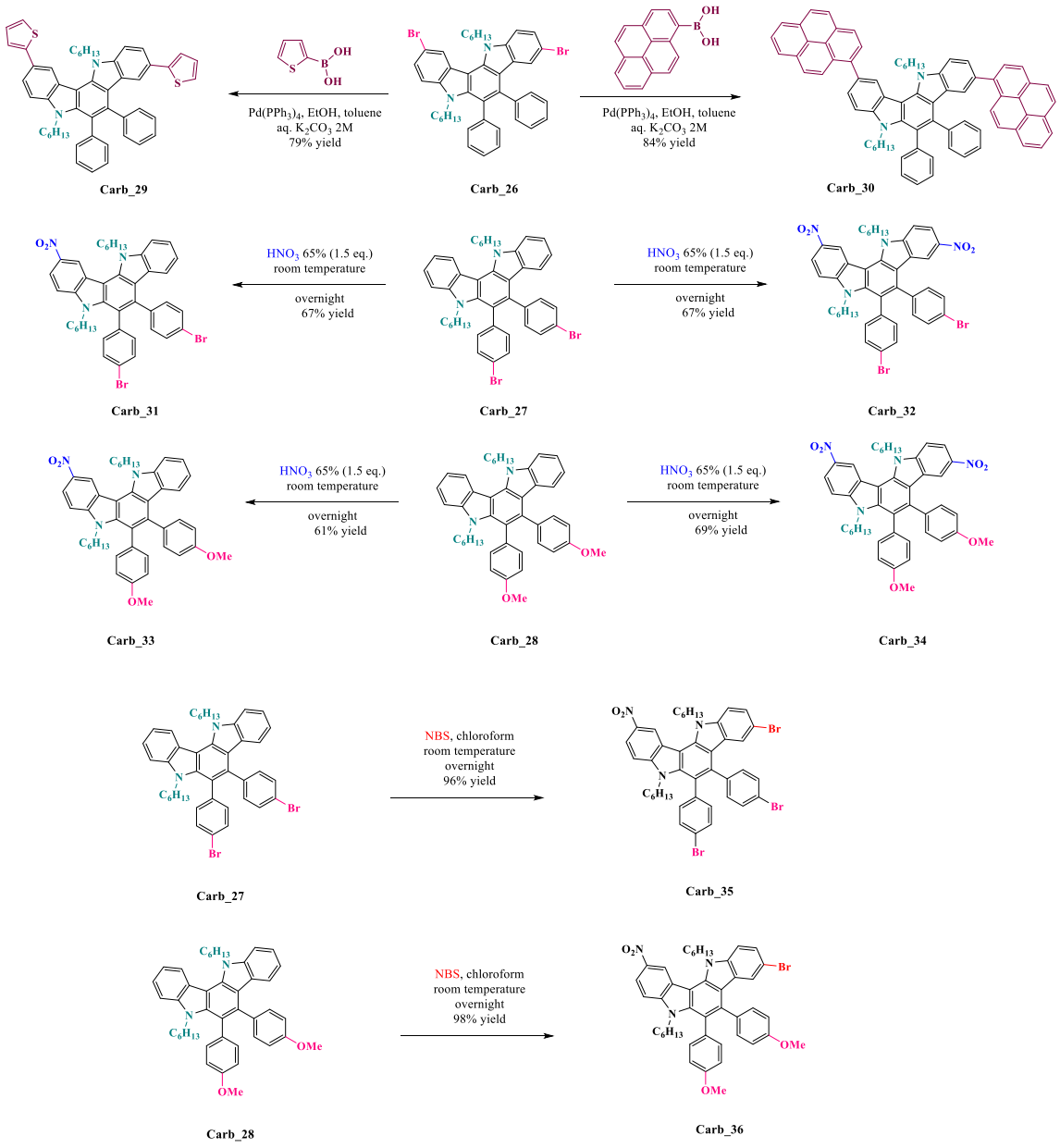

Scheme 9. Synthetic routes to **Carb_92-Carb_36**.

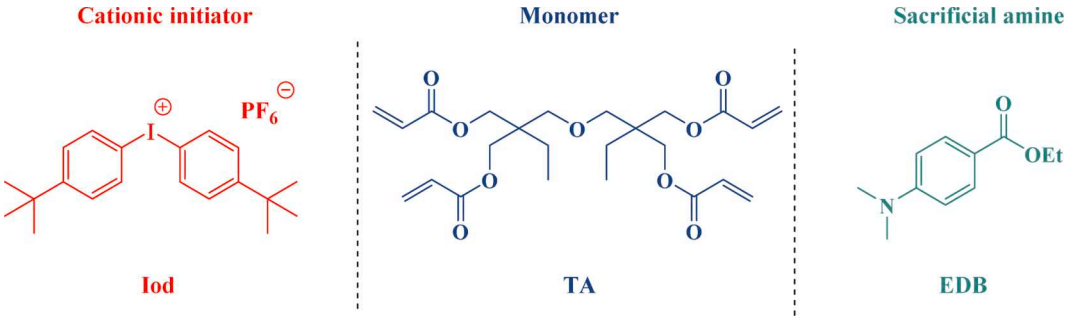

Scheme 10. Chemical structures of monomers and additives used in this study.

dimethylaminobenzoate (EDB; SpeedCure EDB) was obtained from Lambson. The monomer di(trimethylolpropane)tetraacrylate (TA)) was obtained from Allnex. Chemical structures of monomers and additives are shown in the Scheme 10.

2.5. Irradiation source

The following light-emitting diodes (LEDs) were used as irradiation sources: (i) λem = 405 nm (denoted LED@405 nm) with an incident

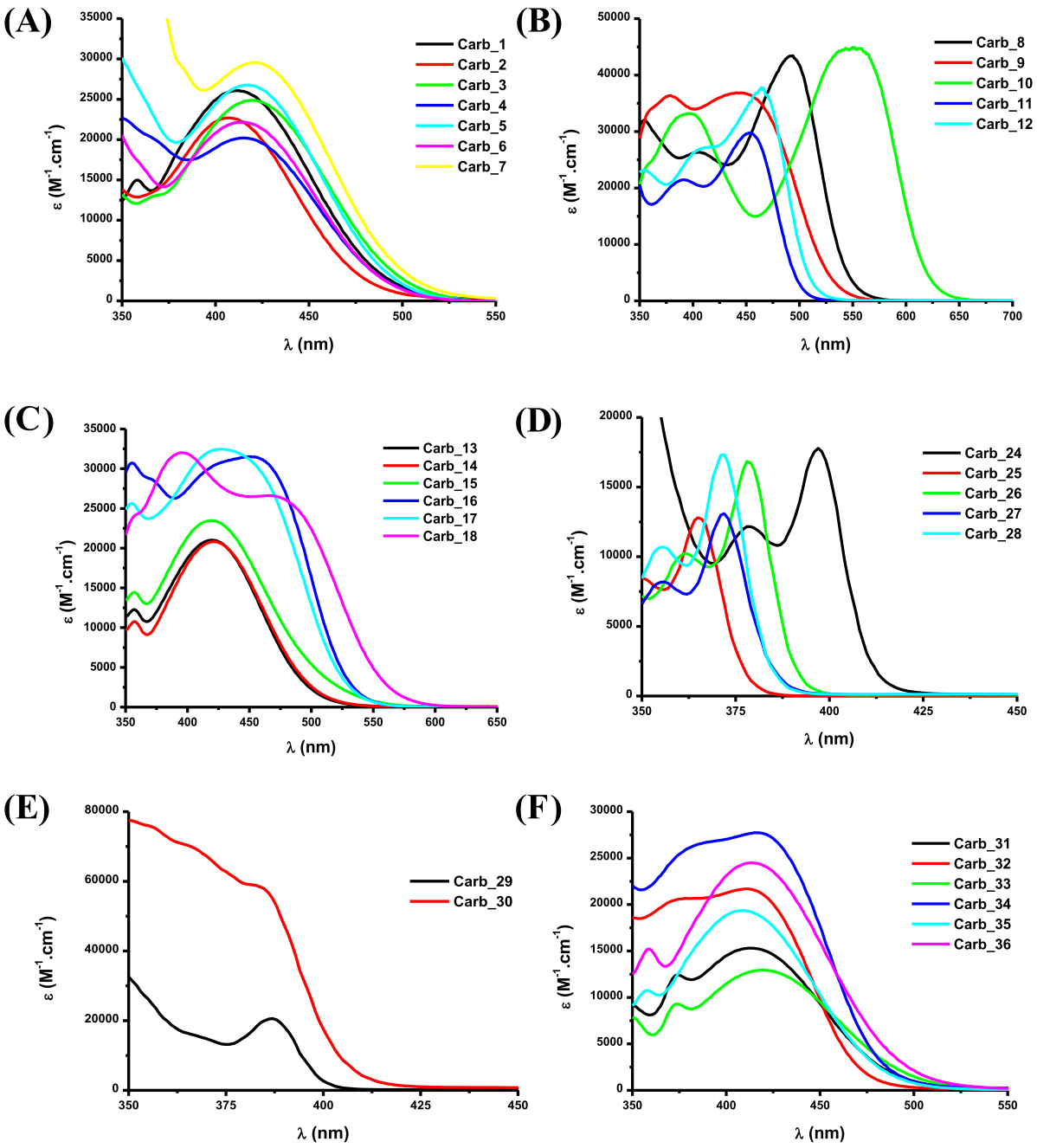

Fig. 1. UV–visible absorption spectra of **Carb_1- Carb_30** in chloroform.

light intensity at the sample surface, $I_0 = 110$ mW cm^{-2} and (ii) λem = 375 nm (denoted as LED@375 nm), $I_0 = 40$ mW cm^{-2}.

2.6. UV–visible absorption and photolysis experiments

UV–visible absorption properties of the different compounds (~10^{-5} M) as well as the steady state photolysis experiments were studied using a JASCO V730 UV–visible spectrometer, in chloroform.

2.7. Photopolymerization kinetics (RT-FTIR)

Experimental conditions used for each photosensitive formulation are indicated in the caption of the figures. All polymerization tests were performed at room temperature and the irradiation was started at t = 10 s. The weight content of the photoinitiating system is calculated from the monomer content. The photoinitiator concentrations in each photosensitive formulation have been chosen to ensure good light absorption at 405 nm. Conversion of the acrylate functions of TA was continuously followed by real time FTIR spectroscopy (JASCO FTIR 4100). For the thin samples (~25 μm of thickness), free radical polymerizations of TA were performed in laminate (the formulation is sandwiched between two polypropylene films to reduce the O_2 inhibition). The decrease of C=C double bond band was continuously monitored from 1581 to 1662 cm^{-1}. For the thicker samples (~1.4 mm of thickness), the formulations were deposited on a polypropylene film inside a 1.4 mm mold under air. Evolution of the C=C band and the epoxide group band were continuously followed from 6117 to 6221 cm^{-1}.

2.8. Steady state fluorescence

Fluorescence spectra were acquired in a quartz cell at room

Table 1
Optical characteristics of different dyes in chloroform as the solvent.

PI	Carb_1	Carb_2	Carb_3	Carb_4	Carb_5	Carb_6	Carb_7
λ (nm)	410	407	420	416	417	416	421
ε ($M^{-1}.cm^{-1}$)	26,100	22,700	24,600	20,200	26,750	22,300	29,600
PI	**Carb_8**	**Carb_9**	**Carb_10**	**Carb_11**	**Carb_12**	**Carb_13**	**Carb_14**
λ (nm)	495	441	550	452	465	419	419
ε ($M^{-1}.cm^{-1}$)	43,550	36,700	45,000	30,000	37,700	21,000	21,000
PI	**Carb_15**	**Carb_16**	**Carb_17**	**Carb_18**	**Carb_24**	**Carb_25**	**Carb_26**
λ (nm)	418	453	428	469	397	365	379
ε ($M^{-1}.cm^{-1}$)	23,500	31,500	32,500	26,426	17,550	12,700	16,800
PI	**Carb_27**	**Carb_28**	**Carb_29**	**Carb_30**	**Carb_31**	**Carb_32**	**Carb_33**
λ (nm)	371	370	387	381	414	410	418
ε ($M^{-1}.cm^{-1}$)	12,900	17,200	20,350	58,700	15,200	21,700	12,850
PI	**Carb_34**	**Carb_35**	**Carb_36**				
λ (nm)	416	409	413				
ε ($M^{-1}.cm^{-1}$)	27,700	19,350	24,500				

temperature using a JASCO FP-750 spectrofluorometer. The same spectrometer was used for the fluorescence quenching experiments of the different dyes (~10^{-5} M) in chloroform.

2.9. Redox potentials

Oxidation potentials (E_{ox}) were measured in acetonitrile by cyclic voltammetry using tetrabutylammonium hexafluorophosphate (0.1 M)

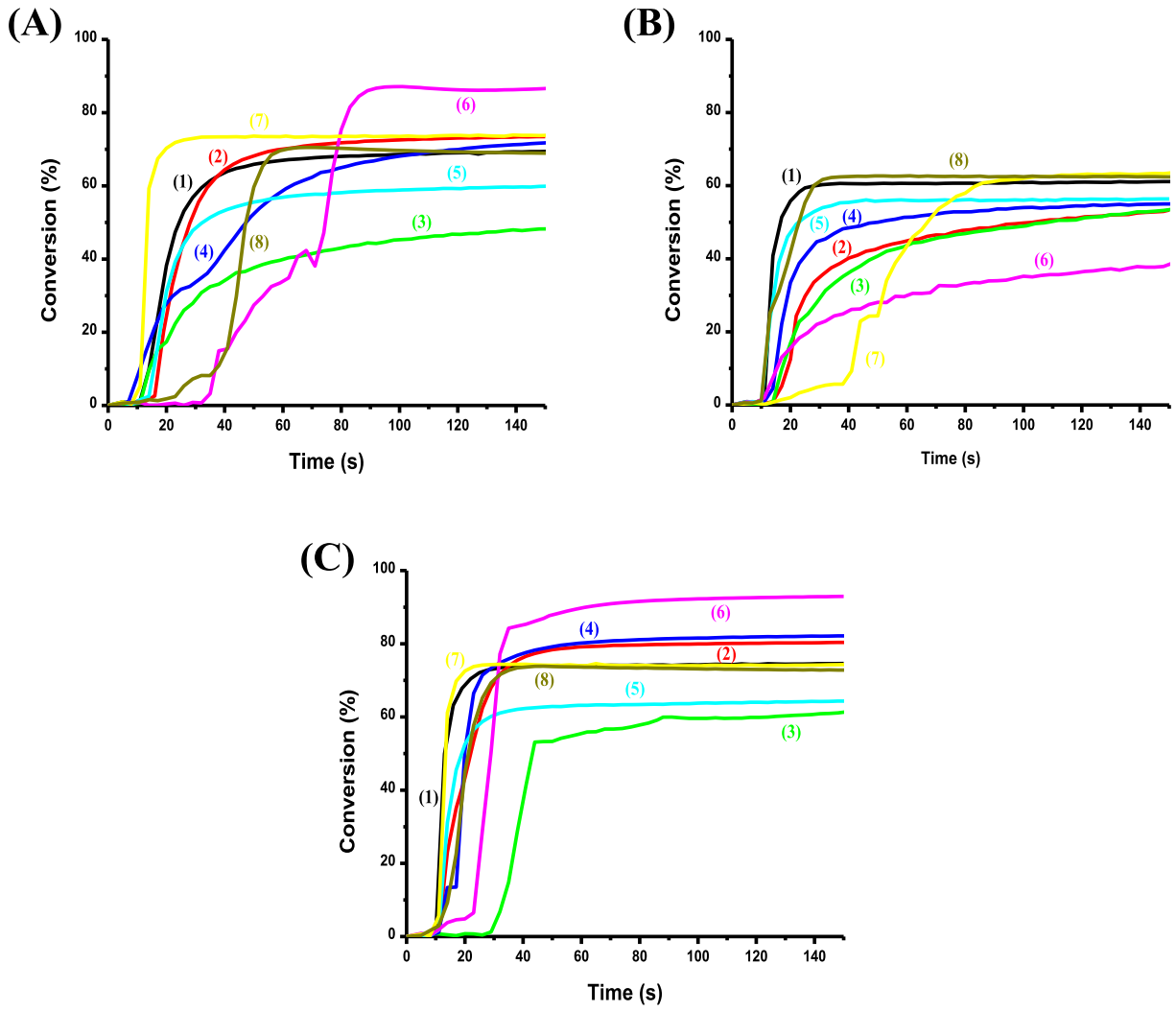

Fig. 2. Photopolymerization profiles of TA (acrylate function conversion vs. irradiation time) in laminate (thickness = 25 μm) upon exposure to LED light λ = 405 nm in the presence of two- and three-component photoinitiating systems based on carbazole compounds: (A) PI/Iod (0.1/1% w/w): (1) **Carb_6**/Iod, (2) **Carb_8**/Iod, (3) **Carb_10**/Iod, (4) **Carb_11**/Iod, (5) **Carb_15**/Iod, (6) **Carb_27**/Iod, (7) **Carb_29**/Iod, and (8) **Carb_36** (B) PI/EDB (0.1/1% w/w): (1) **Carb_6**/EDB, (2) **Carb_8**/EDB, (3) **Carb_10**/EDB, (4) **Carb_11**/EDB, (5) **Carb_15**/EDB, (6) **Carb_27**/EDB, (7) **Carb_29**/EDB, and (8) **Carb_36**/EDB (C) PI/Iod/EDB (0.1/1%/1% w/w/w): (1) **Carb_6**/Iod/EDB, (2) **Carb_8**/Iod/EDB, (3) **Carb_10**/Iod/EDB, (4) **Carb_11**/Iod/EDB, (5) **Carb_15**/Iod/EDB, (6) **Carb_27**/Iod/EDB, (7) **Carb_29**/Iod/EDB, and (8) **Carb_36**/Iod/EDB. The irradiation starts for t = 10 s.

as the supporting electrolyte (potential vs. Saturated Calomel Electrode – SCE). The free energy change ΔG_{et} for an electron transfer reaction was calculated from eqn (1) [100], where E_{ox}, E_{red}, E*, and C are the oxidation potential of the electron donor (the carbazole derivatives), the reduction potential of the electron acceptor (the iodonium salt), the excited state energy and the coulombic term for the initially formed ion pair, respectively. Here, C is neglected for polar solvents.

$$\Delta G_{et} = E_{ox} - E_{red} - E^* + C \quad (1)$$

2.10. Direct laser write

For direct laser write experiments, a laser diode emitting at 405 nm (spot size around 50 μm) was used for the spatially controlled irradiation. The photosensitive resin was polymerized under air and the generated 3D patterns were analyzed using a numerical optical microscope (DSX-HRSU from Olympus Corporation).

2.11. Near-UV conveyor

Light-sensitive resins were deposited on the glass fibers used for reinforcement. Curing of the deposited resins was realized using an LED conveyor @ 395 nm (4 W/cm^2). The distance from the belt to the LED was set at 15 mm, and the belt speed was set at 2 m/min (3 s of irradiation per pass).

3. Results and discussion

3.1. UV–visible absorption properties of the different dyes

UV–visible absorption spectra of all dyes were recorded in chloroform as the solvent and the results are presented in the Figs. 3-9. Different groups of molecules could be identified, depending on their absorption spectra. In the first group comprising **Carb_1-Carb_7**, all dyes comprise a nitro group in their scaffold enabling their absorptions to be centered in the visible range. For these dyes, an absorption maximum centered around 420 nm could be determined. The highest molar extinction coefficient was found for **Carb_7** bearing a pyrene group as the substituent (See Fig. 1 (A) and Table 1). Conversely, once an electron accepting group is connected to **Carb_2**, a significant redshift of the absorption maxima could be found (See Fig. 1(B)). Thus, by improving the electron-withdrawing ability from **Carb_11** to **Carb_10**, position of the intramolecular charge transfer band shifted from 454 nm for **Carb_11** to 549 nm for **Carb_10**. Interestingly, while comparing the absorption of **Carb_8** and **Carb_9** differing by the spacer between the carbazole structure and the pyridinium group, a blueshift of the absorption maxima was detected, the absorption peak shifting from 494 nm for **Carb_8** to 447 nm for **Carb_9**. This blueshift was assigned to the isolation of the electron donating carbazole in **Carb_9** due to the consecutive presence of two phenyl groups that adversely affects the electronic delocalization.

While comparing the absorption of **Carb_13-Carb_15** to that of **Carb_17** and **Carb_18**, replacement of the single bond in **Carb_13-Carb_15** by a double bond significantly modified the absorption spectra compared to that of **Carb_17** and **Carb_18.** Due to the lack of conjugation with the electron accepting groups in **Carb_13-Carb_15**, similar absorption maxima peaking at 420 nm could be found for the three dyes. In the case of **Carb_16-Carb_18**, the lack of conjugation of the electron donating carbazole with the rest of the molecule was confirmed. Indeed, by improving the electron-withdrawing ability, almost no modification of the absorption maxima was found (See Fig. 1(C)).

By varying the substitution pattern of **Carb_24-Carb_28**, interesting trends could be determined. Thus, introduction of cyano groups onto **Carb_24** enabled to produce a dye absorbing until 425 nm. Conversely, for **Carb_25-Carb_28**, almost no absorption was detected in the visible range, making these dyes poor candidates for photoinitiation in the visible range (See Fig. 1(D)). A similar deduction can be evidenced for **Carb_29** and **Carb_30** in which no electron-withdrawing groups have been introduced (See Fig. 1(E)).

Finally, introduction of one or two nitro groups onto **Carb_31-Carb_36** enabled to redshift the absorption spectra of these dyes compared to that of their parent structures **Carb_26-Carb_28** (See Fig. 1 (F)). Interestingly, introduction of one or two nitro groups did not significantly modify the position of the absorption maxima, as shown in the Table 1.

Table 2
Final Acrylate Monomer Conversion (FC) for TA after 100 s.

	Thickness = 25 μm (In laminate)			Thickness = 1.4 mm (Under air)		
	PI/Iod (0,1%/ 1% w/ w)	PI/EDB (0,1%/ 1% w/ w)	PI/Iod/ EDB (0,1%/ 1%/1% w/w/w)	PI/Iod (0,1%/ 1% w/ w)	PI/EDB (0,1%/ 1% w/ w)	PI/Iod/ EDB (0,1%/ 1%/1% w/w/w)
Carb_1	56%	48%	58%	77%	78%	89%
Carb_2	62%	54%	62%	60%	79%	78%
Carb_3	72%	63%	70%	53%	63%	75%
Carb_4	69%	59%	71%	56%	79%	51%
Carb_5	70%	48%	75%	68%	69%	74%
Carb_6	69%	61%	75%	55%	75%	54%
Carb_7	45%	14%	66%	20%	11%	77%
Carb_8	73%	53%	80%	41%	34%	45%
Carb_9	66%	60%	66%	34%	11%	74%
Carb_10	48%	53%	61%	10%	1%	16%
Carb_11	72%	55%	82%	11%	32%	25%
Carb_12	61%	72%	71%	69%	46%	39%
Carb_13	71%	62%	73%	49%	77%	76%
Carb_14	75%	63%	76%	63%	72%	35%
Carb_15	60%	56%	64%	61%	74%	63%
Carb_17	64%	31%	65%	61%	28%	34%
Carb_18	70%	66%	74%	38%	41%	41%
Carb_24	67%	31%	71%	79%	56%	91%
Carb_25	1%	42%	71%	15%	6%	86%
Carb_26	87%	49%	86%	64%	7%	80%
Carb_27	87%	39%	93%	70%	5%	86%
Carb_28	73%	63%	73%	69%	12%	64%
Carb_29	74%	63%	74%	63%	14%	91%
Carb_30	68%	41%	64%	70%	9%	87%
Carb_31	58%	68%	60%	78%	78%	82%
Carb_32	65%	66%	68%	50%	81%	77%
Carb_33	71%	84%	71%	35%	70%	71%
Carb_34	90%	89%	89%	53%	72%	75%
Carb_35	49%	79%	52%	65%	68%	83%
Carb_36	69%	62%	73%	73%	78%	87%
Iod/EDB (1%/ 1% w/ w)	52%	66%				

3.2. Free radical polymerization (FRP) of acrylates

Different combinations based on 5,12-dihydroindolo[3,2-*a*]carbazole derivatives (Carb/Iod, or Carb/EDB (0.1/1% w/w) and Carb/Iod/EDB (0.1%/1%/1% w/w/w)) have been tested for the FRP of TA in thin films (25 μm, in laminate) and thick samples (1.4 mm, under air). High final acrylate function conversions (FCs) are shown for the different dyes while using the different photoinitiating systems (PISs) (Fig. 2 and Table 2). It should be noted that the different dyes, Iod, or EDB examined separately were unable to initiate the FRP of TA under the same conditions, clearly showing that the presence of the dyes was required for an efficient process. For the Iod/EDB system (without Carb), a polymerization occurs in agreement with a Charge Transfer Complex (CTC) behavior. However, the polymerization rate is much slower and an inhibition time is found (Fig. S1 in Supporting Information). Therefore,

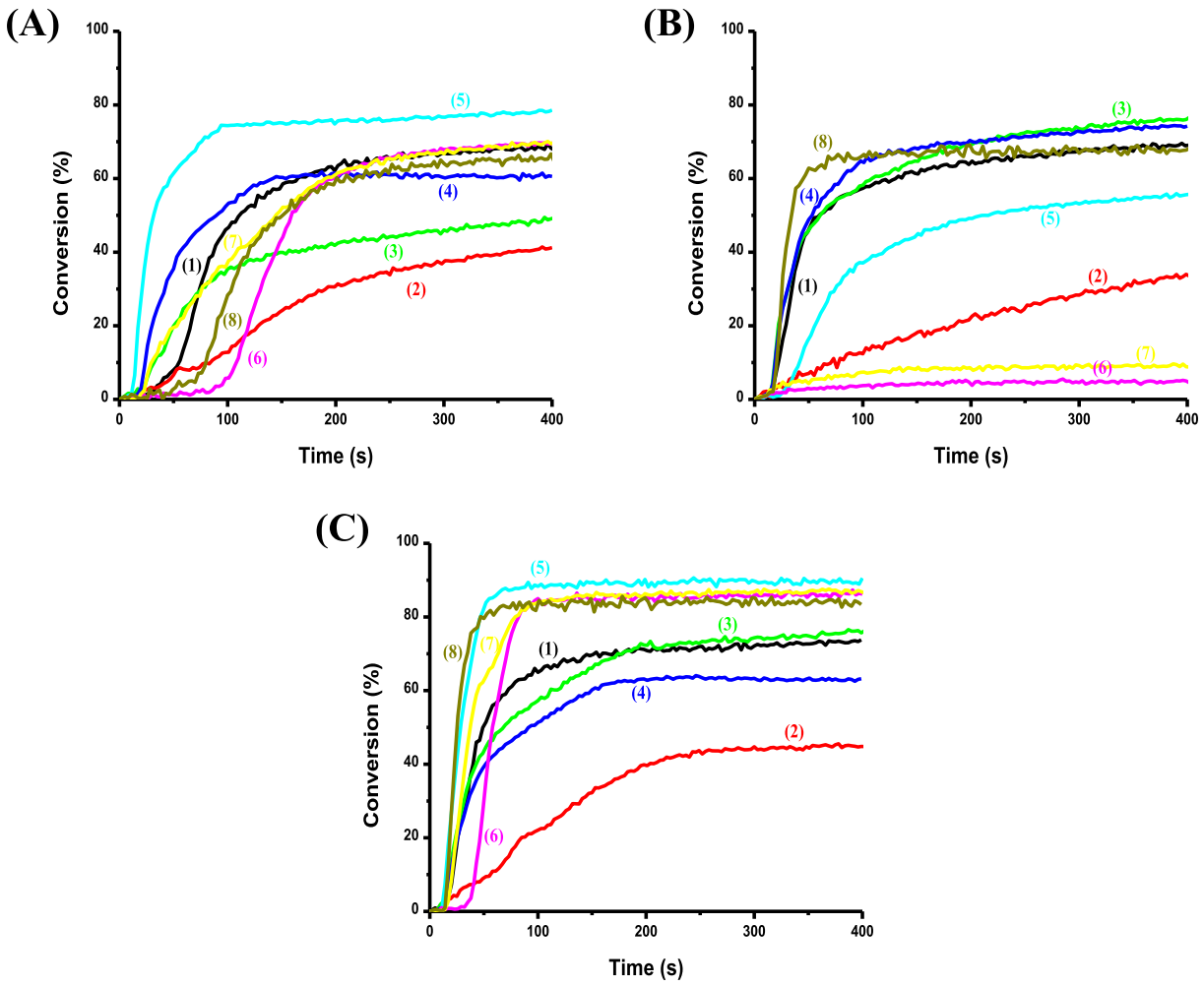

Fig. 3. Photopolymerization profiles of TA (acrylate function conversion vs. irradiation time) under air (thickness = 1.4 mm) upon exposure to LED light λ = 405 nm in the presence of two- and three-component photoinitiating systems based on carbazole compounds: (A) PI/Iod (0.1/1% w/w): (1) **Carb_5**/Iod, (2) **Carb_8**/Iod, (3) **Carb_13**/Iod, (4) **Carb_15**/Iod, (5) **Carb_24**/Iod, (6) **Carb_27**/Iod, (7) **Carb_30**/Iod, and (8) **Carb_35** (B) PI/EDB (0.1/1% w/w): (1) **Carb_5**/EDB, (2) **Carb_8**/EDB, (3) **Carb_13**/EDB, (4) **Carb_15**/EDB, (5) **Carb_24**/EDB, (6) **Carb_27**/EDB, (7) **Carb_30**/EDB, and (8) **Carb_35**/EDB (C) PI/Iod/EDB (0.1/1%/1% w/w/w): (1) **Carb_5**/Iod/EDB, (2) **Carb_8**/Iod/EDB, (3) **Carb_13**/Iod/EDB, (4) **Carb_15**/Iod/EDB, (5) **Carb_24**/Iod/EDB, (6) **Carb_27**/Iod/EDB, (7) **Carb_30**/Iod/EDB, and (8) **Carb_35**/Iod/EDB. The irradiation starts for t = 10 s.

the presence of Carb clearly leads to better polymerization processes.

When the iodonium salt was combined with the different dyes, good photopolymerization profiles could be obtained (see Fig. 2(A), Fig. 3(A) and Table 2). In fact, the Carb/Iod interaction corresponds to an electron transfer reaction finally leading to an aryl radical $Ar^{\bullet}$ (r1) and (r2). $Ar^{\bullet}$ is considered as the initiating species for the free radical polymerization:

$$Carb\ (h\nu) \rightarrow {}^{1}Carb \qquad (r1)$$

$${}^{1}Carb + Ar_2I^{+} \rightarrow Carb^{\bullet+} + Ar_2I^{\bullet} \rightarrow Carb^{\bullet+} + Ar^{\bullet} + ArI \qquad (r2)$$

FRP of TA in thin films (laminate) in the presence of the different Carb/Iod couples was efficient using a LED@405 nm, while Iod alone or the dyes alone could not initiate the polymerization (e.g. **Carb_29**/Iod FC = 74%; Fig. 2(A), curve 7). Same efficiency was observed in thick samples (1.4 mm, under air) using the Carb/Iod systems, but for some dyes, the monomer conversion was low compared to the results obtained in thin samples (e.g., **Carb_8**, Fig. 2(A), curve 2 FC = 73% vs. Fig. 3(A) curve 2 FC = 41%). This behaviour can be attributed to an internal filter effect (see also Table 2). Consequently, the studied compounds were quite efficient in photo-oxidation processes (electron transfer from Carb to Iod) to initiate a FRP in combination with Iod (the chemical mechanism is discussed below, using different techniques such as cyclic voltammetry, photoluminescence spectroscopy and photolysis experiments).

Parallel to this, 5,12-dihydroindolo[3,2-*a*]carbazole derivatives were also examined as Type-II photoinitiators with an amine (EDB), leading also to an efficient photo-reduction process for FRP. After irradiating a Carb/EDB system at 405 nm, a reaction could take place between the excited state of the dyes ^{1}Carb and EDB. Following the reactions (r3, r4), $EDB^{\bullet}_{(-H)}$ was formed and this species was responsible for the initiation of FRP. Firstly, an electron was transferred from EDB to Carb (r3), followed by a hydrogen abstraction (r4) leading to the formation of $EDB^{\bullet}{}_{(-H)}$ radicals responsible for initiating FRP.

$${}^{1}Carb + EDB \rightarrow Carb^{\bullet-} + EDB^{\bullet+} \rightarrow Carb\text{-}H^{\bullet} + EDB^{\bullet}_{(-H)} \qquad (r3, r4)$$

Markedly, FRP of TA in the presence of the different Carb/EDB (0.1%/1% w/w) couples was efficient using LED@405 nm, while EDB alone, or Carb alone could not initiate FRP processes. Typical acrylate function conversion–time profiles are given in Fig. 2(B) for thin films (25 μm, in laminate), Fig. 3(B) for thick samples (1.4 mm, under air) and the FCs are summarized in Table 2. High FCs could be reached in Carb/EDB systems (e.g. **Carb_35**/EDB FC = 68%; Fig. 3(B), curve 8 using LED@405 nm).

With the regard to the three-component photoinitiating systems (PISs), in both thin (25 μm, in laminate) (Fig. 2) and thick samples (1.4

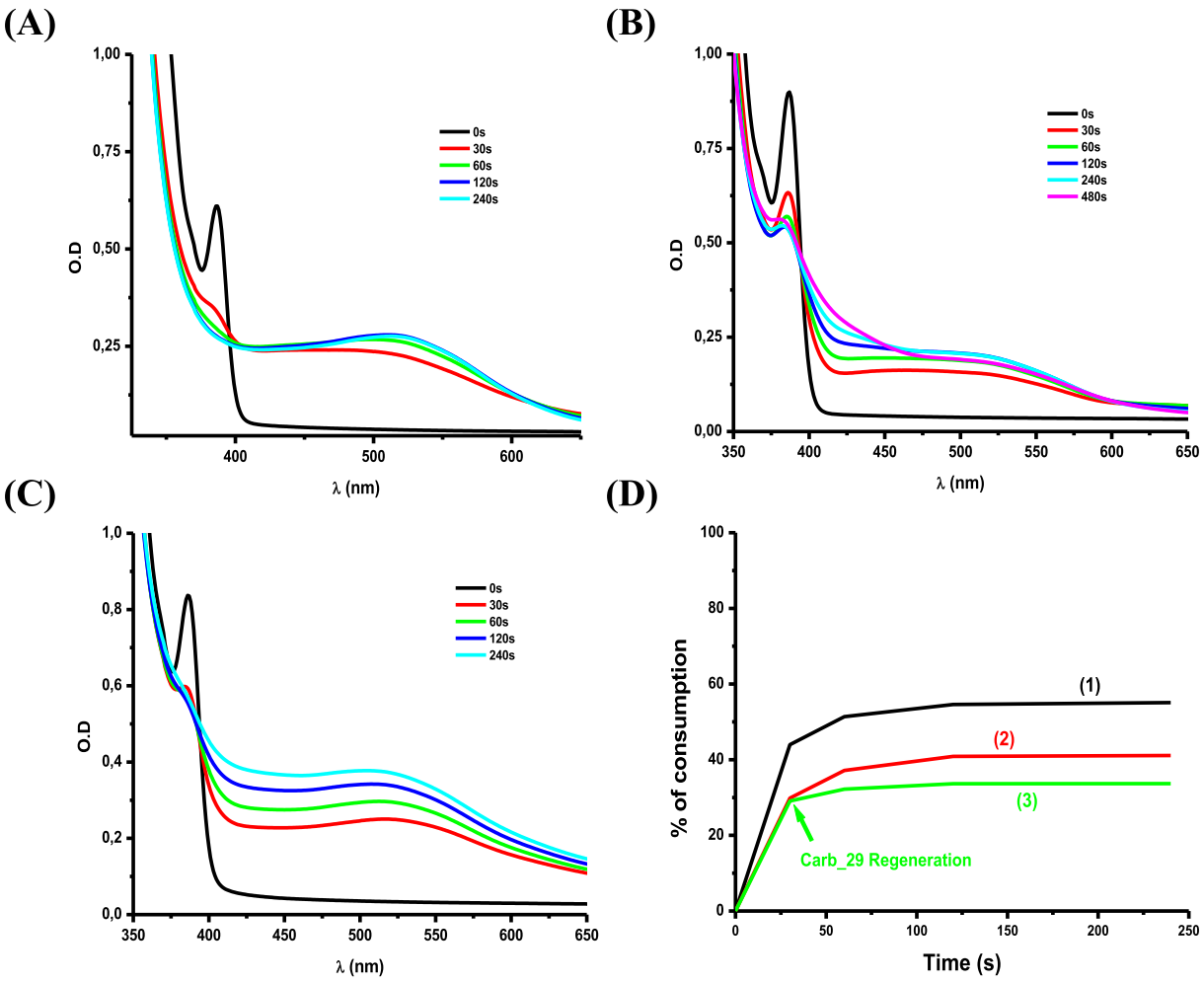

Fig. 4. Photolysis of **Carb_29** in chloroform upon irradiation with a LED@375 nm (A) with Iod (10^{-2} M); (B) with EDB (10^{-2} M); (C) with Iod/EDB (10^{-2} M/10^{-2} M); and (D) Consumption of **Carb_29**: (1) with Iod salt; (2) with EDB; and (3) with Iod/EDB.

mm, under air), better performances were obtained when a third component was added to the photosensitive formulations. Indeed, using a three-component system, the maximum acrylate function conversions (FCs) and the polymerization rates (R_p) achieved in these conditions were higher than those obtained with the two-components PISs (e.g. **Carb_6**/Iod FC = 69% Fig. 2(A) curve 1 or **Carb_6**/EDB FC = 61% Fig. 2 (B) curve 1 vs. **Carb_6**/Iod/EDB FC = 75% Fig. 2(C) curve 1, and **Carb_35**/Iod FC = 65% Fig. 3(A) curve 8 or **Carb_35**/EDB FC = 68% Fig. 3(B) curve 8 vs. **Carb_35**/Iod/EDB FC = 83% Fig. 3(C) curve 8). This fact was also partly ascribed to the formation of a charge transfer complex (CTC) between Iod and EDB which is able to generate reactive species when it absorbs light. Additionally, $Carb^{\bullet+}$ can react with EDB (r5) or Carb-H$^{\bullet}$ with Iod (r6) (see also Scheme 11). Finally, the dye can be regenerated (See also scheme 11 and see the steady state photolysis results below) [3,83,101–103].

$$Carb^{\bullet+} + EDB \rightarrow Carb + EDB^{\bullet+} \quad (r5)$$

$$Carb\text{-}H^{\bullet} + Ar_2I^{+} \rightarrow Carb + Ar^{\bullet} + ArI + H^{+} \quad (r6)$$

Overall, in this series of dyes, seven of them could furnish monomer conversions higher than 87%, namely **Carb_1, Carb_24, Carb_25, Carb_27, Carb_29, Carb_30** and **Carb_36** (See Table 2). Concerning **Carb_1, Carb_24, Carb_30** and **Carb_36**, the high reactivity of these four dyes can be assigned to the high molar extinction coefficients of these dyes at 405 nm. On the opposite, **Carb_25, Carb_27** and **Carb_29** exhibit low molar extinction coefficients at 405 nm. Their remarkable reactivities can be assigned in this case to the highly negative free energy changes determined for the electron transfer reactions. Indeed, these dyes exhibit the most negative free energy changes for the electron transfer reaction of the series. Therefore, high performance of the seven dyes is the result of high molar extinction coefficients at 405 nm or appropriate redox properties providing highly negative free energy changes for the electron transfer from the dye towards the iodonium salt.

3.3. Chemical mechanisms

3.3.1. Steady state photolysis

Steady-state photolysis of the Carb/Iod (10^{-2} M), Carb/EDB (10^{-2} M) and Carb/Iod/EDB (10^{-2} M/ 10^{-2} M) systems was performed in chloroform under light irradiation, using a LED@375 nm. It is remarkable that, for example the photolysis of **Carb_29**/Iod system was very efficient (See Fig. 4(A)) with the formation of new photoproducts (characterized by a significant new absorption for $\lambda > 395$ nm) which is due to the Carb/Iod interaction. Isobestic points were found suggesting a clean process without side reactions. In the same way, photolysis of the **Carb_29**/EDB system was also efficient (Fig. 4(B)) but slower than that with the iodonium salt, which can in addition suggest a photochemical reaction between the studied dyes and EDB, in agreement with the results observed in the photopolymerization experiments. Indeed, photolysis of **Carb_29** in the presence of the Iod/EDB couple (Fig. 4(C)) was lower than that observed with Iod or EDB alone (Fig. 4(A, B), clearly showing that **Carb_29** is regenerated in the three-component system (see also the consumption of **Carb_29** with Iod, EDB, and Iod/EDB in

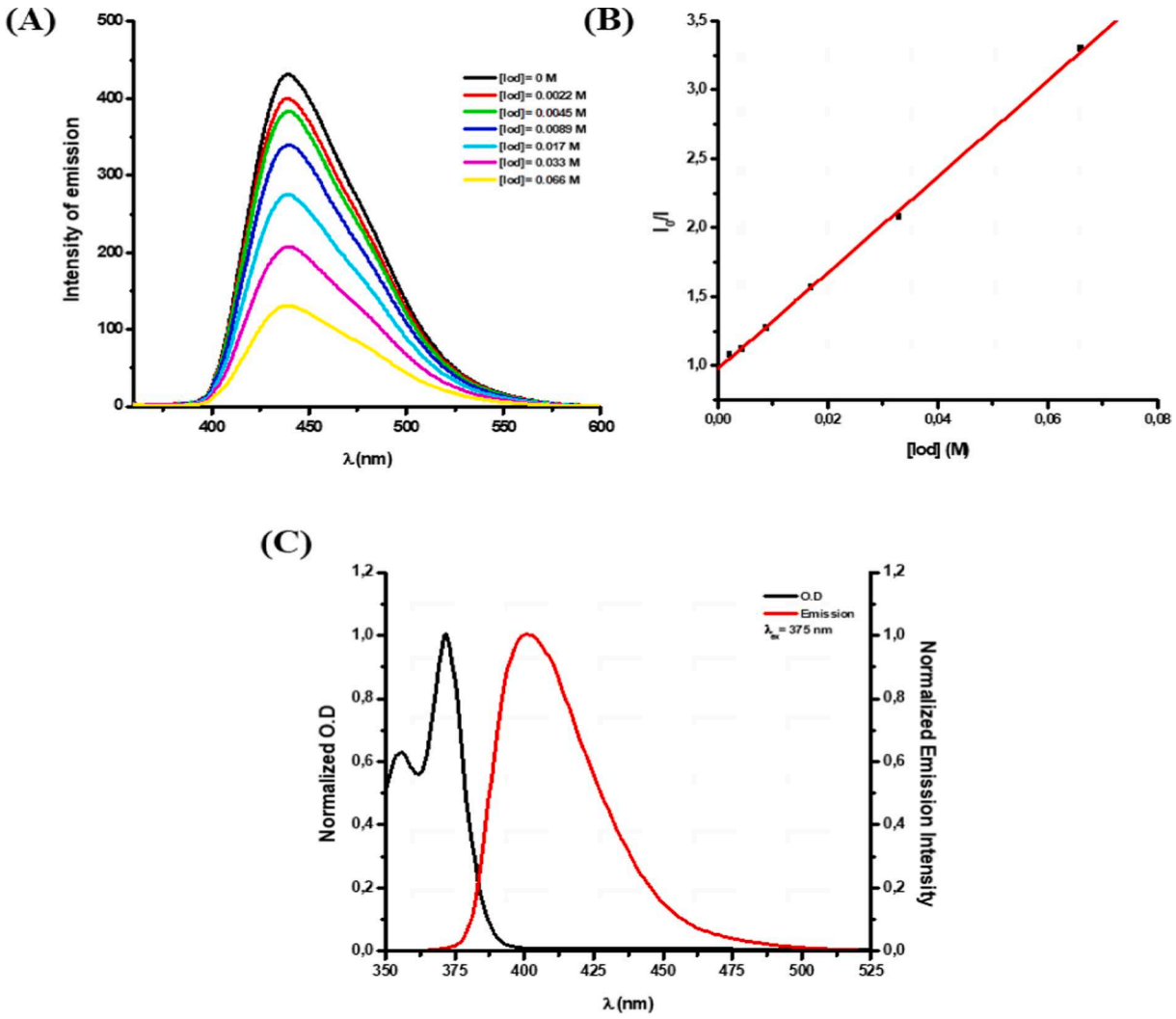

Fig. 5. (A) Quenching of [1]**Carb_30** by Iod in chloroform. (B) Determination of the Stern-Volmer coefficient. (C) UV–visible absorption and emission spectra **Carb_27** in chloroform.

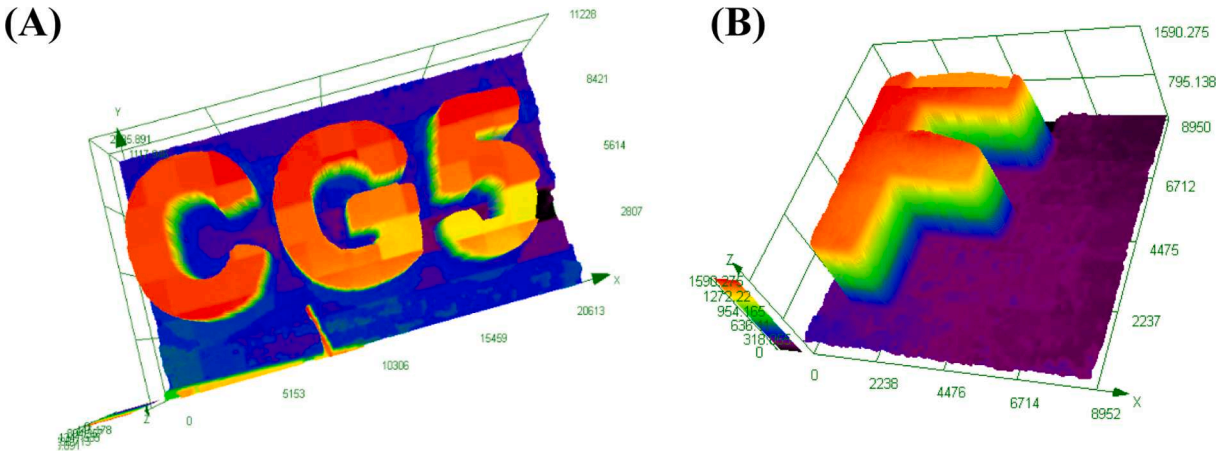

Fig. 6. 3D patterns obtained upon exposure to a laser diode @405 nm: characterization by numerical microscopy; (A): **Carb_5**/Iod/EDB (0.1%/1%/1% w/w/w) in Ebecryl40 (thickness = 2200 μm); (B): **Carb_24**/Iod/EDB (0.1%/1%/1% w/w/w) in Ebecryl40 (thickness = 1590 μm).

Fig. 4(D)).

3.3.2. *Fluorescence quenching*

In order to better understand the interaction existing between the studied dyes and the iodonium salt (Iod), fluorescence quenching experiments were carried out in chloroform. For example, as shown in Fig. 5, a fast fluorescence quenching process of **Carb_30** by Iod was detected (see Fig. 5 and Table 3); this clearly shows a very strong

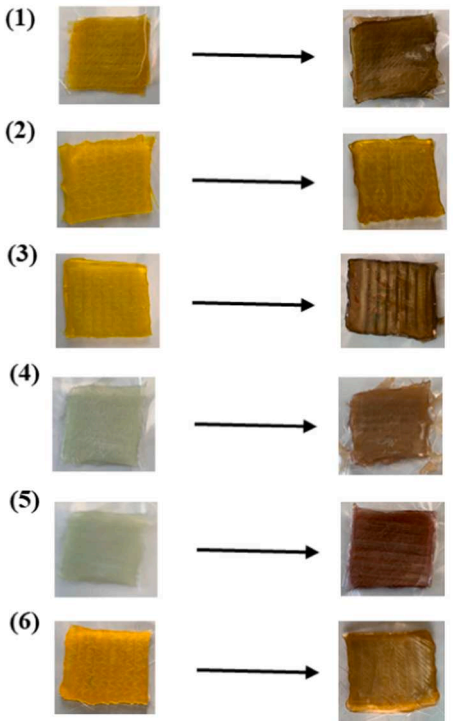

Number of passes to obtained tack-free		
Surface	Bottom	Thickness (mm)
1	20	3.15
3	23	3.63
3	21	3.09
1	15	3.15
1	15	3.22
1	14	2.99

Fig. 7. Photocomposites produced by FRP experiments of acrylate monomer (TA) using a LED conveyor @395 nm Carb/Iod/EDB (0.1%/1%/1% w/w/w): (1) **Carb_5**, (2) **Carb_11**, (3) **Carb_13**, (4) **Carb_24**, (5) **Carb_29** and (6) **Carb_36**.

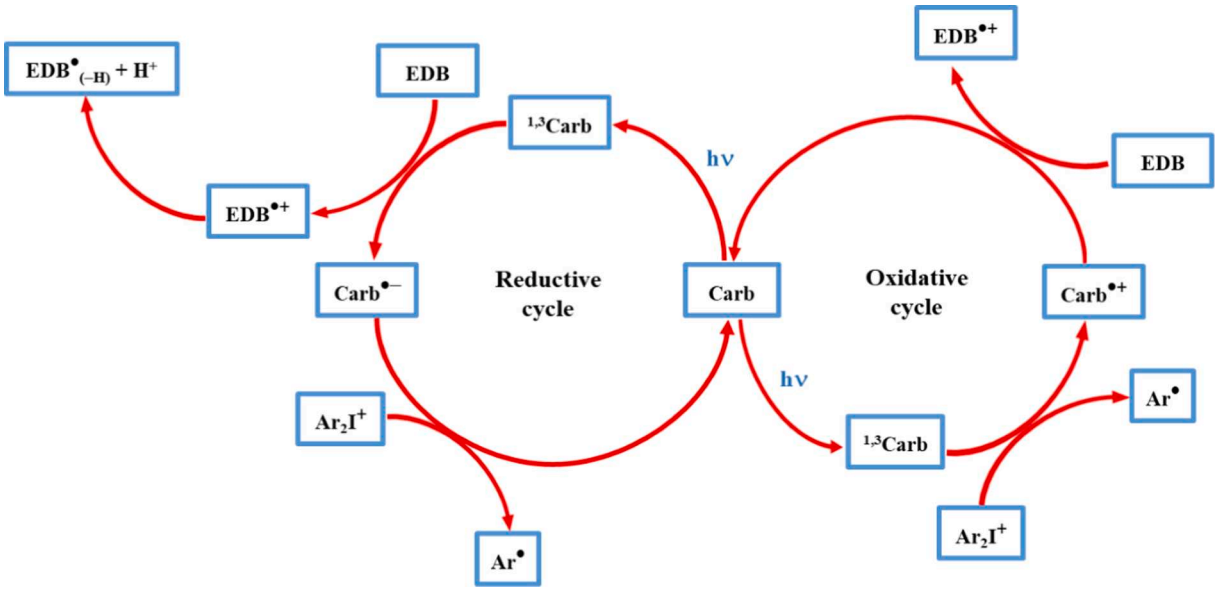

Scheme 11. Proposed photoredox catalytic cycle for the three-component Carb/Iod/EDB system.

interaction of **Carb_30** (and even the other dyes) with the iodonium salt ((r1) and (r2)). The associated electron transfer quantum yields (Φet) were determined according to the following equation: Φet = ksv[Iod]/(1 + ksv[Iod]) and high Φet are found (e.g., Φ = 0.69 for **Carb_30**, Table 3).

In addition, interaction between Carb/Iod (or Carb/EDB) was investigated through the evaluation of the free energy changes (ΔG_{Iod} or ΔG_{EDB}, respectively) for the electron transfer reactions [100,104–106]. According to the equation (1) ($\Delta G_{et} = E_{ox} - E_{red} - E^* + C$), ΔG_{Iod} or ΔG_{EDB} were determined from the oxidation potential E_{ox} (or the reduction potentials) of the studied dyes and their singlet excited state energy (E_{S1}) could be calculated from the crossing point of the

Table 3
Parameters characterizing the chemical mechanisms associated with the studied dyes in chloroform.

PI	E_{S1} (eV)	E_{ox} (V)	E_{red} (V)	$\Delta G_{S1\ (PI/Iod)}$ (eV)[a]	$\Delta G_{S1\ (PI/EDB)}$ (eV)[b]	K_{sv}^{c-1} (Iod) (M	$\Phi_{Iod}^{et(S1)}$
Carb_1	–	1.19	–	–	–	–	–
Carb_2	–	1.24	–	–	–	–	–
Carb_3	–	0.99	−1.02	–	–	–	–
Carb_4	–	0.99	–	–	–	–	–
Carb_5	–	1.09	−1.19	–	–	–	–
Carb_6	–	1.10	−1.08	–	–	–	–
Carb_7	–	0.74	−1.02	–	–	–	–
Carb_8	2.30	1.18	−1.10	−0.42	−0.2	53.33	0.64
Carb_9	2.35	1.16	−1.17	−0.49	−0.18	38.75	0.56
Carb_10	2.05	1.18	−0.98	−0.17	−0.07	22.92	0.43
Carb_11	2.51	1.20	−1.01	−0.61	−0.5	6.43	0.17
Carb_12	2.48	1.50	−1.00	−0.28	−0.48	4.04	0.11
Carb_13	–	1.04	−0.96	–	–	–	–
Carb_14	–	1.03	−0.97	–	–	–	–
Carb_15	–	1.03	−0.99	–	–	–	–
Carb_17	2.37	1.02	−1.14	−0.65	−0.23	7.45	0.11
Carb_18	2.26	1.10	−0.98	−0.46	−0.28	7.59	0.21
Carb_24	3.03	0.92	−1.08	−1.41	−0.95	41.28	0.57
Carb_25	3.31	1.16	−1.12	−1.45	−1.19	25.59	0.62
Carb_26	3.20	0.96	−0.99	−1.54	−1.21	8.69	0.26
Carb_27	3.24	0.95	−1.10	−1.59	−1.14	21.73	0.58
Carb_28	3.25	0.93	−1.03	−1.62	−1.22	18.43	0.54
Carb_29	3.12	1.36	−1.03	−1.06	−1,09	39.52	0.71
Carb_30	3.06	1.34	−1.04	−1.02	−1,02	34.75	0.69
Carb_31	–	1.01	−1.05	–	–	–	–
Carb_32	2.57	1.18	−1.07	−0.69	−0.5	12,02	0.29
Carb_33	–	1.06	−1.07	–	–	–	–
Carb_34	2.56	1.14	−1.06	−0.72	−0.5	15.15	0.34
Carb_35	2.51	1.17	−1.12	−0.64	−0.39	4.59	0.13
Carb_36	–	1.06	−1.13	–	–	–	–

a: evaluated from $\Delta G_{S1\ (PI/Iod)} = E_{ox} - E_{red}(Iod) - E_{S1}$; $E_{red}(Iod) = -0.7$ V.
b: evaluated from $\Delta G_{S1(PI/EDB)} = E_{ox}(EDB) - E_{red} - E_{S1}$; E_{ox} (EDB) = 1 V.
c: Stern-Volmer coefficient (K_{sv}); slope of the quenching curve: $I/I_0=(1 + ksv[Iod])$.

UV–visible absorption and the fluorescence spectra, as shown in Fig. 5 (C). The different results are gathered in Table 3). Favorable ΔG were found in agreement with the strong ^{1}**Carb**/Iod or ^{1}**Carb**/EDB interaction observed above in photopolymerization experiments.

3.4. 3D printing experiments

Due to their high photoreactivity during the FRP of TA, the two three-component systems **Carb_5**/Iod/EDB and **Carb_24**/Iod/EDB were selected for 3D printing experiments upon laser diode irradiation at 405 nm. This experiment was carried out under air. As shown in the Fig. 6, 3D patterns exhibiting a significant thickness could be obtained, together with a high spatial resolution (polymerization process is only produced in the irradiated area). Noticeably, very short irradiation times (~2 min.) were necessary to generate the different 3D patterns (~2 min.). The different letters (C, G, 5 and F) were characterized by numerical optical microscopy (See Fig. 6).

3.5. Near-UV conveyor experiments for access to photocomposites

Photocomposite materials were synthesized by impregnation of glass fibers by TA (50% glass fibers/ 50% resin; thickness of ~ 3 mm) and then irradiation of the sample. The results show that the studied dyes were able to fully cure the composites. An efficient curing polymerization was observed i.e. the surface became tack-free after only one pass of irradiation with the LED @395 nm (See Fig. 7) This character is observed at the bottom of the sample but only after some passes.

4. Conclusion

In this study, a series of 36 new dyes never reported in the literature was synthetized for the elaboration of new high-performance photoinitiating systems capable to efficiently initiate free radical photopolymerizations (FRP) of acrylates upon blue LED irradiation. The FRP results were explained and discussed by a general mechanism proposed using different characterization techniques such as steady-state photolysis, fluorescence quenching, and cyclic voltammetry. It was also noted that, both good light absorption properties and excellent photochemical reactivity in the excited state processes are required for the dyes to reach efficient photoinitiating systems. In addition, the good performance of the investigated dyes paved the way for their use in 3D printing technology, which allows the generation of 3D thick patterns using a laser diode at 405 nm, and the synthesis of thick glass fiber photocomposites. Development of new high-performance photoinitiating systems is currently under progress.

CRediT authorship contribution statement

Fatima Hammoud: Data curation, Writing – original draft, Visualization, Investigation, Writing – review & editing. **Akram Hijazi:** Data curation, Writing – original draft. **Malika Ibrahim-Ouali:** Visualization, Investigation, Writing – review & editing. **Jacques Lalevée:** Conceptualization, Methodology, Software, Data curation, Writing – original draft, Visualization, Investigation, Writing – review & editing. **Frédéric Dumur:** Conceptualization, Methodology, Software, Data curation, Writing – original draft, Visualization, Investigation, Supervision, Writing – review & editing.

Declaration of Competing Interest

The authors declare that they have no known competing financial interests or personal relationships that could have appeared to influence the work reported in this paper.

Acknowledgments

Aix Marseille University and the Centre National de la Recherche Scientifique (CNRS) are acknowledged for financial supports.

Appendix A. Supplementary material

Supplementary data to this article can be found online at https://doi.org/10.1016/j.eurpolymj.2022.111218.

References

[1] A. Bagheri, J. Jin, Photopolymerization in 3D printing, ACS Appl. Polym. Mater. 1 (2019) 593–611, https://doi.org/10.1021/acsapm.8b00165.
[2] A. Andreu, P.-C. Su, J.-H. Kim, C.S. Ng, S. Kim, I. Kim, J. Lee, J. Noh, A. S. Subramanian, Y.-J. Yoon, 4D printing materials for vat photopolymerization, Addit. Manuf. 44 (2021), 102024, https://doi.org/10.1016/j.addma.2021.102024.
[3] H. Chen, G. Noirbent, Y. Zhang, K. Sun, S. Liu, D. Brunel, D. Gigmes, B. Graff, F. Morlet-Savary, P. Xiao, F. Dumur, J. Lalevée, Photopolymerization and 3D/4D applications using newly developed dyes: search around the natural chalcone scaffold in photoinitiating systems, Dyes Pigm. 188 (2021), 109213, https://doi.org/10.1016/j.dyepig.2021.109213.
[4] N. Corrigan, J. Yeow, P. Judzewitsch, J. Xu, C. Boyer, Seeing the light: advancing materials chemistry through photopolymerization, Angew. Chem. Int. Ed. 58 (2019) 5170–5189, https://doi.org/10.1002/anie.201805473.
[5] J.P. Fouassier, X. Allonas, D. Burget, Photopolymerization reactions under visible lights: principle, mechanisms and examples of applications, Prog. Org. Coat. 47 (2003) 16–36, https://doi.org/10.1016/S0300-9440(03)00011-0.
[6] N. Zivic, P.K. Kuroishi, F. Dumur, D. Gigmes, A.P. Dove, H. Sardon, Recent advances and challenges in the design of organic photoacid and photobase generators for polymerizations, Angew. Chem. Int. Ed. 58 (2019) 10410–10422, https://doi.org/10.1002/anie.201810118.
[7] A. Santini, I.T. Gallegos, C.M. Felix, Photoinitiators in dentistry: a review, Prim. Dent. J. 2 (2013) 30–33, https://doi.org/10.1308/205016814809859563.
[8] H. Arikawa, H. Takahashi, T. Kanie, S. Ban, Effect of various visible light photoinitiators on the polymerization and color of light-activated resins, Dent. Mater. J. 28 (2009) 454–460, https://doi.org/10.4012/dmj.28.454.
[9] S.H. Dickens, J.W. Stansbury, K.M. Choi, C.J.E. Floyd, Photopolymerization kinetics of methacrylate dental resins, Macromolecules 36 (2003) 6043–6053, https://doi.org/10.1021/ma021675k.
[10] T. Dikova, J. Maximov, V. Todorov, G. Georgiev, V. Panov, Optimization of photopolymerization process of dental composites, Processes. 9 (2021) 779, https://doi.org/10.3390/pr9050779.
[11] A. Maffezzoli, A.D. Pietra, S. Rengo, L. Nicolais, G. Valletta, Photopolymerization of dental composite matrices, Biomaterials 15 (1994) 1221–1228, https://doi.org/10.1016/0142-9612(94)90273-9.
[12] M.G. Neumann, C.C. Schmitt, G.C. Ferreira, I.C. Corrêa, The initiating radical yields and the efficiency of polymerization for various dental photoinitiators excited by different light curing units, Dent. Mater. 22 (2006) 576–584, https://doi.org/10.1016/j.dental.2005.06.006.
[13] M. Topa, J. Ortyl, Moving towards a finer way of light-cured resin-based restorative dental materials: recent advances in photoinitiating systems based on iodonium salts, Materials 13 (2020) 4093, https://doi.org/10.3390/ma13184093.
[14] F. Yoshino, A. Yoshida, Effects of blue-light irradiation during dental treatment, Jpn. Dent. Sci. Rev. 54 (2018) 160–168, https://doi.org/10.1016/j.jdsr.2018.06.002.
[15] I. Dika, F. Diot, V. Bardinal, J.-P. Malval, C. Ecoffet, A. Bruyant, D. Barat, B. Reig, J.-B. Doucet, T. Camps, O. Soppera, Near infrared photopolymer for micro-optics applications, J. Polym. Sci. 58 (2020) 1796–1809, https://doi.org/10.1002/pol.20200106.
[16] C. Dietlin, S. Schweizer, P. Xiao, J. Zhang, F. Morlet-Savary, B. Graff, J.-P. Fouassier, J. Lalevée, Photopolymerization upon LEDs: new photoinitiating systems and strategies, Polym. Chem. 6 (2015) 3895–3912, https://doi.org/10.1039/C5PY00258C.
[17] P. Xiao, J. Zhang, F. Dumur, M.A. Tehfe, F. Morlet-Savary, B. Graff, D. Gigmes, J. P. Fouassier, J. Lalevée, Visible light sensitive photoinitiating systems: recent progress in cationic and radical photopolymerization reactions under soft conditions, Prog. Polym. Sci. 41 (2015) 32–66, https://doi.org/10.1016/j.progpolymsci.2014.09.001.
[18] M.-A. Tehfe, F. Dumur, P. Xiao, M. Delgove, B. Graff, J.-P. Fouassier, D. Gigmes, J. Lalevée, Chalcone derivatives as highly versatile photoinitiators for radical, cationic, thiol–ene and IPN polymerization reactions upon exposure to visible light, Polym. Chem. 5 (2014) 382–390, https://doi.org/10.1039/C3PY00922J.
[19] H. Mokbel, J. Toufaily, T. Hamieh, F. Dumur, D. Campolo, D. Gigmes, J. Pierre Fouassier, J. Ortyl, J. Lalevée, Specific cationic photoinitiators for near UV and visible LEDs: iodonium versus ferrocenium structures, J. Appl. Polym. Sci. 132 (46) (2015) n/a–n/a.
[20] J. Lalevée, S. Telitel, P. Xiao, M. Lepeltier, F. Dumur, F. Morlet-Savary, D. Gigmes, J.-P. Fouassier, Metal and metal-free photocatalysts: mechanistic approach and application as photoinitiators of photopolymerization, Beilstein J. Org. Chem. 10 (2014) 863–876, https://doi.org/10.3762/bjoc.10.83.
[21] S. Liu, D. Brunel, K. Sun, Y. Xu, F. Morlet-Savary, B. Graff, P. Xiao, F. Dumur, J. Lalevée, A monocomponent bifunctional benzophenone–carbazole type II photoinitiator for LED photoinitiating systems, Polym. Chem. 11 (2020) 3551–3556, https://doi.org/10.1039/D0PY00644K.
[22] T.-L. Huang, Y.-H. Li, Y.-C. Chen, Benzophenone derivatives as novel organosoluble visible light Type II photoinitiators for UV and LED photoinitiating systems, J. Polym. Sci. 58 (2020) 2914–2925, https://doi.org/10.1002/pol.20200437.
[23] X. Qin, G. Ding, Y. Gong, C. Jing, G. Peng, S. Liu, L. Niu, S. Zhang, Z. Luo, H. Li, F. Gao, Stilbene-benzophenone dyads for free radical initiating polymerization of methyl methacrylate under visible light irradiation, Dyes Pigm. 132 (2016) 27–40, https://doi.org/10.1016/j.dyepig.2016.04.035.
[24] S. Liu, D. Brunel, G. Noirbent, A. Mau, H. Chen, F. Morlet-Savary, B. Graff, D. Gigmes, P. Xiao, F. Dumur, J. Lalevée, New multifunctional benzophenone-based photoinitiators with high migration stability and their applications in 3D printing, Mater. Chem. Front. 5 (2021) 1982–1994, https://doi.org/10.1039/D0QM00885K.
[25] J. Lalevée, M.-A. Tehfe, F. Dumur, D. Gigmes, B. Graff, F. Morlet-Savary, J.-P. Fouassier, Light-harvesting organic photoinitiators of polymerization, Macromol. Rapid Commun. 34 (2013) 239–245, https://doi.org/10.1002/marc.201200578.
[26] M.-A. Tehfe, F. Dumur, B. Graff, F. Morlet-Savary, D. Gigmes, J.-P. Fouassier, J. Lalevée, Design of new Type I and Type II photoinitiators possessing highly coupled pyrene–ketone moieties, Polym. Chem. 4 (2013) 2313–2324, https://doi.org/10.1039/C3PY21079K.
[27] M.-A. Tehfe, F. Dumur, B. Graff, J.-L. Clément, D. Gigmes, F. Morlet-Savary, J.-P. Fouassier, J. Lalevée, New cleavable photoinitiator architecture with huge molar extinction coefficients for polymerization in the 340–450 nm range, Macromolecules 46 (2013) 736–746, https://doi.org/10.1021/ma3024359.
[28] P. Xiao, F. Dumur, B. Graff, D. Gigmes, J.P. Fouassier, J. Lalevée, Variations on the benzophenone skeleton: novel high performance blue light sensitive photoinitiating systems, Macromolecules 46 (2013) 7661–7667, https://doi.org/10.1021/ma401766v.
[29] J. Zhang, N. Zivic, F. Dumur, P. Xiao, B. Graff, D. Gigmes, J.P. Fouassier, J. Lalevée, A benzophenone-naphthalimide derivative as versatile photoinitiator of polymerization under near UV and visible lights, J. Polym. Sci., Part A: Polym. Chem. 53 (2015) 445–451, https://doi.org/10.1002/pola.27451.
[30] E. Andrezajewska, K. Grajek, Recent advances in photo-induced free-radical polymerization, MOJ Polym Sci. 1 (2017) 58–60, https://doi.org/10.15406/mojps.2017.01.00009.
[31] F. Dumur, Recent advances on pyrene-based photoinitiators of polymerization, Eur. Polym. J. 126 (2020), 109564, https://doi.org/10.1016/j.eurpolymj.2020.109564.
[32] F. Dumur, Recent advances on ferrocene-based photoinitiating systems, Eur. Polym. J. 147 (2021), 110328, https://doi.org/10.1016/j.eurpolymj.2021.110328.
[33] F. Dumur, Recent advances on visible light photoinitiators of polymerization based on Indane-1,3-dione and related derivatives, Eur. Polym. J. 143 (2021), 110178, https://doi.org/10.1016/j.eurpolymj.2020.110178.
[34] F. Dumur, Recent advances on iron-based photoinitiators of polymerization, Eur. Polym. J. 139 (2020), 110026, https://doi.org/10.1016/j.eurpolymj.2020.110026.
[35] F. Dumur, Recent advances on visible light metal-based photocatalysts for polymerization under low light intensity, Catalysts 9 (9) (2019) 736.
[36] F. Dumur, Recent advances on perylene-based photoinitiators of polymerization, Eur. Polym. J. 159 (2021), 110734, https://doi.org/10.1016/j.eurpolymj.2021.110734.
[37] N. Giacoletto, M. Ibrahim-Ouali, F. Dumur, Recent advances on squaraine-based photoinitiators of polymerization, Eur. Polym. J. 150 (2021), 110427, https://doi.org/10.1016/j.eurpolymj.2021.110427.
[38] N. Giacoletto, F. Dumur, Recent advances in bis-chalcone-based photoinitiators of polymerization: from mechanistic investigations to applications, Molecules 26 (2021) 3192, https://doi.org/10.3390/molecules26113192.
[39] M. Ibrahim-Ouali, F. Dumur, Recent advances on chalcone-based photoinitiators of polymerization, Eur. Polym. J. 158 (2021) 110688.
[40] G. Noirbent, F. Dumur, Recent advances on naphthalic anhydrides and 1,8-naphthalimide-based photoinitiators of polymerization, Eur. Polym. J. 132 (2020), 109702, https://doi.org/10.1016/j.eurpolymj.2020.109702.
[41] G. Noirbent, F. Dumur, Recent advances on copper complexes as visible light photoinitiators and (photo) redox initiators of polymerization, Catalysts 10 (9) (2020) 953.
[42] C. Pigot, G. Noirbent, D. Brunel, F. Dumur, Recent advances on push–pull organic dyes as visible light photoinitiators of polymerization, Eur. Polym. J. 133 (2020), 109797, https://doi.org/10.1016/j.eurpolymj.2020.109797.
[43] F. Dumur, Recent advances on visible light thiophene-based photoinitiators of polymerization, Eur. Polym. J. 169 (2022) 111120.
[44] F. Dumur, Recent advances on anthracene-based photoinitiators of polymerization, Eur. Polym. J. 169 (2022) 111139.
[45] F. Dumur, Recent advances on visible light triphenylamine-based photoinitiators of polymerization, Eur. Polym. J. 166 (2022), 111036, https://doi.org/10.1016/j.eurpolymj.2022.111036.
[46] F. Dumur, Recent advances on visible light Phenothiazine-based photoinitiators of polymerization, Eur. Polym. J. 165 (2022), 110999, https://doi.org/10.1016/j.eurpolymj.2022.110999.

[47] F. Dumur, Recent advances on coumarin-based photoinitiators of polymerization, Eur. Polym. J. 163 (2022), 110962, https://doi.org/10.1016/j.eurpolymj.2021.110962.
[48] P. Xiao, F. Dumur, T.T. Bui, F. Goubard, B. Graff, F. Morlet-Savary, J.P. Fouassier, D. Gigmes, J. Lalevée, Panchromatic photopolymerizable cationic films using indoline and squaraine dye based photoinitiating systems, ACS Macro Lett. 2 (2013) 736–740, https://doi.org/10.1021/mz400316y.
[49] F. Dumur, D. Gigmes, J.-P. Fouassier, J. Lalevée, Organic electronics: an El Dorado in the quest of new photocatalysts for polymerization reactions, Acc. Chem. Res. 49 (2016) 1980–1989, https://doi.org/10.1021/acs.accounts.6b00227.
[50] K.H. Choi, J.M. Kim, W.J. Chung, J.Y. Lee, Effects of substitution position of carbazole-dibenzofuran based high triplet energy hosts to device stability of blue phosphorescent organic light-emitting diodes, Molecules 26 (2021) 2804, https://doi.org/10.3390/molecules26092804.
[51] A. van Dijken, J.J.A.M. Bastiaansen, N.M.M. Kiggen, B.M.W. Langeveld, C. Rothe, A. Monkman, I. Bach, P. Stössel, K. Brunner, Carbazole compounds as host materials for triplet emitters in organic light-emitting diodes: polymer hosts for high-efficiency light-emitting diodes, J. Am. Chem. Soc. 126 (2004) 7718–7727, https://doi.org/10.1021/ja049771j.
[52] N. Blouin, A. Michaud, D. Gendron, S. Wakim, E. Blair, R. Neagu-Plesu, M. Belletête, G. Durocher, Y. Tao, M. Leclerc, Toward a rational design of poly (2,7-carbazole) derivatives for solar cells, J. Am. Chem. Soc. 130 (2008) 732–742, https://doi.org/10.1021/ja0771989.
[53] F. Dumur, Carbazole-based polymers as hosts for solution-processed organic light-emitting diodes: simplicity, efficacy, Org. Electron. 25 (2015) 345–361, https://doi.org/10.1016/j.orgel.2015.07.007.
[54] A. Arai, H. Sasabe, K. Nakao, Y. Masuda, J. Kido, π-Extended carbazole derivatives as host materials for highly efficient and long-life green phosphorescent organic light-emitting diodes, Chem. – Eur. J. 27 (2021) 4971–4976, https://doi.org/10.1002/chem.202005144.
[55] F. Dumur, L. Beouch, S. Peralta, G. Wantz, F. Goubard, D. Gigmes, Solution-processed blue phosphorescent OLEDs with carbazole-based polymeric host materials, Org. Electron. 25 (2015) 21–30, https://doi.org/10.1016/j.orgel.2015.06.013.
[56] D. Sun, Q. Fu, Z. Ren, W. Li, H. Li, D. Ma, S. Yan, Carbazole-based polysiloxane hosts for highly efficient solution-processed blue electrophosphorescent devices, J. Mater. Chem. C. 1 (2013) 5344–5350, https://doi.org/10.1039/C3TC31108B.
[57] T.-T. Bui, S.K. Shah, M. Abbas, X. Sallenave, G. Sini, L. Hirsch, F. Goubard, Carbazole-based molecular glasses as hole-transporting materials in solid state dye-sensitized solar cells, ChemNanoMat 1 (2015) 203–210, https://doi.org/10.1002/cnma.201500014.
[58] G. Puckyte, B. Schmaltz, A. Tomkeviciene, M. Degbia, J.V. Grazulevicius, H. Melhem, J. Bouclé, F. Tran-Van, Carbazole-based molecular glasses for efficient solid-state dye-sensitized solar cells, J. Power Sources 233 (2013) 86–92, https://doi.org/10.1016/j.jpowsour.2013.01.137.
[59] T.-T. Bui, F. Goubard, J. Troughton, T. Watson, Simple 3,6-bis(diphenylaminyl) carbazole molecular glasses as hole transporting materials for hybrid perovskite solar cells, J. Mater. Sci.: Mater. Electron. 28 (2017) 17551–17556, https://doi.org/10.1007/s10854-017-7691-y.
[60] N. Berton, R. Nakar, B. Schmaltz, DMPA-containing carbazole-based hole transporting materials for perovskite solar cells: recent advances and perspectives, Synth. Met. 252 (2019) 91–106, https://doi.org/10.1016/j.synthmet.2019.04.004.
[61] M. Lepeltier, F. Appaix, Y.Y. Liao, F. Dumur, J. Marrot, T. Le Bahers, C. Andraud, C. Monnereau, Carbazole-substituted iridium complex as a solid state emitter for two-photon intravital imaging, Inorg. Chem. 55 (2016) 9586–9595, https://doi.org/10.1021/acs.inorgchem.6b01253.
[62] M. Khalid, A. Ali, R. Jawaria, M.A. Asghar, S. Asim, M.U. Khan, R. Hussain, M. Fayyaz ur Rehman, C.J. Ennis, M.S. Akram, First principles study of electronic and nonlinear optical properties of A-D–π–A and D–A–D–π–A configured compounds containing novel quinoline–carbazole derivatives, RSC Adv. 10 (37) (2020) 22273–22283.
[63] L. MayuriM, D. Kadam, N.S. Patil, Fluorescent carbazole based pyridone dyes – synthesis, solvatochromism, linear and nonlinear optical properties, Opt. Mater. 85 (2018) 308–318, https://doi.org/10.1016/j.optmat.2018.08.072.
[64] W.-J. Kuo, G.-H. Hsiue, R.-J. Jeng, All organic NLO sol-gel material containing a one-dimensional carbazole chromophore, Macromol. Chem. Phys. 202 (2001) 1782–1790, https://doi.org/10.1002/1521-3935(20010601)202:9<1782::AID-MACP1782>3.0.CO;2-O.
[65] M. Rajeshirke, M.C. Sreenath, S. Chitrambalam, I.H. Joe, N. Sekar, Enhancement of NLO properties in OBO fluorophores derived from carbazole-coumarin chalcones containing carboxylic acid at the N-alykl terminal end, J. Phys. Chem. C. 122 (2018) 14313–14325, https://doi.org/10.1021/acs.jpcc.8b02937.
[66] B. Souharce, C.J. Kudla, M. Forster, J. Steiger, R. Anselmann, H. Thiem, U. Scherf, Amorphous carbazole-based (Co)polymers for OFET application, Macromol. Rapid Commun. 30 (2009) 1258–1262, https://doi.org/10.1002/marc.200900214.
[67] P. Jha, S.P. Koiry, V. Saxena, P. Veerender, A. Gusain, A.K. Chauhan, A. K. Debnath, D.K. Aswal, S.K. Gupta, Air-stability and bending properties of flexible organic field-effect transistors based on poly[N-9′-heptadecanyl-2,7-carbazole-alt-5,5-(4′,7′-di-2-thienyl-2′,1′,3′-benzothiadiazole)], Org. Electron. 14 (2013) 2635–2644, https://doi.org/10.1016/j.orgel.2013.06.031.
[68] C.-H. Chen, Y. Wang, T. Michinobu, S.-W. Chang, Y.-C. Chiu, C.-Y. Ke, G.-S. Liou, Donor-acceptor effect of carbazole-based conjugated polymer electrets on photoresponsive flash organic field-effect transistor memories, ACS Appl. Mater. Interfaces. 12 (2020) 6144–6150, https://doi.org/10.1021/acsami.9b20960.
[69] M. Bashir, A. Bano, A.S. Ijaz, B.A. Chaudhary, Recent developments and biological activities of N-substituted carbazole derivatives: a review, Molecules 20 (2015) 13496–13517, https://doi.org/10.3390/molecules200813496.
[70] F. Dumur, Recent advances on carbazole-based photoinitiators of polymerization, Eur. Polym. J. 125 (2020), 109503, https://doi.org/10.1016/j.eurpolymj.2020.109503.
[71] J. Zhang, D. Campolo, F. Dumur, P. Xiao, D. Gigmes, J.P. Fouassier, J. Lalevée, The carbazole-bound ferrocenium salt as a specific cationic photoinitiator upon near-UV and visible LEDs (365–405 nm), Polym. Bull. 73 (2016) 493–507, https://doi.org/10.1007/s00289-015-1506-1.
[72] A. Al Mousawi, D.M. Lara, G. Noirbent, F. Dumur, J. Toufaily, T. Hamieh, T.-T. Bui, F. Goubard, B. Graff, D. Gigmes, J.P. Fouassier, J. Lalevée, Carbazole derivatives with thermally activated delayed fluorescence property as photoinitiators/photoredox catalysts for LED 3D printing technology, Macromolecules 50 (2017) 4913–4926, https://doi.org/10.1021/acs.macromol.7b01114.
[73] A. Al Mousawi, P. Garra, F. Dumur, T.-T. Bui, F. Goubard, J. Toufaily, T. Hamieh, B. Graff, D. Gigmes, J.P. Fouassier, J. Lalevée, Novel carbazole skeleton-based photoinitiators for LED polymerization and LED projector 3D printing, Molecules 22 (2017) 2143, https://doi.org/10.3390/molecules22122143.
[74] A.A. Mousawi, A. Arar, M. Ibrahim-Ouali, S. Duval, F. Dumur, P. Garra, J. Toufaily, T. Hamieh, B. Graff, D. Gigmes, J.-P. Fouassier, J. Lalevée, Carbazole-based compounds as photoinitiators for free radical and cationic polymerization upon near visible light illumination, Photochem. Photobiol. Sci. 17 (2018) 578–585, https://doi.org/10.1039/C7PP00400A.
[75] M. Abdallah, D. Magaldi, A. Hijazi, B. Graff, F. Dumur, J.-P. Fouassier, T.-T. Bui, F. Goubard, J. Lalevée, Development of new high-performance visible light photoinitiators based on carbazole scaffold and their applications in 3d printing and photocomposite synthesis, J. Polym. Sci., Part A: Polym. Chem. 57 (2019) 2081–2092, https://doi.org/10.1002/pola.29471.
[76] A. Al Mousawi, F. Dumur, P. Garra, J. Toufaily, T. Hamieh, B. Graff, D. Gigmes, J. P. Fouassier, J. Lalevée, Carbazole scaffold based photoinitiator/photoredox catalysts: toward new high performance photoinitiating systems and application in LED projector 3D printing resins, Macromolecules 50 (2017) 2747–2758, https://doi.org/10.1021/acs.macromol.7b00210.
[77] S. Telitel, F. Dumur, T. Faury, B. Graff, M.-A. Tehfe, D. Gigmes, J.-P. Fouassier, J. Lalevée, New core-pyrene π structure organophotocatalysts usable as highly efficient photoinitiators, Beilstein J. Org. Chem. 9 (2013) 877–890, https://doi.org/10.3762/bjoc.9.101.
[78] A.A. Mousawi, F. Dumur, P. Garra, J. Toufaily, T. Hamieh, F. Goubard, T.-T. Bui, B. Graff, D. Gigmes, J.P. Fouassier, J. Lalevée, Azahelicenes as visible light photoinitiators for cationic and radical polymerization: Preparation of photoluminescent polymers and use in high performance LED projector 3D printing resins, J. Polym. Sci., Part A: Polym. Chem. 55 (2017) 1189–1199, https://doi.org/10.1002/pola.28476.
[79] S. Liu, B. Graff, P. Xiao, F. Dumur, J. Lalevée, Nitro-carbazole based oxime esters as dual photo/thermal initiators for 3D printing and composite preparation, Macromol. Rapid Commun. 42 (2021) 2100207, https://doi.org/10.1002/marc.202100207.
[80] N.A. Kazin, N.S. Demina, R.A. Irgashev, E.F. Zhilina, G.L. Rusinov, Modifications of 5,12-dihydroindolo[3,2-a]carbazole scaffold via its regioselective C2,9-formylation and C2,9-acetylation, Tetrahedron 75 (2019) 4686–4696, https://doi.org/10.1016/j.tet.2019.07.015.
[81] F. Hammoud, A. Hijazi, S. Duval, J. Lalevée, F. Dumur, 5,12-Dihydroindolo[3,2-a]carbazole: a promising scaffold for the design of visible light photoinitiators of polymerization, Eur. Polym. J. 162 (2022), 110880, https://doi.org/10.1016/j.eurpolymj.2021.110880.
[82] F. Bureš, Fundamental aspects of property tuning in push–pull molecules, RSC Adv. 4 (2014) 58826–58851, https://doi.org/10.1039/C4RA11264D.
[83] K.e. Sun, C. Pigot, Y. Zhang, T. Borjigin, F. Morlet-Savary, B. Graff, M. Nechab, P. u. Xiao, F. Dumur, J. Lalevée, sunlight induced polymerization photoinitiated by novel push-pull dyes: indane-1,3-dione, 1H-cyclopenta[b]naphthalene-1,3(2H)-dione and 4-dimethoxyphenyl-1-allylidene derivatives, Macromol. Chem. Phys. 223 (4) (2022) 2100439.
[84] K. Sun, S. Liu, C. Pigot, D. Brunel, B. Graff, M. Nechab, D. Gigmes, F. Morlet-Savary, Y. Zhang, P. Xiao, F. Dumur, J. Lalevée, Novel push-pull dyes derived from 1H-cyclopenta[b]naphthalene-1,3(2H)-dione as versatile photoinitiators for photopolymerization and their related applications: 3D printing and fabrication of photocomposites, Catalysts 10 (2020) 1196, https://doi.org/10.3390/catal10101196.
[85] K. Sun, C. Pigot, H. Chen, M. Nechab, D. Gigmes, F. Morlet-Savary, B. Graff, S. Liu, P. Xiao, F. Dumur, J. Lalevée, Free radical photopolymerization and 3D printing using newly developed dyes: indane-1,3-dione and 1H-cyclopentanaphthalene-1,3-dione derivatives as photoinitiators in three-component systems, Catalysts 10 (2020) 463, https://doi.org/10.3390/catal10040463.
[86] K. Sun, S. Liu, H. Chen, F. Morlet-Savary, B. Graff, C. Pigot, M. Nechab, P. Xiao, F. Dumur, J. Lalevée, N-ethyl carbazole-1-allylidene-based push-pull dyes as efficient light harvesting photoinitiators for sunlight induced polymerization, Eur. Polym. J. 147 (2021), 110331, https://doi.org/10.1016/j.eurpolymj.2021.110331.
[87] P. Xiao, M. Frigoli, F. Dumur, B. Graff, D. Gigmes, J.P. Fouassier, J. Lalevée, Julolidine or fluorenone based push-pull dyes for polymerization upon soft polychromatic visible light or green light, Macromolecules 47 (2014) 106–112, https://doi.org/10.1021/ma402196p.

[88] I.R. Shaikh, Organocatalysis: key trends in green synthetic chemistry, challenges, scope towards heterogenization, and importance from research and industrial point of view, J. Catal. 2014 (2014) 1–35.
[89] V. Oliveira, M. Cardoso, L. Forezi, A brief overview on its evolution and applications, Catalysts 8 (12) (2018) 605.
[90] S. Ardevines, E. Marqués-López, R.P. Herrera, Horizons in asymmetric organocatalysis: en route to the sustainability and new applications, Catalysts 12 (1) (2022) 101.
[91] A. Carlone, L. Bernardi, Enantioselective organocatalytic approaches to active pharmaceutical ingredients – selected industrial examples, Phys. Sci. Rev. 4 (2019), https://doi.org/10.1515/psr-2018-0097.
[92] P.I. Dalko, L. Moisan, Enantioselective organocatalysis, Angew. Chem. Int. Ed. 40 (2001) 3726–3748, https://doi.org/10.1002/1521-3773(20011015)40:20<3726::AID-ANIE3726>3.0.CO;2-D.
[93] W. Liu, H. Cao, H. Zhang, H. Zhang, K.H. Chung, C. He, H. Wang, F.Y. Kwong, A. Lei, Organocatalysis in cross-coupling: DMEDA-catalyzed direct C−H arylation of unactivated benzene, J. Am. Chem. Soc. 132 (2010) 16737–16740, https://doi.org/10.1021/ja103050x.
[94] J. Wilbuer, G. Schnakenburg, B. Esser, Syntheses, structures and optoelectronic properties of spiroconjugated cyclic ketones, Eur. J. Org. Chem. 2016 (2016) 2404–2412, https://doi.org/10.1002/ejoc.201600235.
[95] J.C. Sloop, P.D. Boyle, A.W. Fountain, C. Gomez, J.L. Jackson, W.F. Pearman, R. D. Schmidt, J. Weyand, Novel fluorinated indanone, tetralone and naphthone derivatives: synthesis and unique structural features, Appl. Sci. 2 (1) (2012) 61–99.
[96] V. Nair, V. Nandialath, K.G. Abhilash, E. Suresh, An efficient synthesis of indolo [3,2-a]carbazoles via the novel acid catalyzed reaction of indoles and diaryl-1,2-diones, Org. Biomol. Chem. 6 (2008) 1738–1742, https://doi.org/10.1039/B803009J.
[97] H. Kilic, O. Aydin, S. Bayindir, N. Saracoglu, Condensation of indoline with some 1,2- and 1,3-diketones, J. Heterocycl. Chem. 53 (2016) 2096–2101, https://doi.org/10.1002/jhet.2580.
[98] A. Khorshidi, N. Sadeghi, Application of RuO2 nanoparticles as catalyst in preparation of indolo[3,2-a]carbazoles, J Clust Sci. 27 (2016) 1923–1932, https://doi.org/10.1007/s10876-016-1052-5.
[99] V. Bocchi, G. Palla, Synthesis and characterization of new indole trimers and tetramers, Tetrahedron 42 (1986) 5019–5024, https://doi.org/10.1016/S0040-4020(01)88053-4.
[100] D. Rehm, A. Weller, Kinetics of fluorescence quenching by electron and H-atom transfer, Isr. J. Chem. 8 (1970) 259–271, https://doi.org/10.1002/ijch.197000029.
[101] H. Chen, C. Regeard, H. Salmi, F. Morlet-Savary, N. Giacoletto, M. Nechab, P. Xiao, F. Dumur, J. Lalevée, Interpenetrating polymer network hydrogels using natural based dyes initiating systems: antibacterial activity and 3D/4D performance, Eur. Polym. J. 166 (2022) 111042.
[102] K. Sun, P. Xiao, F. Dumur, J. Lalevée, Organic dye-based photoinitiating systems for visible-light-induced photopolymerization, J. Polym. Sci. 59 (2021) 1338–1389, https://doi.org/10.1002/pol.20210225.
[103] H. Chen, G. Noirbent, S. Liu, Y. Zhang, K. Sun, F. Morlet-Savary, D. Gigmes, P. Xiao, F. Dumur, J. Lalevée, In situ generation of Ag nanoparticles during photopolymerization by using newly developed dyes-based three-component photoinitiating systems and the related 3D printing applications and their shape change behavior, J. Polym. Sci. 59 (2021) 843–859, https://doi.org/10.1002/pol.20210154.
[104] S. Dadashi-Silab, S. Doran, Y. Yagci, Photoinduced electron transfer reactions for macromolecular syntheses, Chem. Rev. 116 (2016) 10212–10275, https://doi.org/10.1021/acs.chemrev.5b00586.
[105] M. Topa, F. Petko, M. Galek, M. Jankowska, R. Popielarz, J. Ortyl, Difunctional 1H-quinolin-2-ones as spectroscopic fluorescent probes for real-time monitoring of photopolymerisation process and photosensitizers of fluorescent photopolymer resin in 3D printing, Eur. Polym. J. 156 (2021), 110612, https://doi.org/10.1016/j.eurpolymj.2021.110612.
[106] D. Rehm, A. Weller, Kinetik und Mechanismus der Elektronübertragung bei der Fluoreszenzlöschung in Acetonitril, Berichte Der Bunsengesellschaft Für Physikalische Chemie 73 (1969) 834–839, doi: 10.1002/bbpc.19690730818.

Partie III : Systèmes Photoamorceurs Monocomposants

TABLE DES MATIÈRES

Table des matières

PARTIE III : SYSTÈMES PHOTOAMORCEURS MONOCOMPOSANTS

Introduction

Au cours des dernières années, les applications des résines photopolymérisables se sont étendues du domaine des revêtements, des encres d'impression et des adhésifs à de nouvelles applications difficiles telles que la stéréolithographie et l'impression 3D à jet d'encre. [1-3]

Un composant essentiel d'une résine photopolymérisable est un photoamorceur (PA) approprié. Il doit produire des espèces réactives appropriées, c'est-à-dire des radicaux ou des ions, en fonction du mécanisme de polymérisation, dans une mesure suffisante et dans un court laps de temps. En outre, le PA doit avoir un spectre d'absorption avec un bon chevauchement avec la source de lumière émettrice et un coefficient d'extinction élevé dans cette région. En fonction de l'application et du système utilisé, la solubilité dans un monomère liquide, dans l'eau ou dans un solvant approprié est essentielle. [2-5]

Cette partie se concentre sur les PAs de Type I, qui subissent un clivage homolytique de la liaison lors de l'irradiation par la lumière proche UV ou visible. Contrairement aux amorceurs de Type II, ces PAs n'ont pas besoin d'une molécule de donneur d'hydrogène supplémentaire pour générer une espèce réactive. Le mécanisme de formation de radicaux dans les PA de Type I peut être divisé en deux types de clivage, à savoir la scission alpha (Type I de Norrish) et la scission bêta. Lors de l'excitation, la molécule présente un état singulet excité et peut subir un croisement inter-système (CIS) vers l'état triplet. La relaxation de l'état triplet peut conduire à la coupure de la liaison en position alpha d'une liaison carbonyle. La scission bêta peut se produire, en plus ou exclusivement, lorsqu'il existe une liaison faible entre le carbone alpha du carbonyle et un hétéro atome, ainsi qu'en position bêta d'un système conjugué. Par conséquent, cela peut conduire à des molécules photoactives sans la présence de groupes carbonyles, comme les dérivés de la trichlorométhyltriazine, où la liaison C-Cl est rompue et où des radicaux Cl sont produits. [6-9]

Au cours de la dernière décennie, la recherche s'est davantage concentrée sur les systèmes monocomposant et les PAs de Type I présentant une réactivité élevée.

Références

[1] J. P. Fouassier, J. Lalevée, Photoinitiators: Structures, Reactivity and Applications in Polymerization, John Wiley & Sons, 2021.

[2] J. P. Fouassier, J. Lalevée, Photoinitiators for polymer synthesis: scope, reactivity, and efficiency, John Wiley & Sons, 2012.

[3] Y. Zhang, Y. Xu, A. Simon-Masseron, J. Lalevée, Radical photoinitiation with LEDs and applications in the 3D printing of composites, Chemical Society Reviews, 2021, 50.6, 3824-3841.

[4] J. Lalevée, J. P. Fouassier, Dyes and chromophores in polymer science, John Wiley & Sons, 2015.

[5] S. Jauk, R. Liska, Photoinitiators with functional groups, 8. Macromolecular rapid communications, 2005, 26.21, 1687-1692.

[6] J. Zhang, F. Dumur, P. Xiao, B. Graff, D. Bardelang, D. Gigmes, J. P. Fouassier, J. Lalevée, Structure design of naphthalimide derivatives: Toward versatile photoinitiators for near-UV/visible LEDs, 3D printing, and water-soluble photoinitiating systems, Macromolecules, 2015, 48.7, 2054-2063.

[7] D. J. Lougnot, J. P. Fouassier, Comparative reactivity of water soluble photoinitiators as viewed in terms of excited states processes, Journal of Polymer Science Part A: Polymer Chemistry, 1988, 26.4, 1021-1033.

[8] H. Kitano, K. Ramachandran, N. B. Bowden, A. B. Scranton, Unexpected visible-light-induced free radical photopolymerization at low light intensity and high viscosity using a titanocene photoinitiator, Journal of Applied Polymer Science, 2013, 128.1, 611-618.

[9] J. E. Baxter, R. S. Davidson, H. J. Hageman, K. A. McLauchlan, D. G. Stevens, The photo-induced cleavage of acylphosphine oxides. Journal of the Chemical Society, Chemical Communications, 1987, 2, 73-75.

Chapitre I : Photoamorceurs Type I à base d'Oxime-Ester

Un très grand nombre de systèmes photo-amorceurs avec des profils d'absorption correspondant aux longueurs d'onde d'émission des diodes électroluminescentes (LEDs) ont été synthétisés, mais la plupart d'entre eux sont multicomposants. Alors que, les performances de ces systèmes multi-composants sont facilement influencées par la solubilité, l'efficacité du transfert d'électrons ou la viscosité des résines. [1-5] Il existe donc un besoin évident d'introduire de nouveaux systèmes de photo-amorceurs Type I à un seul composant, dans lesquels ces différents paramètres ne doivent plus être pris en compte. En tant que photo-amorceurs Type I, les oxime-esters sont connus depuis longtemps pour leur photoréactivité élevée dans le processus de photopolymérisation. Leur efficacité est attribuée au clivage de la liaison N-O sous irradiation lumineuse, pour générer des radicaux iminyle et carbonate, qui peuvent à leur tour subir d'autres réactions de fragmentation ou de décarboxylation (Schéma 1). [6-10]

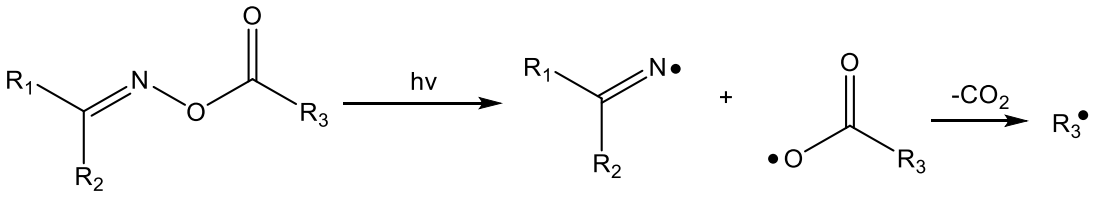

Schéma 1. Mécanisme photochimique des oxime-esters.

L'O-Benzoyl-α-oxooxime (OXE-01) et l'O-acétyloxime (OXE-02) (Schéma 2), deux OXEs commerciaux, sont utilisés pour produire des films épais pour les résines photosensibles des filtres de couleur. Cependant, les bandes d'absorption de OXE-01 et OXE-02 étant situées dans la gamme des UV, ces deux oximes esters fonctionnent faiblement lorsqu'ils sont exposés à des LEDs proches des UV ou visibles. [11-15]

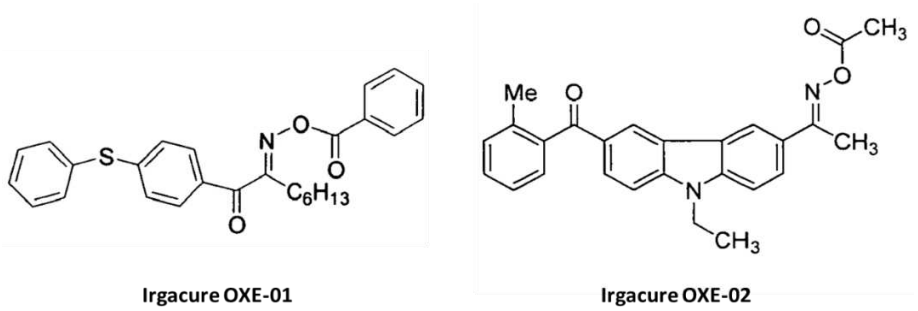

Schéma 2. Structures des photoamorceurs commerciaux à base d'oxime-ester OXE-01 et OXE-02.

PARTIE III : SYSTÈMES PHOTOAMORCEURS MONOCOMPOSANTS

L'idée de base de notre travail, est de tester de nouvelles oxime-esters ayant des longueurs d'onde d'absorption situées dans le visible, afin de mieux correspondre aux différentes sources de lumière LEDs. La capacité de photo-amorçage et la photoréactivité des structures proposées ont été examinées lors de l'exposition des résines à une LED@405 nm, et leur comportement d'amorçage thermique a été évalué par calorimétrie à balayage différentiel (DSC). En outre, et afin de mettre en évidence leur haute efficacité de photopolymérisation, les structures proposées ont été utilisées pour des applications en impression 3D.

Une étude approfondie sur les mécanismes liés aux processus de polymérisation, les techniques de mesure et les différents facteurs affectant l'efficacité de la conversion a été réalisée. Le but de notre recherche est de modifier les structures chimiques des oxime-esters en introduisant différents chromophores ou en variant la substitution du groupe ester, ce qui permet d'obtenir une relation structure/réactivité/efficacité intéressante. La synthèse des différents composés a été majoritairement réalisée à l'institut de chimie radicalaire de Marseille par le Dr. Frédéric Dumur. De plus, d'autres composés utilisés ont été préparés en collaboration avec le département d'ingénierie chimique et des matériaux de l'Université nationale des sciences et technologies de Kaohsiung (Taiwan) par le Dr. Yung-Chung Chen. Les travaux réalisés ont fait l'objet de plusieurs articles publiés dans divers journaux internationaux sous les citations suivantes : F. Hammoud et al, "Novel phenylamine-based oxime ester photoinitiators for LED-induced free radical, cationic, and hybrid polymerization", Journal of Polymer Science, 2021, 59, 1711–1723. Hammoud F. et al, "Substituent effects on the photoinitiation ability of coumarin-based oxime-ester photoinitiators for free radical photopolymerization", Materials Chemistry Frontier, 2021, 5, 8361–8370. Hammoud F. et al, "5,12-Dialkyl-5,12-dihydroindolo[3,2-a]carbazole-based oxime-esters for LED photoinitiating systems and application on 3D printing", Macromolecular Materials and Engineering, 2022. L'ensemble des résultats obtenus sont résumés dans ce chapitre sous la forme d'une revue publiée dans "European polymer journal" qui a rassemblée tous les résultats obtenus et a présenté une comparaison entre les différents chromophores, sous la citation suivante : Hammoud F. et al, "A Review on Recently Proposed Oxime Ester Photoinitiators", European Polymer Journal, 2023, 111901, 0014-3057. Dans ce chapitre, pour des raisons de clarté seul la revue sera présentée.

Références

[1] F. Karasu, C. Croutxé-Barghon, X. Allonas, D. V. Van, G. J. Leendert, Free radical photopolymerization initiated by UV and LED: Towards UV stabilized, tack free coating, J Polym Sci, Part A: Polym Chem, 2015, 52.24, 3597-607.

[2] N. Zivic, M. Bouzrati, S. Villote, F. Morlet-Savary, C. Dietlin, F. Dumur, D. Gigmes, J.P. Fouassier, J. Lalevée, A novel naphthalimide scaffold based iodonium salt as a one-component photoacid/photoinitiator for cationic and radical polymerization under LED exposure, Polymer Chemistry, 2016, 7, 5873-5879.

[3] C. Dietlin, T.T. Trinh, S. Schweitzer, B. Graff, F. Morlet-Savary, P.A. Noirot, J. Lalevée, Rational Design of Acyldiphenylphosphine Oxides as Photoinitiators of Radical Polymerization, Macromolecules, 2019, 52, 7886-7893.

[4] P. Garra, C. Dietlin, F. Morlet-Savary, F. Dumur, D. Gigmes, J.P. Fouassier, J. Lalevée, Photopolymerization processes of thick films and in shadow areas: a review for the access to composites, Polymer Chemistry, 2017, 8.46, 7088-7101.

[5] N. Zivic, M. Bouzrati, S. Villote, F. Morlet-Savary, C. Dietlin, F. Dumur, D. Gigmes, J.P. Fouassier, J. Lalevée, A novel naphthalimide scaffold based iodonium salt as a one-component photoacid/photoinitiator for cationic and radical polymerization under LED exposure, Polymer Chemistry, 2016, 7, 5873-5879.

[6] J. Xu, G. Ma, K. Wang, J. Gu, S. Jiang, J. Nie, Synthesis and photopolymerization kinetics of oxime ester photoinitiators, Journal of Applied Polymer Science, 2012, 123.2, 725-731.

[7] D. E. Fast, A. Lauer, J. P. Menzel, A. M. Kelterer, G. Gescheidt, C. Barner-Kowollik, Wavelength-Dependent Photochemistry of Oxime Ester Photoinitiators, Macromolecules, 2017, 50, 1815-1823.

[8] S. R. Shin, K. Jun, J. I. Shin, S. Y. Park, K. L. An, S. So. Lee, B. S. Moon, B. C. Oh, A. Choi, I. Y. So, Novel fluorene oxime ester compound, photopolymerization initiator and photoresist composition containing the same, U. S. Patent US20150111152A1, 2015.

[9] Z. Li, X. Zou, G. Zhu, X. Liu, R. Liu, Coumarin-based oxime esters: photobleachable and versatile unimolecular initiators for acrylate and thiol-based click photopolymerization under visible light-emitting diode light irradiation, ACS applied materials & interfaces, 2018, 10.18, 16113-16123.

[10] X. Y. Ma, R. Q. Gu, L. J. Yu, W. X. Han, J. Li, X. Y. Li, T. Wang, Conjugated phenothiazine oxime esters as free radical photoinitiators, Polymer Chemistry, 2017, 8, 6134-6142.

[11] Y. Gao, J. Song, S. Shang, D. Wang, J. Li, Synthesis and antibacterial activity of oxime esters from dihydrocumic acid, BioResources, 2012, 7.3, 4150-4160.

[12] D. Wang, S. Ren, H. Wang, H. Yan, J. Feng, X. Zhang, Semisynthesis and antifungal activity of novel oxime ester derivatives of carabrone modified at C (4) against Botrytis cinerea, Chemistry & biodiversity, 2014, 11.6, 886-903.

[13] W. Qiu, J. Zhu, K. Dietliker, Z. Li, Polymerizable Oxime Esters: An Efficient Photoinitiator with Low Migration Ability for 3D Printing to Fabricate Luminescent Devices, ChemPhotoChem, 2020, 4.11, 5296-5303.

[14] X. Y. Ma, D. Cao, H. Y. Fu, J. You, R. Q. Gu, B. F. Fan, J. Nie and T. Wang, Multicomponent photoinitiating systems containing arylamino oxime ester for visible light photopolymerization, Progress in Organic Coatings, 2019, 135, 517-524.

[15] C. Oh, M. Lee, W. J. Lee, Y. Cho, S. R. Shin, J. I. Shin, S. Lee, K. Jun, Novel β-oximester fluorene compound, a photopolymerization initiator comprising same, and photoresist composition, WIPO Patent WO2015108386A1, 2015.

European Polymer Journal 188 (2023) 111901

Contents lists available at ScienceDirect

European Polymer Journal

journal homepage: www.elsevier.com/locate/europolj

A review on recently proposed oxime ester photoinitiators

Fatima Hammoud [a,b,c], Akram Hijazi [c], Michael Schmitt [a,b], Frédéric Dumur [d,*], Jacques Lalevée [a,b,*]

[a] Université de Haute-Alsace, CNRS, IS2M UMR7361, F-68100 Mulhouse, France
[b] Université de Strasbourg, France
[c] EDST, Université Libanaise, Campus Hariri, Hadath, Beyrouth, Lebanon
[d] Aix Marseille Univ, CNRS, ICR UMR 7273, F-13397 Marseille, France

ARTICLE INFO

Keywords:
Oxime esters
Type I photoinitiators
Homolytic cleavage
Photopolymerization
Low light intensity
Dyes
Visible light

ABSTRACT

This review is intended to highlight the recent developments and trends in the chemistry of oxime esters-based photoinitiators. It focuses on the mechanisms underlying the polymerization processes, measurement techniques, and various factors that affect the conversion efficiency. Due to their remarkable reactivities in photopolymerization reactions, oxime esters have attracted a great attention as reliable Type I (one-component) photoinitiators. In recent years, several research studies have been published with the purpose of modifying their chemical structures by introducing different chromophores or by varying the substitution pattern of the ester group, for which an interesting structure/reactivity/efficiency relationship could be achieved. In this review, an overview of the recent advances on oxime esters-based photoinitiators, as well as a comparison of the various scaffolds proposed in the literature is provided and discussed.

1. Introduction

Photochemical engineering of polymers and other modern materials science and technology has led to the creation of complex but effective methods for the fabrication of innovative materials, post-functionalization of polymers and novel synthetic products [1-3]. In these systems, light-activated chemical reaction pathways not only provide an excellent control over the reaction kinetics but also make it simple to carry out complex synthetic protocols [4-7]. Photoinduced polymerization systems may provide more flexible ways to synthesize macromolecules than polymerization systems induced by thermal, chemical, or electrochemical processes. As a result, recent advancements in these technologies have seen widespread being used in fields such as coatings, electronic circuits, digital storage, solar cells, and 3D precision machining. However, the majority of industrial polymerization processes currently under use relies on UV photoinitiating systems, which are facing a number of safety issues [8-12]. Actuality, the risk of UV radiation, which is the source of skin cancers and eye damages, as well as the formation of ozone during polymerization, are the main reasons that UV photopolymerization has been banned from some industrial applications and, more significantly, from consumer apps. High operating costs are also necessary because UV photopolymerization can only be done with pricey and energy-intensive setups [13-15]. The future of the planet now depends on reducing the energy consumption and improving the control of energy usage. Therefore, the search for more ecologically friendly polymerization processes is currently under progress.

Light-emitting diodes (LEDs) are a great choice for visible and secure light sources since these devices are compact and lightweight. LEDs have also low operating costs, long lifetimes, and low power consumption. In addition, these irradiation sources are now easily available [16-18]. In fact, efficiency of the electron transfer in multistep initiating procedures and the viscosity of the resins used to prepare the different photoinitiating systems are the unavoidable difficulties to deal with. At present, a wide range of two- or three component photoinitiating systems with absorption spectra perfectly matching the emission of LEDs are available. However, the complexity of the formulations can constitute a severe limitation for the future uses of these resins. In order to create more easily free radicals directly by the cleavage of chemical bonds, one-component type I PIs are now preferred [19-22].

Only a few Type I photoinitiators, such as phosphine oxides and α-amino ketones, are currently compatible with near-UV and visible LEDs. The high reactivities of oxime esters (OXEs) as Type I photoinitiators in free radical photopolymerization are well known. In these structures, light irradiation can lead to the homolytic cleavage of the N-O bond, generating iminyl and acyloxy radicals. The acyloxy radical is

* Corresponding authors at: Université de Haute-Alsace, CNRS, IS2M UMR7361, F-68100 Mulhouse, France (J. Lalevée).
E-mail addresses: Frederic.dumur@univ-amu.fr (F. Dumur), jacques.lalevee@uha.fr (J. Lalevée).

https://doi.org/10.1016/j.eurpolymj.2023.111901
Received 17 January 2023; Received in revised form 7 February 2023; Accepted 8 February 2023
Available online 17 February 2023

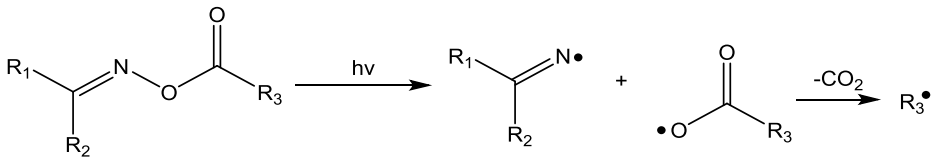

Scheme 1. Photochemical mechanisms involved in the decomposition of oxime esters. Reproduced with the permission from [49].

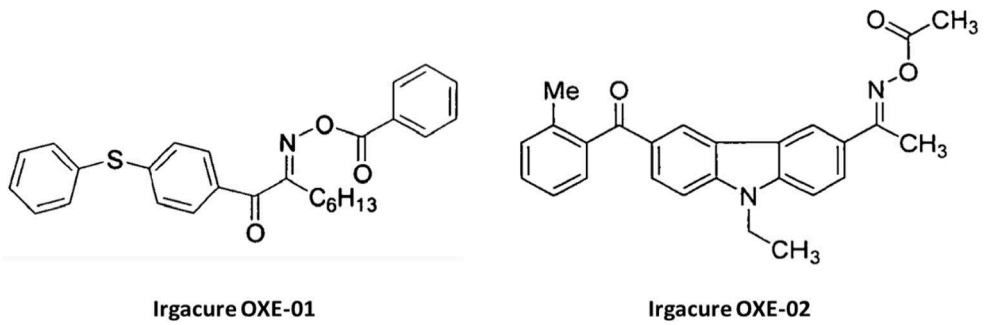

Scheme 2. Structures of commercial oxime ester photoinitiators OXE-01 and OXE-02.

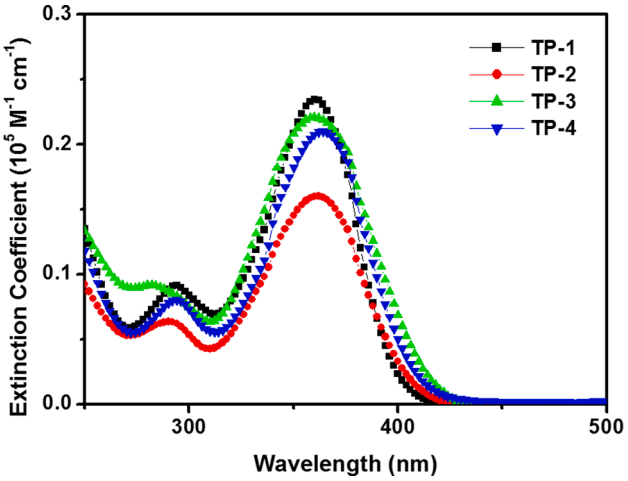

Fig. 1. UV/Vis spectra of **TP-1–TP-4** in DCM solutions (Conc. = $1*10^{-5}$ M). Reproduced with the permission from [36].

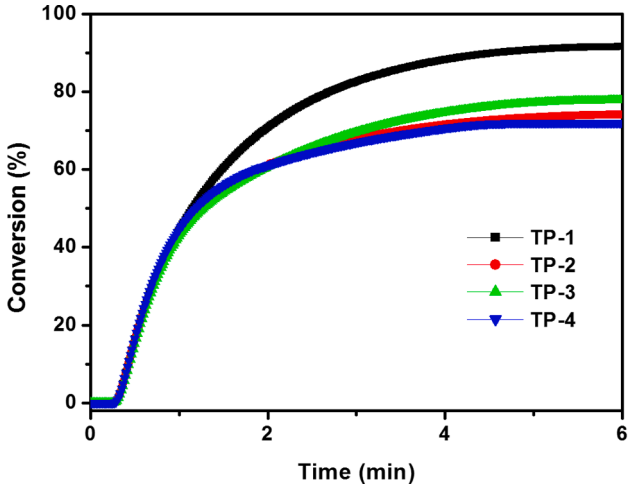

Fig. 2. Conversion versus time of TMPTA photopolymerization initiated by **TP-1–TP-4** (2 wt %) under UV light irradiation. Reproduced with the permission from [36].

next subjected to a decarboxylation process, which results in the production of CO_2 and the formation of an active radical (See Scheme 1) which is quite similar to the known and proven Kolbe and Photo-Kolbe reaction [22-27]. It has to be noticed that during the photoinduced decomposition of oxime esters, only a nontoxic and nonhazardous gas is released within the photocurable resin, namely CO_2. Additionally, after decarboxylation reaction of aryloxy or acyloxy radicals, the probability of radical recombination with iminyl radicals is unfavorable so that aryl or alkyl radicals are more available for polymerization.

O-Benzoyl-*α*-oxooxime (OXE-01) and *O*-acetyloxime (OXE-02) (Scheme 2), two commercial OXEs, are used to produce thick films for color filter resists. However, since OXE-01 and OXE-02′s absorption bands were located in the UV range, these two oxime esters operate poorly if exposed to near-UV or visible LEDs [28-30]. Recently, a number of studies have been devoted to shift the oxime esters absorption wavelength into the visible range in order to better match their absorptions with the emission of various visible light sources. Different chromophores including coumarins, phenothiazines, triphenylamines, anthracenes, pyrenes, fluorenes and carbazoles were notably investigated during the last two years, evidencing the intense research activity in this field.

This review provides an overview of the different oximes esters recently developed by our groups at the Institute of Materials Science of

Table 1
Photo-DSC results derived from **TP-1–TP-4**.

Photoinitiators[b]	Final Conversion (%)	$H_{overall}$ (mW/mg)[c]	H_{max} (mW/mg)[d]	Rp_{max} (S^{-1})[e]	T_{max} (S)[f]
TP-1	91	79	66	89	25
TP-2	74	64	63	86	26
TP-3	77	67	61	84	27
TP-4	72	62	66	90	27

[a]Measured with 80 W/m^2 of UV light for 6 min.
[b]Photo-DSC of the **TP-1–4**/TMPTA at weight ratios of **TP-1–4**: TMPTA = 2: 98.
[c]$H_{overall}$: overall heat flow values within 6 min.
[d]H_{max}: maximum heat flow values.
[e]Rp_{max}: maximum rate of polymerization.
[f]T_{max}: time at maximum heat flow.

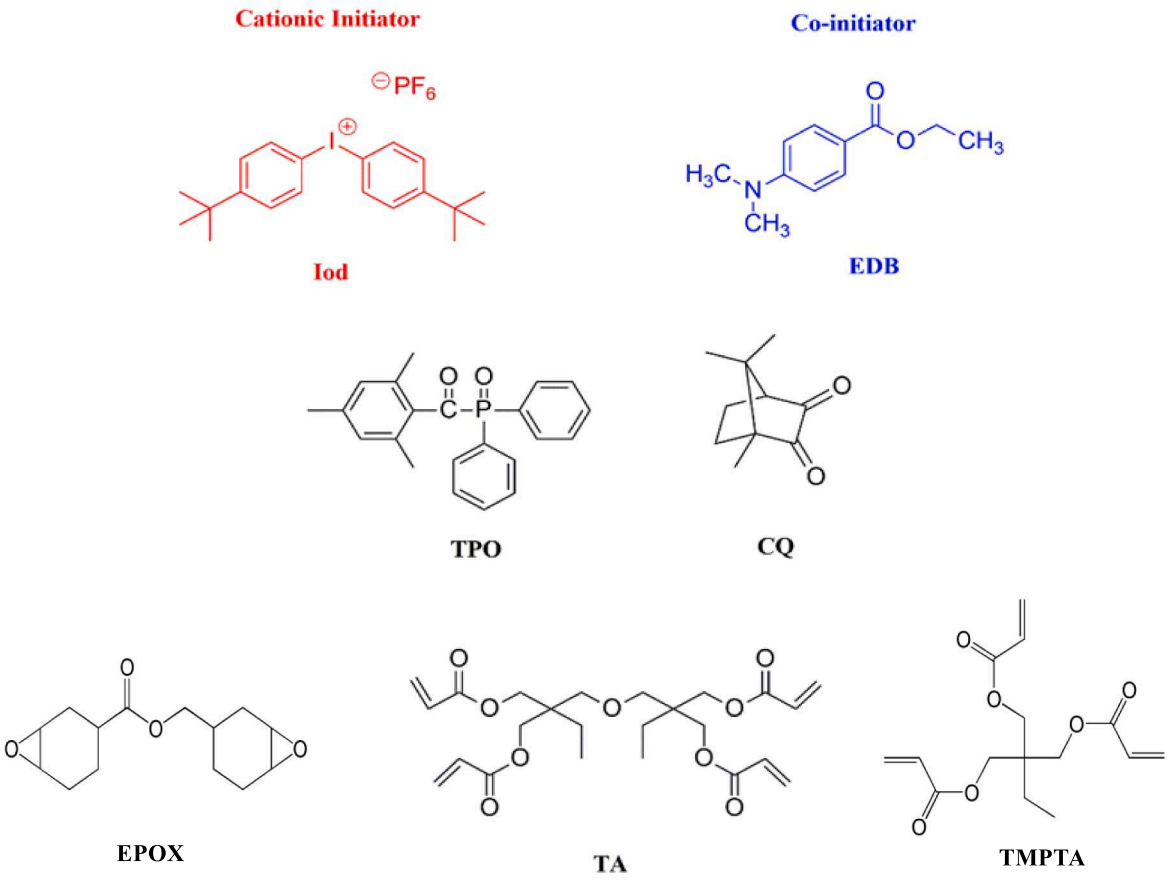

Scheme 3. Chemical structures of additives and monomers.

Mulhouse (IS2M) and the Institute of Radical Chemistry (ICR) of Marseilles. Considering that numerous structures have been investigated, a comparison between the different families of chromophores is provided. Influence of the substitution pattern of the ester function on the photoinitiating ability of oxime esters is also discussed.

2. Triphenylamine based-oxime esters

Triphenylamine is a promising scaffold for the development of visible dyes. Triphenylamine is an electron donating group of low oxidation potential so that, when combined with an electron acceptor, push–pull dyes exhibiting an intense intramolecular charge transfer band extending over the visible range can be obtained [31,32]. The three-dimensional structure of triphenylamine also allows the corresponding dyes to significantly increase the solubility of the dyes produced compared to those made using its parent structure i.e. carbazole exhibiting a higher rigidity. Unlike carbazole, which has a planar structure that favors intermolecular interactions such as π-π staking, the three-dimensionality of triphenylamine is a real advantage to address the solubility issue. Aromatic rings of triphenylamine are excellent candidates for a variety of chemical modifications. Triphenylamine is particularly amenable to the majority of typical chemical reactions that form the core of Organic Chemistry [33-35].

A series of triphenylamine-based oxime esters were investigated by Chen and coworkers in 2020 for their potential use as visible light photoinitiators [36]. In Scheme 4, chemical structures of four different triphenylamine-based Type I photoinitiators (**TP-1-TP-4**) and the synthetic route to access to these structures are shown. The synthetic protocols involve the following crucial steps: (1) a Buchwald-Hartwig C-N-coupling reaction to produce arylamines; (2) a Vilsmeier-Haack reaction to formylate the aromatic ring; (3) an oximation reaction of the aldehyde using sodium acetate as the base and hydroxylamine hydrochloride; and (4) a condensation reaction using benzoic anhydride in the presence of a base used as a catalyst to produce the desired compounds (**TP-1–TP-4**). UV–visible absorption spectra of the studied **TP-1-TP-4** compounds in CH_2Cl_2 are shown in Fig. 1. Absorption maxima of **TP-1-TP-4** were, respectively, 360, 364, 360 and 362 nm. Thus, the triphenylamine unit's substituted groups had a negligible impact on the max values.

Photo-DSC profiles of all the newly developed photoinitiators are shown in Fig. 2 and the results obtained during the photopolymerization experiments are gathered in Table 1. It's interesting to see how the photoreactivity of oxime esters is greatly influenced by the substitution introduced onto the triphenylamine core. According to the results obtained during the photopolymerization studies, the maximum heat flows and polymerization rates both decrease in the order **TP-1** = **TP-4** > **TP-2** > **TP-3** and **TP-1** = **TP-4** > **TP-2** > **TP-3**, respectively. Thus, **TP-1**, **TP-2**, **TP-3**, and **TP-4**'s final conversion efficiencies were determined as being of 92 %, 74 %, 78 %, and 72 %, respectively during the free radical polymerization (FRP) of trimethylolpropane triacrylate (TMPTA) (Scheme 3). Consequently, **TP-1-TP-4**-based photoinitiating systems exhibited excellent polymerization efficiencies. The best conversion efficiency among all of them is achieved by the compound **TP-1** with the highest radical concentration, the highest molar extinction coefficient, the largest difference between E_T and BDE value and good photolysis properties.

A more recent study from the same group proposed four new photoinitiators (PIs) (**TP-2p**, **TP-2m**, **TP-3m** and **Dml-m**) investigated for the free radical polymerization (FRP) of TMPTA, the cationic polymerization (CP) of (3,4-epoxycyclohexane)methyl-3,4-epoxycyclohexylcarboxylate (EPOX) (Scheme 3), and the elaboration of interpenetrated polymer networks (IPN), (see Scheme 5). As

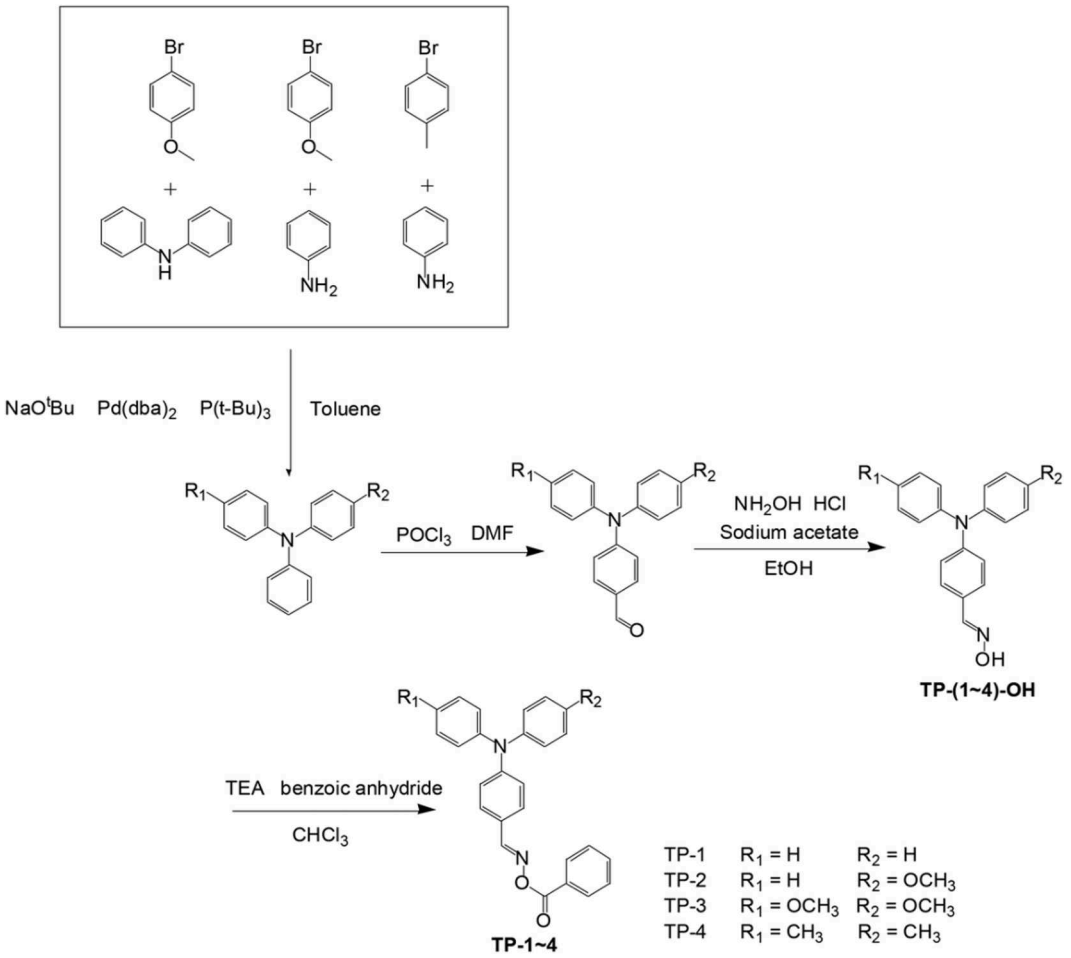

Scheme 4. Synthetic route to triphenylamine-based oxime esters (**TP-1–TP-4**). Reproduced with the permission from [36].

specificities, triphenylamine-based oxime esters comprise two or three oxime ester functions, enabling to tune the reactivity of OXE by mean of the number of photocleavable groups [36]. Synthetic procedures used to access to these structures include first (a) a formylation of the aromatic compound by mean of a Vilsmeier–Haack reaction; (b) an oximation reaction of the formyl group using sodium acetate as the base and hydroxylamine hydrochloride and (c) finally an esterification reaction of the oxime group with benzoic anhydride in the presence of triethylamine used as the base that could afford the different oxime esters in 70 %, 90 %, 70 and 60 % yield respectively for **TP-2p**, **TP-2m**, **TP-3m** and **Dml-m**. These compounds showed an outstanding polymerization photoinitiation ability i.e. high polymerization rates and good final reactive function conversions, when irradiated with a LED@405 nm.

From the absorption point of view, **TP-2p**, **TP-2m**, and **TP-3m** showed mainly an absorption centered in the near UV range (300–425 nm), while **Dml-m** showed an absorption at a shorter wavelength (See Fig. 3), highlighting the crucial role of the triphenylamine chromophore in red-shifting the absorption. **TP-3m** exhibited the highest molar extinction coefficient of the series due to the presence of three oxime ester functionalities in its structure, acting as electron withdrawing groups and increasing the electronic delocalization for this compound (See Fig. 3).

Considering their light absorption properties, all PIs were suitable to initiate the free radical photopolymerization (FRP) of TMPTA under LED@405 nm. Fig. 4 displays typical acrylate conversion vs. irradiation time profiles. With the exception of **Dml-m**, all the examined OXEs exhibited high polymerization rates (See Fig. 4(A, B); curve 4), which demonstrate the importance of the triphenylamine group in order to get a good absorbance at 405 nm in thin samples (25 μm in laminate) and in thick samples (1.4 mm under air) (see the light absorption properties above).

Noticeably, polymerization efficiency of **TP-2p** was lower than that of **TP-2m** during the FRP of TMPTA at 405 nm. This is in stark contrast to the strong reactivity of the phenyl radical (produced in **TP-2p**), whose reaction rate toward the acrylate double bond is more than two orders of magnitude higher than that of the methyl radicals. This phenomenon was therefore assigned to the easier photocleavage of **TP-2m** upon irradiation as well as an easier decarboxylation process of **TP-2m** compared to **TP-2p** after homolytic cleavage of the N-O bond. However, since **TP-3m** has an additional oxime ester functionality in its structure, which can produce more radicals than the **TP-2m/ TP-2p series**, this OXE could furnish slightly higher conversions than **TP-2m** (See Fig. 4).

The cationic polymerization of EPOX under LED illumination at 405 nm was also examined for the different afore-mentioned OXEs. Especially, the different OXEs were used as photosensitizers for an iodonium salt (Iod). Fig. 5 displays the epoxy function conversion obtained vs. irradiation time curves upon irradiation at 405 nm. No polymerization occurred for Iod alone in EPOX, which is consistent with the lack of absorbance of Iod at 405 nm. Actually, the different OXEs can absorb light at 405 nm, and then the corresponding generated excited states of these compounds are expected to interact with Iod to generate the initiating species ($OXE^{\bullet+}$).

It has to be noticed that the photochemical reactivity of the different OXEs with the iodonium salt is certainly affected by the chemical structures of OXEs but also by differences of reactivity of the generated radical cations ($OXE^{\bullet+}$) formed by decomposition of the iodonium salt

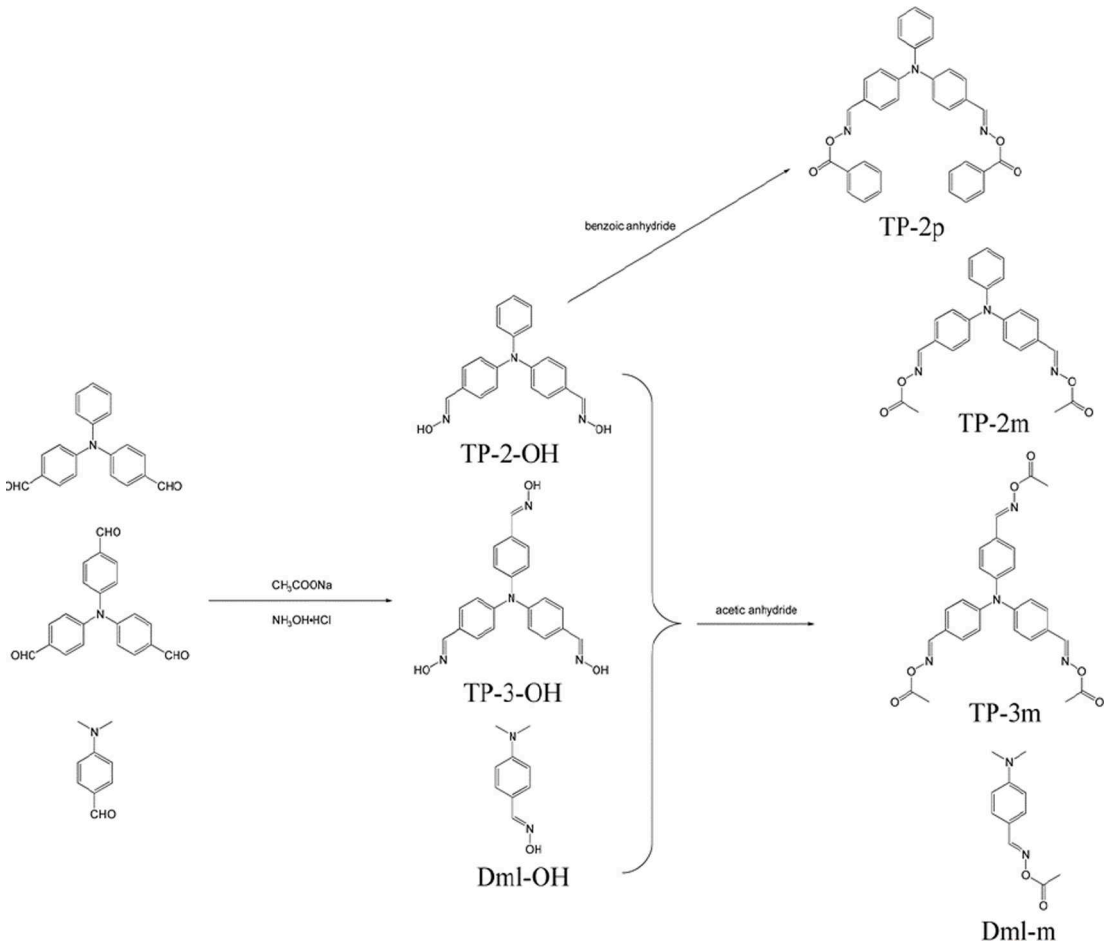

Scheme 5. Synthetic routes and chemical structures of the synthetized phenylamine-based oxime esters used in this research. Reproduced with the permission from Ref [37].

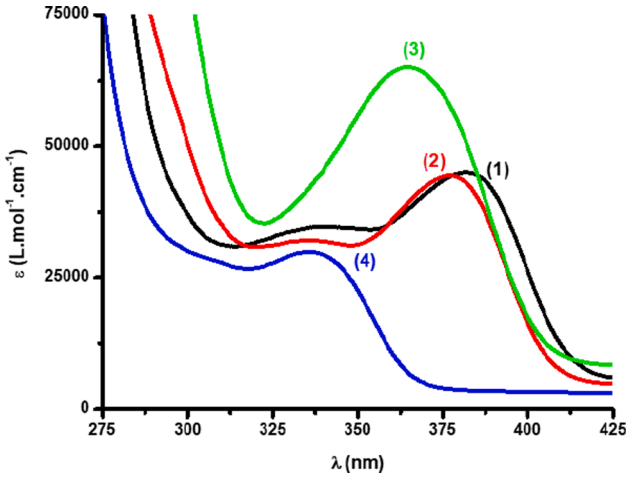

Fig. 3. UV–visible absorption spectra of (1) **TP-2p**, (2) **TP-2m**, (3) **TP-3m** and (4) **Dml-m** in dichloromethane. Reproduced with permission of Ref. [37].

(See equation r2).

Furthermore, it was suggested to combine radical and cationic polymerizations in order to create interpenetrating polymer networks (IPN) that would have the benefits of both techniques without the drawbacks. Table 2 provides a summary of the final acrylate and epoxy function conversions obtained upon irradiation at 405 nm for 800 s. The experimental findings demonstrate that the OXE/Iod systems can induce the hybrid polymerization for a combination of 50 % wt TMPTA and 50 % wt EPOX (See Table 2). Noticeably, in thin films, the acrylate conversion was greatly higher than that of the epoxides, attributable to the higher reactivity of the phenyl radicals compared to the $OXE^{\bullet+}$ radical cations. Conversely, under air, an opposite situation was found, with EPOX conversions on par with that of TMPTA. It can be confidently assigned to oxygen inhibition, adversely affecting the FRP of TMPTA. Indeed, the CP of epoxides being insensitive to oxygen inhibition, higher monomer conversions can be obtained under air compared to that obtained in laminate.

Parallel to the photochemically induced polymerization processes, all OXEs also exhibited an excellent thermal initiating ability. By differential Scanning Calorimetry (DSC), a maximum exothermicity was determined at 155 °C, with an onset temperature of 115 °C. As shown in the Fig. 6, the highest exothermicity was observed for the trifunctional oxime ester i.e. **TP-3m**, furnishing a monomer conversion of 65 %. Following **TP-3m**, the best TMPTA conversions were obtained for the difunctional OXEs **TP-2m** and **TP-2p**, with monomer conversions of 60 and 42 % respectively. It can be thus concluded that in the case of the thermal activation, increase of the number of reactive functions drastically improves the monomer conversion.

Overall, the new series of OXE could efficiently initiate the CP of EPOX and the FRP of TMPTA, as well as the synthesis of interpenetrated polymer networks in which the concomitant polymerization of EPOX and TMPTA can be obtained. Based on their light absorption characteristics, cleavage ability, decarboxylation reaction, and the reactivity of the produced radicals, some pertinent structure/efficiency relationships could be examined. Interestingly, these OXEs could display a dual

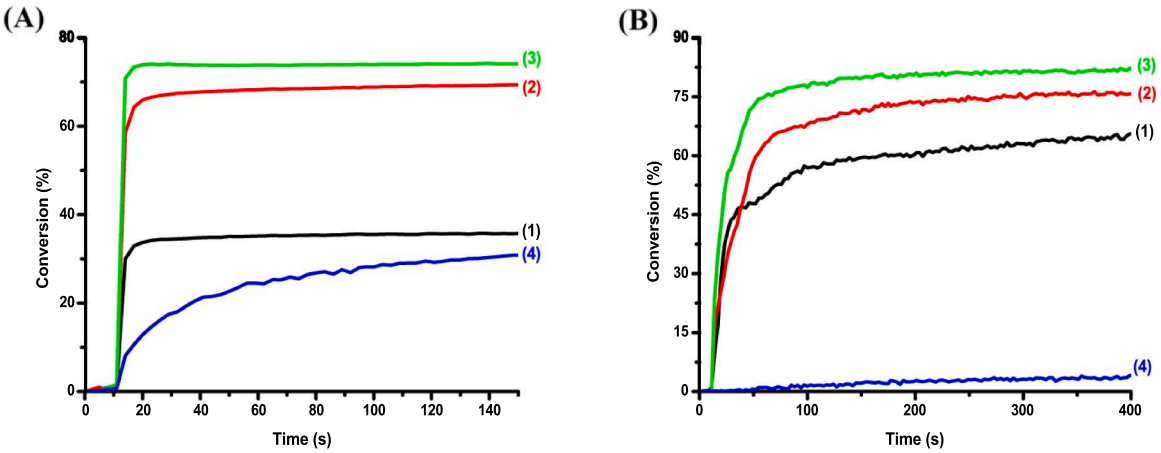

Fig. 4. (A) Polymerization profiles of TMPTA (acrylate function conversion vs. irradiation time) in laminate (thickness = 25 μm) upon exposure to LED lightλ = 405 nm in the presence of: (1) **TP-2p** (1 % w); (2) **TP-2m** (1 % w); (3) **TP-3m** (1 % w); and (4) **Dml-m** (1 % w); respectively. The irradiation starts after t = 10 s. (B) Polymerization profiles of TMPTA (acrylate function conversion vs. irradiation time) under air (thickness = 1.4 mm) upon exposure to LED light λ = 405 nm in the presence of: (1) **TP-2p** (1 % w); (2) **TP-2m** (1 % w); (3) **TP-3m** (1 % w); and (4) **Dml-m** (1 % w); respectively. The irradiation starts after t = 10 s. Reproduced with the permission from Ref [37].

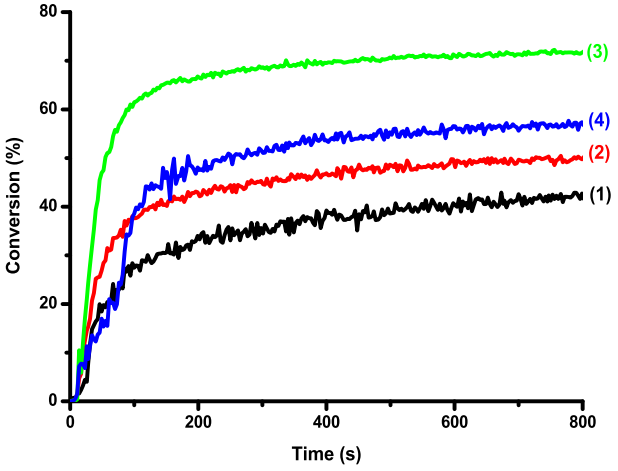

Fig. 5. Polymerization profiles of EPOX (epoxy function conversion vs. irradiation time) under air (thickness = 25 μm) upon exposure to the LED lightλ = 405 nm in the presence of: (1) **TP-2p**/Iod (1 %/2 % w/w); (2) **TP-2m**/Iod (1 %/2 % w/w); (3) **TP-3m**/Iod (1 %/2 % w/w); and (4) **Dml-m**/Iod (1 %/2 % w/w); respectively. The irradiation starts after t = 10 s. Reproduced with the permission from Ref [37].

Table 2
Final acrylate or epoxy function conversion (FCs) for the polymerization of a TMPTA/EPOX blend (50 %/50 % w/w) using different two-component OXE/Iod (1 %/1 % w/w) photoinitiating systems after 800 s of irradiation with a LED (λ = 405 nm).

	Thin sample (25 μm) in laminate		Thick sample (1.4 mm) under air	
	Acrylate function	Epoxy function	Acrylate function	Epoxy function
TP-2p/Iod	77 %	26 %	43 %	42 %
TP-2m/Iod	89 %	14 %	39 %	36 %
TP-3m/Iod	94 %	16 %	38 %	29 %
Dml-m/Iod	69 %	26 %	51 %	21 %

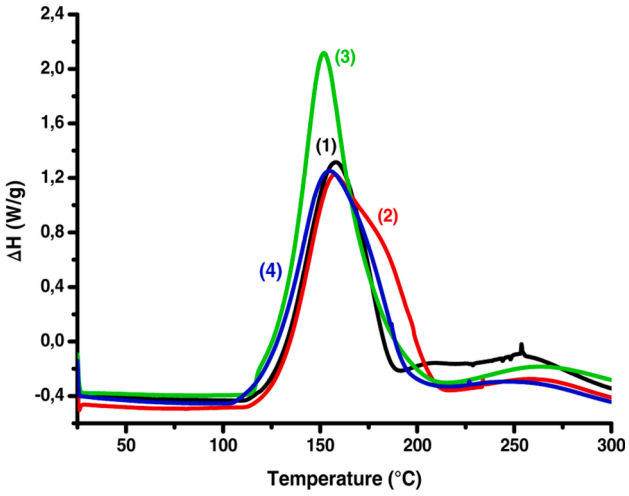

Fig. 6. Thermal polymerization (enthalpy vs. heating temperature) of TMPTA determined at a heating rate of 10 K/min, under nitrogen. (1) 1 % **TP-2p**, (2) 1 % **TP-2m**, (3) 1 % **TP-3m**, and (4) 1 % **Dml-m**. Reproduced with the permission from Ref [37].

$$\text{OXE } (h\nu) \rightarrow {}^{1}\text{OXE} \quad \text{(r1)}$$

$${}^{1}\text{OXE} + Ar_2I^{+} \rightarrow OXE^{\bullet+} + Ar^{\bullet} + ArI \quad \text{(r2)}$$

Scheme 6. Mechanism involved in the polymerization process making use of two-component dye/Iod systems. [36].

thermal and photochemical initiating ability, and to the best of our knowledge, this is the first time that this dual activation mode was demonstrated for oxime esters. This dual ability is of crucial importance, especially when a thermal activation is needed for polymerization in dark areas. In this case, the dual activation mode may offer up an additional curing opportunity in addition to the photochemical one.

3. Coumarin based-oxime esters

As chromophores commonly used for the development of Type II photoinitiators, coumarins, which are present in a variety of bacteria, fungi, and edible plants, have received a specific attention starting from

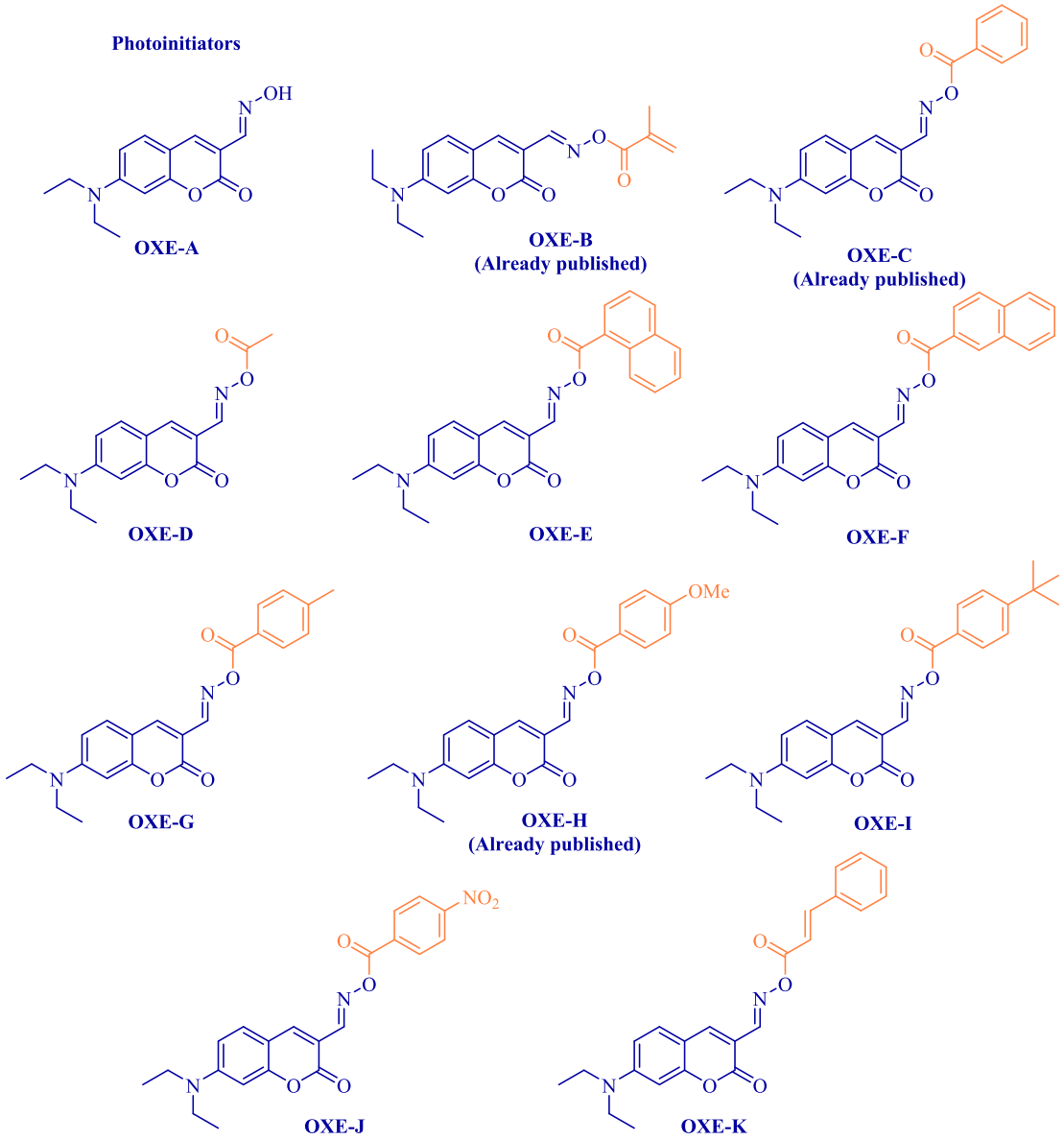

Scheme 7. Chemical structures of the synthetized coumarin-based oxime esters used in Ref [42].

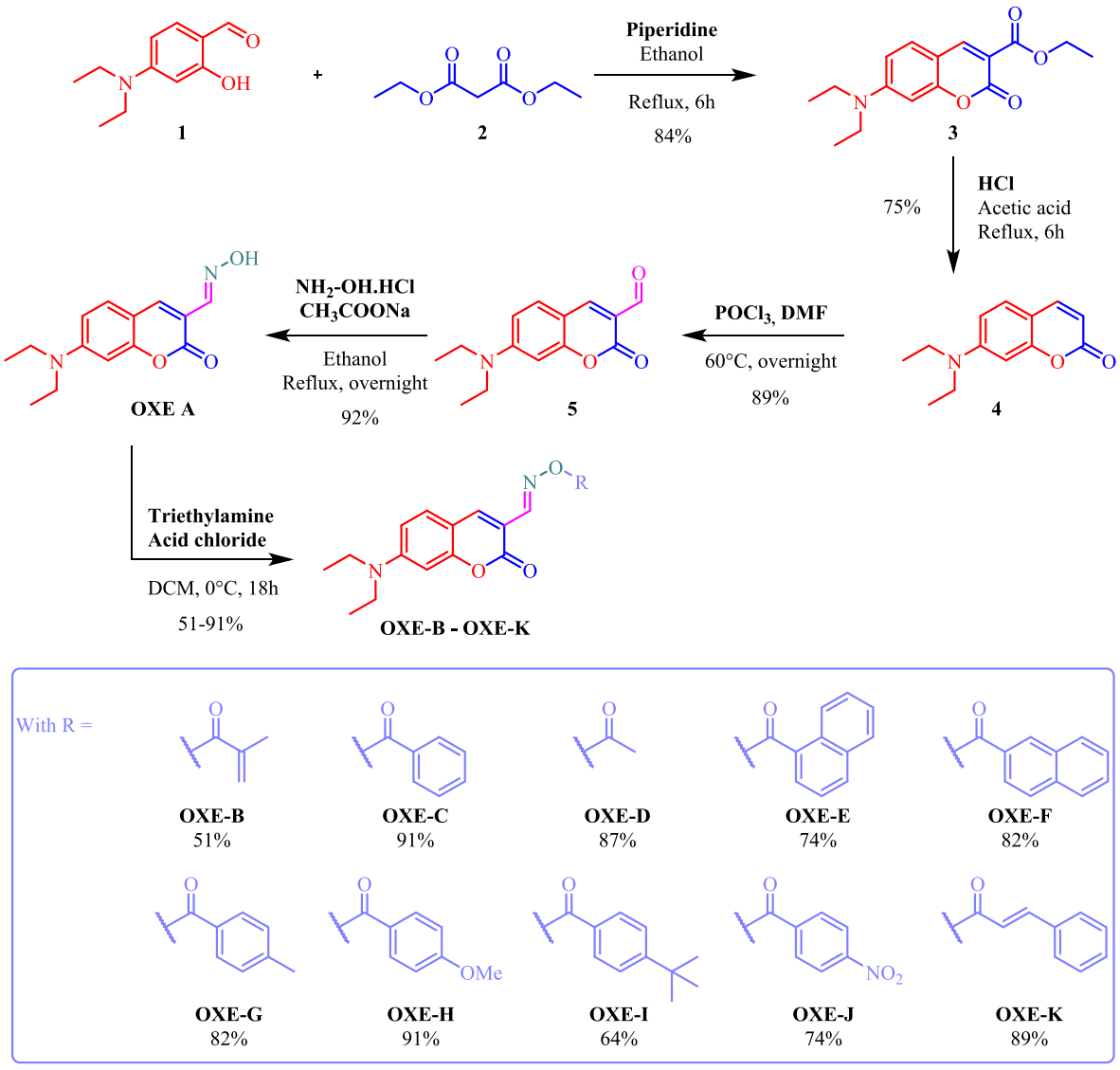

Scheme 8. Synthetic routes to **OXE-B**-**OXE-K**. Reproduced with the permission from [42].

Table 3
Light absorption properties of the investigated compounds; maximum absorption wavelengths (λ_{max}), extinction coefficients at λ_{max} and extinction coefficients at 405 nm.

PI	λ_{max} (nm)	ε_{max} ($M^{-1}cm^{-1}$)	$\varepsilon_{(405nm)}$ ($M^{-1}cm^{-1}$)
OXE-A	418	28,000	25,500
OXE-B	431	33,000	22,000
OXE-C	436	40,500	23,500
OXE-D	431	34,000	22,500
OXE-E	437	28,500	16,500
OXE-F	437	36,000	21,000
OXE-G	436	31,500	18,000
OXE-H	435	26,500	17,000
OXE-I	437	37,000	20,500
OXE-J	441	50,000	25,000
OXE-K	435	31,000	18,000

2019 for the design of oxime esters [38-40]. Indeed, if highly efficient photoinitiating systems could be prepared with coumarins, the only way to get high monomer conversions consisted in using three-component systems. The first coumarin-based oxime esters were reported in 2018 by Liu and coworkers with aim at simplifying the composition of the photocurable resins [41,42]. Unimolecular photoinitiators are currently actively investigated due to the easiness to handle. Indeed, research done recently on oxime esters has amply demonstrated that the efficiency of oxime ester's polymerization was correlated with two key factors: first, the effectiveness of the photocleavage, and second, the capacity of decarboxylation of acyloxy or aryloxy radicals. Recent studies in this area have shown that even if an efficient photocleavage could take place, the inability of aryloxy radicals to evolve into aryl radicals had a significant impact on the monomer conversion. Aryloxy radicals do, in fact, react with acrylic monomers less strongly than aryl radicals. By detecting the release of CO_2 in the reaction media at 2337 cm^{-1}, infrared spectroscopy makes it particularly simple to monitor the absence of decarboxylation and which species is involved in the polymerization process.

In 2021, an interesting study has compared the reactivity of different radicals produced by decarboxylation, the nature of the radicals formed having a significant impact on the polymerization efficiency [43]. This study aimed at comparing ten different oxime esters comprising the same chromophore (namely a coumarin) but exhibiting different substituents on the ester side. Among all OXEs proposed in this work, **OXE-B**, **OXE-C** and **OXE-H** (See Scheme 7) have previously been reported in the literature [29,41,42]. All oxime esters could be obtained in high yields, as shown in Scheme 8.

OXE-B-**OXE-K** exhibited broad absorption spectra with nearly

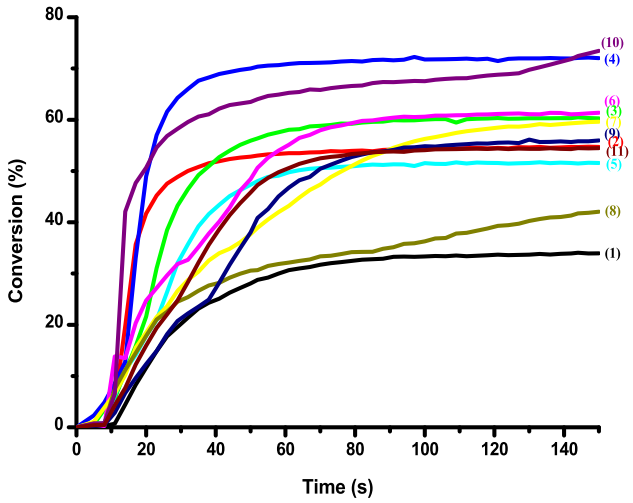

Fig. 7. Photopolymerization profiles of TMPTA (acrylate function conversion vs. irradiation time) in laminate (thickness = 25 μm) upon exposure to LED light λ = 405 nm in the presence of: (1) **OXE-A** (0.5 % w); (2) **OXE-B** (0.5 % w); (3) **OXE-C** (0.5 % w); (4) **OXE-D** (0.5 % w); (5) **OXE-E** (0.5 % w); (6) **OXE-F** (0.5 % w); (7) **OXE-G** (0.5 % w); (8) **OXE-H** (0.5 % w); (9) **OXE-I** (0.5 % w); (10) **OXE-J** (0.5 % w); and (11) **OXE-K** (0.5 % w); respectively. The irradiation starts after t = 10 s. Reproduced with the permission from Ref [42].

identical absorption maxima, as listed in the Table 3. Esterification of the oxime group in **OXE-B**-**OXE-K** resulted in a 20 nm redshift of the absorption maxima compared to that of the parent **OXE-A**, namely a non-esterified oxime (λ_{max} = 418 nm). As a result of this, absorption maxima ranging from 431 nm for **OXE-B** and **OXE-D** up to 441 nm for **OXE-J** could be determined by UV–visible absorption spectroscopy. In this series of oxime esters, **OXE-J** ($\varepsilon = 50\,000$ L.mol^{-1}.cm^{-1}) bearing the strongest electron-withdrawing group on the ester i.e. a nitro group exhibited the highest molar extinction coefficient. All dyes had short excited-state lifetimes that ranged from 1.58 ns for **OXE-I** to 1.92 ns for **OXE-B**. Thus, it can be concluded that the singlet state constitutes the primary deexcitation pathway.

According to the results obtained during the photopolymerization tests using **OXE-A**-**OXE-K** in TMPTA under 405 nm irradiation, **OXE-J** provided the highest final monomer conversion (73 %), followed by **OXE-D** (72 %) (See Fig. 7). As anticipated, **OXE-A**, which is not an oxime ester, had the lowest monomer conversion. In this case, a TMPTA conversion as low as 34 % was determined after 150 s of irradiation. Surprisingly, **OXE-H**, which has been previously reported in the literature, had the worst monomer conversion of the series of oxime esters. In TMPTA, a monomer conversion as low as 42 % was calculated. For all the other oxime esters, monomer conversions ranging between 52 and 61 % were obtained. Considering the diversity of monomer conversions obtained for a series of oxime esters bearing the same chromophore for light absorption, it therefore evidenced the crucial role of the group used to esterify the oxime moiety.

Given that the absorption characteristics of all oxime esters are comparable, differences of their polymerization speeds depend on other factors such as the efficiency of the photocleavage reaction, the efficacy of the decarboxylation reaction, and the reactivity of the produced radicals. All of these variables are crucial to the photopolymerization processes. By calculating the bond dissociation energies (BDE) of all oxime esters, this point could be further explored. According to Table 4, values for **OXE-B** and **OXE-J** ranged from 42.31 kcal/mol and 50.58 kcal/mol, respectively. For the enthalpy of decarboxylation $\Delta H_{decarboxylation}$, more notable differences could be evidenced.

Only **OXE-D** was able to conduct a photoinduced decarboxylation reaction that was energetically favorable ($\Delta H_{decarboxylation} = E(R^{\bullet}) + E(CO_2) - E(RC(=O)O^{\bullet}) = -4.94$ kcal/mol). Thus, the determined highly favorable decarboxylation mechanism for **OXE-D** is consistent with the measured polymerization features. With the appearance of a peak at 2337 cm^{-1} during the polymerization of TMPTA, Fourier Transform Infrared spectroscopy (FTIR) could evidence the occurrence of a decarboxylation process (See Fig. 8). The absence of a CO_2 peak during photopolymerization for all the other oxime esters indicated a low

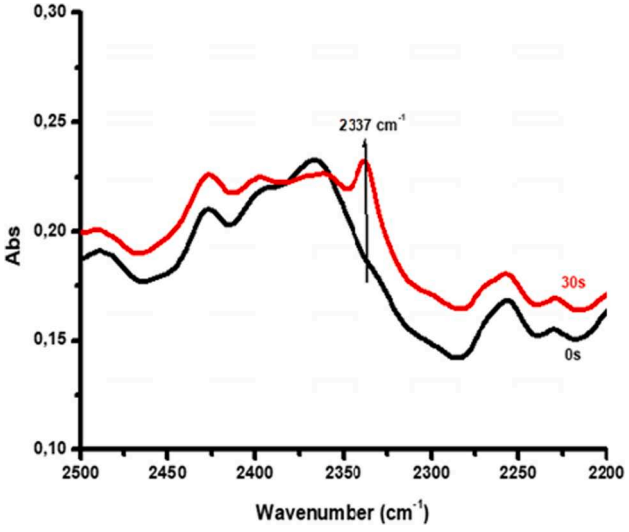

Fig. 8. Detection of CO_2 release during the polymerization with **OXE-D**. Reproduced with permission of Ref [42].

Table 4
Parameters characterizing the investigated OXEs. Some parameters characterizing the proposed oxime esters were calculated by molecular modelling: the Bond Dissociation Energy BDE (N-O), the triplet state energy E_{T1}, the enthalpy $\Delta H_{cleavageT1}$ for cleavage process from T_1, the enthalpy $\Delta H_{decarboxylation}$ for decarboxylation reaction and the spin density. The singlet excited state energy E_{S1}, the enthalpy $\Delta H_{cleavageS1}$ for cleavage process from S_1, and the fluorescence lifetime of the OXEs were measured experimentally.

PI	BDE (N-O) (kcal.mol^{-1})	E_{S1} (kcal.mol^{-1})	$\Delta H_{cleavage\ S1}$ (kcal.mol^{-1})	τ_0 (S1) (ns)	E_{T1} (kcal.mol^{-1})	$\Delta H_{cleavage\ T1}$ (kcal.mol^{-1})	$\Delta H_{decarboxylation}$ (kcal.mol^{-1})	Spin density (R$^{\bullet}$)
OXE-A	64.56	61.8	2.76	3.36	42.70	21.86	–	–
OXE-B	42.31	59.72	−17.41	1.92	47.49	−5.18	0.52	0.999
OXE-C	48.42	59.26	−10.84	1.65	44.67	3.75	5.92	0.989
OXE-D	48.87	60.42	−11.55	1.89	44.83	4.04	−4.94	1.156
OXE-E	45.54	59.49	−13.95	1.64	44.74	0.8	4.36	0.999
OXE-F	48.34	59.26	−10.92	1.61	44.60	3.74	6.24	0.995
OXE-G	48.14	59.03	−10.89	1.65	44.61	3.53	6.92	0.990
OXE-H	47.85	58.57	−10.72	1.79	44.51	3.34	8.77	0.996
OXE-I	48.13	59.49	−11.36	1.58	44.61	3.52	6.97	0.989
OXE-J	50.58	–	–	–	44.78	5.8	3.14	0.998
OXE-K	49.09	59.72	−10.63	0.989	44.42	4.67	7.64	1.076

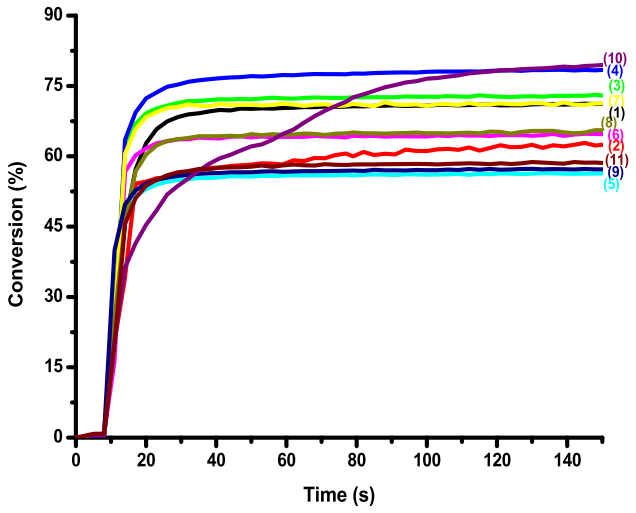

Fig. 9. Photopolymerization profiles of TMPTA (acrylate function conversion vs. irradiation time) in laminate (thickness = 25 μm) upon exposure to LED light λ = 405 nm in the presence of: (1) **OXE-A**/Iod (0.5 %/1 % w/w); (2) **OXE-B**/Iod (0.5 %/1 % w/w); (3) **OXE-C**/Iod (0.5 %/1 % w/w); (4) **OXE-D**/Iod (0.5 %/1 % w/w); (5) **OXE-E**/Iod (0.5 %/1 % w/w); (6) **OXE-F**/Iod (0.5 %/1 % w/w); (7) **OXE-G**/Iod (0.5 %/1 % w/w); (8) **OXE-H**/Iod (0.5 %/1 % w/w); (9) **OXE-I**/Iod (0.5 %/1 % w/w); (10) **OXE-J**/Iod (0.5 %/1 % w/w); and (11) **OXE-K**/Iod (0.5 %/1 % w/w); respectively. The irradiation starts at t = 10 s. Reproduced with permission of Ref [42].

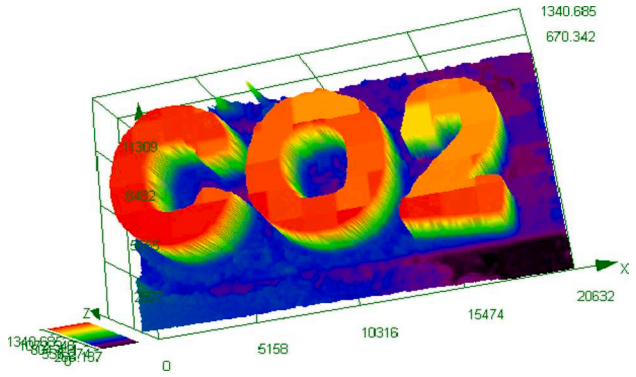

Fig. 10. Optical microscopy of the 3D patterns obtained using the two-component **OXE-D**/Iod (0.1 %/1 % w/w) system in a TA, upon exposure to a laser diode @405 nm. Reproduced with permission of Ref [42].

decarboxylation yield. Reactivity of the radicals (R$^{\bullet}$) once created is another crucial factor. Indeed, once formed, radicals should add onto the C = C double bond but be not too reactive towards formation of mid-chain radicals (MCRs) and/or backbiting, hydrogen transfer [43]. Radical reactivity can be anticipated by analyzing the spin density on the radical center, in this case, carbon-centered radicals. Thus, an improvement of the free radicals reactivity is obtained when the spin is more localized. Too much localization can affect stability and reduce selectivity. Here again, **OXE-D** was discovered as having the highest spin density, demonstrating the extraordinary reactivity of this oxime ester.

Theoretical calculations further showed that the photocleavage step proceeded from the singlet excited state rather than from the triplet excited state due to the unfavorable enthalpy of cleavage (See Table 8).

Parallel to their investigations as Type I photoinitiators, their photoinitiating ability as Type II photoinitiators was also examined when used as photosensitizers for the sensitization of an iodonium salt given that all oxime esters contain the same chromophore i.e. the coumarin unit. When combined in two-component OXE/Iod (0.5 %/1 % w/w) systems for the FRP of TMPTA upon irradiation at 405 nm, all OXE demonstrated higher photoinitiating abilities in two-component OXEs/Iod systems (higher polymerization rates and higher final conversions) than considered alone (See Fig. 9). In two-component systems, it was possible to establish the following reactivity order: **OXE-J** > **OXE-D** > **OXE-C** > **OXE-A** > **OXE-G** > **OXE-H** > **OXE-F** > **OXE-B** > **OXE-K** > **OXE-I** > **OXE-E**. In this case, no CO_2 signal could be seen in the FTIR spectra when utilized as photosensitizers for the decomposition of the iodonium salt, irrespective of the dyes. Notably, no CO_2 signal was detected for **OXE-D** when used as Type II photoinitiators whereas this peak was clearly detectable for **OXE-D** used as type I photoinitiator. These results are indicative that the electron transfer from the coumarin unit towards the iodonium salt was faster than the photocleavage of the oxime esters.

The authors suggested a classical process from a mechanistic point of view. Thus, an electron transfer between the excited dye and the

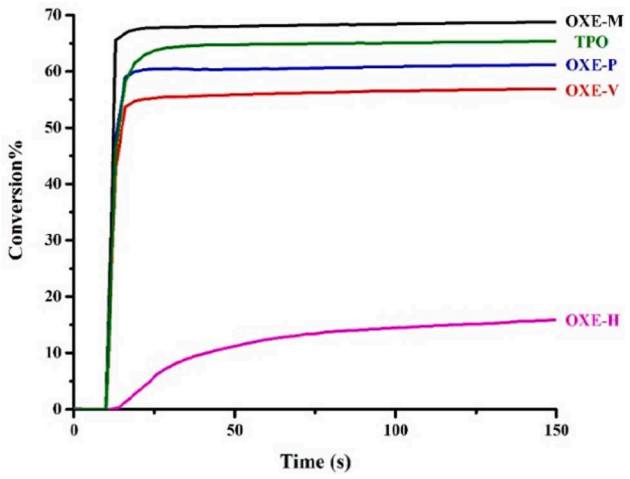

Fig. 11. Photopolymerization profiles of TMPTA upon irradiation at 405 nm using OXE (2×10^{-5} mol/g). Reproduced with permission of Ref. [9].

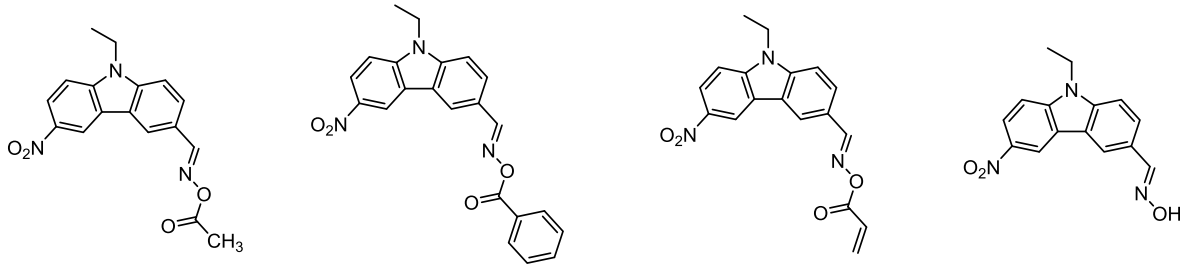

Scheme 9. Chemical structures of the nitrocarbazole-based oxime esters **OXE-M**, **OXE-V**, **OXE-P** and **OXE-H**.

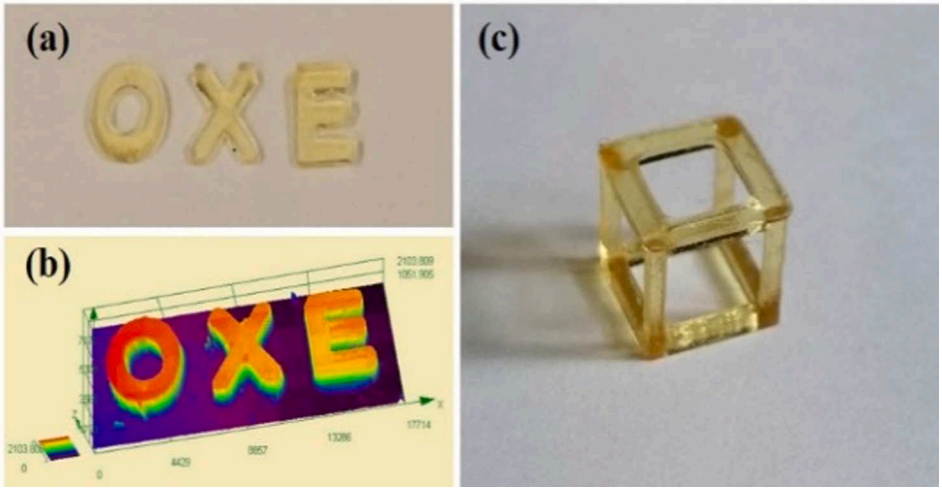

Fig. 12. (a) The letter pattern "OXE" obtained by direct laser write; (b) Characterization of the letter pattern "OXE"; (c) 3D printed object of square frame (7 × 7 × 7 mm). Reproduced with permission of Ref. [9].

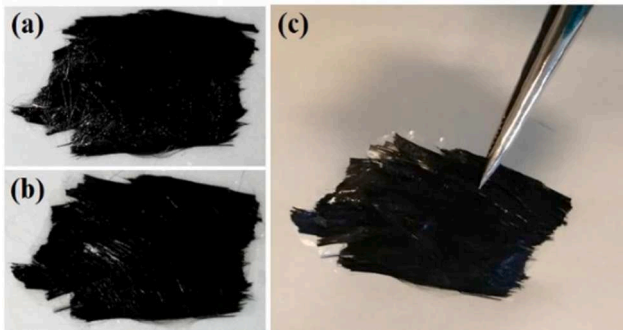

Fig. 13. (a) Prepregs with resin/carbon fiber (50/50, wt %/wt %); (b) Surface cured prepregs; (c) Carbon fiber composite. Reproduced with permission of Ref. [9].

iodonium salt may take place upon irradiation, causing the oxidation of the excited dye and decomposing the iodonium salt as aryl radicals Ar$^{\bullet}$ (See Scheme 6).

Due to the strong reactivity of **OXE-D**, direct laser write experiments could be carried out to create 3D structures. As shown in Fig. 10, the two-component **OXE-D**/Iod (0.1 %/1 % w/w) system enabled the creation of 3D patterns with a high spatial resolution in a relatively little amount of time (within two minutes) using (oxy*bis*(methylene))*bis*(2-ethylpropane-2,1,3-triyl)tetraacrylate (TA) as the monomer.

Finally, the possibility to induce a thermal cleavage of the different oxime esters was examined. Indeed, investigation of the thermal cleavage of oxime esters remains scarce in the literature. Significantly, **OXE-D** once again demonstrated a high efficiency as a thermal initiator compared to the others. Polymerization of TMPTA could begin at temperatures as low as 155 °C (See Table 10). **OXE-D** can therefore function as a powerful photoinitiator for both photochemical and thermal reactions. In particular, the generation of Me$^{\bullet}$ radicals, which are the highly reactive radicals for initiating polymerization processes, is closely correlated with the high reactivity of **OXE-D**.

4. Carbazole based-oxime ester

Due to its polyaromaticity, the planarity of its structure enabling carbazole to exhibit a high thermal and photochemical stability, its excellent electron-donating ability as well as its good solubility in most monomers, carbazole has been identified as a promising scaffold for the design of photoinitiators. Carbazole is an inexpensive starting material that can be used to create economical Type I photoinitiators. It can also be easily chemically modified [9,44-46]. During the last three years, no less than a hundred photoinitiators based on carbazole have been reported in the literature. Several carbazole-based oxime esters have been reported by our group at the Institute of Materials Science of Mulhouse (IS2M).

As photoinitiators for visible light photopolymerization, a series of Type I photoinitiators (PIs) based on the nitrocarbazole scaffold have been developed and tested for the first time in 2021 [47]. Originally, three oxime esters (**OXE-M**, **OXE-V**, and **OXE-P**) with different terminal groups attached via the oxime ester group (acetyl, acryloyl, and benzoyl) were synthesized (See Scheme 9). In this work, the nitrocarbazole scaffold was considered as an appropriate structure for the design of visible light photoinitiators. Indeed, absorption of carbazole is strongly UV-centered and carbazole do not naturally absorb in the visible range. To address this issue, introduction of a nitro group enabled to get the desired absorption in the visible range while facilitating the purification. Indeed, the nitro group is well-known to reduce the solubility of dyes so that the different oxime esters could be purified by a simple precipitation with ether.

As anticipated, the substitution pattern of the oxime ester group had no influence on the absorption maxima of all dyes, for which absorption maxima were detected at 376 nm. This is consistent with the chromophore moiety centered onto the carbazole unit and not on the oxime substituent. Due to the existence of an extra aromatic ring over **OXE-M** ($\varepsilon = 13\,000\ M^{-1}.cm^{-1}$) and **OXE-V** ($\varepsilon = 12\,400\ M^{-1}.cm^{-1}$), **OXE-P** was found to have the highest molar extinction coefficient ($\varepsilon = 13\,800\ M^{-1}.cm^{-1}$). In order to conduct the polymerization studies at 405 nm, molar extinction coefficients of 4100, 3900, and 4100 $M^{-1}.cm^{-1}$ were found at this wavelength. In fact, photolysis of oxime esters was monitored in real time, which revealed a new peak at 2337 cm^{-1}. These experiments successfully proved that CO_2 was released during irradiation.

As anticipated, **OXE-H** did not produce any CO_2 during irradiation as this molecule is not esterified and this compound was thus unable to initiate a decarboxylation reaction. The energy of bond dissociation could be determined theoretically. Thus, N-O bond energies of 49.50, 48.62, and 48.07 kcal mol^{-1} could be calculated for **OXE-V**, **OXE-M**, and **OXE-P**, respectively. Significantly, energies of the triplet excited states of **OXE-M**, **OXE-V**, and **OXE-P** were theoretically calculated and indicated the triplet state to be higher than their N-O bond dissociation energies, so that photocleavage of oxime esters could occur from the triplet excited state. Cleavage enthalpies of **OXE-M**, **OXE-V**, and **OXE-P** were determined to be −4.03, 3.16, and −5.29 kcal.mol^{-1}, respectively.

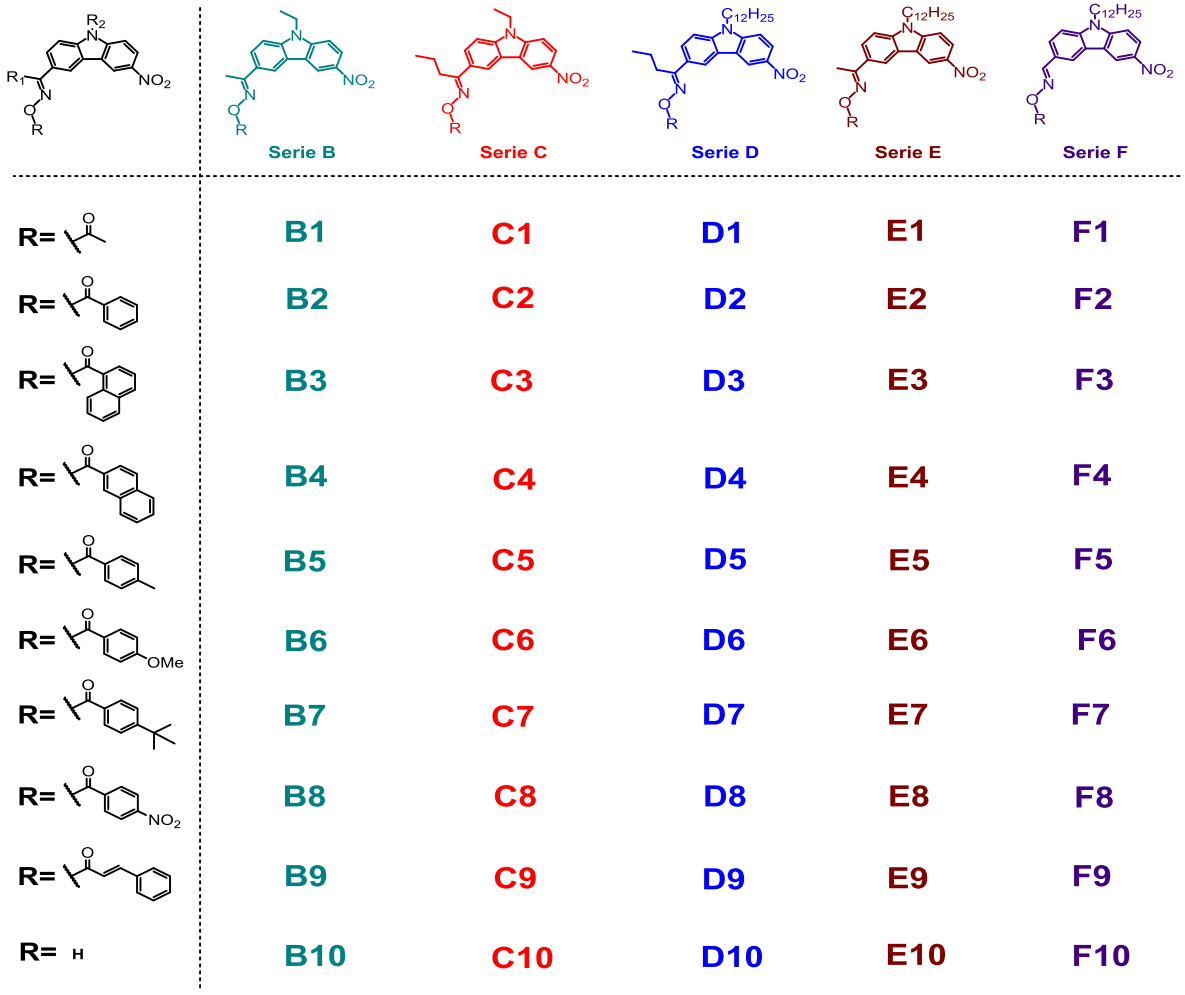

Fig. 14. Chemical structures of nitrocarbazole-based oxime esters. Reproduced with permission of Ref. [47].

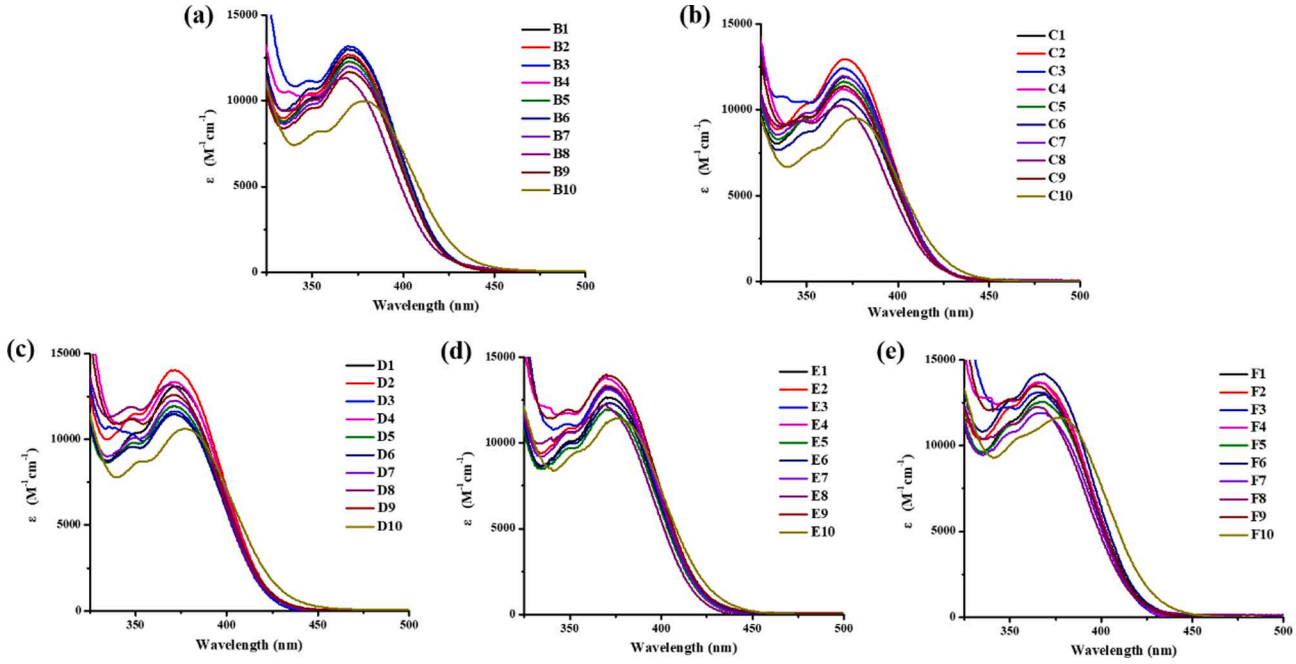

Fig. 15. UV–visible absorption spectra of oxime esters in acetonitrile (a) OXEs based on Series B; (b) OXEs based on Series C; (c) OXEs based on Series D; (d) OXEs based on Series E; (e) OXEs based on Series F. Reproduced with permission of Ref. [47].

Table 5
The final function conversions (FCs) of TMPTA at 405 nm in the presence of OXEs.

PI	B1	B2	B3	B4	B5	B6	B7	B8	B9	B10
FC (%)	64	54	30	50	42	43	48	15	47	23
PIs	**C1**	**C2**	**C3**	**C4**	**C5**	**C6**	**C7**	**C8**	**C9**	**C10**
FC (%)	67	58	53	61	50	46	54	37	54	34
PI	**D1**	**D2**	**D3**	**D4**	**D5**	**D6**	**D7**	**D8**	**D9**	**D10**
FC (%)	68	62	56	61	59	58	58	41	55	35
PI	**E1**	**E2**	**E3**	**E4**	**E5**	**E6**	**E7**	**E8**	**E9**	**E10**
FC (%)	64	53	55	51	40	48	50	35	41	34
PI	**F1**	**F2**	**F3**	**F4**	**F5**	**F6**	**F7**	**F8**	**F9**	**F10**
FC (%)	68	56	54	58	45	51	53	36	57	38

Table 6
Enthalpies for the decarboxylation reactions for different acyloxy and aryloxy groups. Reproduced with permission of Ref. [47].

Decarboxylation reactions	$\Delta H_{decarboxylation}$ (kcal mol^{-1})
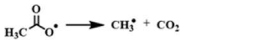	−4.94
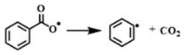	5.92
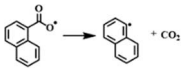	4.36
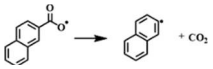	6.24
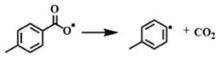	6.92
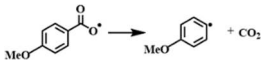	8.77
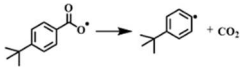	6.97
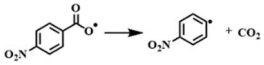	3.14
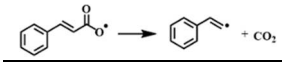	7.64

OXE-M was found to be able to outperform the final monomer conversion obtained with the reference compound diphenyl(2,4,6-trimethylbenzoyl)phosphine (TPO) (69 % versus 65 % for TPO) during the photopolymerization tests of TMPTA at 405 nm utilizing the different OXEs at 2 × 10^{-5} mol/g. This is directly related to the formation of methyl radicals by photocleavage and subsequent decarboxylation reaction. These radicals are carbon-centered radicals and methyl radicals are undoubtedly the most reactive ones. The best monomer conversions were attained with **OXE-M** for this reason. **OXE-P** and **OXE-V**, on the other hand, had lower monomer conversions (61 and 57 %, respectively) due to the formation of less reactive radicals. Indeed, decarboxylation in this situation results in the production of aryl and vinyl radicals, which have lower reactivity than methyl radicals and support the lower monomer conversions reported with **OXE-P** and **OXE-V**. Finally, **OXE-H** (18 %) had the lowest conversion, which is consistent with the fact that it is not an oxime ester and this molecule cannot, thus, cause any photocleavage (See Fig. 11). The generation of methyl radicals, which are more reactive than aryl radicals (generated by photodecomposition of **OXE-P**) or vinyl radicals, is responsible of the higher monomer conversion attained with **OXE-M**. This reactivity trend is in line with results previously reported in the literature [9].

Due to the strong reactivity of **OXE-M**, direct laser writing and 3D printing experiments were conducted with this oxime ester (See Fig. 12). Patterns with a high spatial resolution could be found in both cases.

In this study, the dual photo/thermal initiation behaviors of **OXE-M**, **OXE-V** and **OXE-P** were also evidenced. DSC tests carried out in the dark revealed that **OXE-M** had the lowest onset temperature (113 °C). Conversely, **OXE-V** and **OXE-P** showed higher initiation temperatures, above 150 °C. The thermal initiation ability of **OXE-M** allowed the successful preparation of composites. TMPTA was combined with 50 % carbon fiber to create prepregs, which were then heated at 150 °C for 30 min to achieve a deep polymerization. The prepregs were then irradiated at 395 nm to polymerize the surface. Interestingly, fully cured carbon fiber-based composites could be obtained using this approach (See Fig. 13).

In 2022, our group evaluated 50 nitrocarbazole-based oxime esters, which were separated into five different series (See Fig. 14). This study closely examined the influence of the oxime ester groups (acyloxy or aryloxy groups) on the photoinitiating ability but also the influence of the solubility of oxime esters in resins on the polymerization performance by adjusting the length of the carbazole chains or the length of the side chains. The use of nitrocarbazole as a common scaffold for the design of all of these dyes has been a crucial element in the development of this large series of oxime esters and to establish a structure/performance relationship [47].

It's interesting to note that the absorption maxima for all oxime esters stands between 370 and 372 nm (See Fig. 15). Given that the molar extinction coefficients of all dyes are equivalent, influence of the solubility of oxime esters introduced by the functionalizing groups utilized to create oxime esters on the photoinitiating ability can thus be thoroughly investigated.

TMPTA was used as the monomer for the different polymerization experiments and the photoinitiating abilities of oxime esters **B1**–**B9**, **C1**–**C9**, **D1**–**D9**, **E1**–**E9**, and **F1**–**F9** were examined for TMPTA resins exposed to 405 nm light. According to Table 5, **OXEs 1** and **OXEs 2** containing acetyl or benzoyl groups continued to display the highest monomer conversions among the different series of oxime esters. **OXEs 8** bearing a nitrobenzoyl group, however, produced the worst monomer conversions. The reduced reactivity of the nitrobenzoyl radicals in this case was assigned to the electron-withdrawing ability of the nitro group, thereby deactivating the corresponding radicals. By comparing the different series of oxime esters, it is clear that the series D, which possesses a dodecyl chain on the carbazole unit and a butyryl group as the lateral chain could furnish the best monomer conversions. It can be thus concluded that the carbazole compounds with the most solubilizing chains can furnish the best monomer conversions. Only OXEs with an acetyl substituent (**B1**, **C1**, **D1**, **E1**, and **F1**) were able to exceed the benchmark photoinitiator when their monomer conversions were compared to that obtained with TPO (66 % conversion). Again, among the five series of oxime esters, **C1**, **D1**, and **F1** had the longest solubilizing chains. Other OXEs such as **D4** and **D5** showed remarkable performances compared to their analogues of the other series. Considering that all dyes have been designed to exhibit similar absorption properties, other parameters such as the decarboxylation reaction but also the reactivity of the generated radicals drastically impacted their photoinitiation abilities. Determination of the enthalpy for the decarboxylation reaction revealed the decarboxylation process to be only favorable for oxime esters bearing an acetyl group. For all the others, a less favorable decarboxylation process was evidenced, supporting the lower reactivity of the **B/C/D/E/F 2**–**9** series compared to the **B/C/D/E/F 1** series (See Table 6).

Analysis of their thermal initiating abilities revealed **B1** and **D1** to exhibit the lowest initial polymerization temperatures, according to the study done on the thermal initiating properties of **B1**, **C1**, **D1**, **E1**, and **F1**. For **B1** and **D1**, temperatures as low as 83 and 82 °C were found respectively. Noticeably, the 50 oxime esters examined in this work showed this dual thermal/photochemical initiating behavior.

Still in 2022, a significant increase of the molar extinction coefficients could be obtained in the visible range by combining two carbazole units together. In this work, the 5,12-dihydroindolo[3,2-*a*] carbazole scaffold was used for elaborating a series of nine *bis*-oxime

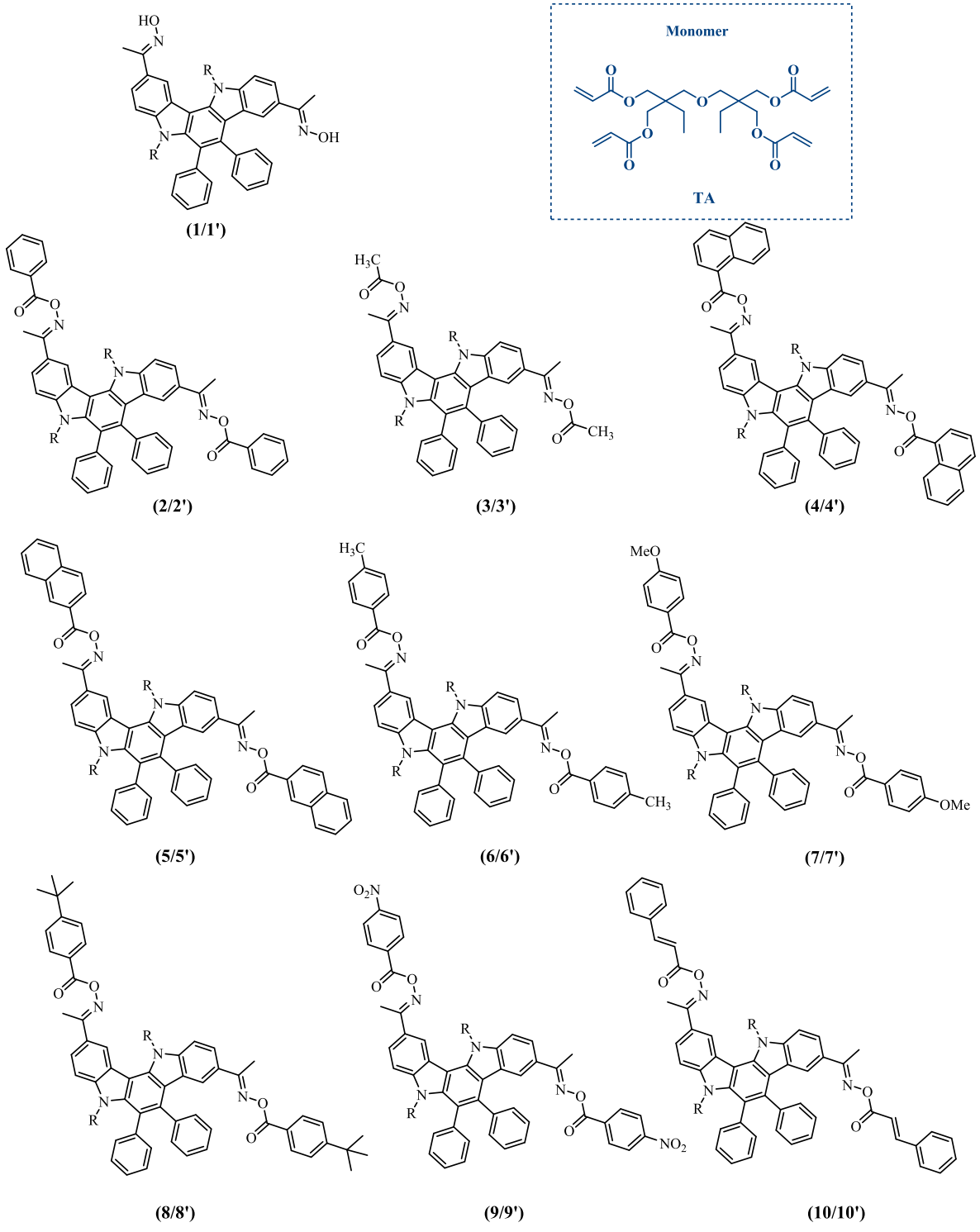

Fig. 16. Chemical structures of 5,12-dialkyl-5,12-dihydroindolo[3,2-*a*]carbazole-derived oxime esters **2**–**10** and **2′**-**10′** and the monomer (TA). From ref. [48].

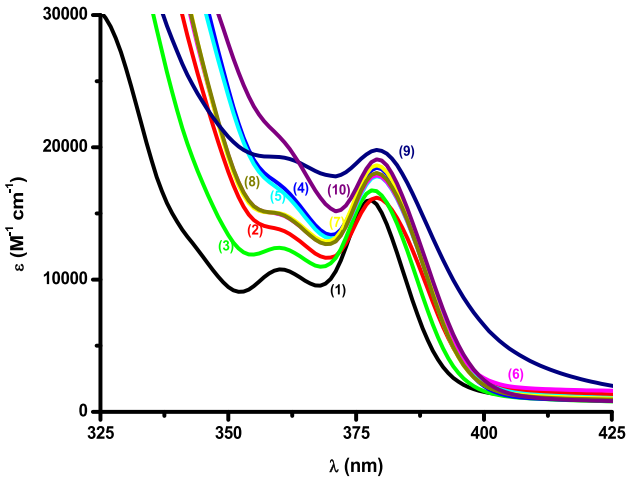

Fig. 17. UV–visible absorption spectra of oxime esters **(1)-(10)** in toluene. Reproduced with permission of Ref. [48].

esters (see Fig. 16) [48]. Derivatives of *O*-acyloxy or *O*-benzoyloxy were therefore synthesized and developed. It should be noted that despite the fact that the 5,12-dialkyl-5,12-dihydroindolo[3,2-*a*]carbazole scaffold was originally described in 2019, only a small number of studies focused on its chemistry, particularly on asymmetrizing the substitution of this *bis*-carbazole structure. Since all oxime esters have comparable absorption characteristics, it was possible to precisely determine the reactivity of each group linked to the oxime function (See Fig. 16). As a result of the polyaromatic structure of 5,12-dialkyl-5,12-dihydroindolo [3,2-*a*]carbazole, absorption maxima at 379 nm for all dyes could be identified (See Fig. 17). All dyes exhibited a tail extending in the visible range until ca. 410 nm except for **9** for which an absorption spectrum extending until 425 nm could be determined. In particular, the nitrobenzoyl derivatives (**dye 9**) showed the best absorption and outperformed the other dyes in terms of molar extinction coefficients (see Fig. 17). Based on their absorptions, polymerization tests could be performed at 405 nm. An important issue in photopolymerization is the solubility of photoinitiators in resins as it can negatively impact the final monomer conversions. For this reason, a second series of compounds, called **2′-10′**, was prepared. These compounds **2′-10′** differ from the **2–10** series in that they have shorter alkyl chains (a methyl chain for **2′-**

Table 7
Final acrylate function conversions (FCs) and polymerization rates for TMPTA using one component (0.5% w) photoinitiators after irradiation with LED light (λ = 405 nm).

OXE	Thin sample (25 μm) in laminate	OXE	Thin sample (25 μm) in laminate	OXE	Thick sample (1.4 mm) under air	OXE	Thick sample (1.4 mm) under air
(1)	42 %	(1′)	29 %	(1)	8 %	(1′)	15 %
(2)	58 %	(2′)	38 %	(2)	50 %	(2′)	61 %
(3)	81 %	(3′)	82 %	(3)	84 %	(3′)	81 %
(4)	64 %	(4′)	66 %	(4)	58 %	(4′)	38 %
(5)	52 %	(5′)	49 %	(5)	39 %	(5′)	34 %
(6)	51 %	(6′)	41 %	(6)	45 %	(6′)	58 %
(7)	35 %	(7′)	47 %	(7)	21 %	(7′)	35 %
(8)	57 %	(8′)	54 %	(8)	65 %	(8′)	54 %
(9)	45 %	(9′)	28 %	(9)	5 %	(9′)	19 %
(10)	48 %	(10′)	49 %	(10)	39 %	(10′)	41 %

Table 8
Parameters characterizing the investigated OXEs **(1)-(10)**. Some parameters were calculated by molecular modelling: the bond dissociation energy BDE (N-O), the triplet state energy E_{T1} and the enthalpy $\Delta H_{cleavage\ T1}$ for the cleavage from T_1. The singlet excited state energy E_{S1}, the enthalpy $\Delta H_{cleavage\ S1}$ for the cleavage from S_1, and the fluorescence lifetime of the OXEs were measured experimentally.

OXE	BDE (N-O) (kcal.mol^{-1})	E_{S1} (kcal mol^{-1})	$\Delta H_{cleavage\ S1}$ (kcal mol^{-1})	E_{T1} (kcal mol^{-1})	$\Delta H_{cleavage\ T1}$ (kcal mol^{-1})
(1)	–	74.25	–	62.21	–
(2)	41.55	73.1	−31.55	62.22	−20.67
(3)	47.02	73.56	−26.54	52.15	−5.13
(4)	40.56	72.87	−32.31	58.09	−17.53
(5)	41.35	73.33	−31.98	52.14	−10.79
(6)	41.28	73.33	−32.05	62.16	−20.88
(7)	40.88	73.33	−32.45	62.15	−21.27
(8)	41.25	73.1	−31.85	62.20	−20.95
(9)	43.71	–	–	62.07	−18.36
(10)	42.97	66.88	−23.91	52.45	−9.48

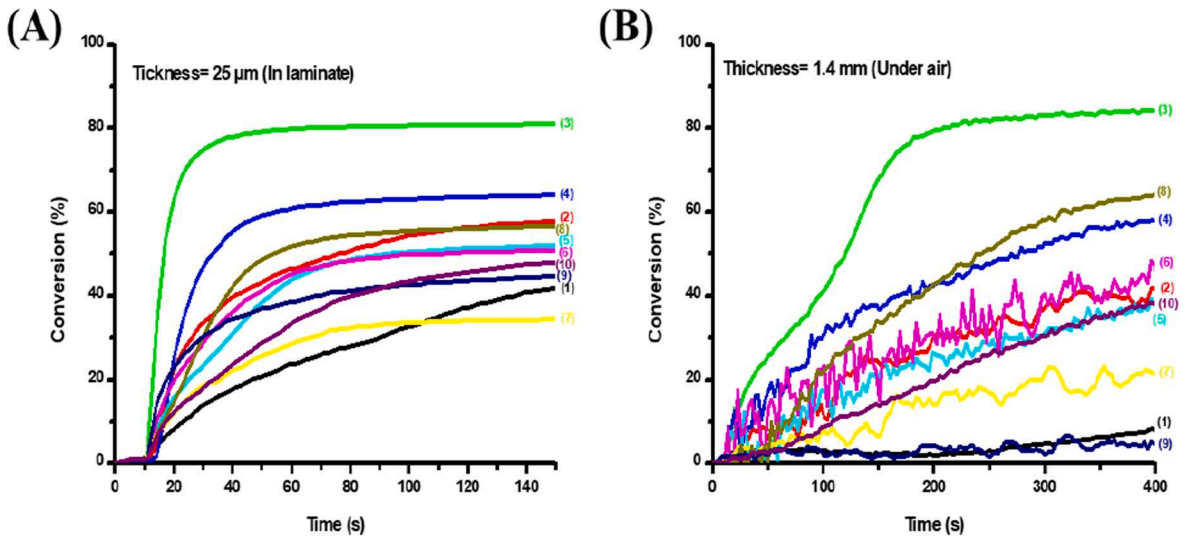

Fig. 18. (A) Polymerization profiles of oxime esters **(1)-(10)** (0.5 % w) in TMPTA in laminate (thickness = 25 μm) upon exposure to LED light λ = 405 nm using OXE (0.5 % w). (B) Polymerization profiles of oxime esters **(1)-(10)** (0.5 % w) in TMPTA under air (thickness = 1.4 mm) upon exposure to LED light λ = 405 nm using OXE (0.5 % w). Reproduced with permission of Ref. [48].

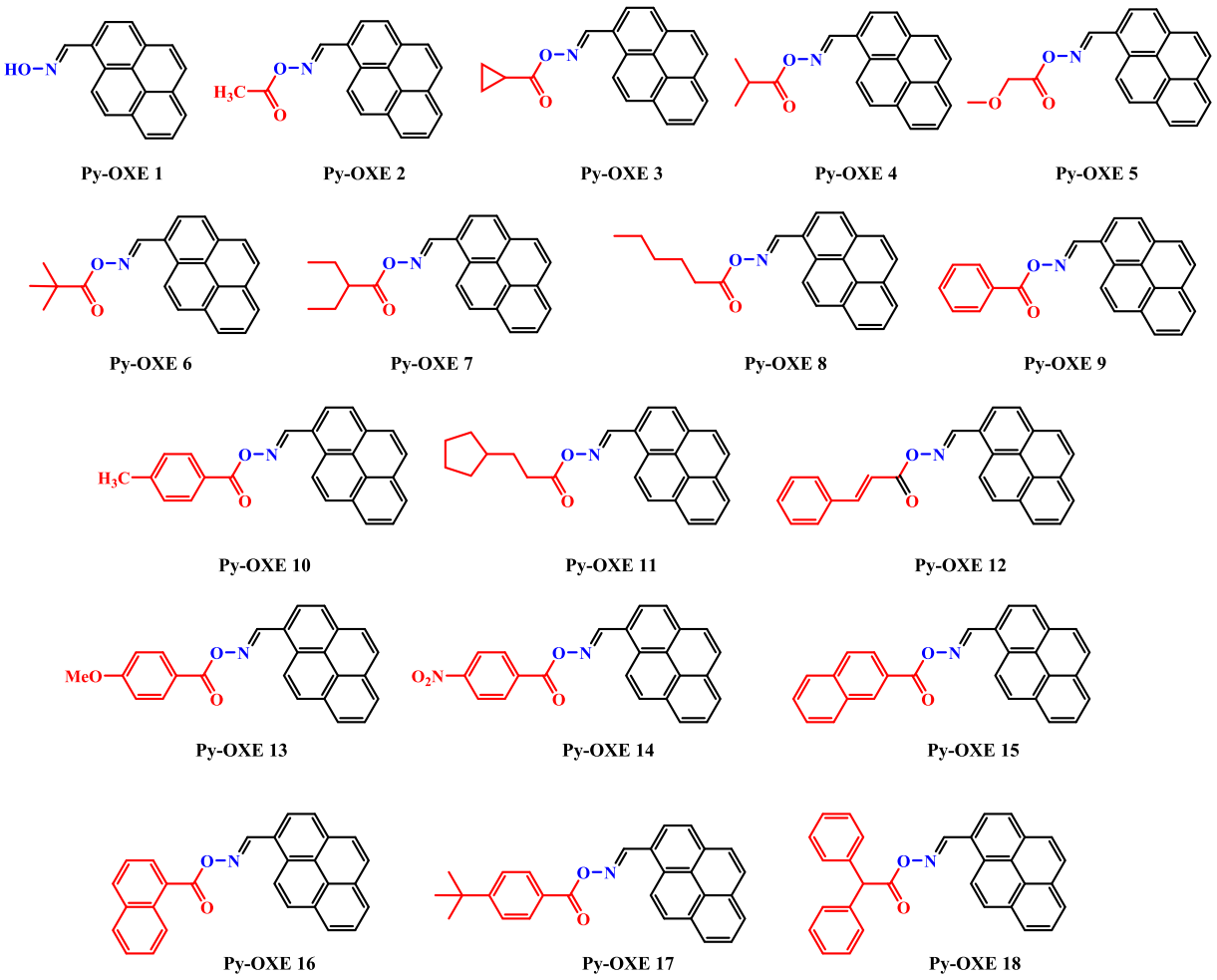

Fig. 19. Chemical structures of the Py-OXE series investigated. Reproduced with the permission from [60].

10′ versus a hexyl chain for **2**–**10**). It has to be noticed that the absorption spectra of the **2**–**10** and **2′**-**10′** series were identical, enabling to compare their photoinitiating abilities with regards to their differences of solubility. In fact, dye solubility can be a significant issue that negatively impacts the capacity to initiate photopolymerization.

The higher reactivity of the methyl radicals over the others in thick and thin films was once again demonstrated during the polymerization tests performed in TMPTA after being exposed to a LED emitting at 405 nm. The TMPTA conversion could be improved by ca 20 % using dye 3, as illustrated in Fig. 18 and Table 7. The TMPTA conversions for **7**/**7′** and **9**/**9′**, which bear an electron-withdrawing or an electron-releasing group (OMe and NO_2 groups respectively) were the lowest. In the case of **9**/**9′**, low monomer conversions can be confidently assigned to the low solubility of the nitro derivatives in resins, even for compound **9** substituted with a hexyl chain.

Again, proving that the reactivity is controlled by the solubility of oxime esters in resins, reduction of the solubilizing chain in **2′**-**10′** caused a significant decrease in the monomer conversion.

The bond dissociation energy for the N-O bonds in all oxime esters was calculated to be between 41 and 43 kcal/mol. For this series of carbazole, photocleavage was also found to occur from the singlet excited state, since the process was unfavorable from the triplet excited state, according to the determination of the enthalpy of cleavage (See Table 8).

Interestingly, it could be established in these different works how much more reactive were the aliphatic radicals compared to the aryl radicals. The solubility issue has negatively impacted the photoinitiating ability of numerous dyes, even though numerous high-performance photoinitiating systems could be developed with these scaffolds. Up to now, most of the oxime esters reported in this review exhibited an absorbance standing in the 450–500 nm range. Future work will consist in creating oxime esters with absorptions more redshifted than those now attained in order to achieve an enhanced light penetration within the photocurable resins. Future research will also focus on creating oxime esters with this dual capability for triggering thermal and photochemical reactions.

5. Polyaromatic oxime esters: Naphthalene, pyrene and anthracene chromophores

Naphthalene and its derivatives, polyaromatic hydrocarbons based on fused aromatic rings have also been developed to act as Type I photoinitiators. It is anticipated that a naphthalene-based photoinitiator, due to the remarkable planarity of naphthalene will favor the electron delocalization. Polyaromaticity is also favorable for the preparation of dyes with high molar extinction coefficients. Recently, a series of naphthalene-based oxime esters was elegantly proposed, these structures exhibiting a significant absorption for $\lambda < 400$ nm [50]. It should be noted that the naphthalene-based oxime ester which contains 1-naphthalene with an o-methoxy substituent showed the rather redshifted absorption region with the highest final conversion yield under UV lamp irradiation (46 %) and 405@nm LED (41 %). In order to get a bathochromic shift of the absorption maxima, other polyaromatic structures were proposed. The family of Polycyclic Aromatic Hydrocarbons (PAHs), which includes pyrene, a polyaromatic structure made up of four fused aromatic rings, is the focus of interdisciplinary research

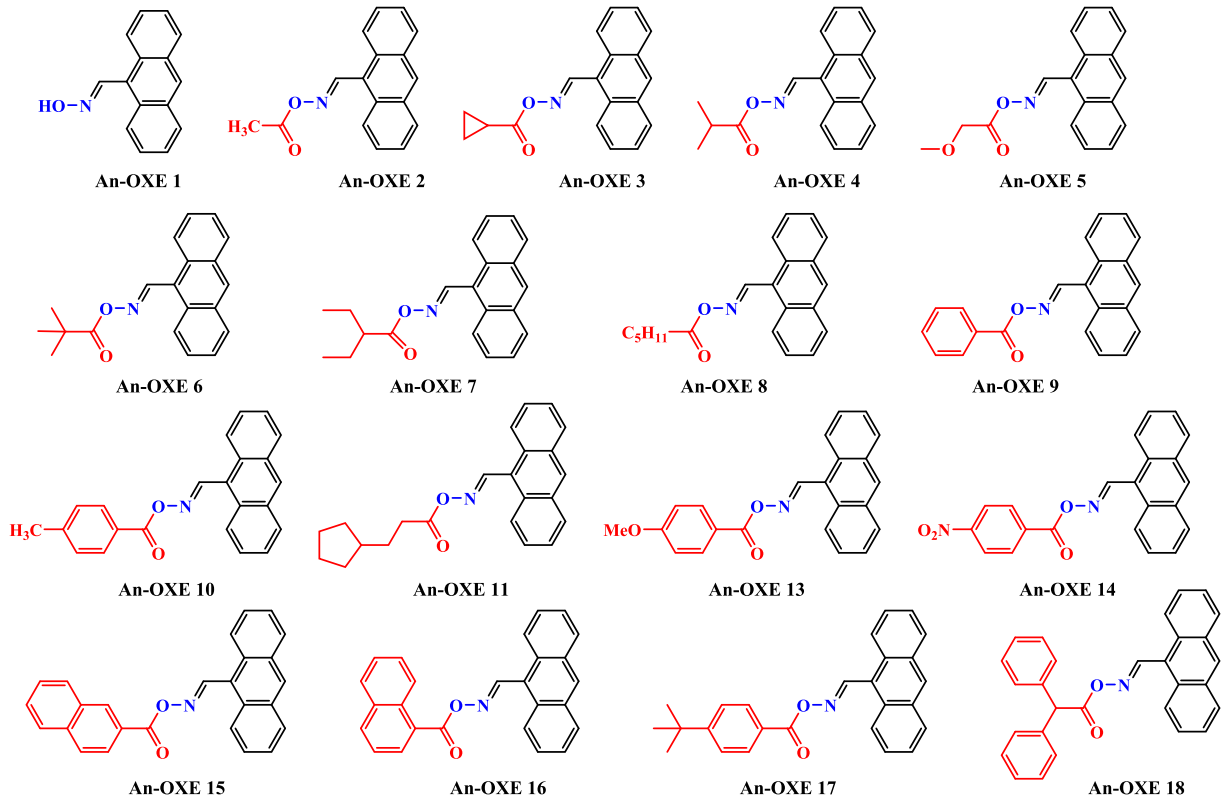

Fig. 20. Chemical structures of the An-OXE series examined. Reproduced with the permission from [60].

in the domains of chemistry, physics, materials science, and biology. More particular, pyrene has undergone substantial research for the development of photoluminescent materials. In the solid form, pyrene has a photoluminescence quantum yield of 0.68. However, pyrene has a strong tendency to dimerize at high concentrations, which has a negative impact on its solubility in the majority of common organic compounds, as frequently found for planar polyaromatic structures [50-52]. Many empirical and semi-empirical models have been proposed in the literature to explain this phenomenon [7]. At the same time, the fluorescence of pyrene frequently coexists with that of excimers due to pyrene dimerization. *Tert*-butyl groups are often added to the 2,7-positions of pyrene to address the solubility issue, but since this chemical is still quite expensive, research is still ongoing to find a simple substitution technique for pyrene. Pyrene remains a useful building block for the preparation of photoinitiators due to its long excited state lifetime (50–90 ns), ease of functionalization by simple reactions such as bromination, Vilsmeier-Haak or Friedel-Crafts acylation processes, and many other standard reactions. Photophysical properties of pyrenes have been thoroughly studied and documented in the literature, making them a reliable basis for the development of visible light photoinitiators. In addition, anthracene has been found to be a promising scaffold in the search for new Type I structures, as it works well as a UV photoinitiator [53-55]. Anthracene is a polyaromatic structure frequently used in Organic Electronics to create fluorescent probes, singlet emitters for organic light-emitting diodes, and dyes for solar cells. The low oxidation potential of this structure, its good film-forming ability make it an excellent candidate for elaborating multilayered devices [56-59]. However, photopolymerization is also part of the range of applications of anthracene. Recently, our group have used an innovative approach to develop novel type I photoinitiators through a combination of these two chromophores i.e. pyrene and anthracene that could act as Type I photoinitiators when linked to an oxime ester group [60]. Two series of oxime esters were prepared (See Figs. 19 and 20). The anthracene chromophore (An-OXE) is present in the first family composed of 17 compounds, and the pyrene moiety is present in the second family composed of 18 compounds (Py-OXE). The two structures, namely pyrene and anthracene, were selected for this study as pyrene and anthracene respectively react from their first excited singlet (S1) and triplet (T1) states. Therefore, impact of the chromophore (pyrene vs. anthracene) on their photochemical characteristics and photoinitiating abilities could be investigated in this work. The newly proposed PIs (An-OXEs and Py-OXEs) were characterized by good near-UV and visible absorption properties.

Starting with the readily available 9-anthracenecarboxaldehyde or 1-pyrenecarboxaldehyde, all oxime esters examined in this work were produced in two steps. The two oximes could be prepared in the first step by reacting the appropriate aldehyde with hydroxylamine hydrochloride under basic conditions. Specifically, sodium acetate, a water-soluble base, was chosen. Methanol, THF, and water were used as a mixture of three solvents to carry out the reaction. Reaction yields greater than 96 % enabled the production of the two oximes. Surprisingly, when oxime esterification was studied, the anthracene-9-carbaldehyde oxime (**An-OXE 1**) failed to form esters if triethylamine was used as a base. Instead, a dehydration reaction was observed, producing the unusual reaction product anthracene-9-carbonitrile. By slowly evaporating chloroform, crystals of this compound could be obtained, allowing X-ray diffraction to clearly identify the substance's chemical structure. Surprisingly, the different oxime esters could be prepared without using base. Thus, anthracene-9-carbaldehyde oxime was combined with one equivalent of the appropriate acid chloride and could produce the different anthracene-based oxime esters in high yields. The various esters were prepared using 17 distinct acid chlorides, ranging from aromatic to aliphatic acid chlorides (See Scheme 10). The possibility of generating aromatic but also aliphatic primary, secondary, and tertiary radicals, stabilized and destabilized radicals during the cleavage and decarboxylation reaction of radicals served as a notable justification for the diversity of acid chlorides. Only the cinnamoyl derivative, or **An-OXE 12**, could not be obtained in the case of the

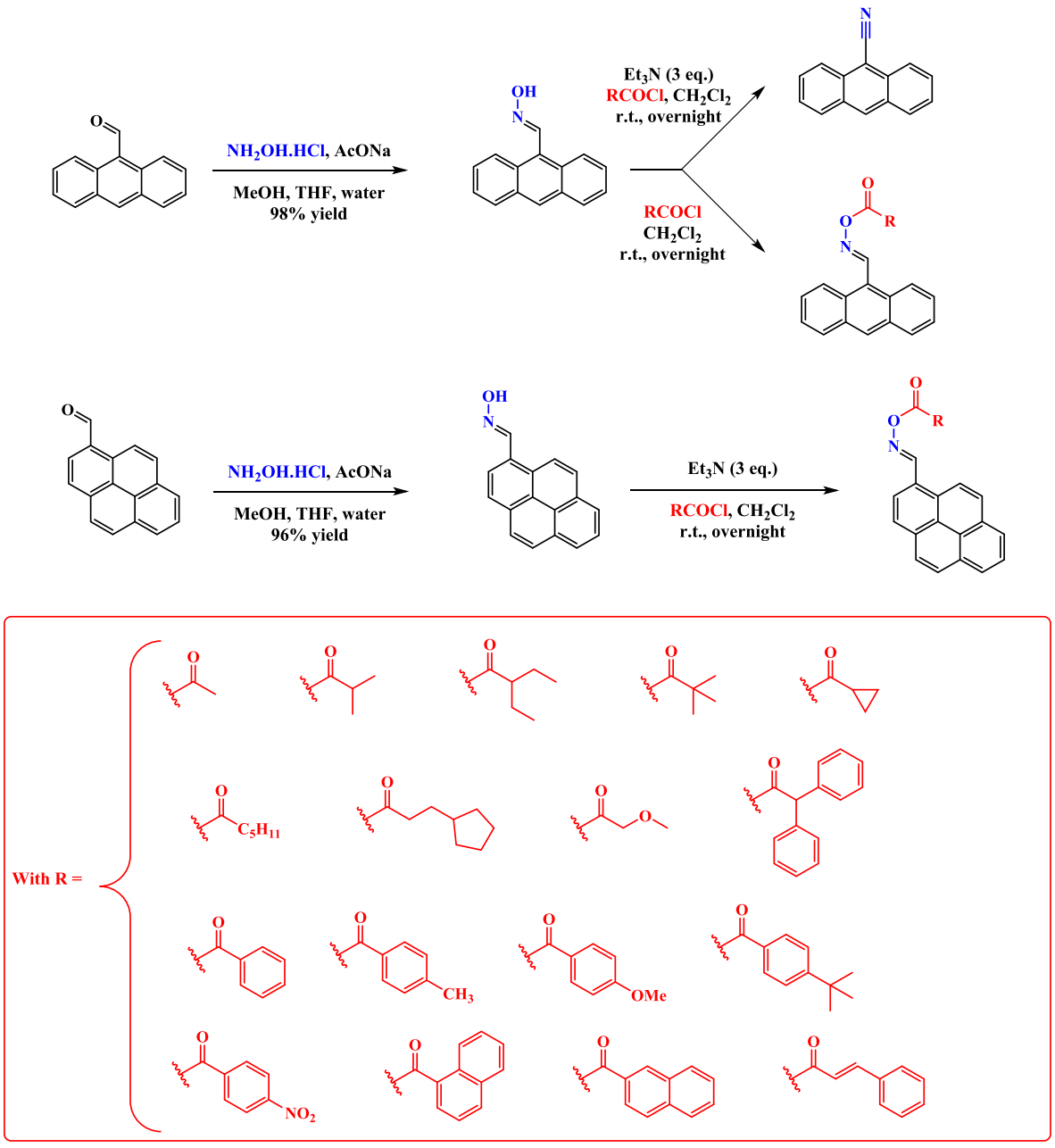

Scheme 10. Synthetic routes to the different anthracene and pyrene-based oxime esters.

Table 9
Reaction yields obtained during the esterification of the two oximes.

esters	**Py-OXE 1**	**Py-OXE 2**	**Py-OXE 3**	**Py-OXE 4**	**Py-OXE 5**	**Py-OXE 6**	**Py-OXE 7**	**Py-OXE 8**	**Py-OXE 9**
reaction yields (%)	96	86	81	84	83	80	94	91	80
esters	**Py-OXE 10**	**Py-OXE 11**	**Py-OXE 12**	**Py-OXE 13**	**Py-OXE 14**	**Py-OXE 15**	**Py-OXE 16**	**Py-OXE 17**	**Py-OXE 18**
reaction yields (%)	80	83	68	87	93	86	81	83	85
esters	**An-OXE 1**	**An -OXE 2**	**An -OXE 3**	**An -OXE 4**	**An -OXE 5**	**An -OXE 6**	**An -OXE 7**	**An -OXE 8**	**An -OXE 9**
reaction yields (%)	98	78	89	88	82	76	77	88	82
esters	**An -OXE 10**	**An -OXE 11**	**An -OXE 12**	**An -OXE 13**	**An -OXE 14**	**An -OXE 15**	**An -OXE 16**	**An -OXE 17**	**An -OXE 18**
reaction yields (%)	88	84	n.o.[1]	72	86	74	78	88	92

[1] : not obtained.

anthracene-based oxime esters, despite numerous attempts. For the pyrene-based oxime esters, the different compounds **Py-OXE 2-Py-OXE 18** could be prepared under standard conditions by deprotonation of pyrene-1-carbaldehyde oxime (**Py-OXE 1**) with an excess of triethylamine and by esterification with the proper acid chlorides. Table 9 provides a summary of the reaction yields.

Table 10
Absorption properties of Py-OXEs at λ_{max} and 405 nm in acetonitrile (ACN).

	λ_{max} (nm)	ε_{max} (M^{-1} cm^{-1})	ε_{405nm} (M^{-1} cm^{-1})
Py-OXE1	359	40,500	0
Py-OXE2	361	52,000	1340
Py-OXE3	362	42,500	1160
Py-OXE4	361	21,760	580
Py-OXE5	362	28,830	535
Py-OXE6	362	27,560	770
Py-OXE7	362	33,300	1100
Py-OXE8	362	41,560	960
Py-OXE9	362	22,000	1530
Py-OXE10	362	42,190	2620
Py-OXE11	362	26,570	545
Py-OXE12	364	40,600	4110
Py-OXE13	363	34,630	1200
Py-OXE14	362	28,640	6400
Py-OXE15	364	42,600	4400
Py-OXE16	364	46,300	3400
Py-OXE17	363	37,720	2720
Py-OXE18	362	34,250	1560

Fig. 21 presents the UV–visible absorption spectra of the different pyrene-based OXEs in acetonitrile (ACN) (See also Table 10). Following is a comparison with the different absorptions of An-OXEs. For example,$\varepsilon_{Py\text{-}OXE}$ = 52 000 $M^{-1}{\cdot}cm^{-1}$ at 361 nm for **Py-OXE2**; 42 500 $M^{-1}{\cdot}cm^{-1}$ at 362 nm for **Py-OXE3**; and 40 600 $M^{-1}{\cdot}cm^{-1}$ at 364 nm for **Py-OXE12** are examples of organic compounds with a broad absorption band and a strong ability to absorb light in the near-UV and visible range between 300 and 425 nm. Indeed, these oxime esters exhibit good absorption properties at 405 nm, ensuring a good overlap with the emission spectra of the LEDs utilized in this work (λ_{exc} = 405 nm).

TA was used as a benchmark monomer for FRP tests in thin samples employing An-OXEs as Type I photoinitiators (0.5 % w/w) at 405 nm. Fig. 22 depicts the various FRP profiles (conversion vs. irradiation time), and Table 11 provides an overview of the conversion data. First of all, the different oxime esters based on anthracene exhibited moderate polymerization efficiencies, leading the majority of An-OXEs to furnish low final acrylate function conversions (FCs) when exposed to an irradiation at 405 nm. For example, for **An-OXE2** FC = 32 %, for **An-OXE4 FC** = 50 %, and for **An-OXE6**, FC = 34 %. No polymerization occurred for TA (without PIs), indicating the crucial role of An-OXEs in the monomer conversion.

When a pyrene group was used instead of the anthracene chromophore (Py-OXE), a different trend was found. Here again, polymerization tests were carried out in laminate, in thin films upon irradiation at 405 nm (I = 110 mW/cm^2) with a LED. Fig. 23 displays the photopolymerization profiles, and Table 17 contains the results obtained during the FRP of TA in laminate. When comparing the monomer conversions obtained during the FRP of TA by the different Py-OXE (0.5 % w) systems to those obtained with the An-OXE analogues, for instance, monomer conversions of 79 % for **Py-OXE2**; 63 % for **Py-OXE3**; 74 % for **Py-OXE4**; and 76 % for **Py-OXE 7** were obtained, greatly higher than that obtained for the An-OXE analogues. Thus, conversions of 32 % for **An-OXE2**; 43 % for **An-OXE3**; and 50 % for **An-OXE4** were determined after 200 s of irradiation. Working with pyrene derivatives resulted in significantly increased polymerization. In contrast to the oxime esters, which contain an anthracene chromophore that has limited photoinitiation capacity, these data clearly demonstrate the substantial impact of pyrene on the polymerization profiles of acrylate functionalities. The findings also demonstrated that Py-OXE with alkyl substituents on the ester moieties have greater polymerization efficiency, as demonstrated by FC = 79 % for **Py-OXE2** with methyl group against 25 % for **Py-OXE15** with a naphthyl group.

It is important to note that these oxime esters showed great efficiency compared to the reference structures (**Py-OXE1** or **An-OXE1**) which possess a N-OH group unable to fragment and generate radicals. This clearly shows the interest of the oxime ester functions in the photopolymerization process e.g. FC = 14 % for **Py-OXE1** vs. 79 % **Py-OXE2**.

These results can be explained in terms of bond dissociation energy. Indeed, for **Py-OXE1**, the bond dissociation energy of the N-O bond is higher than that determined for the different oxime esters. Thus, a BDE N-O = 61.15 kcal/mol could be determined for **Py-OXE1** vs. 47.86, 45.65, 47.39, and 47.82 kcal/mol for **Py-OXE2,3,4,5**, respectively (See Table 12), accompanied by an elongated excited state lifetime for **Py-OXE1** compared to Py-OXEs, which strongly suggests a singlet state cleavage process (τ_0 = 6.8 ns for **Py-OXE1** vs. 3.8, 3.66, 3.8, 3.14 ns for **Py-OXE2,3,4,5**) (See Table 12). Cleavage from the singlet excited state S_1 is shown to be more favorable (ES1 > BDE (N-O)), whereas cleavage from the triplet excited state is less favorable (E_{T1} BDE (N-O)), as shown for example for **Py-OXE2** (E_{S1} = 71.72 kcal/mol; E_{T1} = 41.56 kcal/mol vs. BDE (N-O) = 47.86 kcal/mol.

Figs. 23 and 24 and Table 17 compare how the anthracene and the pyrene chromophores affect the absorption characteristics of the corresponding oxime esters and therefore the photoinitiating ability. The results obtained showed that the oxime esters comprising the pyrene chromophore had a higher initiation ability than those prepared with

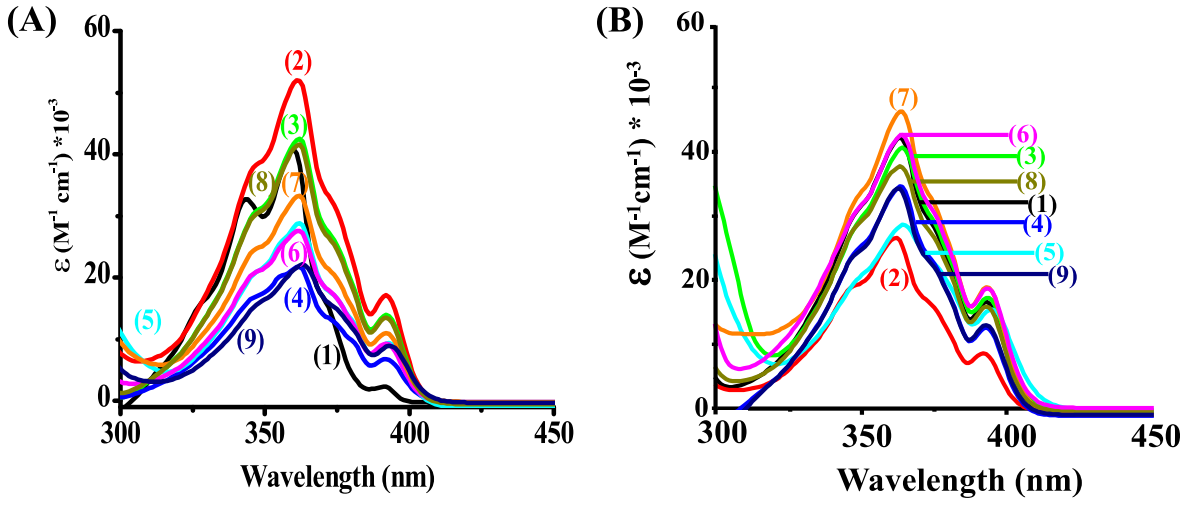

Fig. 21. UV–visible absorption spectra of the Py-OXE derivatives in ACN: (1) **Py-OXE 1**, (2) **Py-OXE 2**, (3) **Py-OXE 3**, (4) **Py-OXE 4**, (5) **Py-OXE 5**, (6) **Py-OXE 6**, (7) **Py-OXE 7**, (8) **Py-OXE 8**, (9) **Py-OXE 9**. (B) UV–visible absorption spectra of the Py-OXE derivatives in ACN: (1) **Py-OXE 10**, (2) **Py-OXE 11**, (3) **Py-OXE 12**, (4) **Py-OXE 13**, (5) **Py-OXE 14**, (6) **Py-OXE 15**, (7) **Py-OXE 16**, (8) **Py-OXE 17**, (9) **Py-OXE 18**. Reproduced with permission of Ref.[59].

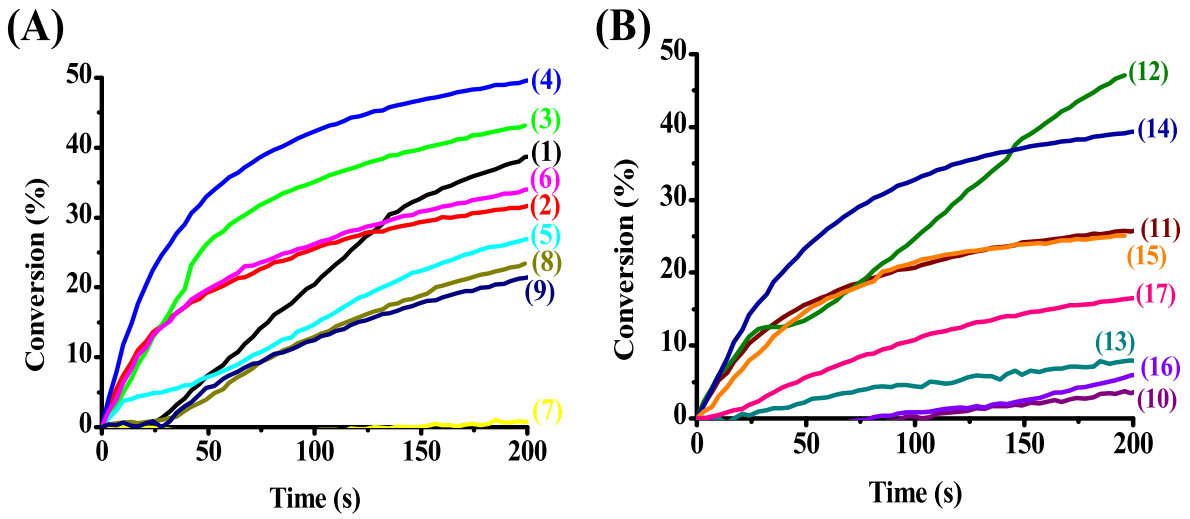

Fig. 22. (A), (B) Photopolymerization profiles of acrylates functions using the TA monomer (acrylate function vs. irradiation time) performed in Thin sample in laminate upon irradiation at 405 nm using one-component PISs (0.5 %): **(1) An-OXE 1**, **(2) An-OXE 2**, **(3) An-OXE** 3, **(4) An-OXE 4**, **(5) An-OXE 5**, **(6) An-OXE 6**, **(7) An-OXE 7**, **(8) An-OXE 8**, **(9) An-OXE 9**, **(10) An-OXE 10**, **(11) An-OXE 11**, **(12) An-OXE 13**, **(13) An-OXE 14**, **(14) An-OXE 15**, **(15) An-OXE 16** **(16) An-OXE 17**, **(17) An-OXE 18**. Irradiation starts at t = 0 s. Reproduced with permission of Ref.[59].

Table 11
Final reactive (acrylate) function conversions (FC%) for TA using Py-OXEs or An-OXEs upon visible light irradiation using the LED @405 nm in laminate.

	Py-OXE	An-OXE
OXE-1	14 %	39 %
OXE-2	79 %	32 %
OXE-3	63 %	43 %
OXE-4	74 %	50 %
OXE-5	72 %	27 %
OXE-6	76 %	34 %
OXE-7	76 %	23 %
OXE-8	78 %	0 %
OXE-9	36 %	22 %
OXE-10	60 %	0 %
OXE-11	72 %	26 %
OXE-12	28 %	–
OXE-13	54 %	47 %
OXE-14	42 %	0 %
OXE-15	25 %	39 %
OXE-16	19 %	25 %
OXE-17	66 %	0 %
OXE-18	64 %	16 %

anthracene. For example, is the final conversion 32 % for **An-OXE2** and 79 % for **Py-OXE 2**, Table 17. Pyrene derivatives are more reactive which is in agreement with their higher cleavage capacity, despite the fact that anthracene-based oxime esters absorb more light at 405 nm than pyrene oxime esters ($\varepsilon = 4000$ vs. 1580 $M^{-1}cm^{-1}$ for **An-OXE 2** and **Py-OXE 2**, respectively) (see Fig. 24). Overall, from these comparisons, it can be concluded that photocleavage of these oxime esters is more favorable from the singlet excited state than the triplet state, the fast photocleavage of oxime esters improving the monomer conversion by limiting radicals recombination.

The different results revealed that the newly proposed oxime esters, particularly those based on pyrene had extremely good photoinitiating abilities competing with other families such as coumarins or carbazoles. This discovery paves the way for the development of brand-new Type I photoinitiators based on pyrene that exhibits a more redshifted absorption towards the visible range.

6. Phenothiazine based-oxime esters

Phenothiazine (PTZ) is an inexpensive compound that is simple to modify. Due to the inclusion of this molecule in numerous drugs, its chemistry was extensively studied in the 1970 s so that photopolymerists could benefit from these advances in phenothiazine chemistry [61-63]. In-depth research on phenothiazine was also done to develop chromophores specifically designed for dye-sensitized solar cells. In relation to photopolymerization, Margerum and coworkers published in 1969 the first study indicating the use of phenothiazines as photoinitiators of polymerization. In this groundbreaking study, phenothiazine was used as a photooxidant capable to oxidize methylene blue or thionine in the excited state, thus producing initiating radicals for the FRP of barium diacrylate. Following this research, phenothiazine was frequently used as a UV photoinitiator for photoinduced charge transfer polymerization of acrylonitrile through the formation of an exciplex between phenothiazine and acrylonitrile, the polymerization of tetrahydrofuran using triphenylsulfonium hexafluoroarsenate, and upon sensitization of the reaction by phenothiazine. More recently, various two-component phenothiazine/sulfonium salt initiating systems have been employed as photochemical initiators for the CP of epoxides and the FRP of acrylates [63-66].

A series of oxime esters based on phenothiazine were recently synthesized and proposed as high-performance photoinitiating systems (Scheme 11) (Unpublished results from IS2M). Photoreactivity of the studied compounds was evaluated after exposure of the resins to LEDs emitting at 405 nm.

PTZ has a high molar extinction coefficient (about 7000 $M^{-1}.cm^{-1}$), as shown in Fig. 25. As a result, the absorption characteristics of the investigated oxime ester enabled a good overlap with the emission spectra of the visible LED used in this work.

Photopolymerization experiments done under LED@ 405 nm revealed the good reactivity of PTZ. Moreover, **PTZ** showed a reactivity very close to that of the commercial photoinitiator TPO (see Fig. 26).

7. Oxime esters analogues

7.1. Naphthoquinone-based imidazolyl esters

Functional metabolites based on naphthoquinone derivatives (NQs) can be found in nature in a variety of sources, including plants, bacteria, and marine species. They are readily available and easy to obtain without complex synthetic procedures and these compounds are also well-known to exhibit anticancer properties [67]. Additionally, the naphthoquinone structure can have various functional groups added on

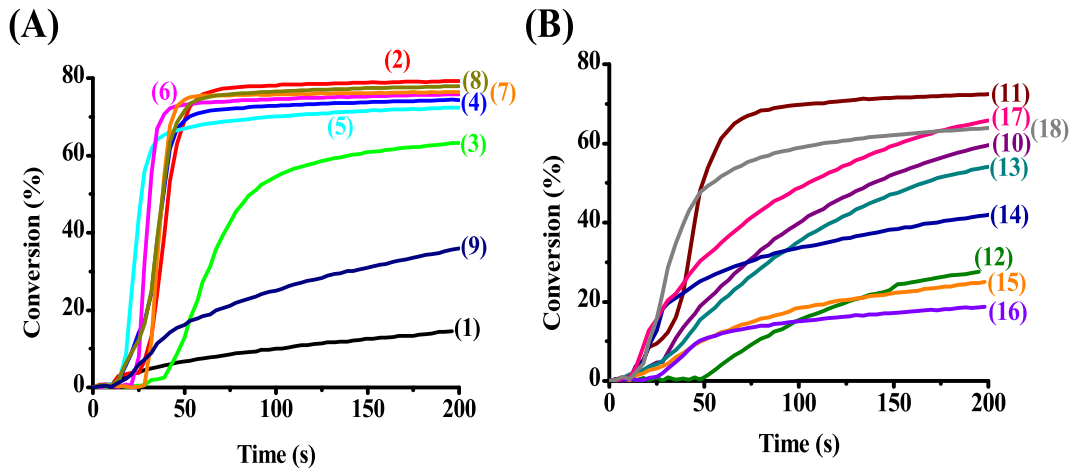

Fig. 23. (A), (B) Photopolymerization profiles of acrylates functions using the TA monomer (acrylate function vs. irradiation time) performed in Thin sample in laminate upon irradiation at 405 nm using one-component PISs (0.5 %): **(1) Py-OXE 1**, **(2) Py-OXE 2**, **(3) Py-OXE 3**, **(4) Py-OXE 4**, **(5) Py-OXE 5**, **(6) Py-OXE 6**, **(7) Py-OXE 7**, **(8) Py-OXE 8**, **(9) Py-OXE 9**, **(10) Py-OXE 10**, **(11) Py-OXE 11**, **(12) Py-OXE 12**, **(13) Py-OXE 13**, **(14) Py-OXE 14**, **(15) Py-OXE 15** **(16) Py-OXE 16**, **(17) Py-OXE 17**, **(18) Py-OXE 18**. Irradiation starts at t = 15 s. Reproduced with permission of Ref.[59].

Table 12
Parameters characterizing the An-OXEs and Py-OXEs. Some parameters characterizing the proposed PIs were calculated by molecular modelling: the bond dissociation energy BDE (N–O), the triplet state energy E_{T1}, the singlet excited state energy E_{S1} (evaluated experimentally from the experimental absorption and fluorescence spectra). The S_1 excited state lifetimes were determined by time resolved fluorescence spectroscopy.

PI	BDE_{N-O} (kcal/mol)	E_{S1} (kcal/mol)	τ_0 (S_1) (ns)	E_{T1} (kcal/mol)
1	63.25[a]	68.95 [a]	4.58 [a]	33.75 [a]
	61.15[b]	74.49[b]	6.8[b]	41.70[b]
2	44.95 [a]	66.41 [a]	1.5[a]	39.54 [a]
	47.86[b]	71.72[b]	3.8[b]	41.56[b]
3	45.74 [a]	n.d	3.66[b]	34.48 [a]
	45.65[b]			41.48[b]
4	44.73 [a]	n.d	3.8[b]	34.08 [a]
	47.39[b]			41.56[b]
5	46.98 [a]	n.d	3.14[b]	34.34[a]
	47.82[b]			41.39[b]
6	43.78 [a]	n.d	3.75[b]	39.72 [a]
	46.70[b]			41.53[b]
7	43.72 [a]	n.d	3.7[b]	39.55 [a]
	46.84[b]			41.55[b]
8	46.33 [a]	n.d	3.79[b]	34.28 [a]
	46.66[b]			41.40[b]
9	44.48 [a]	n.d	3.02[b]	39.48 [a]
	47.34[b]			41.43[b]
10	46.60 [a]	n.d	2.56[b]	34.47 [a]
	47.17[b]			41.43[b]
11	44.92 [a]	n.d	2.57[b]	39.48 [a]
	47.94[b]			41.57[b]
12	43.65[b]	n.d	n.d	43.45[b]
13	46.29 [a]	n.d	n.d	34.46 [a]
	46.93[b]			41.43[b]
14	46.52 [a]	n.d	n.d	39.37 [a]
	45.00[b]			43.57[b]
15	44.34 [a]	n.d	n.d	39.47 [a]
	42.92[b]			43.65[b]
16	45.59 [a]	n.d	n.d	34.65 [a]
	41.88[b]			43.50[b]
17	46.61 [a]	n.d	n.d	34.50[a]
	47.17[b]			41.43[b]
18	44.61 [a]	n.d	n.d	33.80 [a]
	47.65[b]			41.56[b]

a: An-OXE
b: Py-OXE
n.d: not determined

it, enabling to drastically modify the light absorption and notably to redshift their absorptions towards longer wavelengths. Noticeably, naphthoquinones have never been investigated as Type I photoinitiators before 2022 [13]. Therefore, investigation of naphthoquinone for the design of photoinitiating systems and examination of the impact of the structural variations on their photoinitiating abilities is therefore exciting and important. Recently, a study conducted by Lalevée and coworkers investigated and proposed an unprecedented class of naphthoquinone esters — the 4,9-dioxo-2-phenyl-4,9-dihydro-1*H*-naphtho[2,3-*d*]imidazol-1-yl esters — as high-performance Type I PIs (See Scheme 12) [68]. In order to prepare this series of imidazolyl esters easily, different acid chlorides were used to generate the different esters with 1-hydroxy-2-phenyl-1*H*-naphtho[2,3-*d*]imidazole-4,9-dione. This family of imidazolyl esters, which is novel in the literature and whose structure is comparable to that of the well-known family of oxime esters, is also capable to initiate an homolytic cleavage of the N-O bond upon irradiation. Decarboxylation may also occur after cleavage, generating initiating aryl or alkyl radicals. Considering the similarity of structures between imidazolyl esters and oxime esters, investigation of this new class of PIs and the determination if this family of imidazolyl esters could act as high-performance PIs in comparison to oxime esters or the well-known phosphine oxides was of crucial importance for us (e.g. TPO; Scheme 3). Their abilities to initiate a photopolymerization process under mild conditions (low light intensity using LEDs emitting at 405 nm or 455 nm) was studied. Another indication of their high reactivity is the possibility of using them in photosensitive 3D printing resins.

Concerning the synthesis of these imidazolyl esters, 1,4-naphthoquinone (C1) was used as the starting material to prepare all dyes (See Scheme 13). 2-(Benzylamino)naphthalene-1,4-dione (C4) and 2-((3,4-dimethoxylbenzyl)amino)naphthalene-1,4-dione (C5) were obtained in 92 and 85 % yields, respectively, by a Michael condensation of benzylamine (C2) and 3,4-dimethoxybenzylamine (C3). Compounds 1-hydroxy-2-phenyl-1*H*-naphtho[2,3-*d*]imidazole-4,9-dione (C6) and 2-(3,4-dimethoxyphenyl)-1-hydroxy-1*H*-naphtho[2,3-*d*]imidazole-4,9-dione (C7) could be produced in 67 and 84 % yields, respectively, by a cyclization procedure previously reported by Lavrikova and coworkers. Precisely, derivatives of 1-hydroxy-2-phenyl-1*H*-naphtho[2,3-*d*]imidazole-4,9-dione C6 and C7 were esterified using triethylamine as the base and the appropriate acid chlorides so that compounds 2–15 could be obtained. This method therefore produced compounds that can be regarded as oxime ester analogues. A molecule with a non-cleavable group was also prepared for comparison. Thus, 1-methoxy-2-phenyl-1*H*-naphtho[2,3-*d*]imidazole-4,9-dione (1) could be obtained in pure

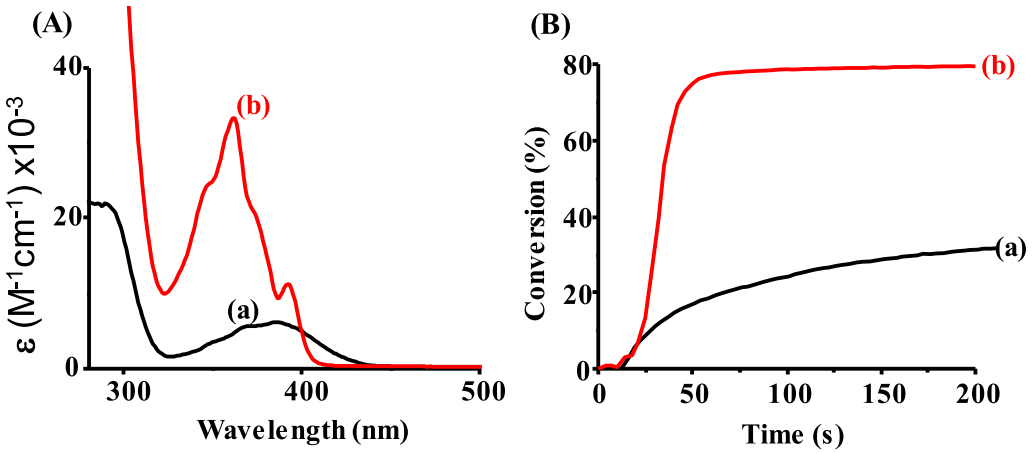

Fig. 24. **(A)** UV–visible absorption spectra of **(a)** An-OXE 2 and **(b)** Py-OXE 2. **(B)** Photopolymerization profiles of acrylates functions using **(a)** An-OXE 2 (0.5 % w) and **(b)** Py-OXE 2 (0.5 % w) as photoinitiators. Reproduced with permission of Ref. [59].

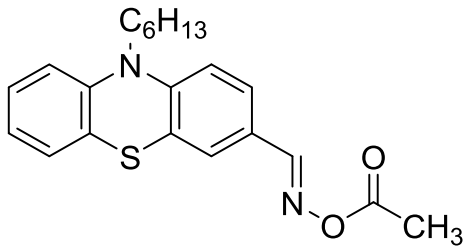

PTZ

Scheme 11. Chemical structure and abbreviation of the synthesized phenothiazine-based OXE.

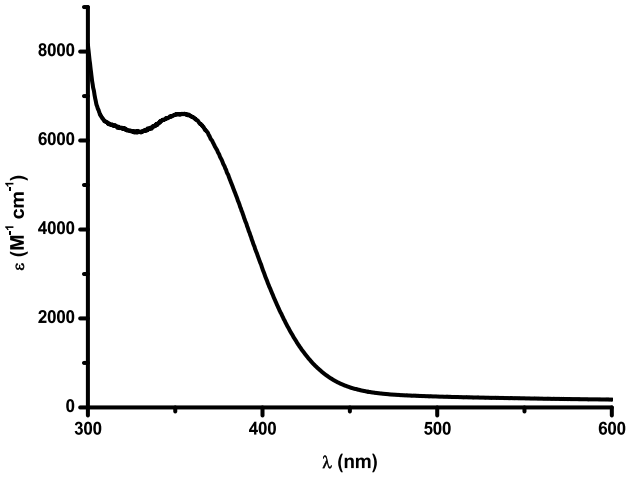

Fig. 25. UV–visible absorption properties of **PTZ** in acetonitrile. Unpublished results @IS2M.

form in 88 % yield after alkylation of C6 with iodomethane in DMF at room temperature and utilizing potassium *tert*-butoxide as the base.

Acetonitrile (ACN) was used as the solvent to acquire the UV–visible absorption spectra of the investigated derivatives (See Fig. 27), and Table 13 lists the main parameters. Compounds **(1)**-**(11)** exhibited a maximum absorption at about 380 nm, but the naphthoquinone-esters showed a blue-shifted absorption maximum after the introduction of the two methoxy groups (See Table 13). All dyes exhibited absorption

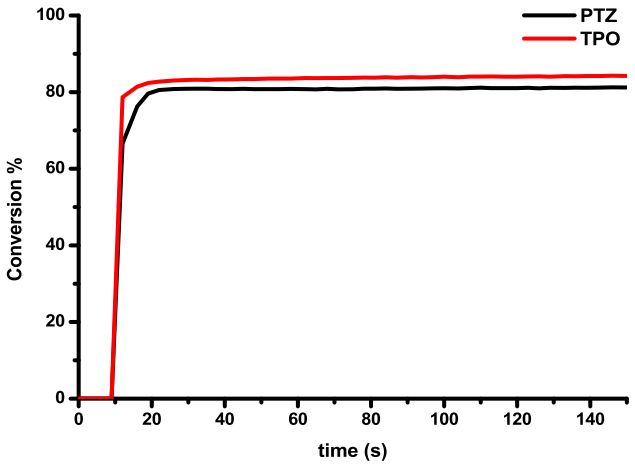

Fig. 26. Photopolymerization profiles of TA (acrylate function conversion vs. irradiation time) in laminate (thickness = 25 μm) upon exposure to a LED (λ = 405 nm) in the presence of PIs (1 %w/w). The irradiation starts at t = 10 s. Unpublished results @IS2M.

maxima perfectly fitting with the emission of LED emitting at 405 and 455 nm, except for the last set of naphthoquinones **(12)**-**(15)** for which blue shifted absorptions were found.

Type I photoinitiating abilities of the studied compounds (0.5 % w) were examined using RT-FTIR in thin (25 μm, in laminate) and thick (1.4 mm under air) samples after exposure to various LEDs (405 nm or 455 nm) using a benchmark monomer i.e. TA. Fig. 27 depicts typical photopolymerization profiles, and Table 14 lists the final acrylate function conversions (FCs) that were attained.

By comparing compound **(1)** to the other structures (**2**–**15**) which all have ester groups, it is clear that the ester group is necessary for compound (**1**) to be able to react as a Type I photoinitiator. As commonly observed, compound **(8)** which has a methyl group on the carboxyl side achieved the highest FC of 88 %, which is also very close to that obtained with the widely used photoinitiator TPO (See Table 14). By comparing compounds with aryl substituents to those with alkyl substituents on the carboxyl side, it is clear that the alkyl substituted naphthoquinones exhibited higher photoinitiation performances (See Fig. 27(A), as evidenced for compounds **(2)**, **(3)**, **(4)**, **(7)**, and **(8)** that exhibited rapid polymerization rates as well as high final conversions. If the methoxy groups were added onto the structures of naphthoquinones in order to improve their solubility in resins, unexpectedly, a severe reduction of

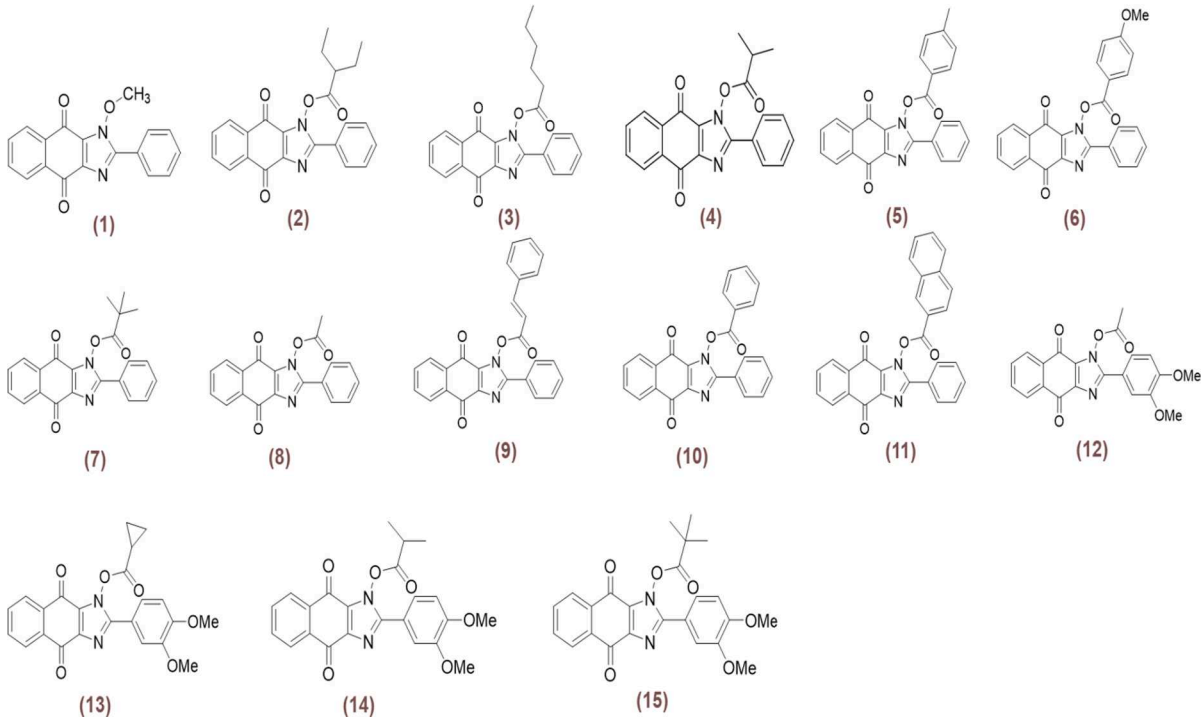

Scheme 12. Chemical structures of the synthesized naphthoquinone-based imidazolyl esters. Reproduced with the permission from Ref. [69].

the photoinitiating ability was evidenced. In fact, the ability of these compounds to initiate photopolymerization was greatly poorer than that of their analogues without methoxy groups (See compounds **(12)**, **(13)**, **(14)**, and **(15)** vs. compounds **(8)**, **(4)**, and **(7)** in Table 14). Therefore, it is important to consider additional variables that may impact the ability to photopolymerize, such as the cleavage yields and the reactivity of the generated radicals. This clearly demonstrates that the photoinitiation ability of the studied compounds is not only associated to their light absorption properties.

Additionally, photopolymerization experiments were also carried out using a LED emitting at 455 nm in order to demonstrate the reactivity of the investigated structures at longer wavelengths. To the best of our knowledge, no oxime esters have been tested at such a redshifted irradiation wavelength. The results notably demonstrated several naphthoquinone derivatives to exhibit a high photoinitiation performance, particularly for compounds **(8)**, **(2)**, **(3)**, **(4)**, and **(7)** (with alkyl substituents on the carboxyl side) (See Fig. 27 and also Table 14). Even under LED@455 nm, compound **(8)** had the strongest reactivity, with a FC of 87 % in thin samples and 84 % in thick samples. When compared to commercial references such as the two-component system camphorquinone/ethyl dimethylaminobenzoate (CQ/EDB) (0.5 %/0.5 % w/w) or even Titanocene (Irgacure 784) (0.5 % w) (see Fig. 27 (A)), compound **(8)** could outperform these two reference systems, indicating that it could constitute a viable alternative to these benchmark photoinitiators. Comparatively, compounds **(9)**, **(10)**, **(11)**, **(12)** and **(15)** exhibited a reduced photoinitiating ability compared to the others, once again due to the fact that these esters are substituted with aromatic groups. To evidence the interest of compound **(8)** as a photoinitiator, the stability in resin was examined. The TA-based resin mixture containing 0.5 % w compound (**8**) was stored without light and at room temperature for one month, and the photoinitiating effect was checked weekly. As can be seen in Fig. 27 (B), a good storage stability was demonstrated without a significant decrease in performance.

By FTIR, occurrence of a decarboxylation reaction could be clearly demonstrated for compound (**8**) in TA monomer when exposed to irradiation at 405 nm. For all derivatives bearing an alkyl group, such as compound **(8)**, appearance of a peak at 2337 cm^{-1} was detected after irradiation, demonstrating the release of CO_2 (See Fig. 28 (A)). Derivatives with an aryl group, such as compound **(10)**, did not release CO_2, as shown in Fig. 28 (C). Since the CO_2 release directly affects the polymerization efficiency (see Fig. 28 (B) and (D) which highlight the connection between the two profiles), CO_2 release is primordial to get a high polymerization efficiency. A low radical launching efficiency is anticipated in the absence of CO_2 release.

For each of the studied compounds, the bond dissociation energy of the associated N-O bond (BDE) and the excited state energies (singlet and triplet excited state energies) could be determined by theoretical calculations and the results are listed in Table 15. From the singlet and triplet excited states where the dissociation enthalpies from the S_1 and T_1 states are negative and favorable, the N-O bond cleavage process is energetically favorable for the compounds **(2)** - **(11)**. Cleavage from the singlet state, however, is more advantageous because the ΔH values are lower. Compounds **(12)** - **(15)** did not have photoluminescence, so that the energy of the singlet state could not be calculated. However, they have negative triplet enthalpy values, indicating that the cleavage is favorable from this energy state. Fluorescence lifetimes of the different naphthoquinone-based imidazolyl esters were also examined (See Table 15). Compound **(1)**, a derivative without ester functionality, had the longest lifetime of 3.45 ns, consistent with its photochemical results. Addition of the ester group resulted in shorter lifetimes, suggesting a cleavage from the S_1 state.

Compound **(8)** (with a methyl substituent in the carboxyl side) in this new family of naphthoquinone-based imidazolyl ester structures exhibited excellent photoinitiating performance so that it could replace well-established references such as TPO as photoinitiator.

7.2. *N-naphthalimide Ester derivatives*

Naphthalimide-based PIs have been the subject of many chemical modifications during the last decade. Different substituents were notably introduced to finely tune the absorption properties of naphthalimide derivatives. Noticeably, until 2020, naphthalimide derivatives were only investigated to elaborate two- and three-component photoinitiating systems. Besides, some works were also devoted to design

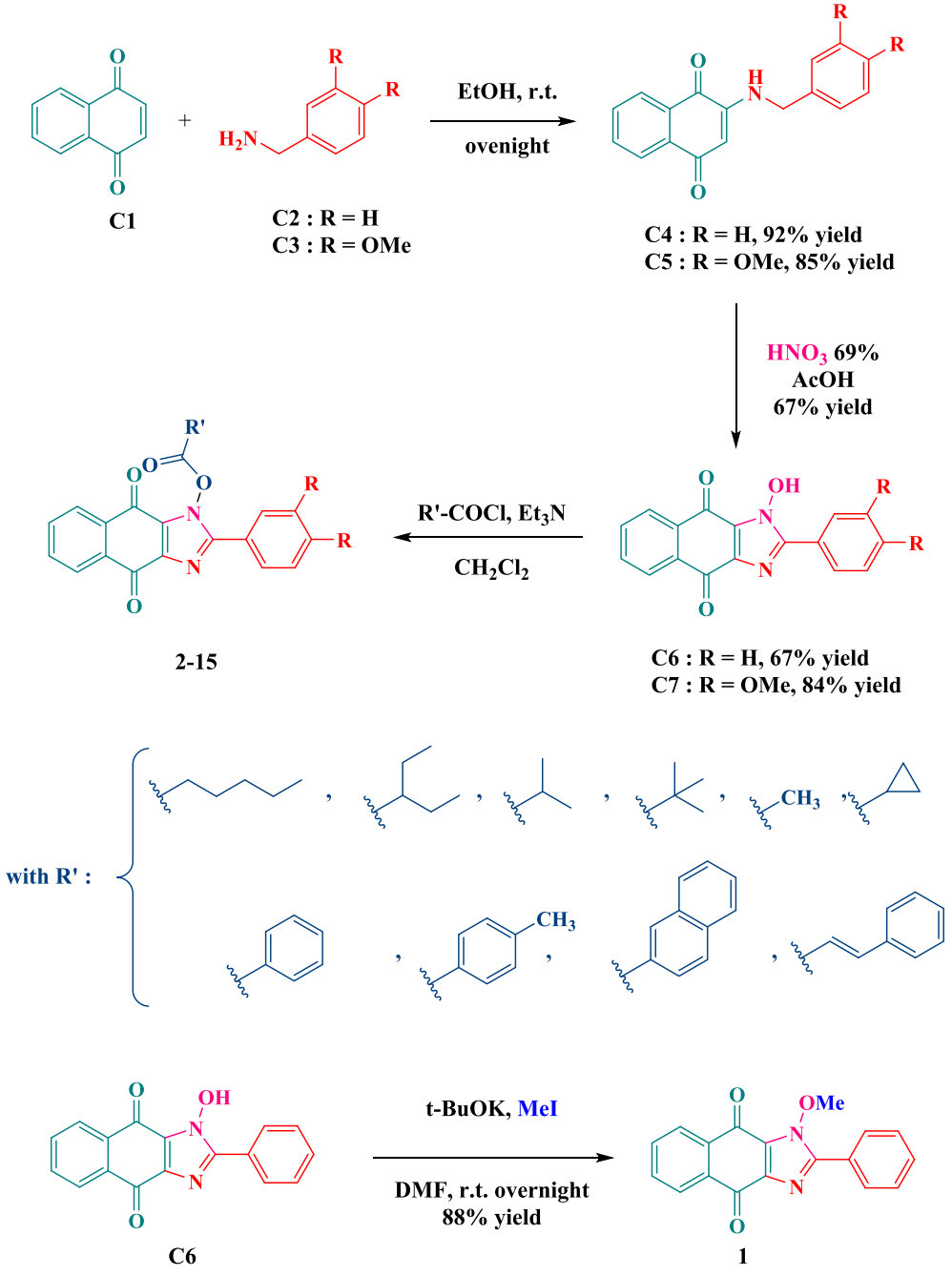

Scheme 13. Synthetic routes to the different dyes. Reproduced with the permission from Ref. [69].

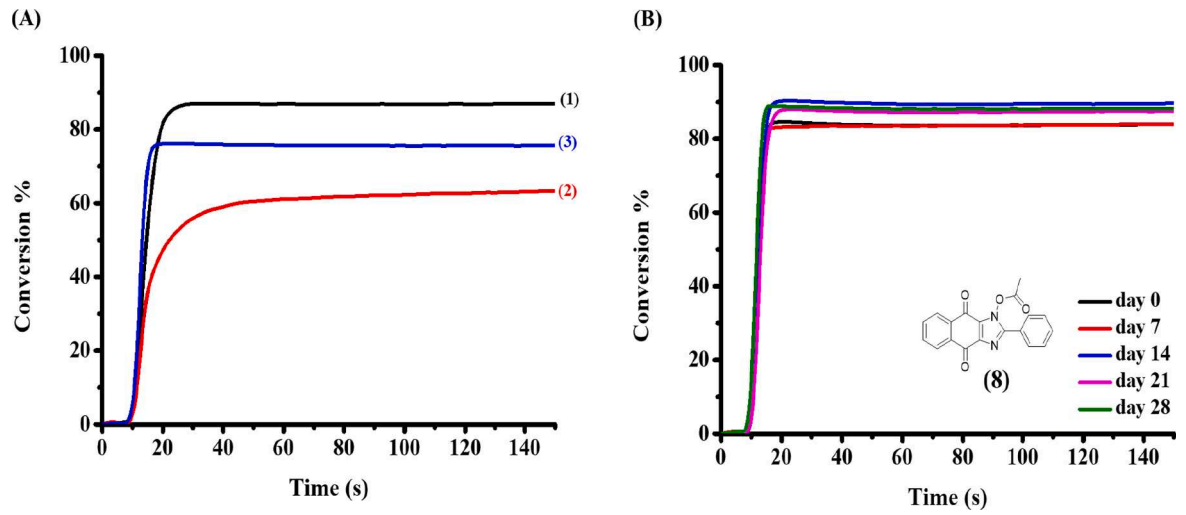

Fig. 27. **(A)** Photopolymerization profiles of TA in laminate (thickness = 25 μm) of (1) compound **(8)** (0.5 % w), (2) CQ/EDB (0.5 %/0.5 % w/w) and (3) Titanocene (0.5 % w), upon exposure to a LED light (λ = 455 nm). **(B)** Photopolymerization profiles of TA using compound **(8)** (0.5 % w) for different storage times in TA monomer. The irradiation starts at t = 10 s. Reproduced with the permission from Ref. [69].

Table 13
Light absorption properties of the investigated compounds: maximum absorption wavelength (λ_{max}), molecular extinction coefficients at λ_{max}, 405 and 455 nm.

PIs	λ_{max} (nm)	ε_{max}(M^{-1} cm^{-1})	ε_{405} (M^{-1} cm^{-1})	ε_{455} (M^{-1} cm^{-1})
(1)	330	500	260	30
(2)	380	1950	1500	90
(3)	382	1350	1070	100
(4)	378	1980	1510	40
(5)	383	970	810	100
(6)	388	2300	2010	260
(7)	383	2000	1670	130
(8)	382	1700	1360	170
(9)	387	1800	1550	210
(10)	385	1800	1630	570
(11)	388	2370	2110	360
(12)	333	3960	810	220
(13)	334	6110	1100	120
(14)	336	5700	960	70
(15)	339	4670	1290	360

Table 14
FCs using one component (0.5 % w) photoinitiators after 100 s of irradiation with LED light (λ = 405 and 455 nm).

PIs	Thin Samples (25 μm) in laminate @405 nm	Thin Samples (25 μm) in laminate @455 nm	Thick Samples (1.4 mm) under air @405 nm	Thick Samples (1.4 mm) under air @455 nm
TPO	90 %	61 %	95 %	77 %
(1)	65 %	48 %	25 %	1 %
(2)	82 %	80 %	78 %	78 %
(3)	68 %	71 %	84 %	81 %
(4)	81 %	83 %	83 %	85 %
(5)	49 %	55 %	78 %	74 %
(6)	34 %	53 %	48 %	68 %
(7)	79 %	76 %	86 %	80 %
(8)	88 %	87 %	88 %	84 %
(9)	42 %	24 %	48 %	65 %
(10)	18 %	32 %	54 %	54 %
(11)	39 %	32 %	63 %	66 %
(12)	56 %	65 %	76 %	78 %
(13)	71 %	73 %	74 %	78 %
(14)	68 %	59 %	78 %	61 %
(15)	54 %	48 %	76 %	67 %

naphthalimides usable as monocomponent photoinitiating systems [70-72]. In a recent study by Lalevée and coworkers, 2,6-dioxopiperidin-1-yl esters were prepared with naphthalimides. Irradiation could lead to the homolytic cleavage of the N-O bond, allowing the acyloxy or the aryloxy groups to undergo a decarboxylation process and produce an alkyl radical [72]. These free radicals could initiate the polymerization of monomers. Nine *N*-naphthalimide esters (**NPIE1**-**NPIE9**) were examined as Type I photoinitiators. To maximize the photocleavage efficiency, various cleavable groups were linked directly to the chromophore using the oxime ester group. For comparison, a second series of naphthalimide derivatives was also prepared, in which the oxime ester group was separated from the chromophore by mean of an aliphatic spacer. This second series of oxime esters was found to be almost incapable to initiate a polymerization, demonstrating the critical importance of the distance between the photocleavable group and the light absorbing chromophore.

The different naphthalimide-based photoinitiators **NPIE1**-**NPIE9** were prepared in three steps, starting from 6-bromo-1*H*,3*H*-benzo[*de*]isochromene-1,3-dione **1**. First, in basic conditions, 6-(octylthio)-1*H*,3*H*-benzo[*de*]isochromene-1,3-dione **2** could be produced in 87 % yield by nucleophilic substitution with octanethiol. Then, using sodium acetate and hydroxylamine hydrochloride, oxime **3** could be obtained in 98 % yield. Finally, using triethylamine as the base and the proper acid chloride, esterification of the oxime group could be obtained. According to Scheme 14, the reaction yields for **NPIE1**-**NPIE9** ranged from 71 % for **NPIE9** to 93 % for **NPIE7**. In the end, **NPIMO** was prepared as a control substance. Indeed, **NPIMO** is not an oxime ester due to its alkylation with iodomethane. Starting from **3**, this compound could be obtained in 85 % yield.

A second series of molecules, **NO1**-**NO8**, was created to examine the impact of the distance introduced between the chromophore and the cleavable group (See Scheme 15). By using an excess of ethylenediamine and 4-fluoroacetophone **4**, 1-(4-((2-aminoethyl)amino)phenyl)ethan-1-one **5** could be produced in 88 % yield. Then, after two days of reaction in 2-ethoxyethanol, 2-(2-((4-acetylphenyl)amino)ethyl)-6-(octylthio)-1*H*,3*H*-benzo[*de*]isochromene-1,3-dione **6** was produced in 82 % by condensation on 6-(octylthio)-1*H*,3*H*-benzo[*de*]isochromene-1,3-dione with 1-(4-((2-aminoethyl)amino)phenyl)ethan-1-one **5**. The oxime could be obtained by reacting the ketone **6** with sodium acetate, hydroxylamine hydrochloride in a mixture of solvents. 2-(2-((4-(1-(Hydroxyimino)ethyl)phenyl)amino)ethyl)-6-(octylthio)-1*H*-benzo[*de*]isoquinoline-1,3(2*H*)-dione **7** was obtained in 96 % yield. Oxime esters were prepared by following a similar process to that used for **NPIE1**-

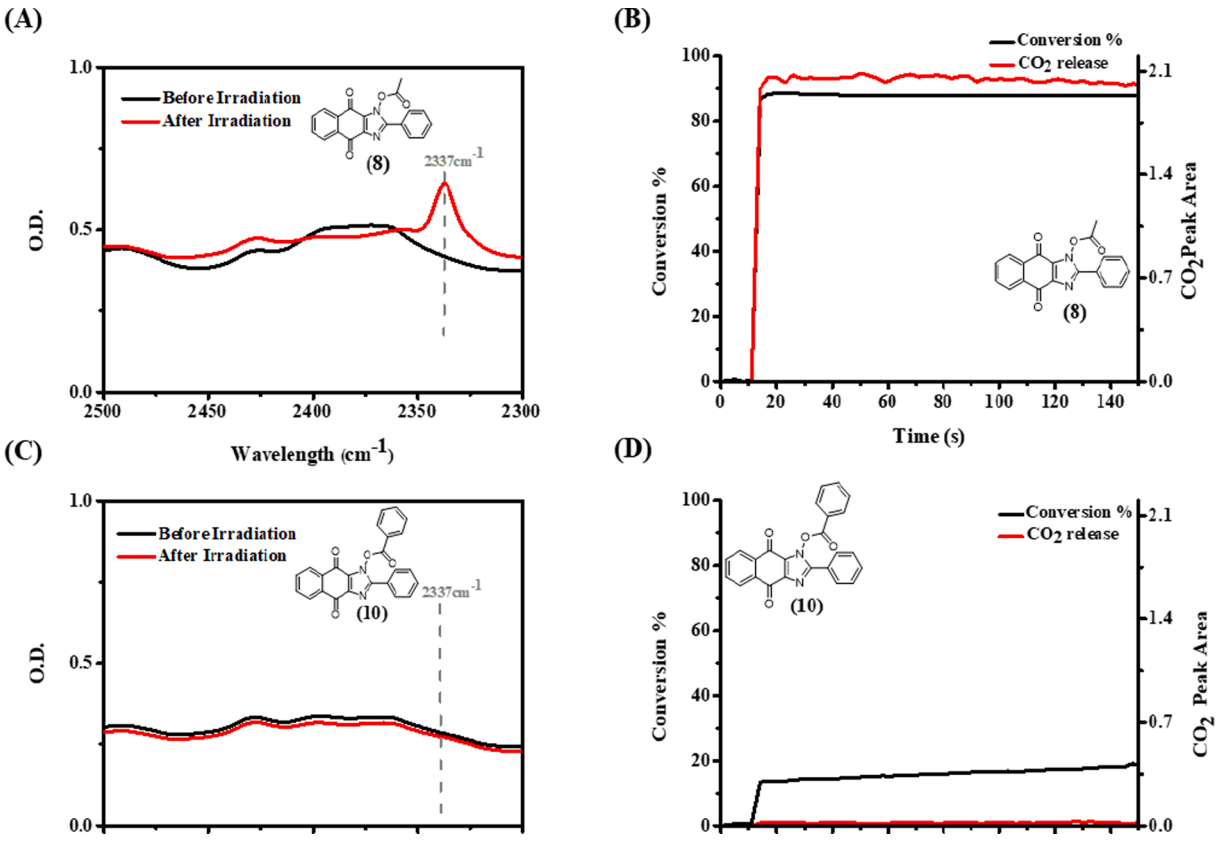

Fig. 28. **(A)** Detection of CO_2 released during photopolymerization using **(8)**, **(B)** Decarboxylation-Conversion correlation using **(8)**, **(C)** Detection of CO_2 released during photopolymerization using **(10)** and **(D)** Decarboxylation-Conversion correlation using **(10);** PI (0.5 % w) in TA (thin film polymerization @405 nm in laminate). Reproduced with the permission from Ref. [69].

Table 15
Parameters characterizing the investigated naphthoquinone-based imidazolyl esters. Parameter calculated by molecular modelling: the bond dissociation energy BDE (N–O), the triplet state energy E_{T1}, the enthalpy ($\Delta H_{cleavageT1}$) for the cleavage process from T_1 ($\Delta H_{cleavageT1} = BDE - E_{T1}$), the singlet excited state energy E_{S1} (evaluated from the experimental absorption and fluorescence spectra), the enthalpy ($\Delta H_{cleavageS1}$) for the cleavage process from S_1 ($\Delta H_{cleavageS1} = BDE - E_{S1}$).

PIs	BDE (kcal/mol)	E_{S1} (kcal/mol)	τ_0 (S_1) (ns)	$\Delta H_{cleavageS1}$ (kcal/mol)	E_T (kcal/mol)	$\Delta H_{cleavageT1}$ (kcal/mol)
(1)	41.78	62.3	3.45	−20.51	50.98	−9.2
(2)	35.76	63.5	2.49	−27.74	50.57	−14.81
(3)	36.54	63.8	2.46	−27.26	50.69	−14.15
(4)	34.95	63.5	1.76	−28.55	50.76	−15.81
(5)	34.90	62.2	2.75	−27.3	50.77	−15.87
(6)	34.94	62.6	2.63	−27.66	50.76	−15.82
(7)	35.03	62.8	3.09	−27.77	50.53	−15.50
(8)	36.19	65.13	2.36	−28.94	50.71	−14.52
(9)	34.92	64.3	2.41	−29.38	50.47	−15.55
(10)	34.87	61.8	2.56	−26.93	50.75	−15.88
(11)	34.78	62.6	2.57	−27.82	50.77	−15.99
(12)	32.68	–	–	–	47.12	−14.44
(13)	32.38	–	–	–	47.56	−15.18
(14)	31.41	–	–	–	47.29	−15.88
(15)	31.89	–	–	–	47.82	−15.93

NPIE9. Reaction yields ranged from 62 % for **NO2** to 75 % for **NO7** respectively.

Fig. 29 shows the UV–visible absorption spectra of PIs in acetonitrile. The maximum absorption wavelength of **NPIMO** (λ_{max}) was 394 nm. The maximum absorption wavelengths of **NPIE**s were slightly redshifted in comparison to **NPIMO**. All **NPIE**s maximum absorption wavelengths were between 397 nm and 398 nm. These results clearly show that the substituents attached to the ester group have only little influence on the light absorption properties of **NPIEs**. Interestingly, molar extinction coefficients of **NPIE**s determined at 405 nm ($\varepsilon_{405\ nm}$), such as $\varepsilon_{405\ nm}$(**NPIE1**) = 15000 $M^{-1}cm^{-1}$ and $\varepsilon_{405\ nm}$ (**NPIE2**) = 14400 $M^{-1}cm^{-1}$ were favorable for polymerization experiments carried out at 405 nm.

The high molar extinction values of the different dyes at 405 nm allowed the authors to examine the photoinitiation performance of **NPIE**s in free radical photopolymerization. Fig. 30a depicts the polymerization profiles of TMPTA (acrylate conversion vs. irradiation duration. Under LED@405 nm, NPIEs showed good photoinitiation capabilities during free radical polymerization. Interestingly, even though the TPO system had a reasonably quick polymerization rate, the acrylate function conversion of TMPTA in the presence of **NPIE1** (FC = 68 %) was higher than that of the benchmark structure TPO (FC = 66 %).

Furthermore, **NPIE7** demonstrated a good photoinitiating ability (FC = 66 %). When exposed to a LED@405 nm while **NPIMO** (without ester group) was present, a function conversion of 41 % was determined. It suggests that the ester group plays a crucial role in these PIs structural composition. Upon exposure to a LED@455 nm, the photoinitiation capacity of **NPIE1** and TPO was also examined (See Fig. 30b). TPO proved to be almost ineffective to initiate a polymerization upon irradiation at 455 nm. Significantly, the ultimate functional conversion of TMPTA in the presence of **NPIE1** was 44 %, which benefited from the efficient absorption of visible light by **NPIE1** (much better absorption than TPO at 455 nm).

The singlet excited state energy (E_{S1}) could be determined at the intersection of the UV–visible absorption and fluorescence emission spectra of **NPIE**s. From computational methods, the triplet state energy (E_T) and the dissociation energy of the N-O bond of **NPIE**s were estimated. Table 16 contains the N-O bond cleavage enthalpies of the singlet

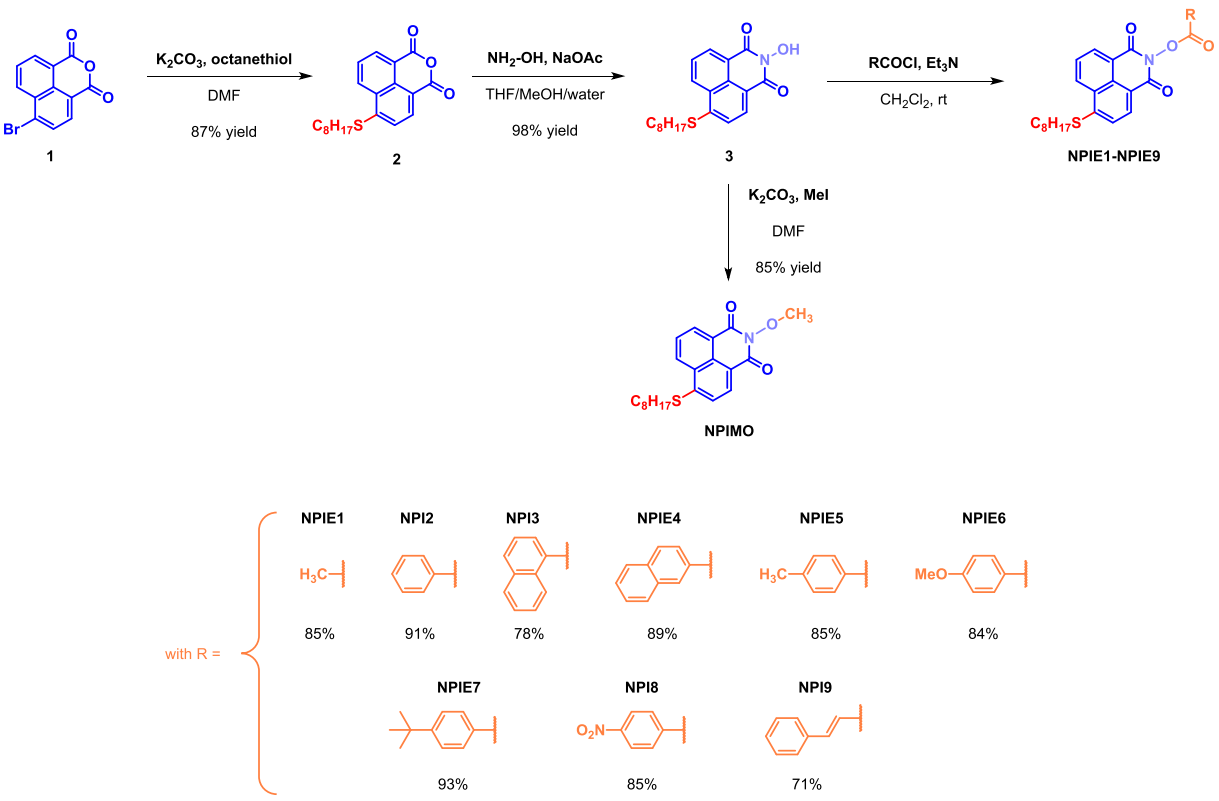

Scheme 14. Synthetic routes to **NPIE1-NPIE9** and **NPIMO**.

state (S_1) and triplet state (T_1). The results ($\Delta H_{cleavage\ S1} < 0$, $\Delta H_{cleavage\ T1} > 0$) indicate that the major pathway involves cleavage of the N-O bond from the singlet state. Additionally, a time-correlated single-photon counting system was used to evaluate the fluorescence lifetimes of PIs in acetonitrile. Table 16 lists the fluorescence lifetimes (τ_0) of PIs. In accordance with the favorable values of cleavage S_1 for the N-O bond cleavage process from the singlet excited state, **NPIE**s have shorter fluorescence lifetimes than **NPIMO**.

Interestingly, photodecomposition of oxime esters upon irradiation could be monitored by RT-FTIR by following the formation of CO_2 during the decarboxylation reaction. Here, photopolymerization experiments involving the decomposition of **NPIE**s in TMPTA after exposure to a LED@405 nm were also examined using RT-FTIR. Fig. 31a and 31b demonstrate that following irradiation, an emerging absorption peak at 2337 cm^{-1} was found in the infrared spectra of the **NPIE1**/TMPTA and **NPIE2**/TMPTA systems. The generated peak was attributed to CO_2. Infrared spectra of the **NPIMO**/TMPTA (Fig. 31c) and TPO/TMPTA systems did not have this peak. According to these findings, irradiation can induce a decarboxylation reaction for both alkoxy or aryloxy radicals, subsequent to photocleavage. Absorbance of **NPIE1** and **NPIE2** during the photolysis tests remains unchanged, evidencing the photostability of the naphthalimide moiety. Fig. 31d illustrates that during the photopolymerization process, intensity of the CO_2 absorption peak for the **NPIE1**/TMPTA system was higher than that of the **NPIE2**/TMPTA system, indicating that more CO_2 was released by the **NPIE1**/TMPTA system. These results demonstrate that the acetoxy group, which is also present in **NPIE1**, can undergo an easier decarboxylation reaction than the benzoyloxy group.

Molecules may be promoted in their excited states upon irradiation of **NPIE**s. The naphthalimide and alkyloxy/aryloxy radicals are produced by a fast cleavage of the N-O bond from the singlet state. Active radicals used during the free radical polymerization of monomers can then be produced by decarboxylation of the alkyloxy/aryloxy radicals. Photoinitiation ability of **NPIE**s is significantly influenced by the substituents R. The production of methyl radicals was facilitated by the efficient decarboxylation of acetyloxy radicals. Thus, among them, the **NPIE1** system showed the highest monomer conversion. The **NPIE7** system was found to have a slightly higher initiation ability than the others. The addition reaction of the electron-deficient double bond of acrylate is facilitated by the radicals produced with electron-rich isopropyl groups. In **NPIE4**/TMPTA and **NPIE8**/TMPTA, the CO_2 peak was not observed, which could be attributed to an unfavorable cleavage or decarboxylation process. Therefore, with these two systems, low monomer conversions were obtained. In addition, the naphthalimide chromophore-based complexes are capable of undergoing a hydrogen abstraction reaction to produce radicals, resulting in the conversion of TMPTA to a low function state in the presence of **NPIMO**. Therefore, photoinitiating ability of **NPIMO** can be assigned to Type II behavior.

Another molecule, **NO1** (See structure in Scheme 15), was prepared in parallel to the **NPIE1**-**NPIE9** series in order to examine the impact of the separation between the chromophore and the photocleavable group. As shown in Fig. 32a, **NO1** had a higher molar extinction coefficient at 405 nm than **NPIE1**, and its maximum absorption wavelength was blue-shifted relative to **NPIE1** (λ_{max} = 397 nm). Fig. 32b shows the photopolymerization of TMPTA in the presence of **NO1** when exposed to an LED at 405 nm. Compared to **NO1**, **NPIE1** displayed a substantially greater capacity for photoinitiation. The naphthalimide chromophore is still responsible from the absorption of **NO1** light absorption band, with a maximum absorption located at ca 397 nm. The spacer in the **NO1** structure prevents the energy from being transferred to the oxime ester group when the naphthalimide moiety in the structure is excited by a LED@405 nm. No active radicals are produced during the oxime ester group's cleavage process; in contrast to **NPIE1**, no CO_2 peak was detected for **NO1**, indicating that the cleavage mechanism is not advantageous for **NO1**. As a result, TMPTA had a low function conversion (38 %) when **NO1** was used as the photoinitiator. With a spacer between the chromophore and the cleavable ester moiety, the other naphthalimide-esters (noted **NO2**-**NO8**) exhibited a similar reactivity.

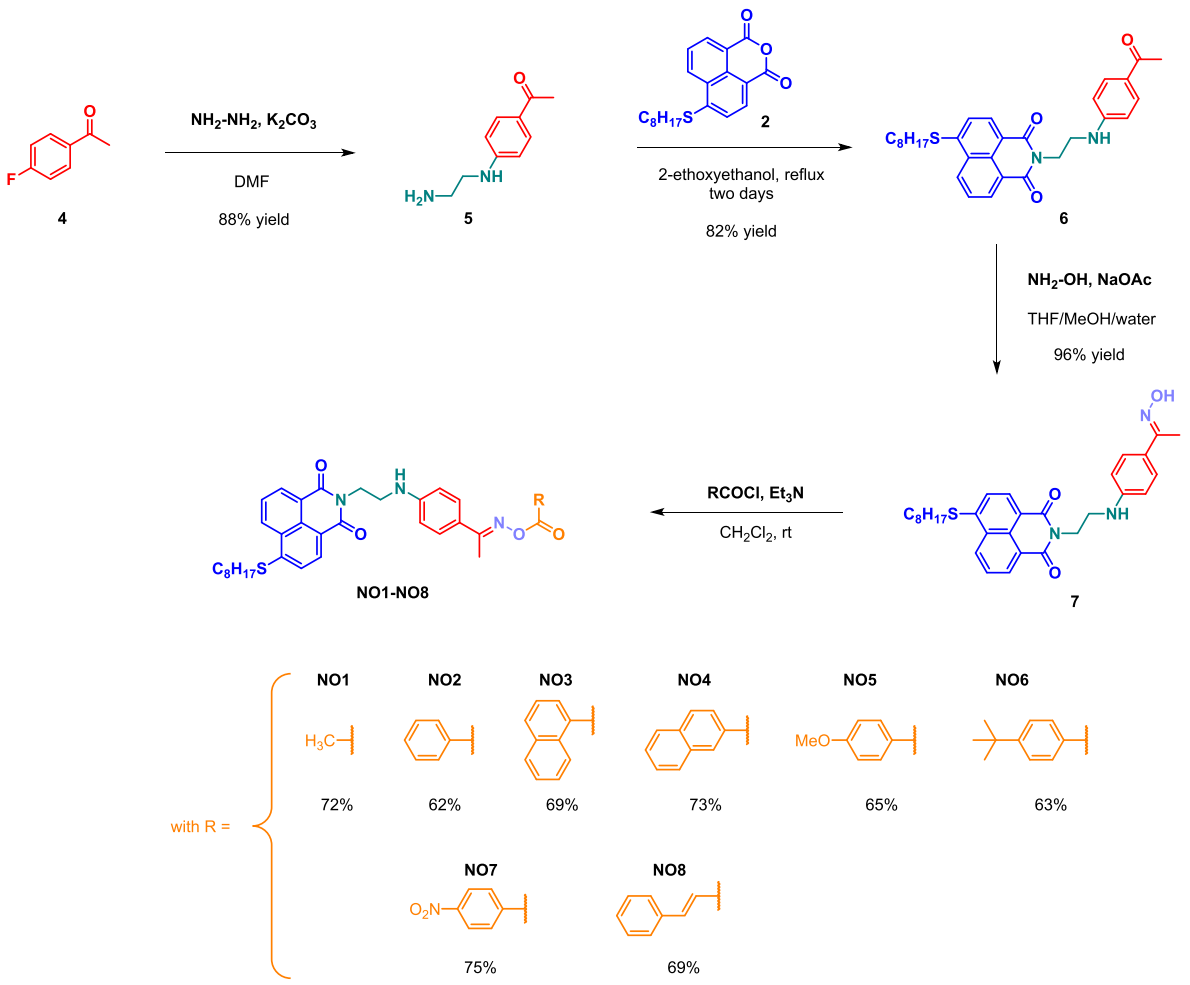

Scheme 15. Synthetic routes to **NO1-NO8**.

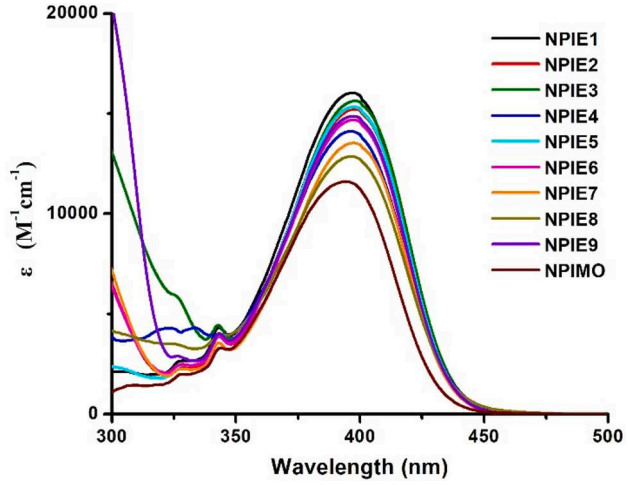

Fig. 29. UV–visible absorption spectra of **NPIE**s and **NPIMO** in acetonitrile. Reproduced with permission of Ref. [73].

Low performance levels are observed, which is consistent with a deficiency in energy transfer. The outcomes further show that NPIEs with the ester group in close vicinity to the naphthalimide chromophore is an important structural parameter in order to optimize the energy transfer efficiency upon photoexcitation.

8. Chromophore effects on photoinitiation ability

In general, as shown by the different studies performed so far, an important number of parameters such as the absorption properties, the efficiency of the photocleavage and the decarboxylation abilities, as well as the reactivity of the generated radicals, can drastically affect the overall mechanism of decomposition of oxime esters and in turn the final monomer conversion (See Scheme 16). In this part, the effect of the choice of the chromophore with regards to these different parameters is presented for the first time.

8.1. *Absorption properties*

Absorption properties of the photoinitiator (PI) are mainly controlled by its chemical structure, including the different groups attached to the chromophore. These groups can determine the position of the absorption spectra on the electromagnetic spectrum. Therefore, the wavelengths that a photoinitiator can absorb are reflected in an absorption spectrum. In addition, the absorption characteristics associated with the photosensitive molecule are revealed by the absorbance of the dye at a specific wavelength. In this review, each chromophore was chosen to shift the absorption wavelength of the oxime ester-based photoinitiators into the visible range. As summarized above, a wide range of chromophores have been examined during the last three years including triphenylamine, coumarin, carbazole, pyrene, anthracene, phenothiazine and other analogues derivatives… The different results have demonstrated that all the proposed structures exhibited good absorption properties in the visible range. Especially, all chromophores are adapted

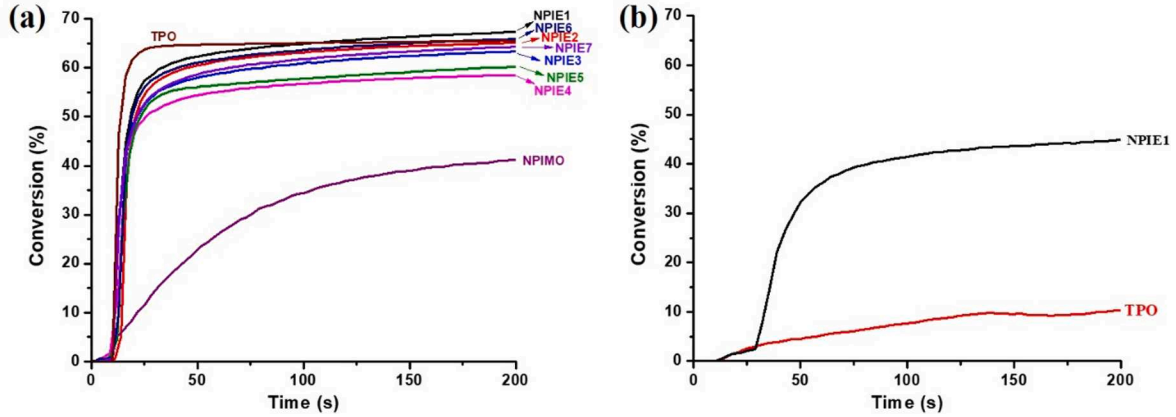

Fig. 30. Photopolymerization profiles of TMPTA in laminate (~25 μm) in the presence of photoinitiators (2×10^{-5} mol/g TMPTA) (a) upon exposure to a LED@405 nm; (b) upon exposure to a LED@455 nm. The irradiation starts at t = 10 s. Reproduced with permission of Ref. [73].

Table 16
Some parameters characterizing the cleavage process of the N − O bond.

NPIEs	N − O BDE (kcal. mol^{-1})	E_{S1} (kcal. mol^{-1})	$\Delta H_{cleavage\ S1}$[a] (kcal. mol^{-1})	E_T (kcal. mol^{-1})	$\Delta H_{cleavage\ T1}$ (kcal. mol^{-1})	τ_0 (ns)
NPIE1	63.17	65.72	−2.55	50.63	12.54	6.09
NPIE2	62.00	65.49	−3.49	50.68	11.32	5.89
NPIE3	61.85	65.58	−3.73	50.67	11.18	5.75
NPIE4	61.94	65.43	−3.49	50.69	11.25	5.69
NPIE5	61.91	65.66	−3.75	50.73	11.18	5.80
NPIE6	61.87	65.51	−3.64	50.79	11.08	5.70
NPIE7	61.98	65.63	−3.65	50.76	11.22	5.71
NPIE8	61.41	65.36	−3.95	50.52	10.89	5.30
NPIE9	63.06	65.61	−2.55	50.79	12.27	5.62
NPIMO	–	–	–	–	–	6.72

[a] $\Delta H_{cleavage\ S1/T1} = BDE(N-O) - E_{S1}/E_T$.

Table 17
Light absorption properties with different chromophore.

Chromophore	λ_{max} (nm)	ε_{max} ($M^{-1}cm^{-1}$)	$\varepsilon_{405\ nm}$ ($M^{-1}cm^{-1}$)
Triphenylamine	370 ↔ 380	30000 ↔ 45000	13000 ↔ 18000
Coumarin	430 ↔ 435	28000 ↔ 50000	16500 ↔ 25500
Carbazole	370 ↔ 380	12000 ↔ 20000	1200 ↔ 5400
Pyrene	360 ↔ 365	22000 ↔ 52000	535 ↔ 6400
Anthracene[1]	370 ↔ 375		
Phenothiazine	320 ↔ 350	6000 ↔ 6700	680 ↔ 2700

[1] : see Fig. 24 for absorption of An-OXE 2 as example.

for light irradiation done at 405 nm, which is a standard wavelength for 3D printers. The following table summarizes the absorption properties for all the chromophores.

The results show that coumarin-based photoinitiators exhibit the highest absorption properties compared to the other chromophores especially when exposed to irradiation done at 405 nm. The trend of efficiency for the absorption properties at 405 nm respects the following order: **Coumarin** > **Triphenylamine** > **Carbazole** > **Pyrene** > **Phenothiazine** > **Anthracene**. This can partially explain the photopolymerization results, but other factors may also have an effect on the photoinitiating ability of the investigated photoinitiators to initiate reactions.

8.2. Cleavage reaction

The usual cleavage in the oxime ester is mainly expected from the triplet state (T_1), but depending on the structure of the OXE, cleavage from the singlet state (S_1) has also been suspected (See Scheme 17). Table 18 summarizes the (N-O) bond dissociation energy and the cleavage process enthalpies from various excited state levels (S_1 or T_1) ($\Delta H_{cleavage\ S1\ or\ T1} = BDE(N\text{-}O) - E_{(S1\ or\ T1)}$) for the various oxime esters.

As we can see in Table 18, the cleavage from S_1 is favorable for all chromophores in the following order: **Carbazole** > **Pyrene** > **Anthracene** > **Triphenylamine** > **Coumarin** > **Phenothiazine**. In addition, for some chromophores such as **Carbazole**, **Coumarin**, and **Triphenylamine**, the possibility of cleavage from T_1 is also energetically favorable.

8.3. Photoinitiation behavior

All the investigated chromophores showed a significant shift towards the visible and consequently a good efficiency in photopolymerization process under LED@405 nm, the associated final acrylate conversions (FCs) are summarized in Table 19 with a trend: **Carbazole** > **Triphenylamine** > **Coumarin** and > **Pyrene** > **Phenothiazine** > **Anthracene**.

Other factors such as the decarboxylation reactions can also have a significant effect on the efficiency as shown in the previously published papers. For example, the decarboxylation is more favorable when alkyl substituents are involved compared to aryl substituents (see previous results), in addition the reactivity of the generated radicals to initiate the polymerization.

9. Conclusion

The design of oxime esters is an active field of research, for which several types of chromophores were examined during the last three years in order to shift the absorption wavelength of these dyes towards the visible range. An overview of the recently proposed structures is given in this review. According to the investigations, different factors including absorption properties, cleavage mechanisms, decarboxylation reactions, and the reactivity of the generated radicals can drastically influence the initiation abilities of oxime esters. In order to select the optimal structures that can act as Type I photoinitiators, it was demonstrated how the chromophore coupled to the oxime ester structure can drastically affect the final monomer conversion. Furthermore, in order to find the radicals that can produce the most efficient polymerization reactions, there is still much work to be done. Indeed, there is a wealth of literature on aromatic and heterocyclic radicals. In addition, current research has conclusively shown that the methyl radicals were the most reactive ones ever described in the literature for oxime esters. Future research on novel oxime esters will focus on the generation of aliphatic radicals that could considerably improve the polymerization efficiency. The excited state involved in the photocleavage of oxime

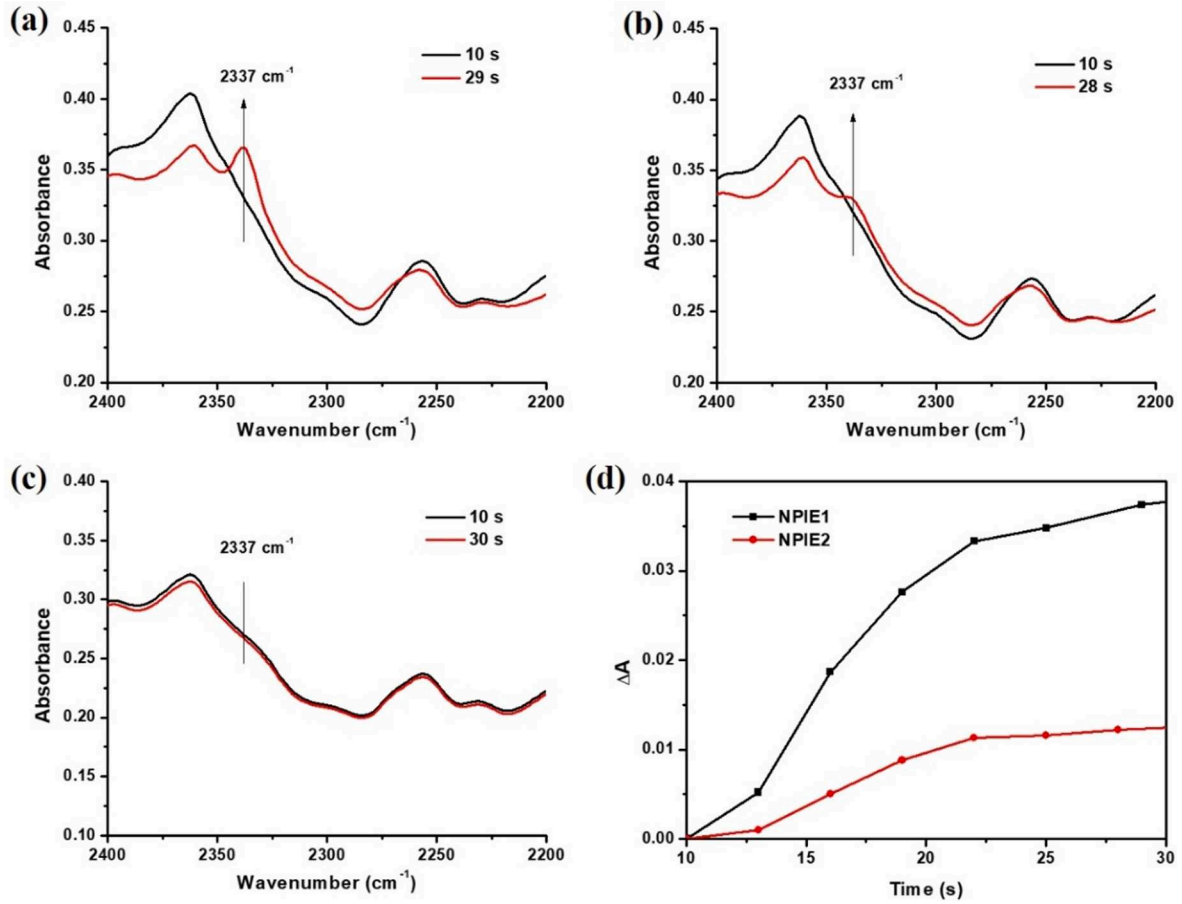

Fig. 31. Infrared spectra of PI/TMPTA in photopolymerization experiments at different times (a) **NPIE1**/TMPTA; (b) **NPIE2**/TMPTA; (c) **NPIMO**/TMPTA; (d) The curve of absorption intensity of CO_2 obtained with the **NPIE1**/TMPTA and **NPIE2**/TMPTA systems ($A = A_t - A_0$, where A_t is the absorbance intensity at t s; A_0 is the absorbance intensity before irradiation (at $t = 10$ s)). Reproduced with permission of Ref. [73].

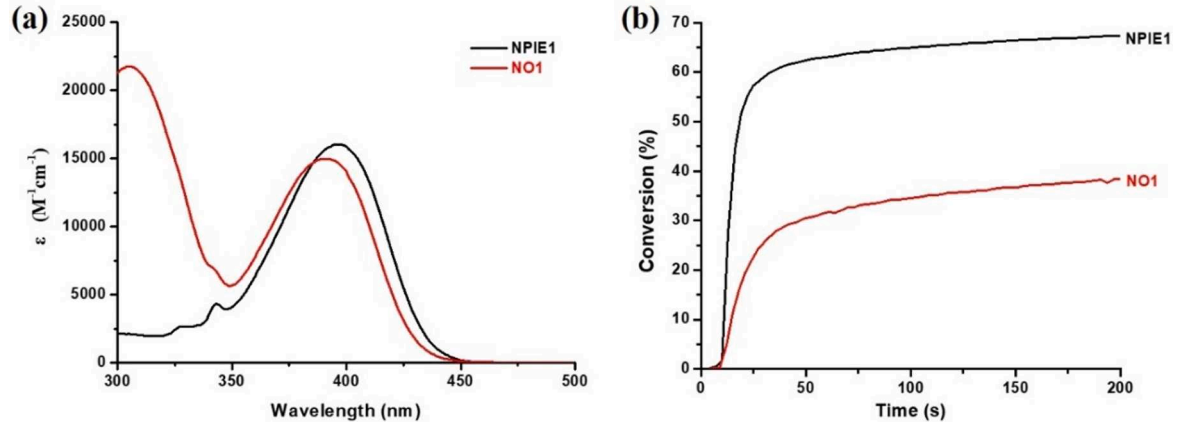

Fig. 32. (a) UV–visible absorption spectra of **NPIE1** and **NO1**; (b) Photopolymerization profiles of TMPTA in laminate (~25 μm) upon exposure to a LED@405 nm in the presence of **NPIE1** and **NO1** (2×10^{-5} mol/g TMPTA). The irradiation starts at t = 10 s. Reproduced with permission of Ref. [72].

Scheme 16. Key steps in OXE photoinitiation efficiency.

esters is another factor to take into account while designing oxime esters. In fact, compared to dyes for which a triplet pathway is found, recent investigations have shown that the singlet deexcitation pathway improves the photocleavage efficiency as well as the monomer conversion.

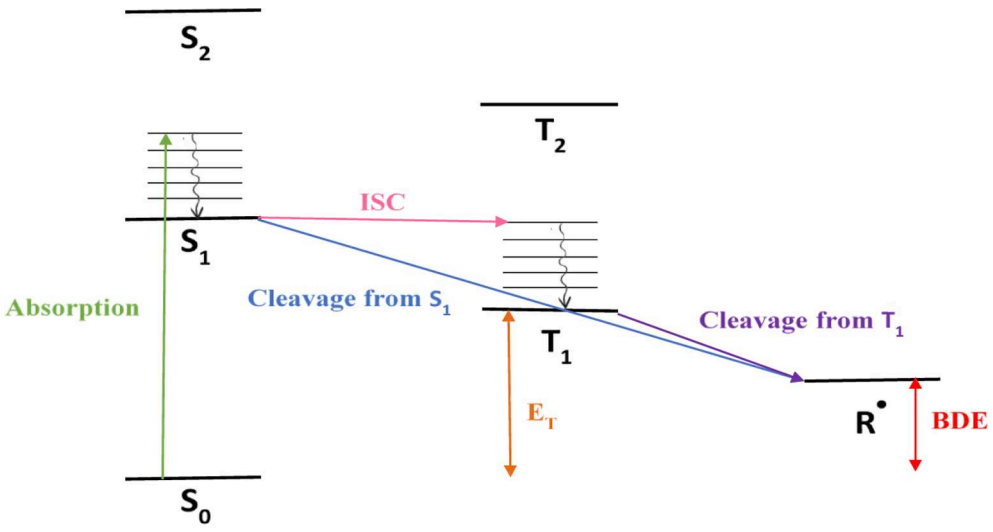

Scheme 17. Jablonski Diagram for cleavage from either S_1 or T_1.

Table 18
Some parameters characterizing the cleavage process of the N − O bond.

Chromophore	N − O BDE (kcal mol^{-1})	$\Delta H_{cleavage\ S1}$ [a] (kcal mol^{-1})	$\Delta H_{cleavage\ T1}$ [a] (kcal mol^{-1})	τ_0 (ns)
Triphenylamine	53 ↔ 57	−14.5 ↔ -21.25	−0.3 ↔ -8.5	1.25 ↔ 1.5
Coumarin	42 ↔ 50.5	−17 ↔ -10.6	−5 ↔ 6	1.6 ↔ 1.9
Carbazole	41 ↔ 44	–32.5 ↔ -26.5	−21 ↔ -5	1.4 ↔ 3.85
Pyrene	43 ↔ 47	–23.85	4 ↔ 6	2.5 ↔ 4
Anthracene	41 ↔ 48	−21.5	5 ↔ 12.5	1.5 ↔ 4.5
Phenothiazine	54 ↔ 54.5	−9 ↔ -11	5.6	7 ↔ 7.65

[a] $\Delta H_{cleavage\ S1/T1} = BDE(N-O) - E_{S1}/E_{T1}$.

Table 19
Final acrylate function conversion (FCs) after 100 s of irradiation with LED light (λ = 405 nm) in laminate.

Chromophore	Final acrylate function conversion (FCs) Thin sample (25 μm) in laminate
Triphenylamine	35 % ↔ 75 % [a]
Coumarin	35 % ↔ 75 % [a]
Carbazole	35 % ↔ 85 % [a]
Pyrene	15 % ↔ 80 % [b]
Anthracene	0 % ↔ 50 % [b]
Phenothiazine	15 % ↔ 55 % [b]

[a] TMPTA based system.
[b] TA based system.

Declaration of Competing Interest

The authors declare that they have no known competing financial interests or personal relationships that could have appeared to influence the work reported in this paper.

Data availability

Data will be made available on request.

References

[1] P. Garra, C. Dietlin, F. Morlet-Savary, F. Dumur, D. Gigmes, J.P. Fouassier, J. Lalevée, Photopolymerization processes of thick films and in shadow areas: a review for the access to composites, Polym. Chem. 8 (46) (2017) 7088–7101.
[2] J.P. Fouassier, J. Lalevée, Photoinitiators: Structures, Reactivity and Applications in Polymerization, Wiley, Weinhein, 2021.
[3] J.P. Fouassier, Photoinitiation, Photopolymerization, and Photocuring: Fundamentals and Applications, Hanser Publishers, New York, 1995.
[4] Y. Yagci, S. Jockusch, N.J. Turro, Photoinitiated polymerization: advances, challenges, and opportunities, Macromolecules 43 (2010) 6245–6260.
[5] J. Lalevée, J. P. Fouassier, Dye Photosensitized Polymerization Reactions: Novel Perspectives, RSC Photochemistry Reports, Ed. A. Albini, E. Fasani, Photochemistry, London, UK, 2015, 42, 215–232.
[6] K. Dietliker, T. Jung, J. Benkhoff, H. Kura, A. Matsumoto, H. Oka, D. Hristova, G. Gescheidt, G. Rist, New developments in photoinitiators, Macromolecular Symposia. Weinheim : WILEY-VCH Verlag, 2004, 217.1, 77-98.
[7] M.A. Tehfe, F. Dumur, B. Graff, F. Morlet-Savary, D. Gigmes, J.P. Fouassier, J. Lalevée, Design of new Type I and Type II photoinitiators possessing highly coupled pyrene–ketone moieties, Polym. Chem. 4 (7) (2013) 2313–2324.
[8] A. Kowalska, J. Sokolowski, K. Bociong, The photoinitiators used in resin based dental composite—a review and future perspectives, Polymers 13 (3) (2021) 470.
[9] M. Abdallah, D. Magaldi, A. Hijazi, B. Graff, F. Dumur, J.P. Fouassier, T.T. Bui, F. Goubard, J. Lalevée, Development of New High-Performance Visible Light Photoinitiators Based on Carbazole Scaffold and Their Applications in 3D Printing and Photocomposite Synthesis, J. Polym. Sci. A Polym. Chem. 57 (2019) 2081–2092.
[10] J. Lalevée, H. Mokbel, J.-P. Fouassier, Recent Developments of Versatile Photoinitiating Systems for Cationic Ring Opening Polymerization Operating at Any Wavelengths and under Low Light Intensity Sources, Molecules 20 (2015) 7201–7221.
[11] P. Xiao, F. Dumur, B. Graff, J.P. Fouassier, D. Gigmes, J. Lalevée, Cationic and Thiol-Ene Photopolymerization upon Red Lights Using Anthraquinone Derivatives as Photoinitiators, Macromolecules 46 (2013) 6744–6750.
[12] C. Dietlin, S. Schweizer, P. Xiao, J. Zhang, F. Morlet-Savary, B. Graff, J. P. Fouassier, J. Lalevée, Photopolymerization upon LEDs: new photoinitiating systems and strategies, Polym. Chem. 6 (21) (2015) 3895–3912.
[13] X. Peng, D. Zhu, P. Xiao, Naphthoquinone derivatives: Naturally derived molecules as blue-light-sensitive photoinitiators of photopolymerization, Eur. Polym. J. 127 (2020), 109569.
[14] M.M. Abdul-Monem, Naturally Derived Photoinitiators for Dental and Biomaterials Applications, Eur. Dental Res. Biomater. J. 1 (02) (2020) 72–78.
[15] C.-H. Chen, Y. Wang, T. Michinobu, S.-W. Chang, Y.-C. Chiu, C.-Y. Ke, G.-S. Liou, Donor-Acceptor Effect of Carbazole-Based Conjugated Polymer Electrets on Photoresponsive Flash Organic Field-Effect Transistor Memories, ACS Appl. Mater. Interfaces 12 (2020) 6144–6150.
[16] A. Bagheri, J. Jin, Photopolymerization in 3D Printing, ACS Appl. Polym. Mater. 1 (2019) 593–611.
[17] M. Topa, J. Ortyl, Moving Towards a Finer Way of Light-Cured Resin-Based Restorative Dental Materials: Recent Advances in Photoinitiating Systems Based on Iodonium Salts, Materials 13 (2020) 4093.
[18] E. Andrezajewska, K. Grajek, Recent advances in photo-induced free-radical polymerization, MOJ Polymer Science 1 (2017) 58–60.
[19] F. Yoshino, A. Yoshida, Effects of blue-light irradiation during dental treatment, Japan. Dental Sci. Rev. 54 (2018) 160–168.
[20] H. Arikawa, H. Takahashi, T. Kanie, S. Ban, Effect of various visible light photoinitiators on the polymerization and color of light-activated resins, Dent. Mater. J. 28 (2009) 454–460.
[21] N. Corrigan, J. Yeow, P. Judzewitsch, J. Xu, C. Boyer, Seeing the Light: Advancing Materials Chemistry through Photopolymerization, Angew. Chem. Int. Ed. 58 (2019) 5170–5189.
[22] M. Schmitt, Synthesis and testing of ZnO nanoparticles for photo-initiation: Experimental observation of two different non-migration initiators for bulk polymerization, Nanoscale 7 (2015) 9532–9544.

[23] E. Vessally, H. Saeidian, A. Hosseinian, L. Edjlali, A. Bekhradnia, A review on synthetic applications of oxime esters, Curr. Org. Chem. 21 (3) (2017) 249–271.
[24] D. Wang, S. Ren, H. Wang, H. Yan, J. Feng, X. Zhang, Semisynthesis and antifungal activity of novel oxime ester derivatives of carabrone modified at C (4) against Botrytis cinerea, Chem. Biodivers. 11 (6) (2014) 886–903.
[25] J. Xu, G. Ma, K. Wang, J. Gu, S. Jiang, J. Nie, Synthesis and photopolymerization kinetics of oxime ester photoinitiators, J. Appl. Polym. Sci. 123 (2) (2012) 725–731.
[26] Y. Gao, J. Song, S. Shang, D. Wang, J. Li, Synthesis and antibacterial activity of oxime esters from dihydrocumic acid, BioResources 7 (3) (2012) 4150–4160.
[27] B. Kraeutler, C.D. Jaeger, A.J. Bard, Direct Observation of Radical Intermediates in Photo-Kolbe Reaction - Heterogeneous Photocatalytic Radical Formation by Electron-Spin Resonance, J. Am. Chem. Soc. 100 (15) (1978) 4903–4905.
[28] W. Qiu, J. Zhu, K. Dietliker, Z. Li, Polymerizable Oxime Esters: An Efficient Photoinitiator with Low Migration Ability for 3D Printing to Fabricate Luminescent Devices, ChemPhotoChem 4 (11) (2020) 5296–5303.
[29] D.E. Fast, A. Lauer, J.P. Menzel, A.M. Kelterer, G. Gescheidt, C. Barner-Kowollik, Wavelength-Dependent Photochemistry of Oxime Ester Photoinitiators, Macromolecules 50 (2017) 1815–1823.
[30] F. Dumur, Recent advances on visible light Triphenylamine-based photoinitiators of polymerization, Eur. Polym. J. 166 (2022), 111036.
[31] D. Ladika, G. Noirbent, F. Dumur, D. Gigmes, A. Mourka, M.G.D. Barmparis, M. Farsari, D. Gray, Synthesis and application of triphenylamine-based aldehydes as photo-initiators for multi-photon lithography, Appl. Phys. A 128 (9) (2022) 1–8.
[32] M. Abdallah, F. Dumur, B. Graff, A. Hijazi, J. Lalevée, High performance dyes based on triphenylamine, cinnamaldehyde and indane-1, 3-dione derivatives for blue light induced polymerization for 3D printing and photocomposites, Dyes Pigm. 182 (2020), 108580.
[33] Y.H. Li, Y.C. Chen, Triphenylamine-hexaarylbiimidazole derivatives as hydrogen-acceptor photoinitiators for free radical photopolymerization under UV and LED light, Polym. Chem. 11 (8) (2020) 1504–1513.
[34] S.C. Yen, Z.H. Lee, J.S. Ni, C.C. Chen, Y.C. Chen, Effect of number and position of methoxy substituents on triphenylamine-based chalcone visible-light-absorbing photoinitiators, Polym. Chem. 13 (25) (2022) 3780–3789.
[35] Z.H. Lee, F. Hammoud, A. Hijazi, B. Graff, J. Lalevée, Y.C. Chen, Synthesis and free radical photopolymerization of triphenylamine-based oxime ester photoinitiators, Polym. Chem. 12 (2021) 1286–1297.
[36] F. Hammoud, Z.H. Lee, B. Graff, A. Hijazi, J. Lalevée, Y.C. Chen, Novel phenylamine-based oxime ester photoinitiators for LED-induced free radical, cationic, and hybrid polymerization, J. Polym. Sci. 59 (2021) 1711–1723.
[37] F. Dumur, Recent advances on coumarin-based photoinitiators of polymerization, Eur. Polym. J. 163 (2021), 110962.
[38] M. Rahal, B. Graff, J. Toufaily, T. Hamieh, F. Dumur, J. Lalevée, Design of keto-coumarin based photoinitiator for Free Radical Photopolymerization: Towards 3D printing and photocomposites applications, Eur. Polym. J. 154 (2021), 110559.
[39] M. Abdallah, A. Hijazi, J.T. Lin, B. Graff, F. Dumur, J. Lalevée, Coumarin derivatives as photoinitiators in photo-oxidation and photo-reduction processes and a kinetic model for simulations of the associated polymerization profiles, ACS Appl. Polym. Mater. 2 (7) (2020) 2769–2780.
[40] Z. Li, X. Zou, G. Zhu, X. Liu, R. Liu, Coumarin-based oxime esters: photobleachable and versatile unimolecular initiators for acrylate and thiol-based click photopolymerization under visible light-emitting diode light irradiation, ACS Appl. Mater. Interfaces 10 (18) (2018) 16113–16123.
[41] W. Qiu, M. Li, Y. Yang, Z. Li, K. Dietliker, Cleavable coumarin-based oxime esters with terminal heterocyclic moieties: photobleachable initiators for deep photocuring under visible LED light irradiation, Polym. Chem. 11 (7) (2020) 1356–1363.
[42] F. Hammoud, N. Giacoletto, G. Noirbent, B. Graff, A. Hijazi, M. Nechab, D. Gigmes, F. Dumur, J. Lalevée, Substituent Effects on Photoinitiation Ability of Coumarin-Based Oxime Ester Photoinitiators for Free Radical Photopolymerization, Mater. Chem. Front. 5 (2021) 8361–8370.
[43] J. Barth, M. Buback, P. Hesse, T. Sergeeva, Termination and Transfer Kinetics of Butyl Acrylate Radical Polymerization Studied via SP-PLP-EPR, Macromolecules 43 (9) (2010) 4023–4031.
[44] F. Dumur, Recent advances on carbazole-based photoinitiators of polymerization, Eur. Polym. J. 125 (2020), 109503.
[45] F. Dumur, Recent advances on carbazole-based oxime esters as photoinitiators of polymerization, Eur. Polym. J. 111330 (2022).
[46] S. Liu, D. Brunel, K. Sun, Y. Xu, F. Morlet-Savary, B. Graff, P. Xiao, F. Dumur, J. Lalevée, A monocomponent bifunctional benzophenone–carbazole type II photoinitiator for LED photoinitiating systems, Polym. Chem. 11 (21) (2020) 3551–3556.
[47] S. Liu, B. Graff, P. Xiao, F. Dumur, J. Lalevée, Nitro-Carbazole Based Oxime Esters as Dual Photo/Thermal Initiators for 3D Printing and Composite Preparation, Macromol. Rapid Commun. 42 (15) (2021) 2100207.
[48] S. Liu, N. Giacoletto, M. Schmitt, M. Nechab, B. Graff, F. Morlet-Savary, P. Xiao, J. Lalevée, Effect of Decarboxylation on the Photoinitiation Behavior of Nitrocarbazole-Based Oxime Esters, Macromolecules 55 (7) (2022) 2475–2485.
[49] F. Hammoud, N. Giacoletto, M. Nechab, B. Graff, A. Hijazi, F. Dumur, J. Lalevée, 5, 12-Dialkyl-5, 12-dihydroindolo [3, 2-a] carbazole-Based Oxime-Esters for LED Photoinitiating Systems and Application on 3D Printing, Macromol. Mater. Eng. 307 (8) (2022) 2200082.
[50] Z.H. Lee, S.C. Yen, F. Hammoud, A. Hijazi, B. Graff, J. Lalevée, Y.C. Chen, Naphthalene-Based Oxime Esters as Type I Photoinitiators for Free Radical Photopolymerization, Polymers 14 (23) (2022) 5261.
[51] F. Dumur, Recent advances on pyrene-based photoinitiators of polymerization, Eur. Polym. J. 126 (2020), 109564.
[52] S. Telitel, F. Dumur, T. Faury, B. Graff, M.A. Tehfe, D. Gigmes, J.P. Fouassier, J. Lalevée, New core-pyrene π structure organophotocatalysts usable as highly efficient photoinitiators, Beilstein J. Org. Chem. 9 (1) (2013) 877–890.
[53] J.V. Crivello, F. Jiang, Development of pyrene photosensitizers for cationic photopolymerizations, Chem. Mater. 14 (11) (2002) 4858–4866.
[54] M.V. Encinas, E.A. Lissi, C. Majmud, J.J. Cosa, Photopolymerization in aqueous solutions initiated by the interaction of excited pyrene derivatives with aliphatic amines, Macromolecules 26 (23) (1993) 6284–6288.
[55] A. Mishra, S. Daswal, Copolymerization of n-butylacrylate with methylmethacrylate by a novel photoinitiator, 1-(bromoacetyl) pyrene, Int. J. Chem. Kinet. 39 (5) (2007) 261–267.
[56] M.V. Encinas, C. Majmud, J. Garrido, E.A. Lissi, Methyl methacrylate polymerization photoinitiated by pyrene in the presence of triethylamine, Macromolecules 22 (2) (1989) 563–566.
[57] F. Dumur, Recent advances on anthracene-based photoinitiators of polymerization, Eur. Polym. J. 169 (2022), 111139.
[58] D.K. Balta, N. Arsu, Y. Yagci, S. Jockusch, N.J. Turro, Thioxanthone− anthracene: A new photoinitiator for free radical polymerization in the presence of oxygen, Macromolecules 40 (12) (2007) 4138–4141.
[59] D.T. Beyazit, B. Gacal, Y. Yagci, An amphipathic thioxanthone-anthracene photoinitiator for free-radical polymerization, Turk. J. Chem. 37 (4) (2013) 525–537.
[60] J.V. Crivello, M. Jang, Anthracene electron-transfer photosensitizers for onium salt induced cationic photopolymerizations, J. Photochem. Photobiol. A Chem. 159 (2) (2003) 173–188.
[61] M. Rahal, H. Bidotti, S. Duval, B. Graff, T. Hamieh, J. Toufaily, F. Dumur, J. Lalevée, Investigation of pyrene vs Anthracene-based oxime esters: Role of the excited states on their polymerization initiating abilities, Eur. Polym. J. 177 (2022), 111452.
[62] F. Dumur, Recent advances on visible light Phenothiazine-based photoinitiators of polymerization, Eur. Polym. J. 165 (2022) 110999–111021.
[63] L. Deng, L. Tang, J. Qu, Novel chalcone-based phenothiazine derivative photoinitiators for visible light induced photopolymerization with photobleaching and good biocompatibility, Prog. Org. Coat. 167 (2022), 106859.
[64] Z. Gomurashvili, J.V. Crivello, Monomeric and polymeric phenothiazine photosensitizers for photoinitiated cationic polymerization, Macromolecules 35 (8) (2002) 2962–2969.
[65] Z. Gomurashvili, J.V. Crivello, Phenothiazine photosensitizers for onium salt photoinitiated cationic polymerization, J. Polym. Sci. A Polym. Chem. 39 (8) (2001) 1187–1197.
[66] M. Rahal, M. Abdallah, T.T. Bui, F. Goubard, B. Graff, F. Dumur, J. Toufaily, T. Hamieh, J. Lalevée, Design of new phenothiazine derivatives as visible light photoinitiators, Polym. Chem. 11 (19) (2020) 3349–3359.
[67] M. Li, B. Bao, J. You, Y. Du, D. Li, H. Zhan, L. Zhang, T. Wang, Phenothiazine derivatives based on double benzylidene ketone structure: Application to red light photopolymerization, Prog. Org. Coat. 173 (2022), 107217.
[68] J.P. Fouassier, F. Morlet-Savary, J. Lalevée, X. Allonas, C. Ley, Dyes as photoinitiators or photosensitizers of polymerization reactions, Materials 3 (12) (2010) 5130–5142.
[69] F. Hammoud, A. Pavlou, A. Petropoulos, B. Graff, M.G. Siskos, A. Hijazi, F. Morlet-Savary, F. Dumur, J. Lalevée, Naphthoquinone-based imidazolyl esters as blue-light-sensitive Type I photoinitiators, Polym. Chem. 13 (2022) 4817–4831.
[70] G. Noirbent, F. Dumur, Recent advances on naphthalic anhydrides and 1, 8-naphthalimide-based photoinitiators of polymerization, Eur. Polym. J. 132 (2020), 109702.
[71] P. Xiao, F. Dumur, M. Frigoli, M.A. Tehfe, B. Graff, J.P. Fouassier, D. Gigmes, J. Lalevée, Naphthalimide based methacrylated photoinitiators in radical and cationic photopolymerization under visible light, Polym. Chem. 4 (21) (2013) 5440–5448.
[72] J. Yang, C. Xu, Y. Xiong, X. Wang, Y. Xie, Z. Li, H. Tang, A green and highly efficient naphthalimide visible photoinitiator with an ability initiating free radical polymerization under air, Macromol. Chem. Phys. 219 (24) (2018) 1800256.
[73] S. Liu, N. Giacoletto, B. Graff, F. Morlet-Savary, M. Nechab, P. Xiao, F. Dumur, J. Lalevée, N-naphthalimide ester derivatives as Type I photoinitiators for LED photopolymerization, Mater. Today Chem. 26 (2022), 101137.

Chapitre II : Photoamorceurs Type I : Analogues d'Oxime-Esters

Les métabolites fonctionnels basés sur les dérivés de naphtoquinone (NQ) peuvent être trouvés dans une variété de sources dans la nature, y compris les plantes, les bactéries et les espèces marines. [1-5] Ils sont facilement disponibles et faciles à obtenir sans procédures synthétiques complexes et ces composés sont également bien connus pour leurs propriétés anti-cancérigènes. [2-3] En outre, divers groupes fonctionnels peuvent être ajoutés à la structure de la naphtoquinone, ce qui permet de modifier considérablement l'absorption de la lumière et notamment de déplacer leur absorption vers des longueurs d'onde plus importantes. Notamment, les naphtoquinones n'ont jamais été étudiées en tant que photoamorceurs de Type I auparavant. Par conséquent, l'étude de la naphtoquinone pour la conception de systèmes photoamorceurs et l'examen de l'impact des variations structurelles sur leurs capacités photoamorçantes sont donc passionnants et importants.

Dans ce chapitre, une classe originale de naphtoquinone-esters (les esters de 4,9-dioxo-2-phényl-4,9-dihydro-1H-naphto[2,3-d]imidazol-1-yl) a été étudiée et proposée en tant que PA de Type I à haute performance. Afin de préparer facilement cette série d'esters d'imidazolyle, différents chlorures d'acide ont été utilisés pour générer les différents esters avec la 1-hydroxy-2-phényl-1H-naphto[2,3-d]imidazole-4,9-dione. Cette famille d'esters d'imidazolyle, dont la structure est comparable à celle de la famille bien connue des oxime-esters, est également capable de produire un clivage homolytique de la liaison N-O sous irradiation. Une décarboxylation peut également se produire après le clivage, générant des radicaux aryles ou alkyles amorceurs. Compte tenu de la similitude des structures entre les esters d'imidazolyle et les oxime-esters, l'étude de cette nouvelle classe de PA et la comparaison aux oxime-esters ou aux oxydes de phosphine bien connus (par exemple, TPO) étaient très importantes pour nous. Leur capacité à amorcer un processus de photopolymérisation dans des conditions douces (faible intensité lumineuse à l'aide de LED émettant à 405 nm ou 455 nm) a été étudiée. Une autre indication de leur grande réactivité est la possibilité de les utiliser dans des résines d'impression 3D photosensibles. La synthèse de ces nouvelles structures a été faite par nos collaborateurs de l'Université d'Aix-Marseille (Dr. Frédéric Dumur). Ce travail a été publié dans "Polymer Chemistry" sous la citation suivante : Hammoud F. et al. "Naphthoquinone-based imidazolyl esters as blue-light-sensitive Type I photoinitiators", Polymer Chemistry, 2022, 13.33, 4817-4831.

Références

[1] X. Peng, D. Zhu, P. Xiao, Naphthoquinone derivatives: Naturally derived molecules as blue-light-sensitive photoinitiators of photopolymerization, European Polymer Journal, 2020, 127, 109569.

[2] M. M. Abdul-Monem, Naturally Derived Photoinitiators for Dental and Biomaterials Applications, European Dental Research and Biomaterials Journal, 2020, 1.02, 72-78.

[3] R. Strzelczyk, R. Podsiadły, Derivatives of 1, 4-naphthoquinone as visible-light-absorbing one-component photoinitiators for radical polymerization, Coloration Technology, 2015, 131.3, 229-235.

[4] G. Noirbent, F. Dumur, Photoinitiators of polymerization with reduced environmental impact: Nature as an unlimited and renewable source of dyes, European Polymer Journal, 2021, 142, 110109.

[5] A. M. Szymczak, R. Podsiadły, K. Podemska, J. Sokołowska, Dyes based on a 1, 4-naphthoquinone skeleton as new type II photoinitiators for radical polymerization, Coloration Technology, 2013, 129.4, 284-288.

Polymer Chemistry

ROYAL SOCIETY OF CHEMISTRY

PAPER

View Article Online
View Journal | View Issue

Cite this: *Polym. Chem.*, 2022, **13**, 4817

Naphthoquinone-based imidazolyl esters as blue-light-sensitive Type I photoinitiators†

Fatima Hammoud, [a,b,c] Aristea Pavlou,[d] Alexandros Petropoulos,[d] Bernadette Graff,[a,b] Michael G. Siskos,[d] Akram Hijazi,[c] Fabrice Morlet-Savary,[a,b] Frédéric Dumur *[e] and Jacques Lalevée *[a,b]

Received 13th June 2022,
Accepted 29th July 2022

DOI: 10.1039/d2py00753c

rsc.li/polymers

In this work, a series of Type I photoinitiators (PIs), based on the naphthoquinone scaffold, were designed and synthesized for the first time in order to induce photopolymerization under visible light. As a result, these PIs exhibit excellent photoinitiation abilities in the presence of acrylate monomers upon LED@405 or @455 nm irradiation. Interestingly, some compounds have better photoinitiation performance than the benchmark Type I phosphine-oxide, *i.e.* diphenyl(2,4,6-trimethylbenzoyl)phosphine oxide (TPO) upon exposure to LED@455 nm. Chemical mechanisms supporting the photopolymerization process were investigated through different techniques as well as theoretical calculations. In addition, the newly proposed structures were also investigated in two-component photoinitiating systems and exhibited a higher efficiency in free radical photopolymerization. Finally, a direct laser writing approach was successfully used to fabricate 3D objects.

1. Introduction

The process of light-induced polymerization is a field that has attracted a lot of interest in the past few years due to its several environmental benefits, including low energy consumption, low or no volatile organic emissions and high efficiency.[1–3] Consequently, this technology is now extensively used for a large number of industrial applications such as 3D printing, adhesives, coatings, and dentistry.[4–6] Indeed, photoinitiators (PIs) are one of the main components for the initiation of photopolymerization reactions since the nature of the PI (*i.e.* its light absorption properties) determines the types of light sources that will be used. They can work as cleavable (Type I PIs) or uncleavable (Type II PIs, based on PI/hydrogen or electron donor couple) compounds.[7–9] However, Type II PIs can be easily influenced by the solubility, the electron transfer efficiency or the resin viscosity, all of which can negatively affect the efficacy of the different bimolecular interactions.[10] Conversely, Type I PIs generate reactive radicals by a direct homolytic bond cleavage without any hydrogen donors (co-initiators), which is beneficial in overcoming the drawbacks of Type II PIs.[10–12]

Although the majority of Type I PIs are sensitive in the UV range, a few PIs such as amino-acteophenones (*e.g.* Irgacure 369) and phosphine oxides such as diphenyl(2,4,6-trimethylbenzoyl)phosphine oxide (TPO) could be activated by excitation at 405 nm.[13–15] Therefore, for mild conditions, the search for new Type I PIs, which are capable of absorbing light at longer wavelengths, has been attracting more and more attention these last few years.

Light-emitting diodes (LEDs) are a valuable alternative to the traditional irradiation systems due to their low cost, compactness, light weight and extended lifetime.[16–18] Some Type I PIs have recently been reported in this context.[19–22]

Naphthoquinone derivatives are well-established bio-sourced chromophores in plants, marine organisms or microbes, *etc.* Interestingly, they can be collected easily without sophisticated synthetic procedures. Studies on naphthoquinone derivatives as Type II PIs (multicomponent photoinitiating systems) were reported recently.[23–25]

In the present work, a series of naphthoquinone esters, namely 4,9-dioxo-2-phenyl-4,9-dihydro-1*H*-naphtho[2,3-*d*]imidazol-1-yl esters, never synthesized previously according to the literature, were investigated and proposed as high-performance Type I PIs (see Scheme 1). More precisely, various acid chlorides could be used to form esters with 1-hydroxy-2-phenyl-1*H*-naphtho[2,3-*d*] imidazole-4,9-dione, enabling the facile preparation of a series of imidazolyl esters. It is noticeable that this series of imidazolyl esters is unprecedented in the literature and can be compared to the well-known oxime ester PIs that are capable of initiating the

[a]*Université de Haute-Alsace, CNRS, IS2M UMR7361, F-68100 Mulhouse, France. E-mail: jacques.lalevee@uha.fr*
[b]*Université de Strasbourg, France*
[c]*EDST, Université Libanaise, Campus Hariri, Hadath, Beyrouth, Liban*
[d]*Department of Chemistry, Section of Organic Chemistry and Biochemistry, University of Ioannina, Ioannina, 45110, Greece*
[e]*Aix Marseille Univ, CNRS, ICR UMR 7273, F-13397 Marseille, France. E-mail: Frederic.dumur@univ-amu.fr*

† Electronic supplementary information (ESI) available. See DOI: https://doi.org/10.1039/d2py00753c

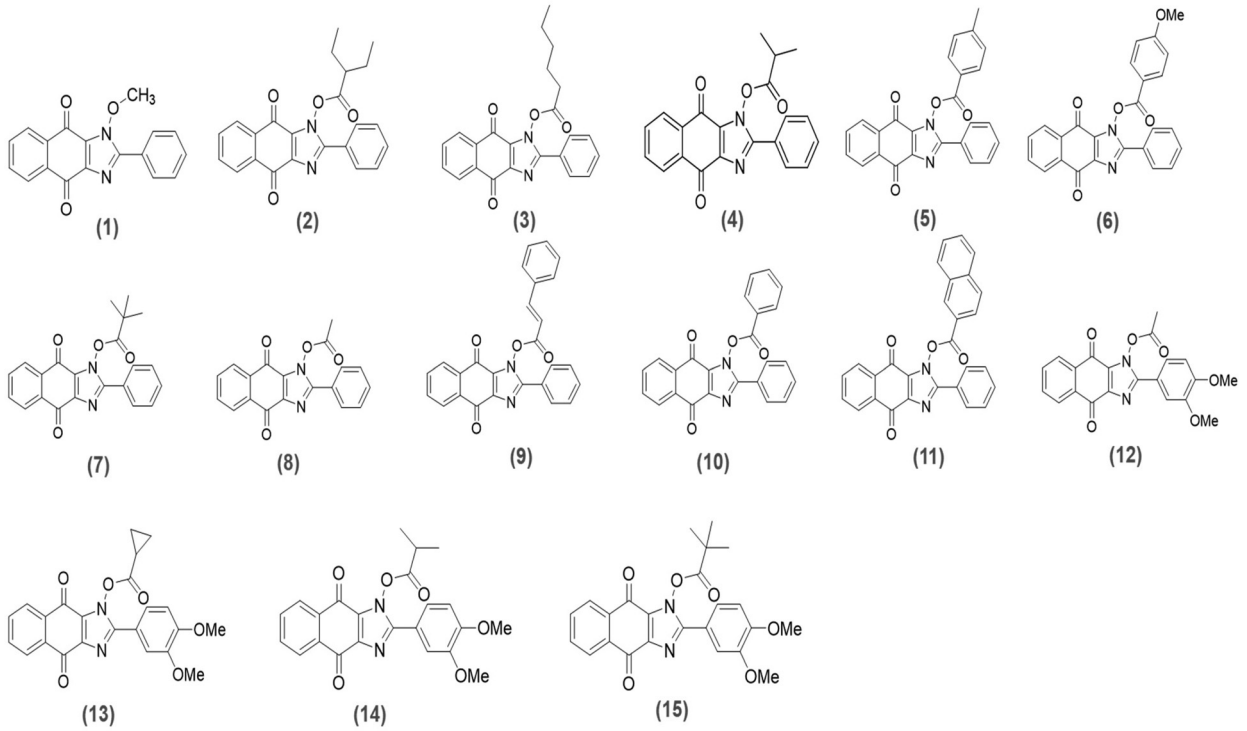

Scheme 1 Chemical structures of the synthesized naphthoquinone-based imidazolyl esters.

cleavage of the N–O bond upon irradiation. Following cleavage, a decarboxylation reaction may also occur, producing initiating aryl or alkyl radicals. It appeared to us to be of interest to investigate this new family of PIs and to examine the possibility of imidazolyl esters behaving as high-performance PIs in comparison with oxime esters or well-established phosphine-oxides (*e.g.* TPO; Scheme 2). Their photoinitiating ability under mild conditions (low intensity and LED@405 nm or 455 nm) was investigated. Their potential use in photosensitive 3D printing resins is also presented as proof of high reactivity.

2. Experimental part

2.1. Other chemical compounds

Bis-(4-*tert*-butylphenyl)iodonium hexafluorophosphate (Iod), diphenyl(2,4,6-trimethylbenzoyl)phosphine oxide (TPO) and ethyl 4-dimethylaminobenzoate (EDB) were obtained from Lambson Ltd (UK) (Scheme 2). Camphorquinone (CQ, Scheme 2) was obtained from Sigma Aldrich. The monomer di (trimethylolpropane)tetraacrylate (TA) or urethane dimethacrylate (UDMA) was obtained from Allnex (Scheme 2).

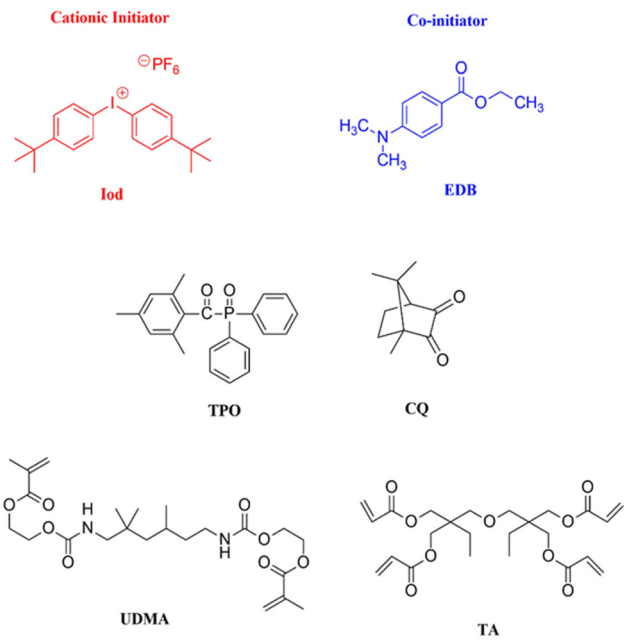

Scheme 2 Chemical structures of the additives and monomers used.

2.2. Irradiation source

Different light emitting diodes (LEDs) were used as irradiation sources (emission spectra are shown in Fig. S1†): (i) λ_{em} = 455 nm (labeled as LED@455 nm, with a light intensity I_0 = 100 mW cm^{-2}); (ii) λ_{em} = 405 nm (labeled as LED@405 nm, with a light intensity I_0 = 110 mW cm^{-2}); and (iii) λ_{em} = 375 nm (labeled as LED@375 nm, with a light intensity I_0 = 40 mW cm^{-2}).

2.3. UV-visible absorption and photolysis experiments

The light absorption properties of PIs as well as their photolysis abilities were investigated by UV-Vis spectroscopy as presented by the authors[19] (see more details in the ESI†).

2.4. Photopolymerization kinetics (RT-FTIR)

The polymerization kinetics were followed under different experimental conditions (see the figure captions) by real-time FTIR (RT-FTIR) spectroscopy (JASCO FTIR 4600) as presented by the authors[26,27] (see more details in the ESI†).

2.5. Computational procedure

The bond dissociation energies (BDE), the excited state energy levels and the absorption properties of the different PIs were calculated using the Gaussian 16 suite of programs as presented by the authors[19] (see more details in the ESI†).

2.6. Fluorescence experiments

The properties of the first singlet excited state (S_1) were probed by steady state fluorescence as well as time-correlated single photon counting (TCSPC) as presented by the authors[19] (see more details in the ESI†).

2.7. ESR spin-trapping (ESR-ST) experiments

The free radicals generated were characterized by ESR-ST experiments (an X-band spectrometer; Bruker EMX-plus) as presented by the authors[19] (see more details in the ESI†). The free radicals generated were trapped by phenyl-*N*-*tert*-butylnitrone (PBN) based on a procedure described in the literature.[26,27] After the end of the experiment, some ESR simulations were carried out using the PEST WINSIM program.

2.8. Direct laser writing

To characterize the spatial control of the reaction, direct laser writing experiments were performed using a laser diode @405 nm (spot size around 50 μm) (see more details in the ESI†). The generated 3D patterns were analyzed using a numerical optical microscope as presented in ref. 19.

3. Results and discussion

3.1. Synthesis of the dyes

All dyes were prepared using 1,4-naphthoquinone (C1) as the starting material (see Scheme 3). Following reaction with benzylamine (C2) and 3,4-dimethoxybenzylamine (C3), products 2-(benzylamino)naphthalene-1,4-dione (C4) and 2-((3,4-dimethoxylbenzyl)amino) naphthalene-1,4-dione (C5) were

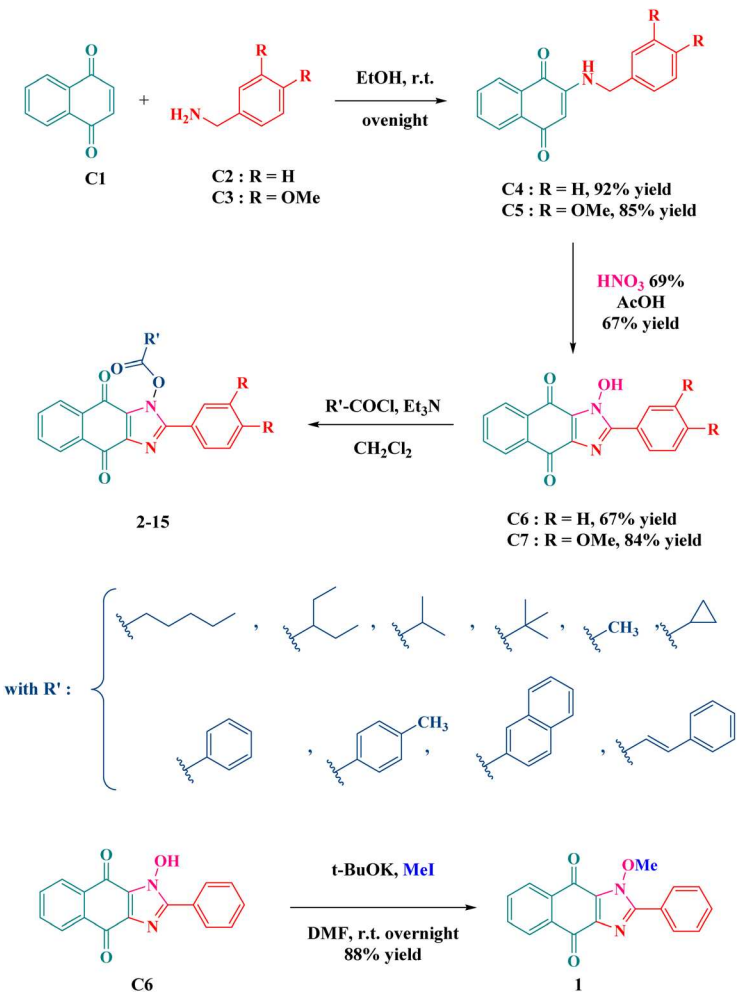

Scheme 3 Synthetic routes to the different dyes.

afforded in 92 and 85% yields, respectively. Using a cyclization reaction previously reported by Lavrikova and coworkers,[28] completed in acetic acid, and following treatment with a mixture of nitric and sulfuric acids, 1-hydroxy-2-phenyl-1*H*-naphtho[2,3-*d*]imidazole-4,9-dione (C6) and 2-(3,4-dimethoxyphenyl)-1-hydroxy-1*H*-naphtho[2,3-*d*]imidazole-4,9-dione (C7) could be obtained in 67 and 84% yields, respectively. 1-Hydroxy-2-phenyl-1*H*-naphtho[2,3-*d*]imidazole-4,9-dione derivatives C6 and C7 were then esterified with different acid chlorides using triethylamine as the base, providing compounds **2–15**. Using this strategy, molecules that can be considered analogues of oxime esters were obtained. For comparison, a molecule bearing a non-cleavable group was prepared. Thus, upon alkylation of C6 with iodomethane in DMF at room temperature and by using potassium *tert*-butoxide as the base, 1-methoxy-2-phenyl-1*H*-naphtho[2,3-*d*]imidazole-4,9-dione (1) could be isolated in pure form in 88% yield.

3.2. UV-visible absorption

UV-visible absorption spectra of the studied derivatives (Fig. 1) were acquired in acetonitrile (ACN) and the measured properties are gathered in Table 1. Compounds **(1)–(11)** have λ_{max} at around 380 nm, while after the introduction of the two methoxy groups the λ_{max} of the naphthoquinone-esters **(12)–(15)** is blue shifted (Fig. 1, Table 1). Besides this blue shift observed for the last series of naphthoquinones, all dyes exhibit a good absorption for the LED light used in this study.

3.3. Type I photoinitiator features

For the benchmark TA monomer, Type I photoinitiation abilities of the investigated compounds (0.5 wt%) were studied using RT-FTIR in thin (25 μm, in laminate) and thick (1.4 mm under air) samples upon irradiation using different LEDs (405 nm or 455 nm). Typical photopolymerization profiles are shown in Fig. 2; the obtained final acrylate function conversions (FCs) are gathered in Tables 2 and 3.

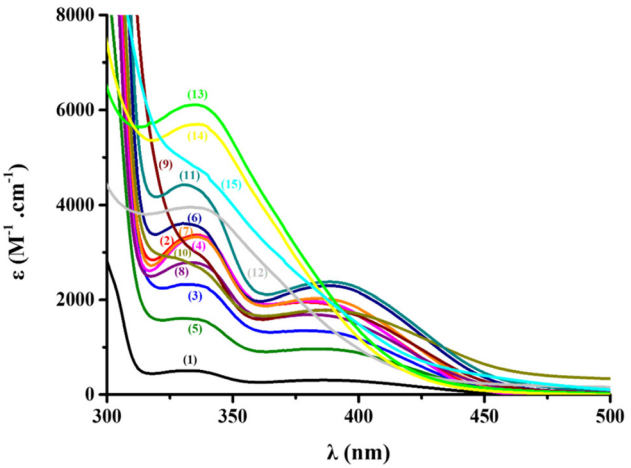

Fig. 1 UV-visible absorption properties of compounds **1–15** in acetonitrile.

Table 1 Light absorption properties of the investigated compounds: maximum absorption wavelength (λ_{max}), molecular extinction coefficients at λ_{max}, @405 and @455 nm

PIs	λ_{max} (nm)	ε_{max} (M^{-1} cm^{-1})	ε_{405} (M^{-1} cm^{-1})	ε_{455} (M^{-1} cm^{-1})
(**1**)	330	500	260	30
(**2**)	380	1950	1500	90
(**3**)	382	1350	1070	100
(**4**)	378	1980	1510	40
(**5**)	383	970	810	100
(**6**)	388	2300	2010	260
(**7**)	383	2000	1670	130
(**8**)	382	1700	1360	170
(**9**)	387	1800	1550	210
(**10**)	385	1800	1630	570
(**11**)	388	2370	2110	360
(**12**)	333	3960	810	220
(**13**)	334	6110	1100	120
(**14**)	336	5700	960	70
(**15**)	339	4670	1290	360

Compound (**1**), which has no ester function, has a very poor photoinitiator behavior compared to the other structures (**2–15**), indicating the role of the ester group as being able to react as a Type I photoinitiator. Compound (**8**) (with a methyl substituent on the carboxyl side) reached the highest FC of 88%, which is also very close to that of the commercial photoinitiator TPO (see Fig. 2 and Table 3). Noticeably, compounds with alkyl substituents on the carboxyl side appear to have excellent photoinitiation performance compared to compounds that have aryl substituents (*e.g.* compounds (**2**), (**3**), (**4**), (**7**), and (**8**) show fast polymerization rates as well as high final conversions compared to the other compounds – Fig. 2(A)). The difference of reactivity (thin *vs.* thick samples) can be associated with an inner filter effect. It is generally well known that light penetration decreases with the optical density, which depends on the molar concentration of the absorbing species, their molar absorptivity and the length of the optical path as determined through the Beer–Lambert law.[2] Moreover, after introduction of methoxy groups into the structure of the compounds that have alkyl substituents in order to increase their absorption properties, it was clearly noticed that their photoinitiation ability was reduced compared to their analogues without methoxy substituents (see compounds (**12**), (**13**), (**14**) and (**15**) *vs.* compounds (**8**), (**4**) and (**7**) in Fig. 2). This can clearly show that the photoinitiation ability of the studied compounds is not only associated with their absorption properties. Hence, it is necessary to consider other factors that can affect their photopolymerization ability, such as the cleavage yields and the reactivity of the generated radicals.

Besides that, considering the difference between the molecular weights of the studied structures, if we vary the percentage of mass to obtain the same molar content (Fig. 3 and Table 2) it can be noticed that there is not a significant difference regarding the reactivity of the investigated compounds; for example, compound (**8**) is always the most reactive and the compounds with alkyl substituents are always better than those with aryl substituents. This is in agreement with the

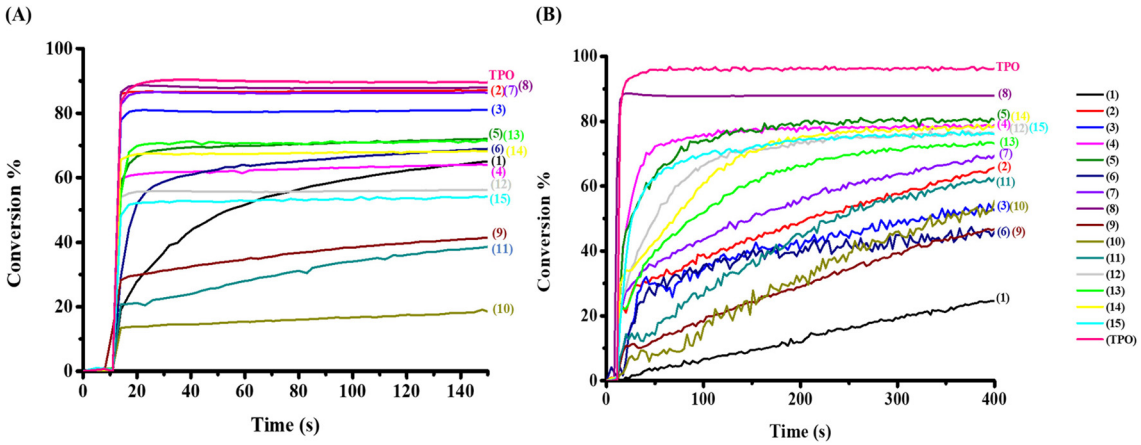

Fig. 2 Photopolymerization profiles of TA (acrylate function conversion *vs.* irradiation time) using different photoinitiators (0.5% w/w) in (A) laminate (thickness = 25 μm) and (B) under air (thickness = 1.4 mm); the irradiation with a LED (λ = 405 nm) starts at t = 10 s.

Table 2 FCs using different photoinitiators: (**1**) (0.34% w/w); (**2**) (0.43% w/w); (**3**) (0.43% w/w); (**4**) (0.4% w/w); (**5**) (0.46% w/w); (**6**) (0.47% w/w); (**7**) (0.42% w/w); (**8**) (0.37% w/w); (**9**) (0.47% w/w); (**10**) (0.44% w/w); (**11**) (0.5% w/w); (**12**) (0.44% w/w); (**13**) (0.47% w/w); (**14**) (0.47% w/w) and (**15**) (0.48% w/w). After 100 s of irradiation with a LED light (λ = 405)

PIs	Thin samples (25 μm) in laminate	Thick samples (1.4 mm) under air
(**1**)	55%	17%
(**2**)	73%	87%
(**3**)	76%	65%
(**4**)	69%	85%
(**5**)	—	74%
(**6**)	47%	75%
(**7**)	79%	87%
(**8**)	81%	86%
(**9**)	56%	70%
(**10**)	41%	65%
(**11**)	41%	68%
(**12**)	47%	71%
(**13**)	63%	75%
(**14**)	57%	77%
(**15**)	40%	75%

importance of the other factors that can influence the photopolymerization process.

In addition, and in order to show the reactivity of the studied structures at longer wavelengths, photopolymerization experiments were also performed using a LED@455 nm where the results showed a high photoinitiation performance, especially for compounds (**8**), (**2**), (**3**), (**4**) and (**7**) (with alkyl substituents on the carboxyl side). Interestingly, at 455 nm, some compounds are much more efficient than the benchmark TPO (Fig. 4; see also Table 3). Again, compound (**8**) showed the highest reactivity, even under LED@455 nm with a FC of 87% for the thin sample and 84% for the thick sample. Markedly, compound (**8**) exhibited a better performance when compared to commercial references, such as camphorquinone/ethyl dimethylaminobenzoate (CQ/EDB) (0.5%/0.5% w/w) or even titanocene (Irgacure 784) (0.5% w) (see Fig. 4(C) and (D)), which demonstrates that compound (**8**) could be considered as a new alternative to benchmark photoinitiators.

Table 3 FCs using one-component (0.5% w/w) photoinitiators after 100 s of irradiation with a LED light (λ = 405 and 455 nm)

PIs	Thin samples (25 μm) in laminate @405 nm	Thin samples (25 μm) in laminate @455 nm	Thick samples (1.4 mm) under air @405 nm	Thick samples (1.4 mm) under air @455 nm
TPO	90%	61%	95%	77%
(**1**)	65%	48%	25%	1%
(**2**)	82%	80%	78%	78%
(**3**)	68%	71%	54%	81%
(**4**)	81%	83%	83%	85%
(**5**)	49%	55%	78%	74%
(**6**)	34%	53%	48%	68%
(**7**)	79%	76%	86%	80%
(**8**)	88%	87%	88%	84%
(**9**)	42%	24%	48%	65%
(**10**)	18%	32%	54%	54%
(**11**)	39%	32%	63%	66%
(**12**)	56%	65%	76%	78%
(**13**)	71%	73%	74%	78%
(**14**)	68%	59%	78%	61%
(**15**)	54%	48%	76%	67%

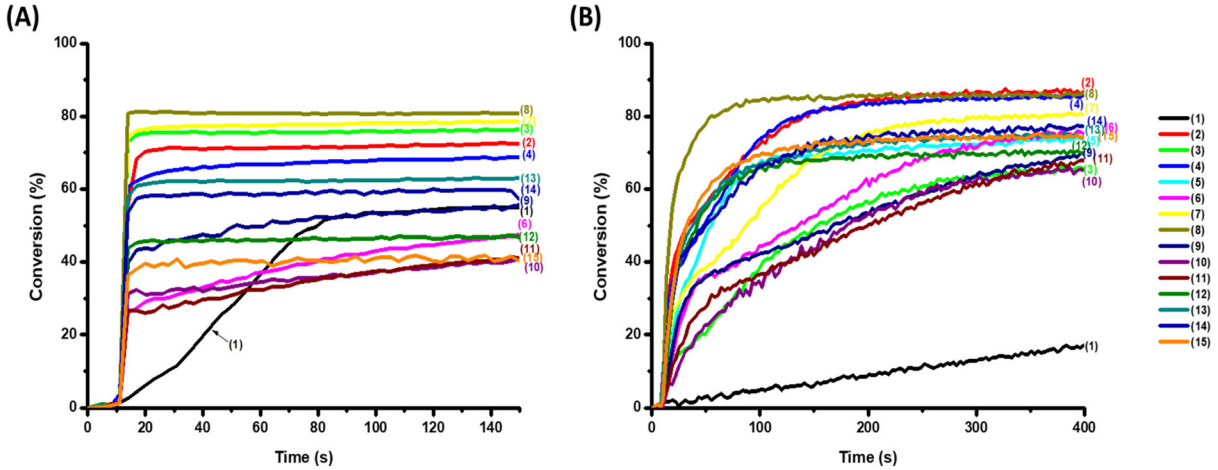

Fig. 3 Photopolymerization profiles of TA (acrylate function conversion *vs.* irradiation time) using different photoinitiators: (**1**) (0.34% w/w); (**2**) (0.43% w/w); (**3**) (0.43% w/w); (**4**) (0.4% w/w); (**5**) (0.46% w/w); (**6**) (0.47% w/w); (**7**) (0.42% w/w); (**8**) (0.37% w/w); (**9**) (0.47% w/w); (**10**) (0.44% w/w); (**11**) (0.5% w/w); (**12**) (0.44% w/w); (**13**) (0.47% w/w); (**14**) (0.47% w/w) and (**15**) (0.48% w/w) in (A) laminate (thickness = 25 μm) and (B) under air (thickness = 1.4 mm); the irradiation with a LED (λ = 405 nm) starts at t = 10 s.

Compounds (**9**), (**10**), (**11**), (**12**) and (**15**) appear to have the poorest abilities compared to the others. Additionally, compound (**8**) in TA was left for a period of 1 month and its initiation ability was tested weekly. As shown in Fig. 4(E), good storage stability was found without significant decrease of performance.

Remarkably, a release of CO_2 was also observed after irradiation of the photoinitiators in the TA monomer, clearly indicating a decarboxylation reaction. Specifically, derivatives with alkyl groups, such as compound (**8**), appeared to have a peak after irradiation at 2337 cm^{-1}, proving the release of CO_2 (Fig. 5(A)). However, derivatives containing an aryl group, such as compound (**10**), did not show CO_2 release as shown in Fig. 5(C). CO_2 release is an important parameter directly governing the efficiency of the polymerization (see Fig. 5(B) and (D) highlighting the link between both profiles). Without CO_2 release, a low yield of initiating radicals is expected.

To better understand the mechanism that occurs after the irradiation of the studied compounds, and more particularly to identify the type of generated radicals, ESR spin trapping experiments have been performed. Remarkably, when compound (**8**) was irradiated in the presence of phenyl-*N*-*tert*-butylnitrone (PBN) as a spin trapping agent, the ESR signal (a_N = 13.50 G, a_H = 1.86 G) could be assigned to the acyloxy radical adduct (RC(=O)O$^{\bullet}$)/PBN (Fig. 6). This showed that the acyloxy radical is generated by the cleavage of the N–O bond, which in turn undergoes further decarboxylation reactions resulting in carbon-centered radicals (Scheme 4), in agreement with the CO_2 release detected by FT-IR during the photopolymerization process (Fig. 5(A)).

Photophysical properties of compounds (**8**) and (**10**) (alkyl *vs.* aryl substituents on the carboxyl side), respectively, are shown in Fig. 7. In particular, compound (**8**) (see Fig. 7(A)) and all derivatives containing an alkyl substituent have faster photolysis in acetonitrile when irradiated with LED light at 375 nm compared to compound (**10**) (Fig. 7(B)), and even all the derivatives containing aryl substituents, for which no or low photolysis yields were observed. Furthermore, derivatives with methoxy groups, (**12**)–(**15**), also show rather rapid photolysis behavior. The above photolysis results are in agreement with the photopolymerization results, *i.e.* high photolysis ability leading to better PI properties.

In Table 4, the corresponding N–O bond dissociation energies (BDE) and excited state properties (singlet and triplet excited state energies) for the studied compounds are given. The N–O cleavage process is energetically favorable from both singlet and triplet excited states from which the dissociation enthalpy of S_1 and T_1 are negative and favorable for compounds (**1**)–(**11**). However, more propitious is the cleavage from the singlet state due to the lower ΔH values. Since compounds (**12**)–(**15**) did not have any photoluminescence, the singlet state energy could not be evaluated, but they have negative enthalpy values from the triplet state showing that the cleavage is favorable from that energy state. The fluorescence lifetimes of the naphthoquinone-based imidazolyl esters were also measured (Table 4, Fig. 7). The derivative without an ester function, namely compound (**1**), had the highest lifetime at 3.45 ns, which approaches agreement with its photochemical results, *i.e.* the addition of the ester group provides lower lifetimes suggesting a cleavage from S_1.

Interesting results were also obtained during the direct laser writing experiments at 405 nm under air, in particular with the derivative (**8**) even for a very low content (0.1 wt%) in TA with a short writing time (~4s). Fig. 8 shows the 3D patterns elaborated in high resolution.

3.4. Type II photoinitiator features

The photoinitiating ability of OXE/Iod or OXE/EDB (0.1%/1% w/w) was also investigated upon irradiation using a

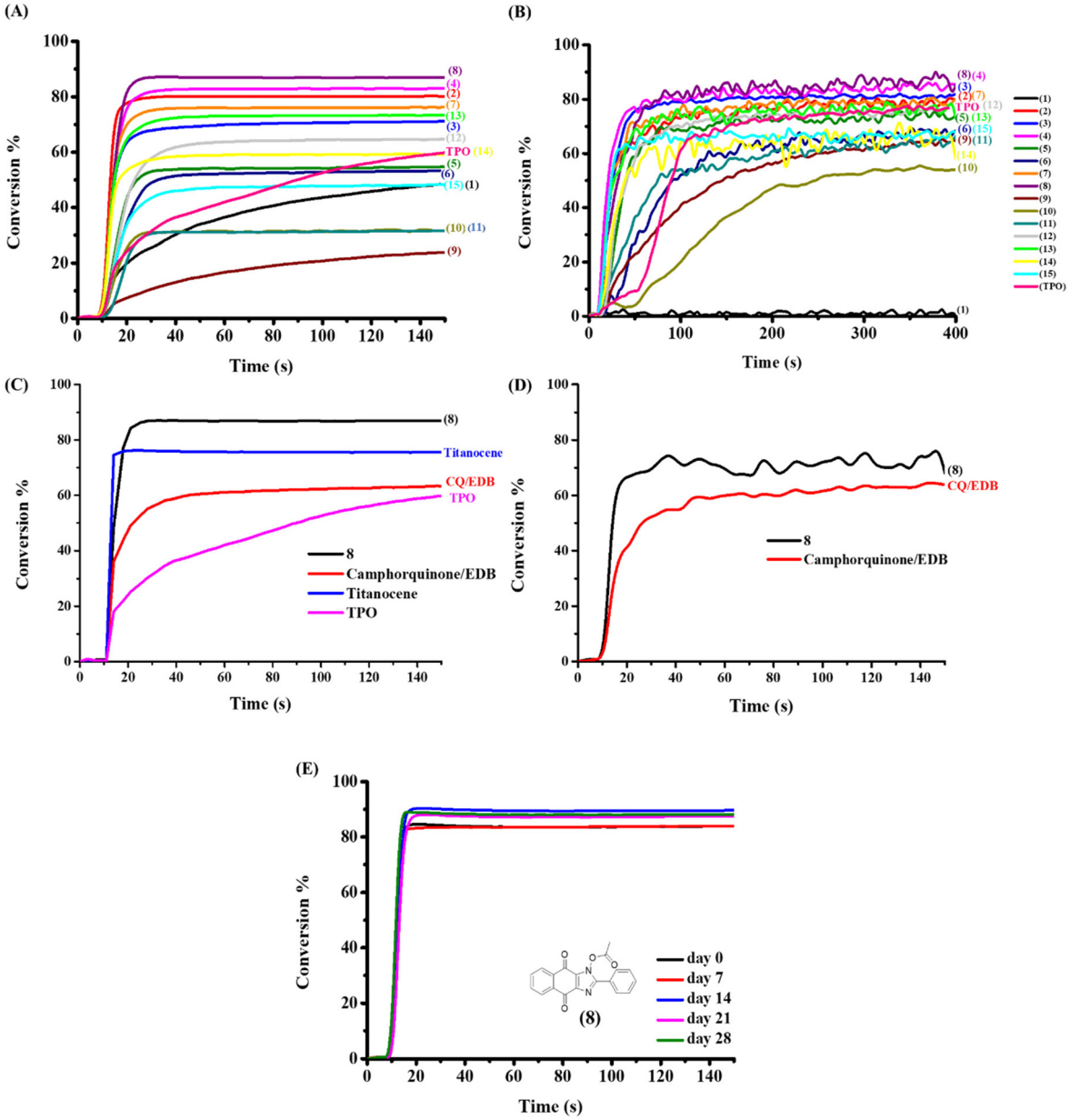

Fig. 4 Photopolymerization profiles of TA (acrylate function conversion *vs.* irradiation time) using different photoinitiators (0.5 wt%) in (A) laminate (thickness = 25 μm) and (B) under air (thickness = 1.4 mm) upon exposure to a LED light (λ = 455 nm). (C) Photopolymerization profiles of TA in laminate (thickness = 25 μm) with: compound (**8**) (0.5% w/w), CQ/EDB (0.5%/0.5% w/w); TPO (0.5% w/w) and titanocene (0.5% w/w). (D) Photopolymerization profiles of UDMA in laminate (thickness = 25 μm) with: compound (**8**) (0.5% w/w), CQ/EDB (0.5%/0.5% w/w) and (E) photopolymerization profiles of TA using compound (**8**) (0.5% w/w) for different storage times in TA monomer. The irradiation starts at t = 10 s.

LED@405 nm. The typical polymerization profiles using compound (**13**) are presented in Fig. 9, and the final acrylate conversions (FCs) for all the FCs with the other compounds are summarized in Table 5.

When the iodonium salt was introduced into the light sensitive formulations, most derivatives showed insignificant improvements in their photopolymerization profiles. There was only one compound that had any great enhancement in its photopolymerization profile, which was compound (**13**). It had a better performance, reaching a FC of 48%, which was much higher than the 25% that was obtained when compound (**13**) was used alone in the thin sample. The same effect was also observed in the thick sample where the FC reached 72% compared to 48% when compound (**13**) was used alone. This fact shows that compound (**13**) is very effective in the photo-oxidation process in initiating a free radical polymerization in combination with Iod (see eqn (r3) below).

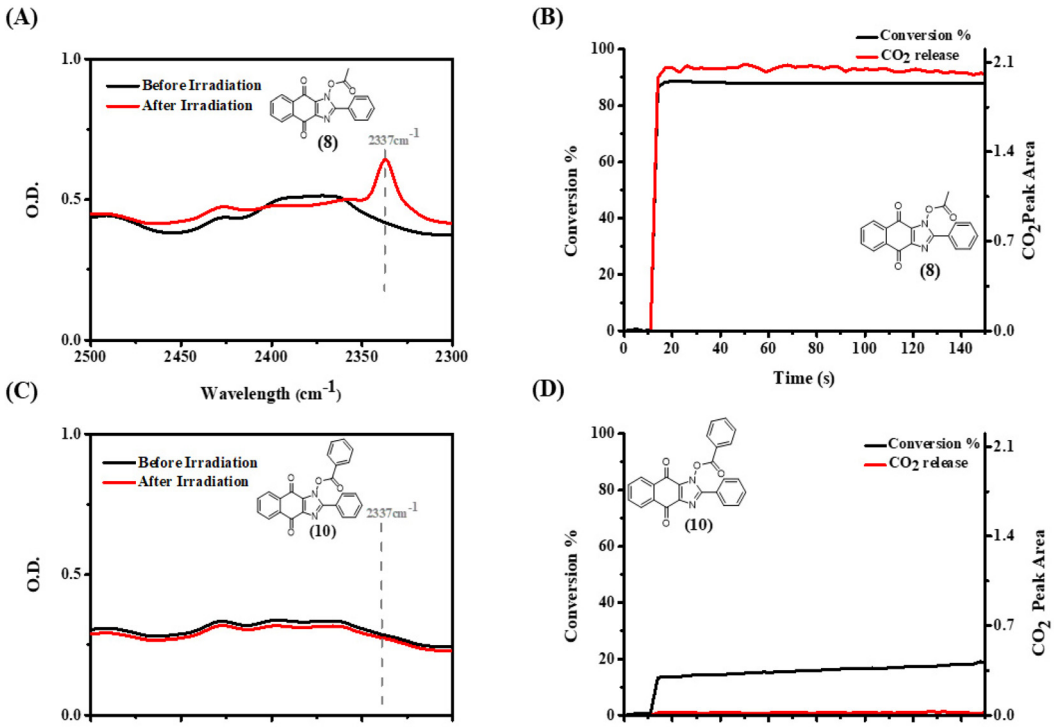

Fig. 5 (A) Detection of CO_2 released during photopolymerization using (**8**), (B) decarboxylation-conversion correlation using (**8**), (C) detection of CO_2 released during photopolymerization using (**10**) and (D) decarboxylation-conversion correlation using (**10**); PI (0.5% w/w) in TA (thin film polymerization @405 nm in laminate).

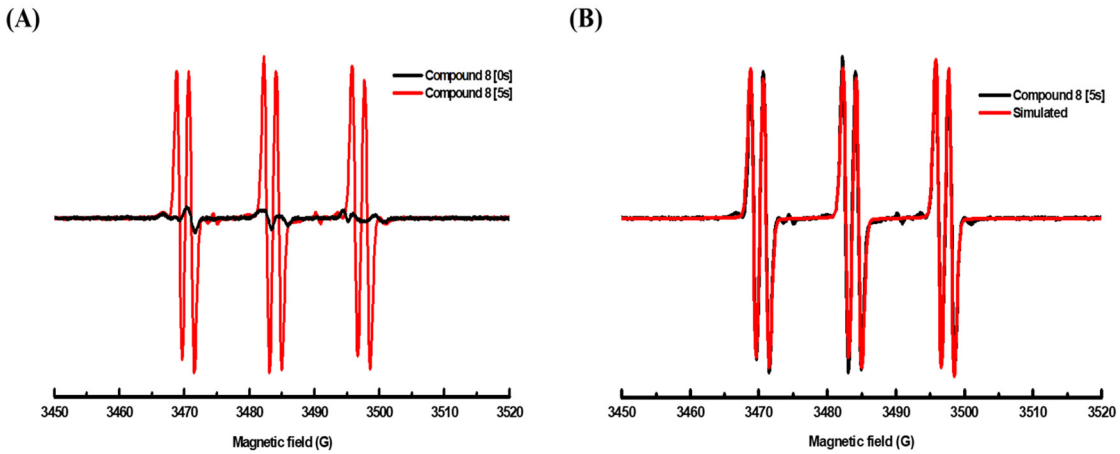

Fig. 6 ESR spectra (in the presence of PBN and in toluene) recorded for compound (**8**): (A) before *vs.* after irradiation (at t = 0 s and t = 5 s); LED@405 nm. (B) Simulated and experimental spectra observed after irradiation (at t = 30 s).

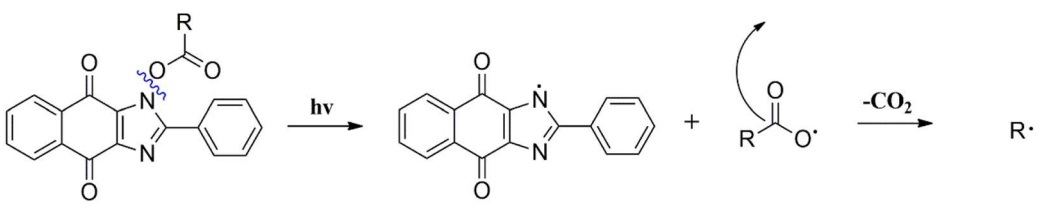

Scheme 4 Proposed photochemical mechanisms for naphthoquinone-based imidazolyl esters.

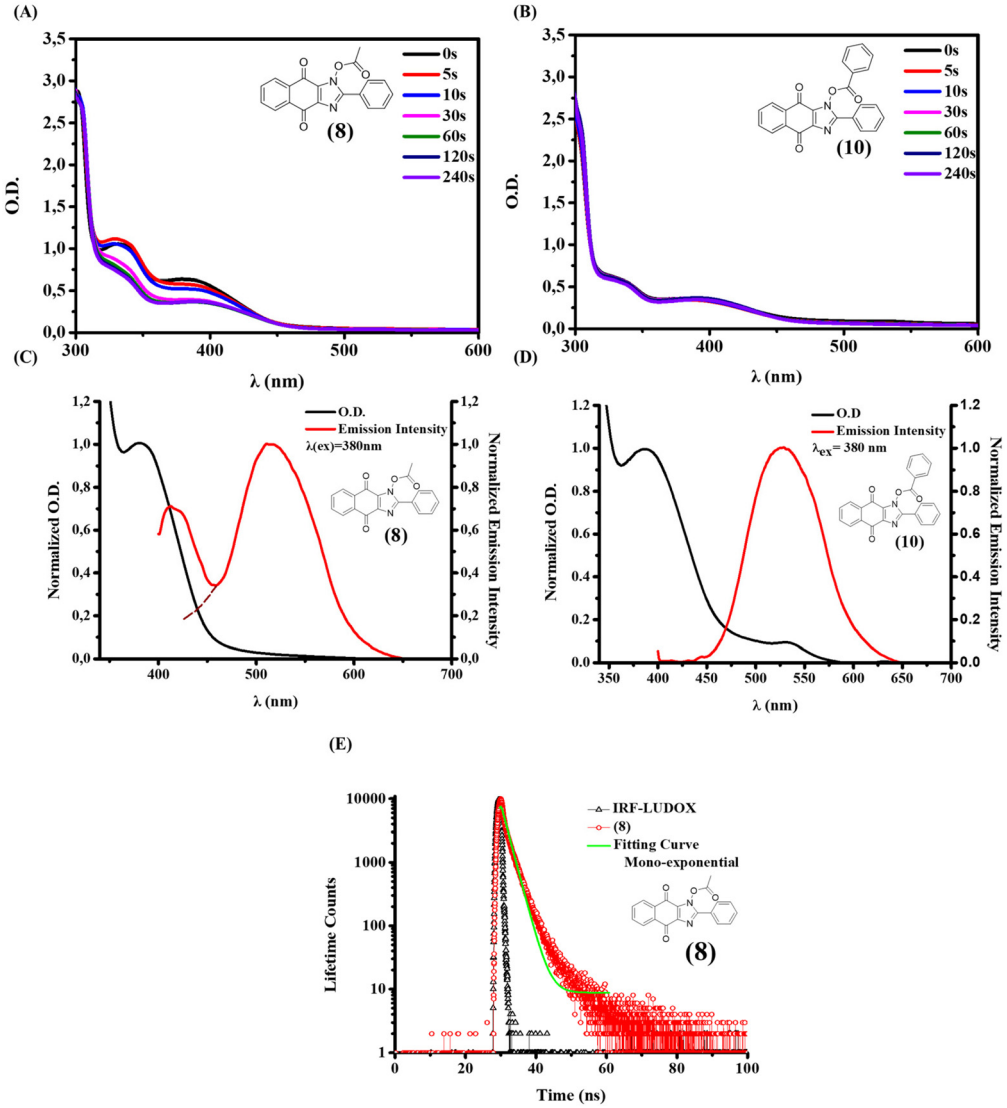

Fig. 7 Photolysis of (A) compound (**8**) and (B) compound (**10**) in acetonitrile using LED light at λ = 375 nm. UV-visible absorption and emission spectra of (C) compound (**8**) and (D) compound (**10**) in acetonitrile. (E) Time correlated single-photon counting of compound (**8**) in acetonitrile, λ_{ex} = 367 nm, λ_{em} = 450 nm, and the associated curve fitting.

On the other hand, when EDB was added to the photosensitive formulations, we observed a clear and significant enhancement of the photopolymerization profiles of all compounds in both thin and thick samples. Again, the most remarkable improvement was obtained for compound (**13**), which achieved a final acrylate conversion of 67%, compared to 25% alone in the thin sample and 48% when combined with Iod. A great enhancement was also seen in the thick sample of compound (**13**) where the final acrylate conversion reached 80% plus EDB, a result that shows that this compound is also very effective in a photo-reduction process to initiate free radical polymerizations (see eqn (r2) below). From the above results, it can easily be understood that these naphthoquinone-based derivatives can work efficiently according to the reactions (r1)–(r3) where $EDB^{\bullet}_{(-H)}$ and $Ar^{\bullet}$ are considered the main initiating species:[3]

$$PI\ (h\nu) \rightarrow {}^{*}PI \rightarrow R^{\bullet} \quad (r1)$$

$$^{1}PI + EDB \rightarrow PI^{\bullet -} + EDB^{\bullet +} \rightarrow PI^{\bullet}\text{-}H + EDB^{\bullet}_{(-H)} \quad (r2)$$

$$^{1}PI + Ar_2I^{+} \rightarrow PI^{\bullet +} + Ar^{\bullet} + ArI \quad (r3)$$

When the compounds were used as Type I photoinitiators, they could undergo a decarboxylation reaction after the bond cleavage takes place (see eqn (r1) above or Scheme 4). This does not seem to be the case when these derivatives are used as Type II photoinitiators with the addition of Iod. As seen in Fig. 10(A) and (B), compound (**13**) does not undergo a de-

Table 4 Parameters characterizing the investigated naphthoquinone-based imidazolyl esters. Parameters calculated by molecular modelling: the bond dissociation energy BDE (N–O), the triplet state energy E_{T1}, the enthalpy ($\Delta H_{cleavageT1}$) for the cleavage process from T_1 ($\Delta H_{cleavageT1}$ = BDE – E_{T1}), the singlet excited state energy E_{S1} (evaluated from the experimental absorption and fluorescence spectra), and the enthalpy ($\Delta H_{cleavageS1}$) for the cleavage process from S_1 ($\Delta H_{cleavageS1}$ = BDE – E_{S1})

Pis	BDE (kcal mol^{-1})	E_{S1} (kcal mol^{-1})	τ_0 (S_1) (ns)	$\Delta H_{cleavageS1}$ (kcal mol^{-1})	E_T (kcal mol^{-1})	$\Delta H_{cleavageT1}$ (kcal mol^{-1})
(**1**)	41.78	62.3	3.45	−20.51	50.98	−9.2
(**2**)	35.76	63.5	2.49	−27.74	50.57	−14.81
(**3**)	36.54	63.8	2.46	−27.26	50.69	−14.15
(**4**)	34.95	63.5	1.76	−28.55	50.76	−15.81
(**5**)	34.90	62.2	2.75	−27.3	50.77	−15.87
(**6**)	34.94	62.6	2.63	−27.66	50.76	−15.82
(**7**)	35.03	62.8	3.09	−27.77	50.53	−15.50
(**8**)	36.19	65.13	2.36	−28.94	50.71	−14.52
(**9**)	34.92	64.3	2.41	−29.38	50.47	−15.55
(**10**)	34.87	61.8	2.56	−26.93	50.75	−15.88
(**11**)	34.78	62.6	2.57	−27.82	50.77	−15.99
(**12**)	32.68	—	—	—	47.12	−14.44
(**13**)	32.38	—	—	—	47.56	−15.18
(**14**)	31.41	—	—	—	47.29	−15.88
(**15**)	31.89	—	—	—	47.82	−15.93

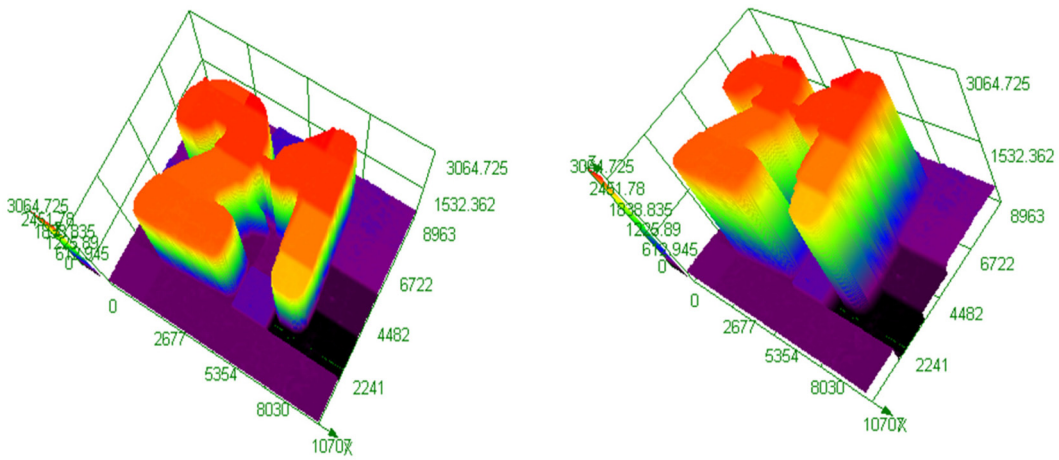

Fig. 8 Characterization of the 3D patterns (thickness on the *z*-axis) obtained from compound (**8**) (0.1% w/w) in TA.

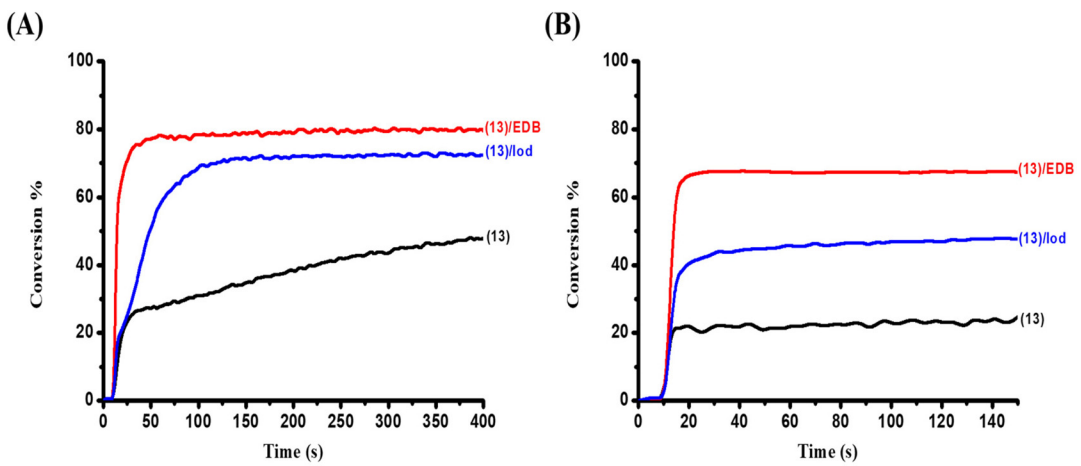

Fig. 9 Photopolymerization profiles of TA (acrylate function conversion *vs.* irradiation time) using compound (**13**) alone (0.1% w/w), compound (**13**)/EDB (0.1%/1% w/w) and compound (**13**)/Iod (0.1%/1% w/w): (A) in laminate (thickness = 25 μm) and (B) under air using a thickness of 1.4 mm; the irradiation with a LED (λ = 405 nm) starts at t = 10 s.

Table 5 Final acrylate function conversion using one-component (0.1% w/w) photoinitiators and two-component (0.1%/1% w/w) photoinitiators with the iodonium salt or EDB after 100 s of irradiation with a LED light (λ = 405 nm)

	Thickness (25 μm) in laminate			Thickness (1.4 mm) under air		
	PI	PI/Iod	PI/EDB	PI	PI/Iod	PI/EDB
(**1**)	60%	28%	83%	16%	56%	64%
(**2**)	43%	63%	74%	62%	84%	87%
(**3**)	43%	48%	53%	69%	84%	85%
(**4**)	37%	60%	61%	65%	85%	86%
(**5**)	30%	27%	54%	58%	73%	84%
(**6**)	48%	47%	67%	52%	70%	85%
(**7**)	32%	56%	69%	64%	81%	86%
(**8**)	29%	59%	73%	70%	84%	85%
(**9**)	44%	38%	66%	47%	63%	88%
(**10**)	45%	31%	62%	62%	76%	84%
(**11**)	41%	61%	49%	66%	70%	86%
(**12**)	39%	52%	55%	37%	46%	81%
(**13**)	25%	48%	67%	48%	72%	80%
(**14**)	23%	46%	51%	48%	75%	81%
(**15**)	62%	46%	6%	42%	57%	78%

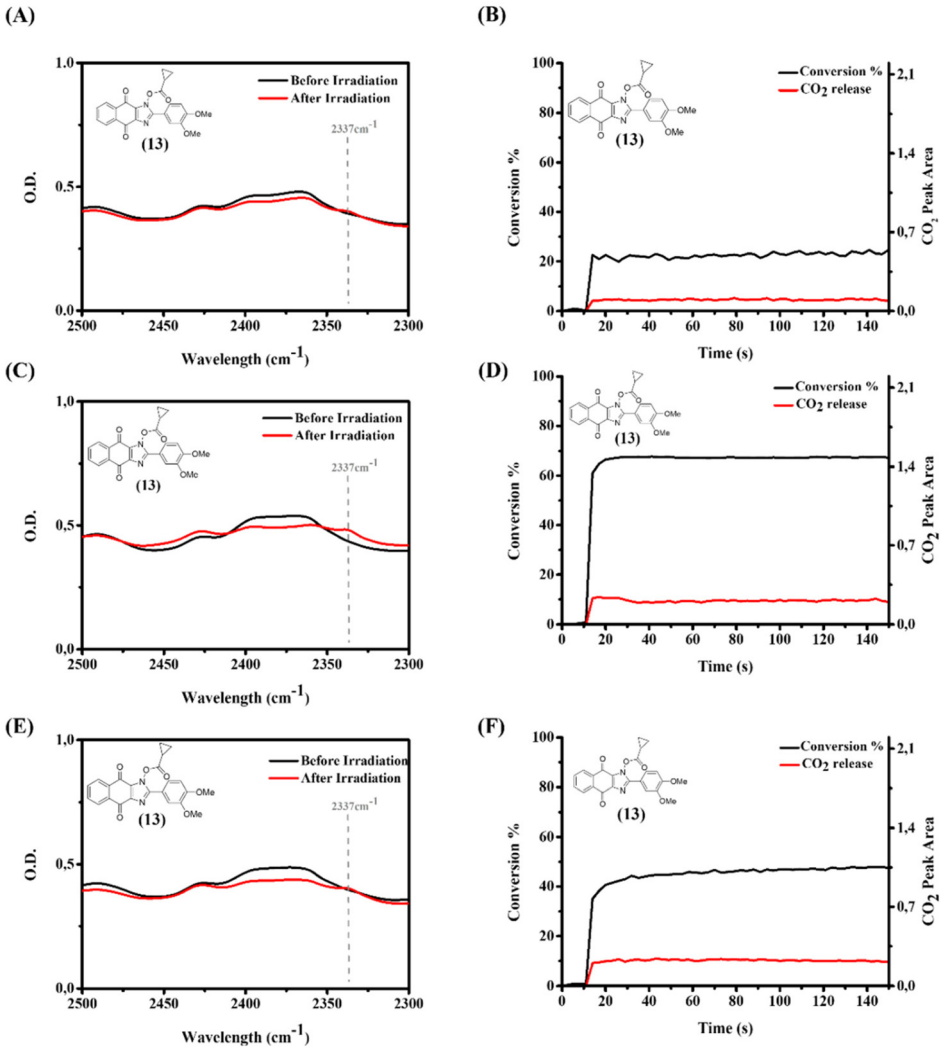

Fig. 10 Photopolymerization of TA upon irradiation with a LED@405 nm: (A) detection of CO_2 with a (**13**) (0.1 wt%) system, (B) decarboxylation-conversion correlation with a compound (**13**) (0.1 wt%) system, (C) detection of CO_2 with a (**13**)/EDB (0.1%/1% w/w) system, (D) decarboxylation-conversion correlation with a (**13**)/EDB (0.1%/1% w/w) system, (E) detection of CO_2 with a (**13**)/Iod (0.1%/1% w/w) system, and (F) decarboxylation-conversion correlation with a (**13**)/Iod (0.1%/1% w/w) system.

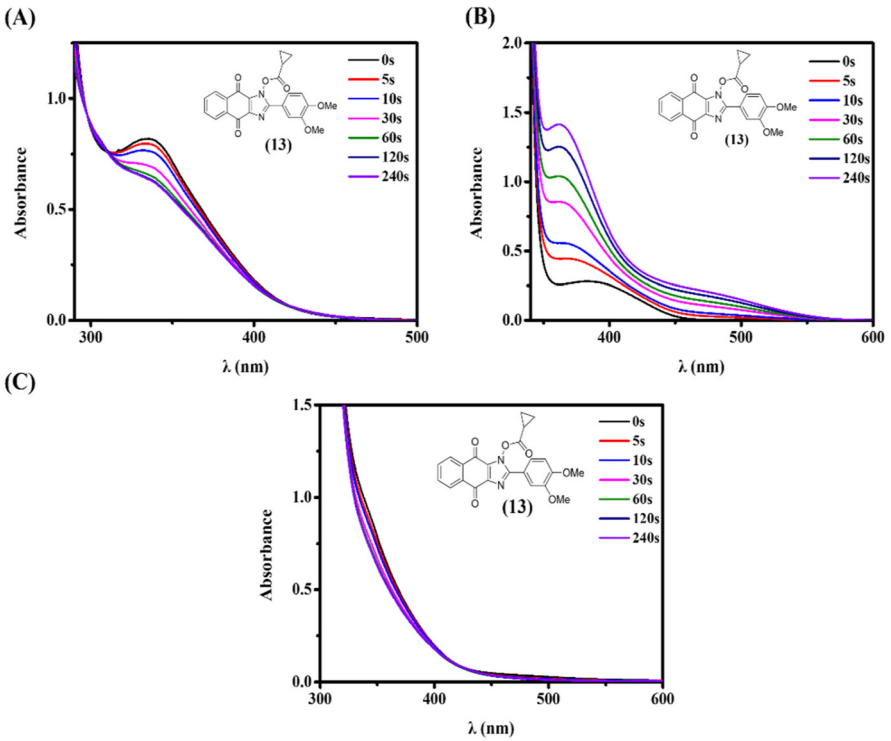

Fig. 11 Photolysis of: (A) (**13**) (0.1 wt%), (B) (**13**)/EDB (10^{-2} M) and (C) (**13**)/Iod (10^{-2} M) in acetonitrile using a LED light at λ = 375 nm.

carboxylation reaction when Iod is present, *i.e.* we can assume that the excited state is mainly quenched by Iod (eqn (r3)) than cleaved through eqn (r1) (eqn (r1) and (r3) being in competition). When the same compound is used in a two-component system with EDB instead of Iod, a decarboxylation reaction takes place, which is in full agreement with the better photopolymerization profile of that derivative plus EDB. This decarboxylation result in the presence of EDB is also in agreement with the decarboxylation of the radical anion of oxime-esters ($PI^{\bullet -}$) found in ref. 29.

Fig. 11 represents the steady state photolysis for (**13**)/Iod or EDB (10^{-2} M) systems in acetonitrile upon irradiation. As observed, there are differences showing that there is an overlap of peaks when combining with an additive (Fig. 11 (A) *vs.* (B) and (C)). Furthermore, the addition of EDB to the system leads to a faster photolysis reaction, which is in agreement with the photopolymerization profiles described above. Regarding the rest of the examined Type II derivatives, higher polymerization rates were observed for all compounds with alkyl groups in the presence of additives. On the other hand, the opposite was noted for compounds containing an aryl substituent attached to the ester function.

For a better understanding of their interactions with Iod or EDB, fluorescence quenching experiments were carried out in acetonitrile for the different PIs being investigated (Fig. 12). The concentration of EDB or iodonium salt was increased successively and each time a fluorescence spectrum was obtained. The fluorescence quenching was determined from the evolution of the first peak (at ~420 nm) for different contents of EDB or Iod. Indeed, the longest wavelength fluorescence peak was affected (see Fig. 12(E)) by the formation of fluorescent photoproducts generated in the photolysis of PI/Iod (or EDB) (see Fig. 12(A) and (B)). From the Stern–Volmer equation, the fluorescence quenching yield was calculated:

$$\frac{\Phi_0}{\Phi} = 1 + k_{sv}[Q] = 1 + k_q\tau_0[Q] \;\; => \Phi_{quenching} = \frac{k_{sv}[Q]}{1 + (k_{sv}[Q])}$$

In this equation, k_{sv}, k_q, τ_0 and [Q] stand for the Stern–Volmer quenching constant, the bimolecular quenching constant, the unquenched lifetime, and the quencher concentration, respectively.[30] All the fluorescence quenching yields are gathered in Table 6.

Choosing the derivative with the best photoinitiating performance so far, the fluorescence quenching results showed that compound (**8**) had one of the highest fluorescence quenching yields when adding the iodonium salt but one of the lowest when adding EDB based on the Stern–Volmer equation (see Fig. 12(C)–(F)). However, compound (**1**), when adding the iodonium salt, had the highest quenching yield, of 97%, but when adding EDB it appeared to be 39%. The iodonium salt results in a higher quenching compared to EDB for derivatives (**1**), (**8**) and (**11**). For the other derivatives, however, the opposite phenomenon was observed. Compounds (**3**), (**4**) and (**9**) appeared to have a blue shift and a hyperchromic

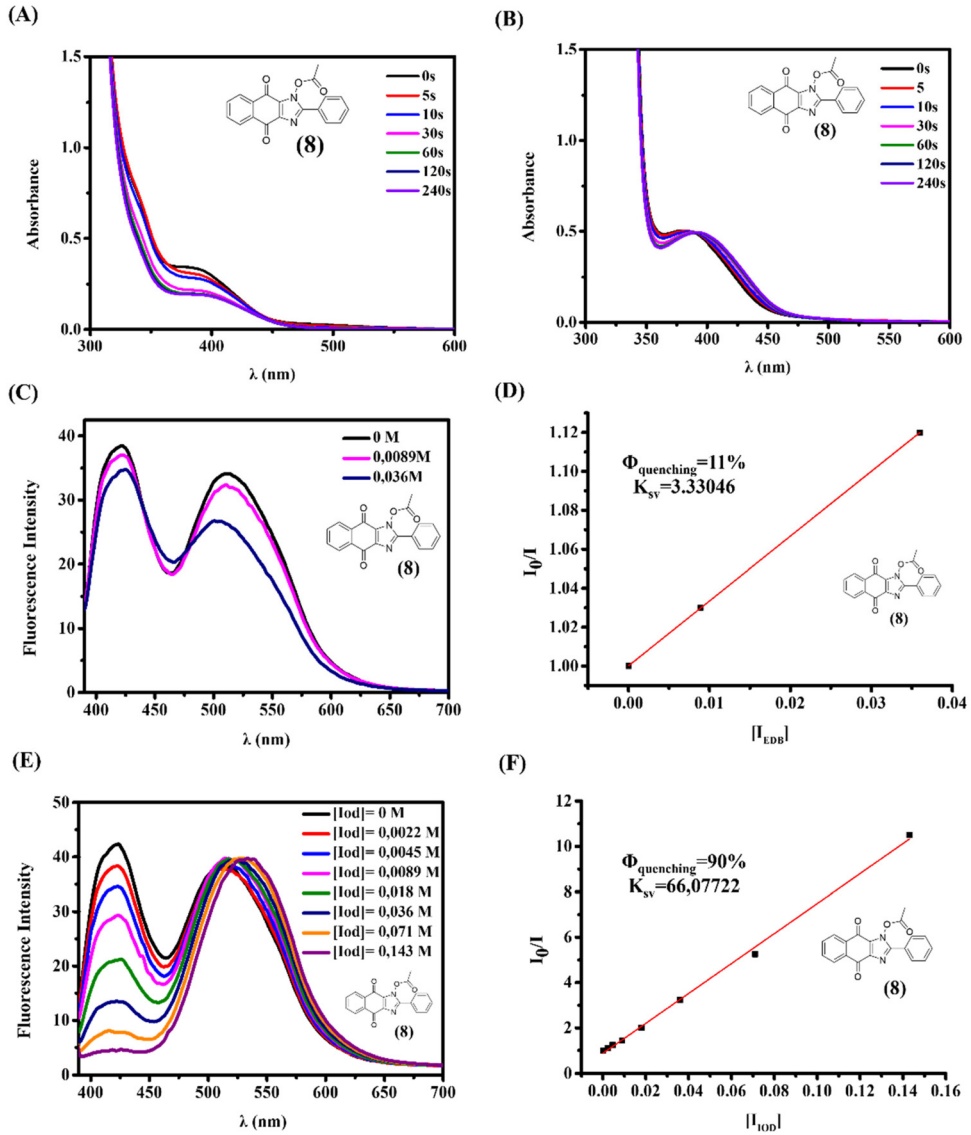

Fig. 12 Photolysis of (A) (**8**)/Iod (10^{-2} M) and (B) (**8**)/EDB (10^{-2} M) in acetonitrile using a LED light at λ = 375 nm. (C) Fluorescence quenching study of compound (**8**) by EDB in acetonitrile and (D) representation of the associated Stern–Volmer plot. (E) Fluorescence quenching study of compound (**8**) by the iodonium salt in acetonitrile and (F) the associated Stern–Volmer plot for (E).

Table 6 Parameters characterizing the photochemical mechanisms associated with ^{1}PI/Iod or ^{1}PI/EDB interactions

	Iod		EDB	
Compounds	$\phi_{quenching}$	k_{sv} (M^{-1})	$\phi_{quenching}$	k_{sv} (M^{-1})
(**1**)	97%	3884	39%	35
(**2**)	18%	6	43%	20
(**5**)	23%	2	29%	22
(**6**)	42%	10	57%	37
(**7**)	22%	15	44%	42
(**8**)	90%	66	11%	3
(**10**)	38%	4	55%	34
(**11**)	50%	7	43%	41

effect on addition of the iodonium salt or EBD, and therefore the quenching yield was not calculated.

4. Conclusion

An unprecedented series of naphthoquinone-based imidazolyl esters were designed and successfully synthesized. All the studied photoinitiators have demonstrated interesting photophysical and photochemical properties. The new compounds could also achieve high photopolymerization conversions as Type I and Type II photoinitiators when a second component was added to the photoinitiating systems. In particular, naphthoquinone-based derivatives with lower conversions as

Type I PIs managed to have higher conversions in Type II systems. This new family of naphthoquinone-based imidazolyl ester structures show great photoinitiating behavior and more specifically compound (**8**) (with a methyl substituent in the carboxyl side) can possibly replace or stand on a par with a well-established reference like TPO. Interestingly, these naphthoquinone derivatives have been used for 3D printing experiments. Specific Type I and Type II photoinitiators based on the naphthoquinone scaffold will be presented in forthcoming studies.

Conflicts of interest

There are no conflicts to declare.

Acknowledgements

This research project was supported by The Agence Nationale de la Recherche (ANR) for the NoPerox project (ANR-19-CE07-0042).

References

1 J. P. Fouassier, *Photoinitiation, Photopolymerization, and Photocuring: Fundamentals and Applications*, Hanser Publishers, New York, 1995.
2 P. Garra, C. Dietlin, F. Morlet-Savary, F. Dumur, D. Gigmes, J. P. Fouassier and J. Lalevée, Photopolymerization processes of thick films and in shadow areas: a review for the access to composites, *Polym. Chem.*, 2017, **8.46**, 7088–7101.
3 J. P. Fouassier and J. Lalevée, *Photoinitiators: Structures, Reactivity and Applications in Polymerization*, Wiley, Weinhein, 2021.
4 Y. Yagci, S. Jockusch and N. J. Turro, Photoinitiated polymerization: advances, challenges, and opportunities, *Macromolecules*, 2010, **43**, 6245–6260.
5 F. Karasu, C. Croutxé-Barghon, X. Allonas, D. V. Van and G. J. Leendert, Free radical photopolymerization initiated by UV and LED: Towards UV stabilized, tack free coating, *J. Polym. Sci., Part A: Polym. Chem.*, 2015, **52.24**, 3597–3607.
6 F. Hammoud, M. Rahal, J. Egly, F. Morlet-Savary, A. Hijazi, S. Bellemin-Laponnaz, M. Mauro and J. Lalevée, Cubane Cu4I4(phosphine)4 complexes as new co-initiators for free radical photopolymerization: towards aromatic amine-free systems, *Polym. Chem.*, 2021, **12**, 2848–2859.
7 J. Lalevée and J. P. Fouassier, Dye Photosensitized Polymerization Reactions: Novel Perspectives, RSC Photochemistry Reports, ed. A. Albini and E. Fasani, in *Photochemistry*, London, UK, 2015, pp. 215–232.
8 J. Xu, G. Ma, K. Wang, J. Gu, S. Jiang and J. Nie, Synthesis and photopolymerization kinetics of oxime ester photoinitiators, *J. Appl. Polym. Sci.*, 2012, **123.2**, 725–731.
9 K. Dietliker, T. Jung, J. Benkhoff, H. Kura, A. Matsumoto, H. Oka, D. Hristova, G. Gescheidt and G. Rist, *New developments in photoinitiators, Macromolecular Symposia*, Weinheim, Wiley–VCH Verlag, 2004, vol. 217.1, pp. 77–98.
10 S. Liu, B. Graff, P. Xiao, F. Dumur and J. Lalevée, Nitro–Carbazole Based Oxime Esters as Dual Photo/Thermal Initiators for 3D Printing and Composite Preparation, *Macromol. Rapid Commun.*, 2021, **42.15**, 2100207.
11 F. Hammoud, N. Giacoletto, M. Nechab, B. Graff, A. Hijazi, F. Dumur and J. Lalevée, 5, 12−Dialkyl−5, 12−-dihydroindolo 3, 2−a carbazole–Based Oxime–Esters for LED Photoinitiating Systems and Application on 3D Printing, *Macromol. Mater. Eng.*, 2022, 2200082.
12 P. Hu, W. Qiu, S. Naumov, T. Scherzer, Z. Hu, Q. Chen, W. Knolle and Z. Li, Conjugated bifunctional carbazole–based oxime esters: Efficient and versatile photoinitiators for 3D Printing under one–and two–photon excitation, *ChemPhotoChem*, 2020, **4.3**, 224–232.
13 A. Kowalska, J. Sokolowski and K. Bociong, The photoinitiators used in resin based dental composite—a review and future perspectives, *Polymers*, 2021, **13.3**, 470.
14 C. Dietlin, T. T. Trinh, S. Schweizer, B. Graff, F. Morlet-Savary, P. A. Noirot and J. Lalevée, New phosphine oxides as high performance near-UV type I photoinitiators of radical polymerization, *Molecules*, 2020, **25.7**, 1671.
15 M. A. Tehfe, F. Dumur, B. Graff, F. Morlet-Savary, D. Gigmes, J. P. Fouassier and J. Lalevée, Design of new Type I and Type II photoinitiators possessing highly coupled pyrene–ketone moieties, *Polym. Chem.*, 2013, **4.7**, 2313–2324.
16 C. Dietlin, S. Schweizer, P. Xiao, J. Zhang, F. Morlet-Savary, B. Graff, J. P. Fouassier and J. Lalevée, Photopolymerization upon LEDs: new photoinitiating systems and strategies, *Polym. Chem.*, 2015, **6.21**, 3895–3912.
17 A. AL Mousawi, F. Dumur, P. Garra, J. Toufaily, T. Hamieh, F. Goubard, T. T. Bui, B. Graff, D. Gigmes, J. P. Fouassier and J. Lalevée, Azahelicenes as Visible Light Photoinitiators for Cationic and Radical Polymerization: Preparation of Photoluminescent Polymers and Use in High Performance LED Projector 3D Printing Resins, *J. Polym. Sci., Part A: Polym. Chem.*, 2017, **55**, 1189–1199.
18 J. Yu, Y. Gao, S. Jiang and F. Sun, Naphthalimide aryl sulfide derivative norrish type I photoinitiators with excellent stability to sunlight under near-UV LED, *Macromolecules*, 2019, **52.4**, 1707–1717.
19 F. Hammoud, N. Giacoletto, G. Noirbent, B. Graff, A. Hijazi, M. Nechab, D. Gigmes, F. Dumur and J. Lalevée, Substituent Effects on Photoinitiation Ability of Coumarin-Based Oxime-Ester Photoinitiators for Free Radical Photopolymerization, *Mater. Chem. Front.*, 2021, **5**, 8361–8370.
20 Z. H. Lee, F. Hammoud, A. Hijazi, B. Graff, J. Lalevée and Y. C. Chen, Synthesis and free radical photopolymerization of triphenylamine-based oxime ester photoinitiators, *Polym. Chem.*, 2021, **12**, 1286–1297.
21 W. Wang, M. Jin, H. Pan and D. Wan, Remote Effect of Substituents on the Properties of Phenyl Thienyl Thioether-based Oxime Esters as LED-sensitive Photoinitiators, *Dyes Pigm.*, 2021, 109435.

22 M. Popal, J. Volk, G. Leyhausen and W. Geurtsen, Cytotoxic and genotoxic potential of the type I photoinitiators BAPO and TPO on human oral keratinocytes and V79 fibroblasts, *Dent. Mater.*, 2018, **34.12**, 1783–1796.

23 X. Peng, D. Zhu and P. Xiao, Naphthoquinone derivatives: Naturally derived molecules as blue-light-sensitive photoinitiators of photopolymerization, *Eur. Polym. J.*, 2020, **127**, 109569.

24 R. Strzelczyk and R. Podsiadły, Derivatives of 1, 4–-naphthoquinone as visible–light–absorbing one–component photoinitiators for radical polymerisation, *Color. Technol.*, 2015, **131.3**, 229–235.

25 M. M. Abdul-Monem, Naturally Derived Photoinitiators for Dental and Biomaterials Applications, *Eur. Dent. Res. Biomater. J.*, 2020, **1.02**, 72–78.

26 F. Hammoud, Z. H. Lee, B. Graff, A. Hijazi, J. Lalevée and Y. C. Chen, Novel phenylamine-based oxime ester photoinitiators for LED-induced free radical, cationic, and hybrid polymerization, *J. Polym. Sci.*, 2021, **59**, 1711–1723.

27 M. Abdallah, D. Magaldi, A. Hijazi, B. Graff, F. Dumur, J. P. Fouassier, T. T. Bui, F. Goubard and J. Lalevée, Development of New High-Performance Visible Light Photoinitiators Based on Carbazole Scaffold and Their Applications in 3D Printing and Photocomposite Synthesis, *J. Polym. Sci., Part A: Polym. Chem.*, 2019, **57**, 2081–2092.

28 L. M. Gornostaev, M. V. Vigant, O. I. Kargina, A. S. Kuznetsova, Y. G. Khalyavina and T. I. Lavrikova, Synthesis of 2-aryl-1-hydroxy-1H-naphtho 2, 3-d imidazole-4, 9-diones by reaction of 2-benzylamino-1, 4-naphthoquinones with nitric acid, *Russ. J. Org. Chem.*, 2013, **49.9**, 1354–1357.

29 K. A. Rykaczewski, E. R. Wearing, D. E. Blackmun and C. S. Schindler, Reactivity of oximes for diverse methodologies and synthetic applications, *Nat. Synth.*, 2022, **1.1**, 24–36.

30 *Principles of fluorescence spectroscopy*, ed. J. R. Lakowicz, Boston, MA, Springer US, 2006.

Partie IV : Combinaison : Photoamorceur & Amorceur Thermique

TABLE DES MATIÈRES

Table des matières

Polymérisation frontale pour la préparation des composites renforcés de fibres

Malgré tous les avantages de la photopolymérisation, l'application de la lumière à la fabrication de matériaux composites est récente et encore assez limitée. Cependant, les difficultés rencontrées au cours d'un processus classique de photopolymérisation peuvent être surmontées avec succès par la polymérisation frontale (FP), qui fait l'objet de recherches depuis de nombreuses années. [1-3] Il s'agit d'une réaction auto-entretenue, dans laquelle un stimulus initial (par exemple, la lumière) induit une zone de réaction localisée, appelée "front de polymérisation". La chaleur créée par la polymérisation exothermique dans cette zone génère une augmentation de température suffisante pour induire une polymérisation supplémentaire à la frontière entre la phase polymère et la phase monomère non réagie, ce qui entraîne généralement une propagation de la réaction. [4-6]

Dans cette partie, de récents développements en matière de comportement prédictif contrôlable pour la photopolymérisation frontale induite par la lumière ont été étudiés afin de préparer des composites renforcés par sept à dix couches de fibres de verre tissées de 1 mm d'épaisseur avec des teneurs en charges de 50 et 70 %. Un certain nombre d'amorceurs thermiques ont été étudiés dans ce travail, ce qui a conduit aux expériences de polymérisation présentées utilisant le peroxybenzoate de tert-butyle (Luperox® P). Les températures des échantillons ont été contrôlées en temps réel par des études d'imagerie thermique. Le nombre de couches polymérisées et la profondeur de polymérisation ont également été déterminés. Les propriétés mécaniques des composites produits ont été étudiées à l'aide de différentes techniques telles que la calorimétrie différentielle à balayage (DSC), l'analyse thermogravimétrique (TGA) et l'analyse mécanique dynamique (DMA). En outre, pour étudier l'impact de divers facteurs sur la polymérisation frontale, des plans d'expériences ont été réalisés. Les diluants réactifs utilisés dans ce travail sont soit le triacrylate de triméthylpropane (TMPTA), soit le diacrylate de 1,6-hexanediole (HDDA). Le HDDA a été choisi pour le plan d'expériences étudié car il est moins visqueux, ce qui peut faciliter l'imprégnation des composites et, par la suite, la diffusion de la chaleur. Le Laromer PE 9074 (BASF), un acrylate de polyester, a été choisi comme oligomère en raison de sa grande réactivité, de sa bonne élasticité, de sa résistance chimique et de sa faible dureté. Cette résine est donc un bon système modèle pour introduire la contrôlabilité de la polymérisation frontale photo-induite.

PARTIE IV : COMBINAISON : PHOTOAMOCEUR & AMORCEUR THERMIQUE

Ce travail est un projet réalisé dans le cadre d'une collaboration industrielle avec BASF à Ludwigshafen (Allemagne), et sera présenté sous la forme d'un article à venir.

Références

[1] B. A. Suslick, J. Hemmer, B. R. Groce, K. J. Stawiasz, P. H. Geubelle, G. Malucelli, A. Mariani, J. S. Moore, J. A. Pojman, and Nancy R. Sottos, Frontal Polymerizations: From Chemical Perspectives to Macroscopic Properties and Applications, Chemical Reviews, 2023, 123.6, 3237-3298.

[2] P. Garra, C. Dietlin, F. Morlet-Savary, F. Dumur, D. Gigmes, J.P. Fouassier, J. Lalevée, Photopolymerization processes of thick films and in shadow areas: a review for the access to composites, Polymer Chemistry, 2017, 8.46, 7088-7101.

[3] M. Ziaee, I. Naseri, J. W. Johnson, K. A. Franklin, M. Yourdkhani, Frontal Polymerization and Three-Dimensional Printing of Thermoset Polymers with Tunable Thermomechanical Properties, ACS Applied Polymer Materials, 2023.

[4] J. Staal, E. Smit, B. Caglar, V. Michaud, Thermal management in radical induced cationic frontal polymerisation for optimised processing of fibre reinforced polymers, Composites Science and Technology, 2023, 110009.

[5] J. T. Cabral, S. D. Hudson, C. Harrison, J.F. Douglas, Frontal photopolymerization for microfluidic applications, Langmuir, 2004, 20.23, 10020-10029.

[6] C. Nason, T. Roper, C. Hoyle, J. A. Pojman, UV-induced frontal polymerization of multifunctional (meth) acrylates, Macromolecules, 2005, 38.13, 5506-5512.

Assessment of Photoinduced Frontal Polymerization Processes for a Stable 1K System

Abstract

Frontal polymerization (FP) has attracted increasing interest in recent years in various applications. This polymerization method can be very promising for the polymerization of thick materials with high fillers content in the range of 50-80% (weight) by local application of a reasonable amount of energy. In this work, recent advances in controllable and predictive behavior for photo-induced frontal photopolymerization are reported. Here, *Tert*-butyl peroxybenzoate (Luperox-P) was selected to initiate thermal polymerization at depth because its decomposition temperature is in a promising range for industrial applications, i.e., neither extremely high nor very low. The choice of the thermal initiator is very important and the stability in monocomponent (1K) systems (all-in-one) of the photoinitiator Diphenyl(2,4,6-trimethylbenzoyl)phosphine oxide (TPO), monomers and Luperox-P for more than 8 weeks at 80°C in the dark opens new opportunities for the FP. Investigations were conducted on the FP of 7 mm thick woven glass fiber reinforced composites (seven layers of 50 and 70% wt woven glass fibers). Thermal imaging experiments were used to follow the temperatures in the samples in real time. The number of cured layers and the depth of cure were also determined. We investigated various factors such as the content of the photoinitiator, the light intensity, resulting in a statistical design of experiments (DoE) with the factors: 1) Content of Luperox-P and the irradiation time used to investigate the influence on photoinduced frontal polymerization. Markedly, FP appears to be fully controllable for a storage-stable, tunable 1K system.

PARTIE IV : COMBINAISON : PHOTOAMOCEUR & AMORCEUR THERMIQUE

1. Introduction

In a world where competition and cost reduction are constant goals, composite materials, which combine lightness and high mechanical strength, are a viable alternative to traditional materials such as metals or plastics. [1-2] Although their range of uses extends from aerospace to high-end sporting equipment, their high production costs seem to be the main obstacle to a universal shift from steel to composites. [3] The majority of work in recent years has been done to increase their level of competitiveness, but there is still much progress to be made in order to solve this persistent problem. Today, thermal curing is the primary method of producing composite materials. [1-3] This means that reactions take place either at high temperatures, requiring a lot of energy, or at ambient temperatures, requiring little control and being slow. The technical drawbacks of thermal curing can be overcome by a further development to a fully UV-controlled procedure. It is a reliable technology that works at room temperature and has reaction times in the order of minutes, rather than hours. Despite all its advantages, light is still only recently and very rarely used in the production of composite materials. [2]

Frontal photo-induced polymerization (FPP), which has been studied for many years, is efficient solution for this problem. In this process, which is driven by an external light source, polymerization/heat fronts form and propagate through the monomer material as traveling plane waves (Figure 1). High optical attenuation, limited mass and heat diffusion, and FPP result in a sharp interfacial profile between the polymer network and the monomer. [7-9] The solidification front first forms a "skin" on the surface closest to the light source before moving into the uncrosslinked medium (Figure 1). Photopolymerization of (millimeter to centimeter) thick material sections illustrates this frontal feature of the polymerization process particularly well, and allows for rapid 3D patterning by modulated or multistage illumination (without the need for lithography and stereo, two-photon, or multistage alignment). Thermal front polymerization (TFP) and isothermal frontal polymerization (IFP), which are autocatalytic reaction processes, are distinct from FPP as a polymerization method. [10] However, propagation is (self-)sustained by the thermal energy released from an exothermic polymerization reaction, despite the fact

that various polymerization techniques also produce wave polymerization fronts. In TFP, a localized heat source initiates the process, and the rate of thermal diffusion and the nonlinear temperature dependence of the polymerization rate constants control the rate of front propagation. FIP, also known as "interfacial gel polymerization," occurs in a viscous or gel matrix that inhibits chain termination. A self-sustaining polymerization front is initiated by the introduction of a polymer seed. A thorough review of the history, nature, and applications of these polymerization methods is provided by Pojman and colleagues. [11-16]

Typically, a certain type of peroxide chemical is used as a thermal initiator to induce polymerization, which is initiated by the heat created by photo-induced polymerization. Thus, to ensure long-term preservation, the thermal initiators should have a particular level of stability (i.e., a relatively high initiation temperature). [17-19] However, extreme decomposition temperatures are not suitable for use with heat-sensitive materials. In addition, toxicity and odor leachability issues of the initiator, especially aromatic leachability, must be resolved. Dibenzoyl peroxide (BPO) is an example of an aromatic peroxide with rather low decomposition temperature, low storage stability, and high aromatic leachability. On the other hand, aromatic hydroperoxides (CHPs) are examples of aromatic hydroperoxides with high decomposition temperature, high storage stability and high aromatic leachability. [20-22] Indeed, the decomposition temperature of the thermal initiator remains the key challenge, as it must be neither very low to avoid stability issues, nor very high, which would cause evaporation cracks or perhaps polymer degradation.

In this paper, recent developments in controllable predictive behavior for photo-induced frontal photopolymerization were investigated in order to prepare composites reinforced with seven to ten layers of 1 mm thick woven glass fibers with 50 and 70% solids content. A number of thermal initiators were investigated in this work (Scheme S1) leading to the presented curing experiments using *Tert*-butyl peroxybenzoate (Luperox® P). Thereby, the temperatures of the samples were monitored in real time by thermal imaging studies. The number of polymerized layers and the depth of polymerization were also determined. The mechanical properties of the produced composites were studied through different techniques such as differential scanning calorimetry (DSC), thermogravimetric analysis (TGA), and dynamic mechanical analysis (DMA). In addition, to study the impact of various factors on the frontal polymerization, design of experiments (DoE) was carried out. The reactive diluents used in this work are either trimethylpropane triacrylate (TMPTA) or 1,6-hexanediole diacrylate (HDDA), where HDDA

was selected for the DoE studied since it is less viscous which can facilitate the impregnation of the composites and subsequently the heat diffusion. Laromer PE 9074 (BASF), which is a polyester acrylate, was chosen as an oligomer due to its high reactivity, good elasticity and chemical resistance, and low hardness. Therefore, this resin is a good model system to introduce the controllability of photo-induced frontal polymerization. Preparation, chemicals, materials and procedures are described in detail in the accompanying information.

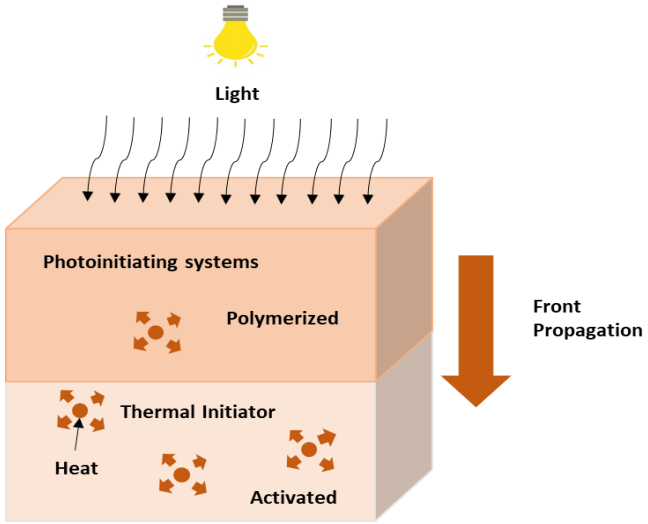

Figure 1. Schematic view of the photoinduced frontal polymerization process.

2. Experimental part

2.1. Chemical compounds

2.1.1. Photoinitiator and thermal initiators

Diphenyl(2,4,6-trimethylbenzoyl)phosphine oxide (TPO) was chosen as photoinitiator and obtained from Lambson Ltd. (Speedcure® TPO). *Tert*-butyl peroxybenzoate (Luperox® P), *tert*-butyl peroxide (Luperox® DI), 1,1-Bis(*tert*-butylperoxy)cyclohexane (Luperox® 331M80), potassium persulfate, ammonium persulfate and 1,1'-azobis(cyclohexanecarbonitrile) were obtained from Sigma Aldrich. Dicumyl peroxide and *tert*-butyl hydroperoxide (70 % wt in water) were purchased from TCI Chemicals. Cumene hydroperoxide was obtained from Alfa Aesar, dibenzoyl peroxide (Peroxan® BP 50) was obtained from Pergan GmbH and BlocBuilder® MA was obtained from Arkema (Scheme 1).

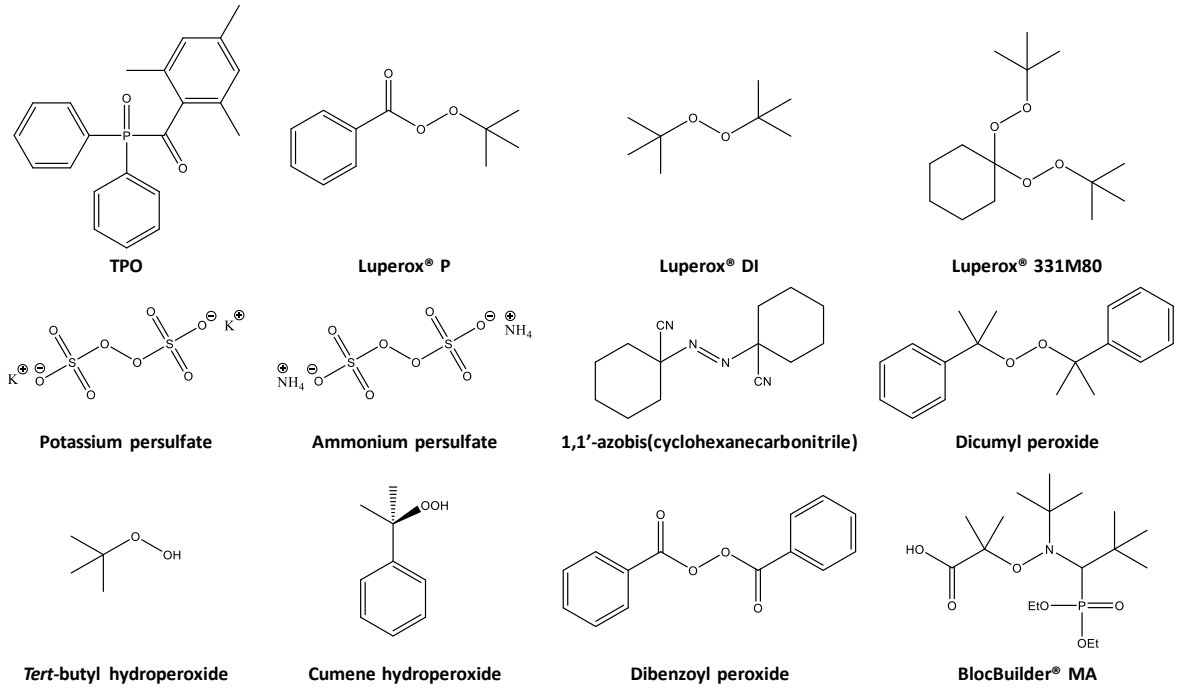

Scheme 1. Chemical structures of the photoinitiator: TPO and the thermal initiators: Luperox® P, Luperox® DI, Luperox® 331M80, potassium persulfate, ammonium persulfate, 1,1'-azobis(cyclohexanecarbonitrile), dicumyl peroxide, tert-butyl hydroperoxide, cumene hydroperoxide, dibenzoyl peroxide and BlocBuilder® MA.

2.1.2. Monomers

All the monomers (**acrylates:** Laromer DPGDA (Dipropylene glycol diacrylate), Laromer GPTA (Propoxylated glycerol triacrylate), Laromer HDDA (1,6-Hexandiol diacrylate), Laromer LR 8986 (Aromatic Epoxy Acrylates), Laromer PE 9074 (polyester acrylate), Laromer PR 9119 (Epoxy acrylates), Laromer TMPTA (trimethylpropane triacrylate), Laromer UA 8987N (Urethane-modified acrylic resin), Laromer UP 35D (Unsaturated polyesters), or **methacrylates:** Visiomer 1,6 HDDMA (1, 6-hexanediol dimethacrylate), Laromer GPTA Variante, Laromer UP 911, Laromer LR 8986 with MA, Laromer LR 8987 MA Variante, Laromer UP 35D Variante, Laromer DPGDA Variante, Laromer PE 9074 with MA, Visiomer TMPTMA) used were received from BASF.

2.2. Fibers

Cut glass fibers (4.5 mm length) were obtained from Polyplan Composites. Woven glass fibers (QX1178, quadriaxial glass fibers, 1177 g.m^{-2}, ~1 mm thickness) were obtained from Sicomin.

2.3. Irradiation sources

A LED centered at 395 nm with a maximal light intensity of 8 $W.cm^{-2}$ (area 2.5 cm x 4 cm) was obtained from TaoYuan (China) and a laser diode centered at 405 nm with a maximal light intensity of 400 $mW.cm^{-2}$ was obtained from Thorlabs (USA).

2.4. Preparation of fiber reinforced composites

The woven glass fibers are cut into squares of 4 cm length and 4 cm width. Each sample is composed of 7 layers of woven glass fibers. The 7 layers of woven glass fibers are weighed in order to determine the corresponding amount of monomer to obtain the desired weight content (e.g. 50 or 70 % wt of glass fibers). The amounts of photoinitiator (about 1% wt) and thermal initiator (3% wt) are determined on the whole weight (fibers + monomer).

The photoinitiator and the thermal initiator are mixed with the monomer in a beaker of the size of 12 mL using the Speedmixer™ DAC 150.1 FVZ-K from Hauschild with a speed of 2000 rpm for 2 min. A polypropylene (PP) film is used as support for the sample and a small amount of the mixture is deposited on the PP film. Then, a first layer of fibers is placed on the previous assembly and mixture is deposited on it. The sample is obtained by the superposition and alternation of fibers and mixture. The sample is covered with a PP film and pressed 3 times by hand. Then, the sample is pressed 3 times with a steel roller. The sample is placed in a vacuum bag and is vacuum sealed with a vacuum sealing machine in order to enhance the impregnation of the fibers by removing the air. After sealing, the sample is placed between two new PP films and placed under the irradiation device to start the frontal polymerization experiment (Figure 2).

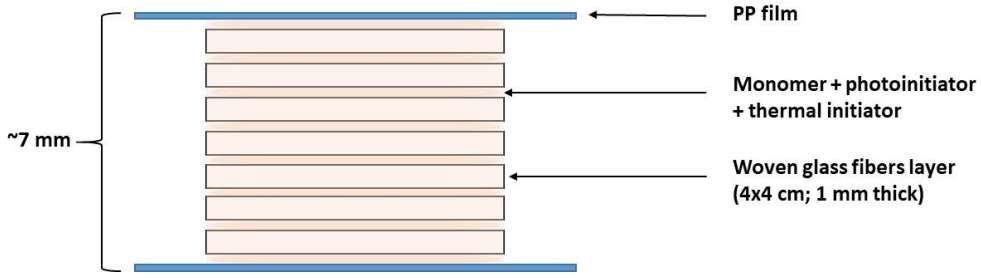

Figure 2. Structure of a woven glass fibers-based sample.

2.5. Thermal measurements

The frontal polymerization is followed in real-time by recording the temperature of the sample using a thermal imaging camera obtained by Fluke TiX500 and a by Optrics GmbH XI-400. The temperatures at 3 different depths of the ~7 mm thick samples are recorded for the side: near to the surface, at 3 mm depth and at 6 mm depth (Scheme 2). After analyzing the measurements, temperature-time diagrams can be created from which the maximum temperatures and the time at which this temperature is reached can be obtained (Figure 3).

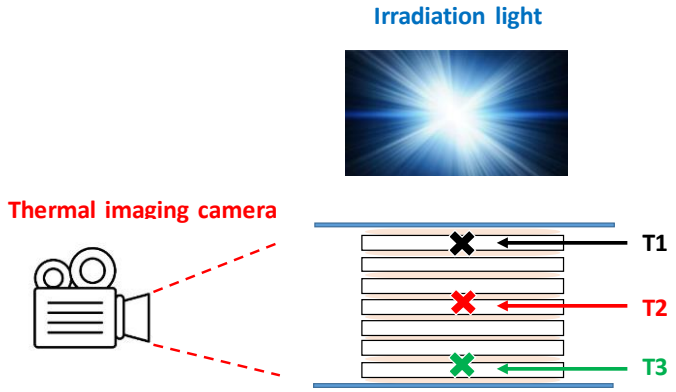

Scheme 2. Experimental setup used for the thermal measurements: the temperature of the sample (7 mm thick) is recorded at 3 different depths (T1 at the surface of the sample, T2 at 3 mm depth and T3 at 6 mm depth), while LED@395 nm is used.

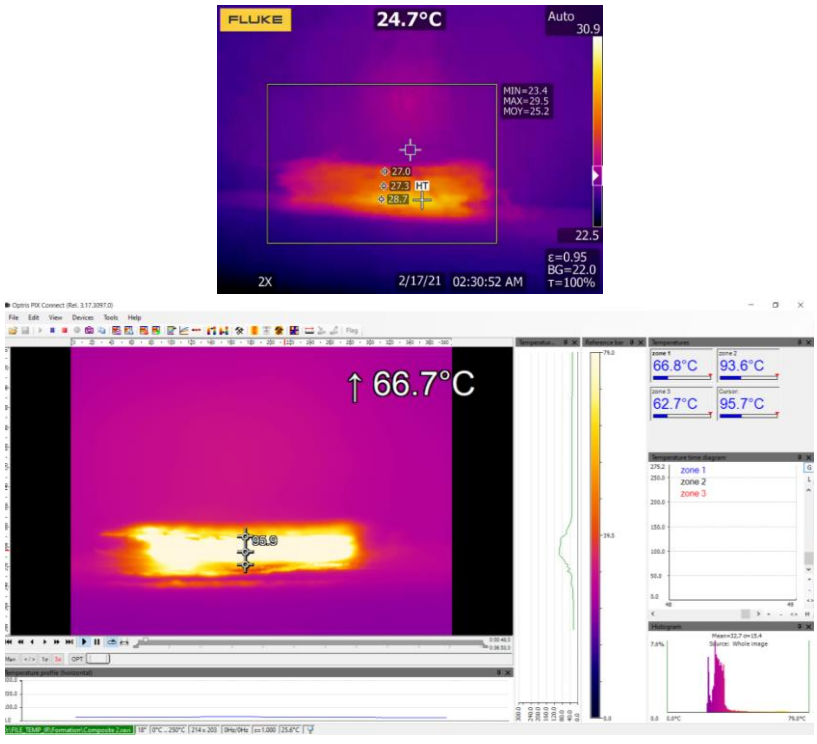

Figure 3. Thermal image of the photocomposite.

2.6. Visual rating of the bottom layer

This parameter is used to evaluate the quality of the last layer. it is rated from 1 to 5: (Figure 4)

1 (best rating): entirely polymerized, good aspect, appropriate exothermicity (no resin + PP layer)

2: entirely polymerized, good aspect, too high exothermicity (huge resin + PP layer)

3: entirely polymerized, burned surface, too high exothermicity (huge resin + PP layer)

4: lower edges polymerized but wet in the middle (last layer)

5 (worst rating): no polymerization (last layer)

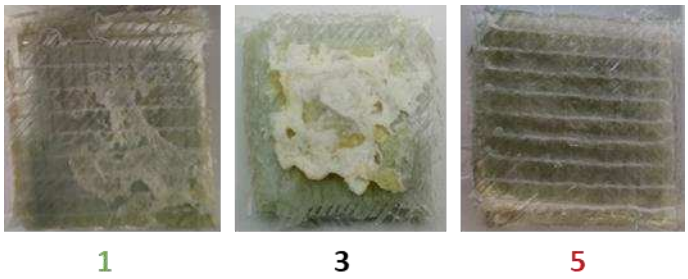

Figure 4. Visual rating for different samples.

2.7. Depth of cure

The depth of cure (DoC) corresponds to the thickness of cured material. For woven glass fibers-based samples, the depth of cure is determined by removing the unpolymerized layers from the rest of the sample. The cured thickness is measured using a Mitutoyo thickness measuring tool and the corresponding number of polymerized layers is determined.

2.8 Deflection measurement

Some samples have a tendency to curve during the polymerization (the edges are rising up) (Figure 5). This characterization was used to evaluate the angle of deflection and this method was used to differentiate well polymerized samples from partially polymerized samples. A seven layers of woven glass fibers composite is prepared by frontal polymerization experiment. The top of the sample is placed against a spirit level to adjust the horizontal level and a photo is taken. The deviation angle is determined using the software ImageJ. High deviation angles correspond to well polymerized samples as the high exothermicity is responsible for the deviation angle.

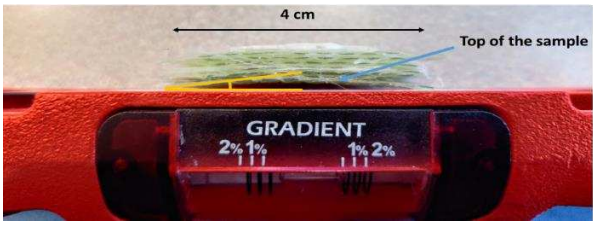

Figure 5. Deviation angle measurement.

2.9. Shore D measurement

Shore D hardness tests from SAUTER, was used to measure to measure the hardness of polymers. Shore hardness tests measure the resistance of material to indentation. Different scales of Shore hardness can be used depending on the hardness of the material to characterize. Shore A scale is used for softer materials whereas Shore D is used for relatively hard materials (Figure 6). Fifteen measurements were done on each surface (top/bottom of the sample) to obtain highly reliable data.

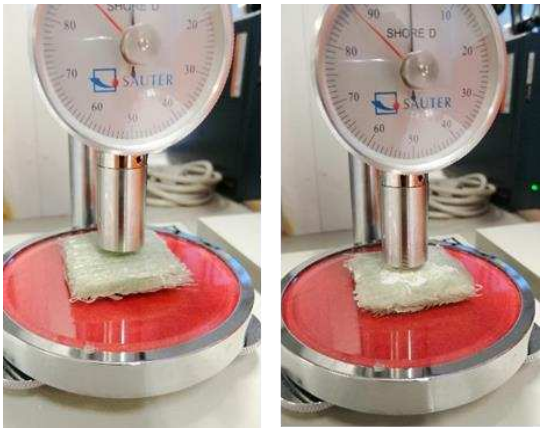

Figure 6. Shore D measurements on the top and the bottom.

2.10. Differential scanning calorimetry (DSC)

The thermal polymerization can be evaluated by DSC with a Mettler-Toledo DSC 1 differential scanning calorimeter. 10 mg of the monomer alone or with the thermal initiator (1 % wt) are inserted in an aluminium crucible. Thermal measurements are performed from 25 to 500 °C with a heating rate of 10 °C.min^{-1} under nitrogen. Different parameters can be extracted from this experiment: the onset temperature, the temperature of the polymerization peak and the enthalpy corresponding to the polymerization peak. The function conversion (FC) can be determined using following formula:

$$FC\ (\%) = \frac{heat\ released\ \times MW}{\Delta Htheory\ \times f} \times 100$$

With:

- heat released: the heat released during the polymerization experiment corresponding to the enthalpy of the polymerization peak determined by DSC in $J.g^{-1}$;
- MW: the molar weight of the monomer in $g.mol^{-1}$;
- ΔHtheory: the heat corresponding to the polymerization of 1 mol of reactive functions leading to 100 % of conversion (78610 $J.mol^{-1}$ for acrylate and 54453 $J.mol^{-1}$ for methacrylate);
- f: the monomer functionality

Some experiments were also carried out for polymerization under air to characterize the oxygen inhibition effect on the thermal initiator ability.

DSC experiments are also used to characterize the woven glass fibers-based composites after frontal polymerization. The upper and the lower layers of the composite are separated from the rest of the sample and a small piece of the center of the upper and lower layers is cut and placed in an aluminium crucible. The sample is heated two times from 0 to 250 °C with a heating rate of 10 $°C.min^{-1}$ under nitrogen. Inhomogeneities in terms of conversion between the top and the bottom of the sample can be characterized by this technique and the content of remaining monomer can be evaluated.

2.11. Thermogravimetric analysis (TGA)

Thermogravimetric experiments are carried out using a Mettler Toledo DSC 1. The degradation of the monomer can be followed as a function of the temperature. The sample is heated from 30 to 500 °C with a heating rate of 10 $°C.min^{-1}$ under nitrogen. The temperatures corresponding to 5 and 10 % weight loss were determined for each monomer.

2.12. Dynamic Mechanical Analysis DMA (Compression test)

The compression tests were performed on a Dynamic Mechanical Analyzer (Metravib VA 4000) with following parameters: static compressive load 10 N, frequency 10 Hz, dynamic strain 5 µm, from ambient temperature to 250 °C with a heating rate of 2 °C/min. Square samples of 10 mm width, 10 mm long and 7-8 mm thick (7 layers of woven glass fibers) were analyzed.

2.13. UV-visible spectroscopy

The UV-visible spectra and the transmittance spectra were recorded using a JASCO V-730 UV/vis spectrophotometer.

3. Results and discussion

3.1. Choice of the thermal initiator by DSC and TGA experiments

The properties of the different thermal initiators are investigated by DSC in order to select the most appropriate one(s) for the frontal polymerization experiments. The structures can be found in Scheme 1. For each thermal initiator the onset temperature, the peak temperature and the corresponding enthalpy and function conversion are determined. For example, for the monomer TMPTA, all of the thermal initiators in combination with TMPTA were investigated by DSC experiments and their order of reactivity based on the maximal temperature of the polymerization peak has been determined (Figure 7).

The temperatures determined by TGA tests for the monomer, corresponding to a weight loss of 5 % and 10 %, were also taken into account in the choice of thermal initiator to ensure that no decomposition of the monomer takes place at the initiation temperature of the chosen thermal initiator.

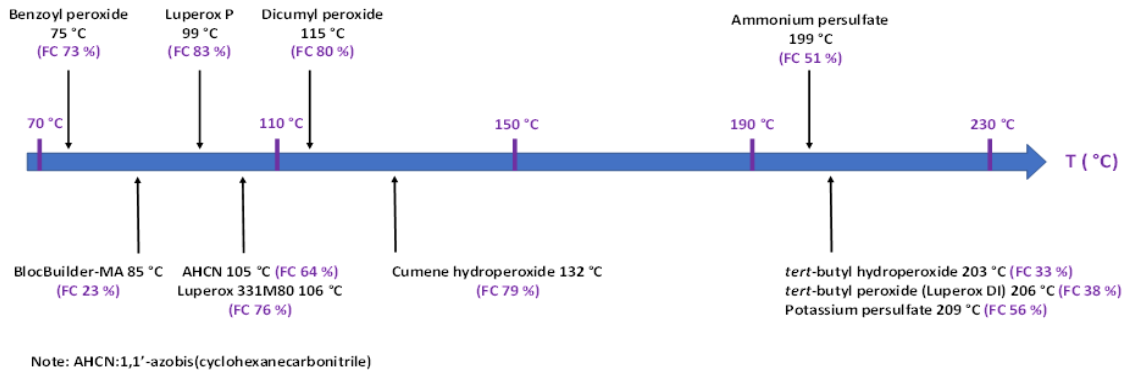

Figure 7. Order of reactivity of the different thermal initiators investigated in Laromer TMPTA based on the maximal temperature of the polymerization peak determined by DSC experiments. FC is the final acrylate function conversion. (See Scheme S1 for the structures)

Based on the TGA experiments of TMPTA without initiator, the temperatures corresponding to 5 and 10 % weight loss have been determined with values respectively equal to 193 and 212 °C. According to the DSC and TGA results and to the frontal polymerization experiments carried out, Luperox P was chosen as thermal initiator. Indeed, the polymerization in presence of Luperox P occurs for a well-adapted temperature range and leads to a high double bond conversion. Markedly, this thermal initiator, was selected to initiate thermal polymerization at depth because its decomposition temperature is with around 100 °C in a promising range for industrial applications, i.e., neither extremely high nor so low that reactivity can be expected under normal conditions (room temperature). The choice of the thermal initiator is very important and the stability in monocomponent (1K) systems (all-in-one) of the photoinitiator Diphenyl(2,4,6-trimethylbenzoyl) phosphine oxide (TPO), monomers and Luperox-P for more than 8 weeks at 80°C in the dark opens new opportunities for photoinduced frontal polymerization.

3.2. Issue of light penetration in filled samples

The light penetration in composites is strongly affected by the light absorption and light scattering by the fillers. This behavior was characterized by the following procedures. A layer of woven glass fibers (70 % wt) was impregnated with 30 % wt trimethylolpropane triacrylate (TMPTA) (see part 1.2 in SI) containing TPO (0.5 % phr, parts per hundred resin) and polymerized with the LED @395 nm with an intensity of 8 $W \cdot cm^{-2}$ for 10 s. A cut glass fibers composite mixture was also prepared by dispersion of cut glass fibers (4.5 mm length, 70 % wt) in TMPTA (30 % wt) containing TPO (0.5 % phr) using the Speedmixer™ and polymerized

with the LED @395 nm. A 1 mm thick slice of the sample was cut. The transmittance spectra of both samples were recorded by UV-visible spectroscopy. The penetration of light that means the absorbance coefficients of the composites were determined using a Beer Lambert model for the LED @395 nm. The irradiance in depth (Figure 8) can be calculated using following equation:

$$I(x) = I(0) \times 10^{(-x \times Abs,TPO@395\ nm)} \times 10^{(-x \times Abs,composite@395\ nm)}$$

With:

I(x): the irradiance at a distance x from the surface in the sample in $W \cdot cm^{-2}$;

I(0): the irradiance at the surface of the sample in $W \cdot cm^{-2}$;

x: the distance from the surface in cm;

AbsTPO@395 nm: the absorbance of TPO at 395 nm which is linked to the molar extinction coefficient of TPO at 395 nm and the concentration of TPO;

Abs, composite@395 nm: the absorbance of the composite at 395 nm (taking into account both the light absorption and scattering), calculated from the transmittance of the composite at 395 nm determined by UV-visible spectroscopy.

Then, the irradiance was calculated using the Beer Lambert model for an unfilled sample and for the samples based respectively on woven glass fibers and cut-glass fibers for depths going from 0 to 0.1 cm in depth (Figure 8). For both filled samples, the irradiance decreases very rapidly in depth such as already no more light penetrates in the sample for 500 µm depth whereas still 7 $W \cdot cm^{-2}$ light intensity penetrates in the case of an unfilled sample.

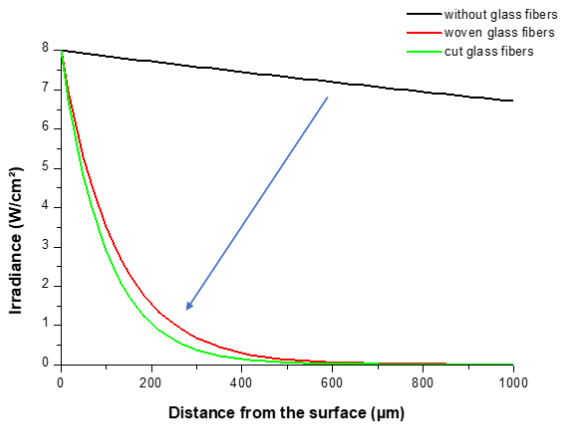

Figure 8. Simulated penetrating irradiance ($W \cdot cm^{-2}$) vs. depth (µm) from a LED @395 nm (8 $W \cdot cm^{-2}$) for TPO (0.5 % phr) in TMPTA without fillers, for woven glass fibers (70 % wt) and in presence of cut glass fibers (70 % wt).

As a conclusion, for filled samples, the light transmittance of the composite must be taken into account. As the penetration of light decreases very rapidly in depth of the samples, frontal polymerization is of particular interest (for thickness > 500 µm).

3.3. Fillers content effect

Two woven glass fibers-based samples containing 50 and 70 % (wt) of woven glass fibers, TMPTA (50 and 30 % wt respectively) and TPO (0.5 % phr, parts per hundred resin) were prepared and polymerized with the LED @395 nm, with an intensity of 8 $W \cdot cm^{-2}$ for 30 s. The temperatures at three different depths of the samples were recorded during the polymerization experiments using thermal imaging experiments, Figure 9 (B). The maximal temperatures reached for the three different depths studied were extracted for the two samples studied and are presented as a function of the woven glass fibers content on Figure 9 (A).

By comparing the maximal temperatures reached for the two different contents of woven glass fibers studied, it is clearly visible that the maximal temperatures reached decrease when the woven glass fibers content increases. Indeed, the maximal temperatures reached in depth of the samples (T2 and T3) are divided by a factor of two (from 166 and 161 °C to 75 and 59 °C) when the woven glass fibers content increases from 50 to 70 % (wt).

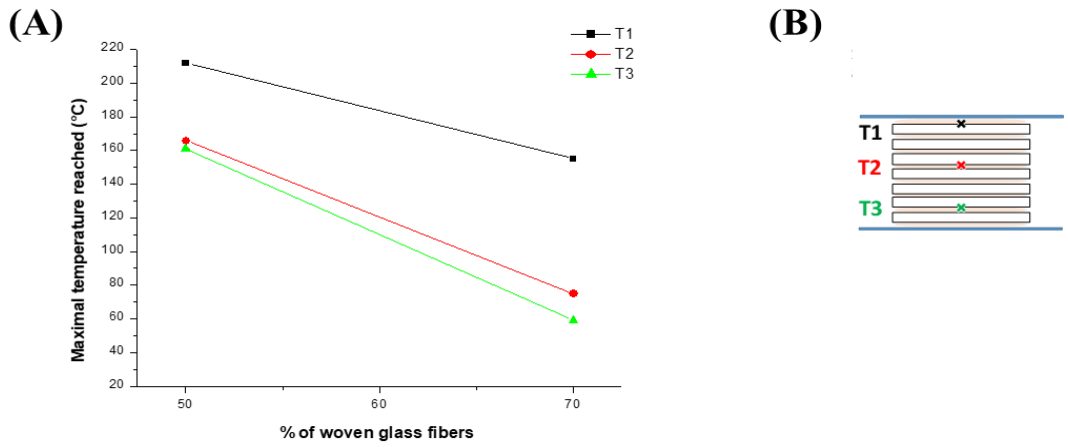

Figure 9. (A) Maximal temperatures reached for T1, T2 and T3 vs. content of woven glass fibers for Laromer TMPTA based samples with 50 and 70 % (wt) of woven glass fibers in presence of TPO (0.5 % phr) (under air) under irradiation with the LED @395nm at 8 $W \cdot cm^{-2}$ for 30 s; thickness=7 mm. (B) Schematic of the sample consisting of seven glass fiber layers and the indicated measuring positions for the temperature (T1 = 1 mm, T2 = 3 mm and T3 = 7 mm).

As the light penetration in depth decreases when the fibers content increases, the temperatures reached in depth also decrease for high fibers contents. Therefore, the polymerization in depth

becomes more and more difficult for increasing fibers contents. Frontal polymerization is of great interest to enhance the polymerization in depth in such difficult conditions.

1.1. Design of experiments to predict frontal polymerization

For the Design of Experiments (DoE) a basic Taguchi model was proposed and Minitab software [23] used in order to investigate the factors that can influence the output in our experiments such as frontal polymerization (yes/no), or the double bond content (DBC).

1.1.1. DoE proposal with PE 9074/HDDA blend

The idea of this DoE is to keep some parameters constant such as the fiber content (66 wt %), the TPO content (1% phr), the irradiation wavelength (395 nm), the intensity (8 W/cm²) and the acrylate double bond content (DBC) (6.5 mol/kg), while the other parameters (input factors) such as Luperox P content and irradiation period, can be varied. The output parameters can be obtained through fast characterizations (such as visual rating, number of polymerized layers, the depth of cure, and the shore D values) or more time consuming techniques (such as thermal measurements: differential scanning calorimetry (DSC) for the residual double bond content on the top or bottom of the sample, or dynamic mechanical analysis (DMA) for tan delta in compression tests. Then a DoE analysis software (Minitab) was used to analyze the series of experiments (see Table 1). As already mentioned, the various procedures are also described in the supporting information.

The experimental results (Table 1) show that for the HDDA/PE 9074 blend, long irradiation periods (90 s) as well as high Luperox P contents (3 or 4 % phr) are required to allow frontal polymerization to occur. And this can be clearly seen from the fast characterization techniques (Table 1), where high temperatures in depth were attenuated just with 3 or 4 % phr Luperox P under 90 s of irradiation (e.g. with 4% phr Luperox P under 90s irradiation the temperatures can reach ~85°C, see Table 1). The difference with the reference samples without Luperox P, where only 3 layers can be polymerized, can also be seen. Moreover, the Shore D values observed in the base are high only in the presence of Luperox P and 90 s irradiation, and the tan delta values were lower (indicating much better mechanical properties), which could also be proved by the remaining double bond content of the acrylate functions in the base, which was quite low (Table 1). Hence, the lowest layer which is nearly 6 mm from the light source was completely solidified / polymerized.

The results of the DoE analysis demonstrated the influence of several parameters such as the number of polymerized layers, the depth of cure, T3, Shore D at the bottom and the content of remaining acrylate functions at the bottom. Figure 10 could suggest the presence of a main effect, in which the factor's levels have a different effect on the response. As a result, the magnitude of the main effect is proportional to the slope of the line. The optimum inputs (irradiation time and thermal initiation content) were extracted by the DoE software by selecting the parameters to enhance the FP process without too high temperature (T_3 was selected close to 80°C). Markedly, the predicted outputs (Table 1) for the optimal formulations were found very close to those obtained experimentally using these inputs, confirming the predictable behavior.

Table 1. The input factors (content of Luperox P and irradiation time) and the output parameters of HDDA/PE9074 FP in laminate in the presence of glass fibers (66 % wt). LED@395 nm at 8 W/cm²; thickness = 7 mm. The irradiation starts at t=10 s. The Luperox P content refers to the resin phase and not to the whole system.

	INPUT		OUPUT											
Experiment	**Luperox P content (%** phr)	**Irradiation period (s)**	**Visual rating**	**Number of polymerized layers**	**DoC (mm)** *Average*	**T2 (°C)**	**T3 (°C)**	**Deviation angle (°)** *average*	**FP?**	**Shore D top** *average*	**Shore D bottom** *average*	**Remaining acrylate top**	**Remaining acrylate bottom**	**tan delta**
1	1	30	4	2	2.9	75	67	0	No	82	12	3	26	0.150
2	3	30	4	2	2.3	73	62	0	No	76	13	7	24	0.143
3	1	90	4	3	3.6	82	63	0	No	80	15	3	22	0.152
4	3	90	1	7	7.1	85	74	0	Yes	81	68	3	8	0.090
5	1	30	4	1.5	1.9	73	52	0	No	83	15	1	29	0.165
6	3	30	4	2.5	2.8	87	63	0	No	83	15	5	36	0.157
7	1	90	4	3.5	3.3	78	69	0	No	84	20	6	23	0.152
8	3	90	1	7	7.0	86	92	0	Yes	80	66	5	11	0.103
9	2	60	4	2.5	2.8	77	63	0	No	84	12	3	31	0.154
10	2	60	4	2.5	2.7	82	62	2	No	79	15	8	32	0.170
11	2	60	4	2.5	2.7	85	66	0	No	84	13	5	25	0.139
12	4	30	4	2.5	2.8	90	74	0	No	83	13	7	27	0.154
13	4	30	4	3	2.9	90	72	1	No	81	13	5	26	0.150
14	4	90	1	7	6.8	87	81	0	Yes	82	71	6	14	0.115
15	4	90	1	7	7.0	87	80	0	Yes	82	64	6	10	0.106
16	0	30	4	1	1.3	83	71	1	-	83	16	1	27	0.130
17	0	30	4	1	1.7	94	70	0	-	86	10	1	34	0.157
18	0	90	4	2	2.1	84	66	2	-	78	17	2	16	0.142
19	0	90	4	3	3.0	83	73	0	-	84	22	2	17	0.160
Experimental	4	90	1	7	6.8	87.2	81	0	1	82	71	6	14	0.115
Proposed	4	90	1.32	6.8	6.7	89.0	82.6	0.2	*	81	63	6	12	0.108

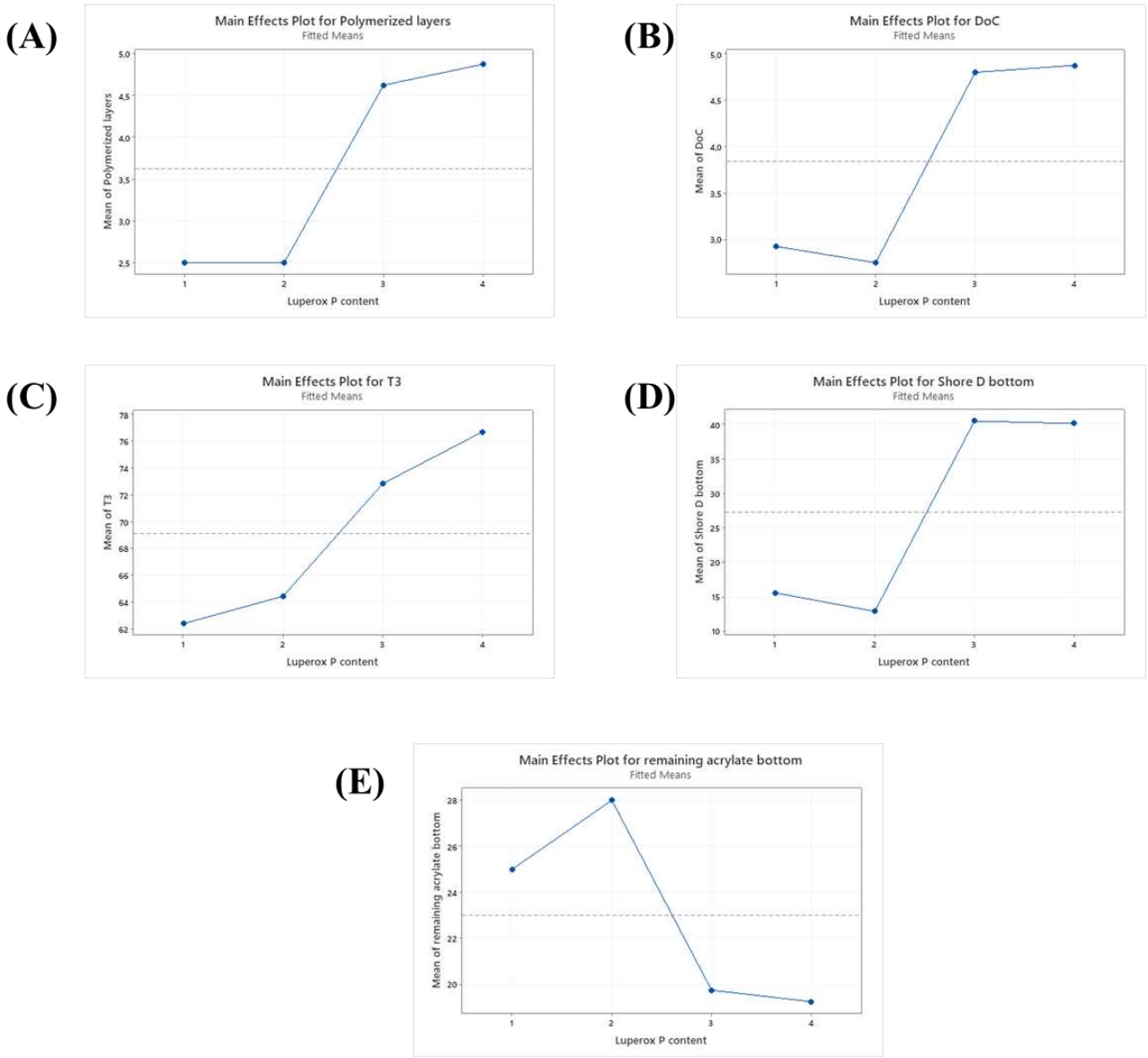

Figure 10. MiniTab analysis: example of analysis of the effect diagrams for Luperox P content: (A) Polymerized layers; (B) Depth of cure; (C) Temperature T3; (D) Shore D bottom; (E) Content of remaining acrylate functions at the bottom.

1.1.2. Comparison of different acrylate and methacrylate blends

In this part, the idea is to compare the different reactive diluents acrylates and methacrylates analogues with PE 9074 or PE9074 methacrylate analogue as oligomer, for a ratio (60%/40% w/w), hence the double bond content was not the same for all the blends tested. The following parameters were kept constant: the optimum fibers content (66 %), the content of TPO (1 % phr), the irradiation wavelength (λ= 395 nm), the intensity (8 W/cm²), and the irradiation time (90s).

The experimental results show that the temperatures reached with methacrylates are much lower than that of acrylates, and this can be expected from the lower heat release for methacrylates (it is about ~52 kJ/mol for methacrylates and 78 kJ/mol for acrylates). [24] For example, Table 2 shows that for the acrylate blend TMPTA/PE9074, the temperatures reached in depth are more than about 110 °C, which is significantly higher in comparison to the temperatures obtained with the analog methacrylate blend TMPTMA/PE9074 variant (which are just about 50 °C, i.e. lower than the initiation temperature of the used thermal initiator), showing that there is a frontal polymerization just in the case of TMPTA/PE9074. Then, the experimental results show that the frontal polymerization was restricted to HDDA and TMPTA (see Table 2), but that DBC is different in this comparison.

Table 2. The input factors and the output parameters of the different tested blends monomer/oligomer for FP in laminate in the presence of glass fibers (66 % wt). LED@395 nm at 8 W/cm²; thickness = 7 mm. The irradiation starts at t=10 s. Double bond content (DBC) and Luperox P refer to the resin phase and not to the whole system.

Monomer/Oligomer	DBC (mol/kg)	Luperox P Content (phr)	Visual rating	Real fiber content (%)	Number of layers polymerized	DoC (mm) average	T2 (°C)	T3 (°C)	Deviation angle (°) average	FP ?	Shore D top average	Shore D bottom average
TMPTA/PE9074	6.9	3	3	68	7	8.4	130	111	3	Yes	80	52
TMPTMA/PE9074 methacrylate	7	3	5	74	3	3.1	49	48	0	No	78	13
HDDA/PE9074	6.4	4	1	77	7	6.8	87	81	0	Yes	82	71
HDDMA/PE9074 methacrylate	6.4	4	5	77	3	3.5	72	62	0	No	80	14
DGPDA/PE9074	6.2	3	4	78	4	4,2	72	64	0	No	80	19
DPGDA Variante /PE9074 methacrylate	5.2	3	4	78	3	3.3	54	48	0	No	78	14
GPTA /PE9074	4.9	3	4	78	3	3.3	70	59	0	No	74	14
GPTA Variante/PE9074 methacrylate	4.9	3	4	74	3	3.2	54	47	0	No	77	12

1.2. Thickness and fiber content variations

1.2.1. 10 layers and 66 %wt filler content

In order to determine the maximum number of layers that could be polymerized by FP, an experiment was performed by increasing the number of layers to 10 using the best TMPTA\PE9074 blend. In fact, the fibers content is the key point of the heat dissipation. The temperature profiles of the compose using the blend TMPTA/PE9074 (72/28 % w/w) (temperature of the sample vs. irradiation time), as well as the pictures of the top and the bottom of the sample after polymerization are gathered in Figure 11.

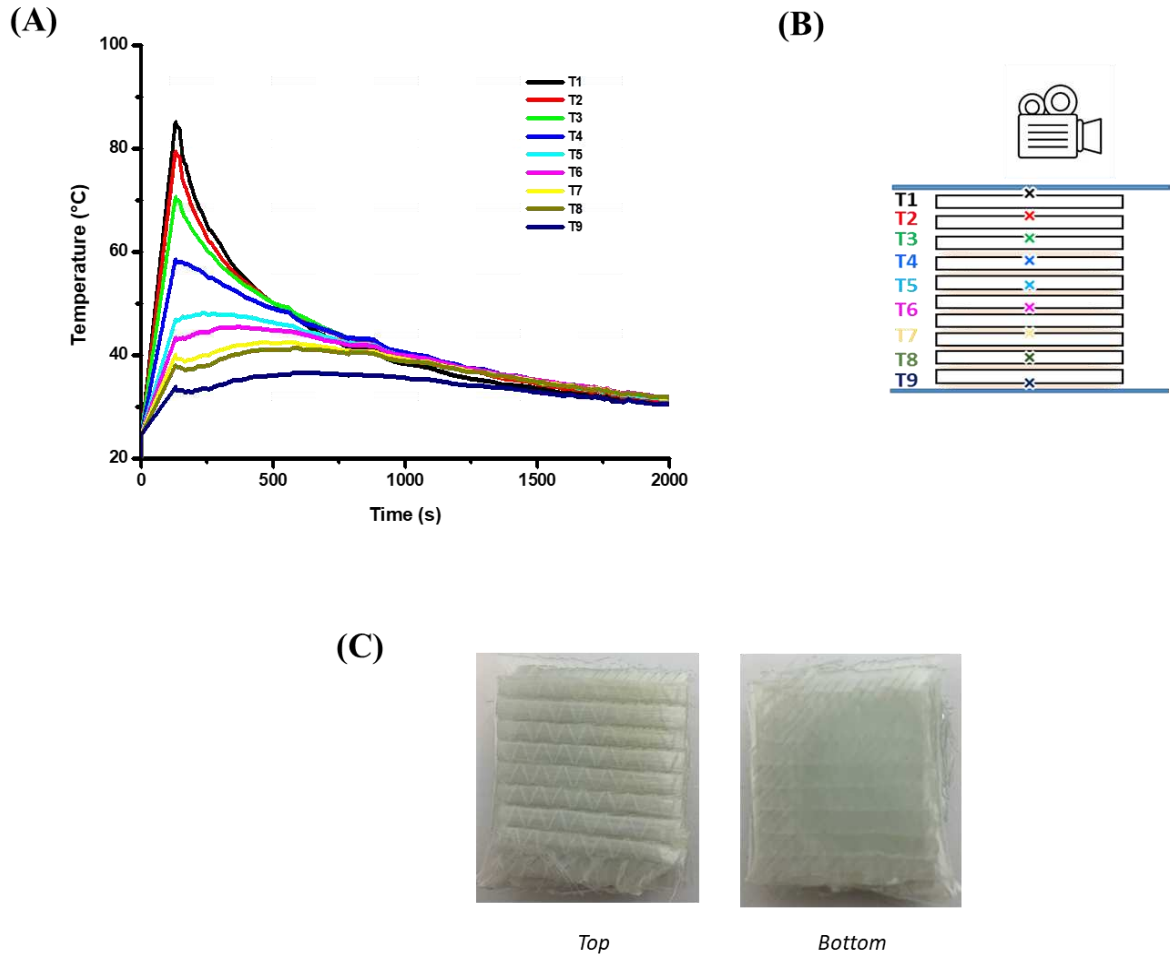

Figure 11. (A) Temperature profiles of Laromer TMPTA and Laromer PE 9074 (72/28 % w/w) laminated (temperature of the sample vs. irradiation time) in the presence of TPO (1.0 % phr), Luperox P (3 % phr) and glass fibers (66 % wt). LED@395 nm at 8 W/cm²; thickness = 10 mm. (B) Schematic of the sample consisting of ten glass fiber layers and the indicated measuring positions for the temperature (T1-T9). (C) Pictures of the top and the bottom of the sample.

Since after sample preparation, there is a loss of resin, the real fiber content was very high, about 72% compared to the resin, which means that very severe conditions were applied.

Therefore, in this case, 8 layers are cured (see Figure 11 (B)) and it is also noticeable that the temperatures in depth were not very high with such high fiber content (Figure 11 (A)).

1.2.2. 10 layers and 50 % wt filler content

In order to improve FP process, the idea of this part is to increase the resin content up to 50% wt. In such case the real fiber content after preparation is about 60% wt, so there is a clear difference between the temperatures in depth reached and all 10 layers are completely polymerized (see Figure 12). This again shows that the fiber content is a key parameter that can influence the frontal polymerization (see also part 3.3).

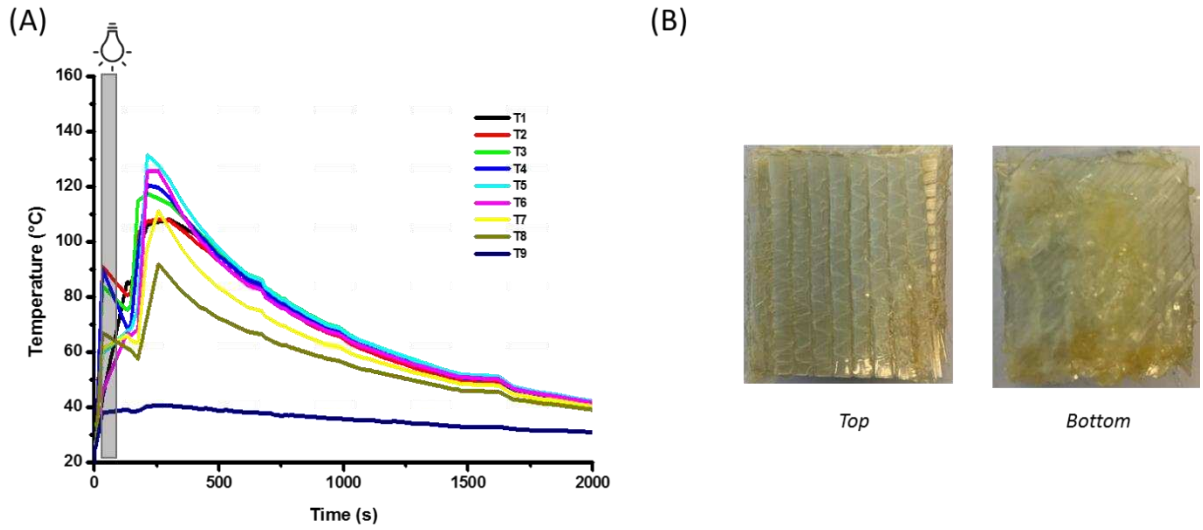

Figure 12. (A) Temperature profiles for the composite with the blend Laromer TMPTA and Laromer PE 9074 (72/28 % w/w) in laminate (temperature of the sample vs irradiation time) in the presence of TPO (1.0 % phr), Luperox P (3 % phr) and glass fibers (50 % wt). LED@395 nm at 8 W/cm²; thickness = 10 mm. The irradiation starts at t=10 s. (B) Pictures of the top and the bottom of the sample. (T9 in this case is not included in the sample).

2. Conclusion and perspectives

Photo-induced frontal polymerizations of acrylic ester systems have been successfully carried out and analyzed for resin blends with high filler content (> 50 wt %). The optical transmittance of the composites so low that almost no light penetrates the samples already for 500 µm in depths. In this work the great interest of frontal polymerization to enhance the polymerization in depth of composites was demonstrated. DSC experiments were undertaken in order to select an appropriate thermal initiator for the frontal polymerization experiments.

Woven glass fibers composites have been successfully prepared by frontal polymerization with the system based on TPO and Luperox P in HDDA/PE9074. Sufficient high temperatures were reached in the depth of the samples, as well as improved depths of cure and larger numbers of polymerized layers (embedded glass fiber layers) for the samples obtained by frontal polymerization compared to those obtained using the photochemical system alone. Designs of experiments were carried out in order to investigate the influence of different parameters on the frontal polymerization. Different characterizations techniques for the composites were done in order to define the appropriate outputs for the design of experiments. An excellent predictive controllable behavior was found for FP. This clearly underlines our statement that the photo induced frontal polymerization can be controlled. Other FP processes will be characterized in following works for composites preparation.

5. References

[1] J. P. Fouassier, Photoinitiation, Photopolymerization, and Photocuring: Fundamentals and Applications, Hanser Publishers, New York 1995.

[2] P. Garra, C. Dietlin, F. Morlet-Savary, F. Dumur, D. Gigmes, J.P. Fouassier, J. Lalevée, Photopolymerization processes of thick films and in shadow areas: a review for the access to composites, Polymer Chemistry, 2017, 8.46, 7088-7101.

[3] J. P. Fouassier, J. Lalevée, Photoinitiators: Structures, Reactivity and Applications in Polymerization, Wiley, Weinhein, 2021.

[4] F. Petko, A. Swiezy, J. Ortyl, Photoinitiating systems and kinetics of frontal photopolymerization processes-the prospects for efficient preparation of composites and thick 3D structures, Polymer Chemistry, 2021.

[5] Z. Li., X. Zou, G. Zhu, X. Liu, and R. Liu, Coumarin-based oxime esters: photobleachable and versatile unimolecular initiators for acrylate and thiol-based click photopolymerization under visible light-emitting diode light irradiation, ACS applied materials & interfaces, 2018, 10.18, 16113-16123.

[6] Z. Tang, Y. Gao, S. Jiang, J. Nie, F. Sun, Cinnamoylformate derivatives photoinitiators with excellent photobleaching ability and cytocompatibility for visible LED photopolymerization, Progress in Organic Coatings, 170, 106969., Shengling, et al. Cinnamoylformate derivatives photoinitiators with excellent photobleaching ability and cytocompatibility for visible LED photopolymerization, Progress in Organic Coatings, 2022, 170, 106969.

[7] J. T. Cabral, S. D. Hudson, C. Harrison, J. F. Douglas, Frontal photopolymerization for microfluidic applications, Langmuir, 2004, 20.23, 10020-10029.

[8] A. Vitale, M. G. Hennessy, O. K. Matar, J. T. Cabral, Interfacial profile and propagation of frontal photopolymerization waves, Macromolecules, 2015, 48.1, 198-205.

[9] M. G. Hennessy, A. Vitale, J. T. Cabral, O. K. Matar, Role of heat generation and thermal diffusion during frontal photopolymerization, Physical Review E, 2015, 92.2, 022403.

[10] M. Retailleau, A. Ibrahim, X. Allonas, Dual-cure photochemical/thermal polymerization of acrylates: a photoassisted process at low light intensity, Polymer Chemistry, 2014, 5.22, 6503-6509.

[11] M. G. Hennessy, A. Vitale, J. T. Cabral, O. K. Matar, Role of heat generation and thermal diffusion during frontal photopolymerization, Physical Review E, 2015, 92.2, 022403.

[12] M. Belk, K. G. Kostarev, V. Volpert, T. M. Yudina, Frontal photopolymerization with convection, The Journal of Physical Chemistry B, 2003, 107.37, 10292-10298.

[13] D. P. Gary, S. Bynum, B. D. Thompson, B. R. Groce, A. Sagona, I. M. Hoffman, C. Morejon-Garcia, C. Weber, J. A. Pojman, Thermal transport and chemical effects of fillers on free-radical frontal polymerization, Journal of Polymer Science, 2020, 58.16, 2267-2277.

[14] J. A. Pojman, V. M. Ilyashenko, A. M. Khan, Free-radical frontal polymerization: Self-propagating thermal reaction waves. Journal of the Chemical Society, 1996, Faraday Transactions, 92.16, 2825-2837.

[15] J. A. Pojman, R. Craven, A. Khan, W. West, Convective instabilities in traveling fronts of addition polymerization. The Journal of Physical Chemistry, 1992, 96.18, 7466-7472.

[16] C. Nason, T. Roper, C. Hoyle, J. A. Pojman, UV-induced frontal polymerization of multifunctional (meth) acrylates, Macromolecules, 2005, 38.13, 5506-5512.

[17] C. Noè, M. Hakkarainen, S. Malburet, A. Graillot, K. Adekunle, M. Skrifvars, M. Sangermano, Frontal-Photopolymerization of Fully Biobased Epoxy Composites. Macromolecular Materials and Engineering, 2022, 307.6, 2100864.

[18] C. Ebner, J. Mitterer, J. Gonzalez-Gutierrez, G. Rieß, W. Kern, Resins for Frontal Photopolymerization: Combining Depth-Cure and Tunable Mechanical Properties, Materials, 2021, 14.4, 743.

[19] S. A. Chesnokov, V. M. Treushnikov, Y. V. Chechet, V. K. Cherkasov, O. N. Mamysheva, General conditions and experimental design of sustained frontal photopolymerization in photopolymerizable liquid compositions, Polymer Science Series A, 2008, 50.3, 291-298.

[20] V. V. Ivanov, C. Decker, Kinetic study of photoinitiated frontal polymerization, Polymer international, 2001, 50.1, 113-118.

[21] J. V. Crivello, Hybrid free radical/cationic frontal photopolymerizations, Journal of Polymer Science Part A: Polymer Chemistry, 2007, 45.18, 4331-4340.

[22] A. Mariani, S. Bidali, S. Fiori, M. Sangermano, G. Malucelli, R. Bongiovanni, A. Priola, UV-ignited frontal polymerization of an epoxy resin, Journal of Polymer Science Part A: Polymer Chemistry, 2004, 42.9, 2066-2072.

[23] P. G. Mathews, Design of Experiments with MINITAB, Quality Press, 2004.

[24] D. Price, L. K. Cunliffe, K. J. Bullet, T. R. Hull, G. J. Milnes, J. R. Ebdon, B. J. Hunt, P. Joseph, Thermal behavior of covalently bonded phosphonate flame-retarded poly (methyl methacrylate) systems, Polymers for Advanced Technologies, 2008, 19.6, 710-723.

Conclusion Générale et Perspectives

Conclusion Générale et Perspectives

Les objectifs fixés au début de la thèse ont été effectivement atteints par les résultats obtenus au cours de ce travail de doctorat, et ils ont également contribué à des avancées scientifiques intéressantes. Principalement, le développement de nouveaux systèmes de photoamorceurs à haute performance (ayant d'excellentes vitesses de polymérisation et caractérisés par des conversions finales élevées en fonctions réactives) a constitué une réalisation importante. Afin d'évaluer la capacité des systèmes photoamorceurs sensibles à la lumière bleue nouvellement développés à amorcer la polymérisation radicalaire (FRP) rapidement et à un coût raisonnable, des diodes électroluminescentes (LEDs) de faible puissance ont été utilisées comme source lumineuse. Ces diodes peuvent remplacer les lampes UV traditionnelles, qui présentent un grand nombre d'inconvénients. Notre recherche s'est concentrée sur une variété de groupes de photoamorceurs (PAs), chacun d'entre eux ayant des réactivités et des propriétés particulières. Ces recherches ont contribué à l'étude des relations entre la structure, la réactivité et l'efficacité des différents nouveaux systèmes photoamorceurs étudiés. Les mécanismes photochimiques correspondants ont été fournis. Ces nouveaux systèmes photoamorceurs (présentant de très bonnes réactivités et d'excellentes capacités de photoamorçage) ont été utilisés précisément pour préparer des motifs de polymère en 3D. En outre, comme les processus de photopolymérisation ne sont pas encore suffisamment appliqués dans le domaine des composites parce que la pénétration de la lumière dans ces matériaux est très limitée, la stratégie de photopolymérisation frontale a été présentée comme une approche puissante pour la préparation de composites hautement chargés.

Dans la première partie de la thèse, une introduction générale a été fournie tout en soulignant l'importance des processus de polymérisation induite par la lumière, le problème de recherche, ainsi que les questions, les défis et l'originalité du travail, les objectifs de recherche et enfin, la structuration du travail.

CONCLUSION GÉNÉRALE ET PERSPECTIVES

Dans la deuxième partie de la thèse, une étude approfondie sur le développement de nouveaux systèmes photoamorceurs multicomposants capables d'amorcer les processus de polymérisation radicalaire ainsi que les procédés de polymérisation cationique des époxydes dans des conditions d'irradiation douces, notamment sous la LED à 405 nm a fait l'objet du travail. Une grande famille de molécules à base de biscarbazole a été sélectionnée et examinée en tant que photoamorceur sensible à la lumière visible. Ces molécules ont été testées pour leur capacité à amorcer les processus de polymérisation radicalaire et cationique sous lumière bleue (LED à 405 nm) à travers soit un processus de photo-oxydation une fois combinées avec les sels d'iodonium, soit un processus de photo-réduction en présence d'une amine (e.g. EDB). D'excellentes performances ont été obtenues en présence de ces nouveaux systèmes proposés, cela revient à leurs fortes absorptions dans la région proche-UV et visible ainsi que leurs potentiels d'oxydation et de réduction appropriés, et finalement leurs variations d'énergie libre (ΔG_{et}) et rendements quantiques de transfert d'électron (Φ_{et}) très favorables. Outre la très grande capacité de photoamorçage observée pour les systèmes à deux composants, ces dérivés sont également capables d'amorcer efficacement la réaction de polymérisation lorsqu'ils sont incorporés dans des systèmes photoamorceurs à trois composants (Biscarbazole/Iod/EDB). Ces nouveaux systèmes photoamorceurs radicalaires et/ou cationiques ont été utilisés pour des applications d'impression 3D ainsi que pour la préparation de photocomposites. Les travaux ont également porté sur le développement de nouveaux additifs de polymérisation ou co-amorceurs comme alternatives intéressantes aux amines aromatiques toxiques, dans le but d'accéder à des systèmes photoamorceurs sûrs sans amines.

Dans la troisième partie de la thèse, le développement de nouveaux systèmes photoamorceurs monocomposants (Type I) a été initié. Plusieurs chromophores (tels que la triphenylamine, la coumarine ou le biscarbazole) ont été introduits dans la structure d'oxime-ester pour décaler leur longueur d'onde d'absorption vers le rouge, afin de mieux correspondre aux différentes sources de lumière LED. La capacité de photo-amorçage et la photoréactivité des structures proposées ont été examinées lors de l'exposition des résines à une LED@405 nm, et leur comportement d'amorçage thermique a été évalué par calorimétrie à balayage différentiel

(DSC). En outre, et afin de mettre en évidence leur haute efficacité de photopolymérisation, les structures proposées ont été utilisées pour des applications en impression 3D.

La quatrième et dernière partie de la thèse était associée aux polymérisations frontales photoinduites pour les systèmes à base d'ester acrylique, réalisées et analysées avec succès pour des mélanges de résines à forte teneur en charges (> 50 % en poids). Ce travail a démontré le grand intérêt de la polymérisation frontale pour améliorer la polymérisation en profondeur des composites.

Un travail futur pourrait être de développer de nouvelles oxime-esters et d'étudier en détail leurs aspects de photogénérateur de bases qui peuvent être à la source de l'amorçage des processus de polymérisation thiol-époxy, susceptibles d'être intéressants pour améliorer les propriétés mécaniques des polymères obtenus. Par ailleurs, une étude approfondie de la toxicité de nos composés, notamment dans la matrice polymère, pourra être envisagée ultérieurement. Il est également souhaitable de développer des structures naturelles efficaces ayant des propriétés biologiques ou pharmacologiques afin de réduire la toxicité des composés chimiques utilisés aujourd'hui comme photoamorceurs, ce qui permettrait l'utilisation de ces composés dans des applications médicales. Le développement de nouveaux photoamorceurs présentant des propriétés d'absorption encore plus décalées, en particulier dans le proche infrarouge, peut également s'avérer avantageux. Cela pourrait assurer une meilleure pénétration de la lumière dans l'épaisseur de l'échantillon, favorisant ainsi la génération de polymères encore plus épais, en particulier pour l'impression 3D et la préparation de composites.